UNIVERSITEIT VAN PRETORIA
UNIVERSITY OF PRETORIA
YUNIBESITHI YA PRETORIA

Mineralogical investigation of the Nepheline syenite Franspoort, South Africa for beneficiation.

University of Pretoria
Department of Geology

February 2010

Lelanie Gryffenberg
M.Sc. Applied Mineralogy

UNIVERSITEIT VAN PRETORIA
UNIVERSITY OF PRETORIA
YUNIBESITHI YA PRETORIA

Mineralogical investigation of the Nepheline syenite Franspoort, South Africa for beneficiation.

By

Lelanie Gryffenberg
M.Sc. Applied Mineralogy

Submitted in partial fulfilment of the requirements for the degree of

Magister Scientiae Applied Mineralogy

in the Faculty of Natural and Agricultural Sciences,

University of Pretoria

Pretoria

February 2010

UNIVERSITEIT VAN PRETORIA
UNIVERSITY OF PRETORIA
YUNIBESITHI YA PRETORIA

I, Lelanie Gryffenberg, declare that the thesis/dissertation, which I herby submit for the degree Magister Scientiae Applied Mineralogy at the University of Pretoria, is my own work and has not previously been submitted by me for a degree at this or any other tertiary institution.

SIGNATURE:……

DATE:……..

In memory of Dad and Mom

Abstract

Mamelodi Quarries, which currently mine the Franspoort nepheline syenite, produces aggregate and crusher sand for the local building industry. The mine is located northeast of Pretoria, South Africa on the road to Cullinan.

The aim of this study is to investigate the use of the Franspoort nepheline syenite as an alumina and alkali resource for the glass and ceramics industry at Mamelodi Quarries, and to evaluate the production of a concentrate of zircon and rare earth elements as economic by-products. International standards require a nepheline product with a ferric oxide content of less than 0.35 weight percent.

The Franspoort nepheline syenite contains 3.37 weight percent of ferric oxide. The iron-containing minerals present are aegirine, aegirine-augite, magnetite, ilmenite and pyrite. The removal of iron-bearing minerals was attempted by high-intensity wet magnetic separation, low-intensity dry magnetic separation, spiral gravity separation, and heavy liquid separation to produce a saleable nepheline product. This product is the cleaned final concentrate, of the different separation tests, which contains the lowest iron concentration for application in the glass and ceramic industry.

The mineral assemblage was determined with a petrographic study as well as X-ray diffraction and electron microprobe analyses. Material from the different separation tests was analysed with X-ray fluorescence to obtain the chemical composition and to evaluate the final iron content of the nepheline product.

The dry magnetic separation method produced the best results. The nepheline product has a ferric oxide content of 0.68 weight percent compared to the starting concentration of 3.37 weight percent. The ferric oxide concentration is, however, above the accepted levels for the glass and ceramics industry. The ferric oxide content is attributed to small iron-rich mineral inclusions, which are locked in feldspar and nepheline. The final nepheline product is not suitable for the use in the glass and ceramic industry.

Zircon was concentrated the best by the use of heavy liquid separation. Zircon is in most cases locked in the minerals albite, microcline, and nepheline. The rare earth elements are mostly associated with zircon and fluorite and therefore it will not be viable to produce it as a by-product.

Table of Contents

List of Tables

List of Figures

List of abbreviations and definitions used

Abbreviation	Explanation
%	Percentage
By-product	A secondary material having economic value. Concentrated in the process of extracting a main mineral from an ore deposit
EMPA	Electron microprobe analysis
Flux	A material that lowers the melting temperature of a mixture or single mineral. The particle size and different melting temperatures will influence the melting temperature
FNS	Franspoort nepheline syenite
FP	Final product
Fuse	The process causing the formation of glass in a furnace
Fusibility	How easily a specific mineral or particle melts and mixes with other minerals at a given temperature
g	Grams
HLRH	Heavy liquid separation ROM heavy portion
HLRL	Heavy liquid separation ROM light portion
HLRSM	Heavy liquid separation ROM starting material
kV	Kilovolt
l.d	lowest limit of detection
LOI	Loss on ignition
Ma	Millions of years before present time
mass %	mass percent
mA	Milli-ampere
ml	Millilitre
MQ	Mamelodi Quarries
MQ1	Mamelodi Quarries 1 (grey nepheline syenite)
MQ2	Mamelodi Quarries 2 (xenolith)
Msr	Measured values
n.d	Not detected
Nugget effect	The effect of high-elevated concentration of a specific element due to statistical distribution or natural enrichment
ppm	Parts per million
REE	Rare Earth Elements
REO	Rare Earth Oxide
ROM	Run of mine
RPM	Roll per minute
sec	Second
Std	Certified reference value
UP	University of Pretoria
wt %	weight percent
XRD	X-ray diffraction
XRF	X-ray fluorescence

1 INTRODUCTION

1.1 General

The aim of this study is to investigate the mineralogical composition of the Franspoort nepheline syenite as an alumina and alkali resource for the glass and ceramics industry. Mamelodi Quarries mine the Franspoort nepheline syenite (FNS) and produce an aggregate and crusher sand for the building industry. Mamelodi Quarries wanted to investigate the possibility of producing a nepheline product to supply the South African glass and ceramics industry.

Compared to the different nepheline syenites from Canada and Norway, the Franspoort nepheline syenite has a higher iron concentration (Table 1). This is challenging for glass and ceramic production. In South Africa, the Pilansberg Complex, which contains nepheline syenite rocks, has been investigated as a potential resource for Rare Earth Elements (REE) (Schürmann and Harmer 1998). In this study the REE and zirconium content of the nepheline syenite will be investigated to evaluate different processes to concentrate these elements as a potential future by-product for the mine for economic reasons.

Table 1. Composition of Franspoort nepheline syenite and different nepheline syenites from Norway and Canada.

	Norway clear glass grade*	**Norway colour glass grade***	**Canada clear glass grade***	**Canada colour glass grade***	**Norway ceramic grade***	**Franspoort starting material****
SiO_2	57.00	56.50	60.30	60.70	57.00	54.95
Al_2O_3	23.80	22.50	23.70	23.30	23.80	20.82
Fe_2O_3	**0.10**	**0.40**	**0.10**	**0.07**	**0.12**	***3.37***
TiO_2	0.10	-	-	-	-	0.33
CaO	1.30	2.50	0.30	0.70	1.10	1.09
Na_2O	7.90	7.50	10.40	9.80	7.80	10.00
K_2O	9.00	8.20	5.00	4.60	9.10	4.88
MgO	-	-	-	0.10	-	0.04
F	< 40ppm	< 40ppm	-	-	< 40ppm	0.75
LOI	1.20	-	0.30	0.70	-	3.29

* Harben (1995); ** data from this study

By combining microscopy with analytical techniques, the different separation processes were evaluated, in order to determine the most economical method for removing iron-containing minerals to produce a nepheline product. The same separation processes were assessed for the concentration of REE and zircon.

1.2 Different uses of nepheline syenite, feldspar, and REE

1.2.1 Nepheline syenite

Nepheline syenite is a medium to course-grained igneous rock containing alkali feldspars and nepheline with one or more ferromagnesian minerals (Nockolds et al.1978).

Nepheline syenite is used as a source for Al_2O_3, Na_2O, and K_2O for the glass and ceramics industry. The alumina enhances the workability of molten glass, as well as protection against chemical corrosion, whilst the hardness and durability of the glass improves. The alkalis (Na_2O and K_2O) act as a flux (a material that lowers the melting temperature of a mixture or single mineral where particle size plays a role), to lower the temperature and the rate at which the glass will melt, and thus to conserve energy (Potter 2007).

In ceramics, a low fuse temperature is required and nepheline syenite is used as an effective agent for the formation of a glassy phase in the ceramic body. The long firing range of nepheline syenite contributes to the physical strength of the final ceramic product (Harben 1995). Table 2 is a summary of the uses of nepheline syenite in different industries (Harben 1995).

The major producers of nepheline syenite products for the glass and ceramics industry are Canada and Norway (Potter 2007). Minor producers for glass and ceramics products are: United States of America, Italy, Poland, Germany, United Kingdom, Netherlands, France, Australia, Singapore, Taiwan, Japan, Sweden, Greece, Portugal, Ireland, China, and Spain (Harben 1995 and Potter 2007).

Table 2. Summary of the different uses of nepheline syenite (after Harben 1995).

Uses	**Description**
Filler:	Anti-blocking agent, adhesives, caulks, sealants.
Coatings:	Latex and alkaloid paints, metal primers, wood strainers, sealers, undercoats, plastic including PVC and epoxy.
Low resin demand:	High loading rates in plastics, categorized as "generally recognized as safe" (GRAS) for indirect food contact, transparent to microwaves surface.
Paint:	Particle size control lead to a satin smooth service, eggshell and flat interior wall paints, powder coating to levels of 30 %.
Mild abrasive:	Scouring powders.

1.2.2 Feldspar

Feldspars are aluminosillicates with varying amounts of K, Na, and Ca in solid solution series (Deer et al. 1997). The feldspars are: albite (sodium rich), microcline, orthoclase, sanidine (potassium rich) and anorthite (calcium rich) (Deer et al. 1997 Figure 1). Microcline or oligoclase are usually referred to as potassium feldspar, potash spar or K-feldspar and must contain at least 10 weight percent (wt %) or more K_2O, while albite or sodium plagioclase (soda spar or Na spar) must contain 7 wt% or more Na_2O (Harben 1995). The economically important sources of feldspars are pegmatites and alaskite (leucocratic granite containing orthoclase, microcline, and quartz; Boelema 1998).
Table 3 summarises the different uses of feldspar. The major producers of feldspar in the world are shown in Table 4.

In South Africa, feldspar is mainly mined from pegmatites in the Limpopo Province and the Northern Cape Province. The feldspar is mined together with other commodities like mica, quartz, beryl, and tantalite / columbite (Boelema 1998).

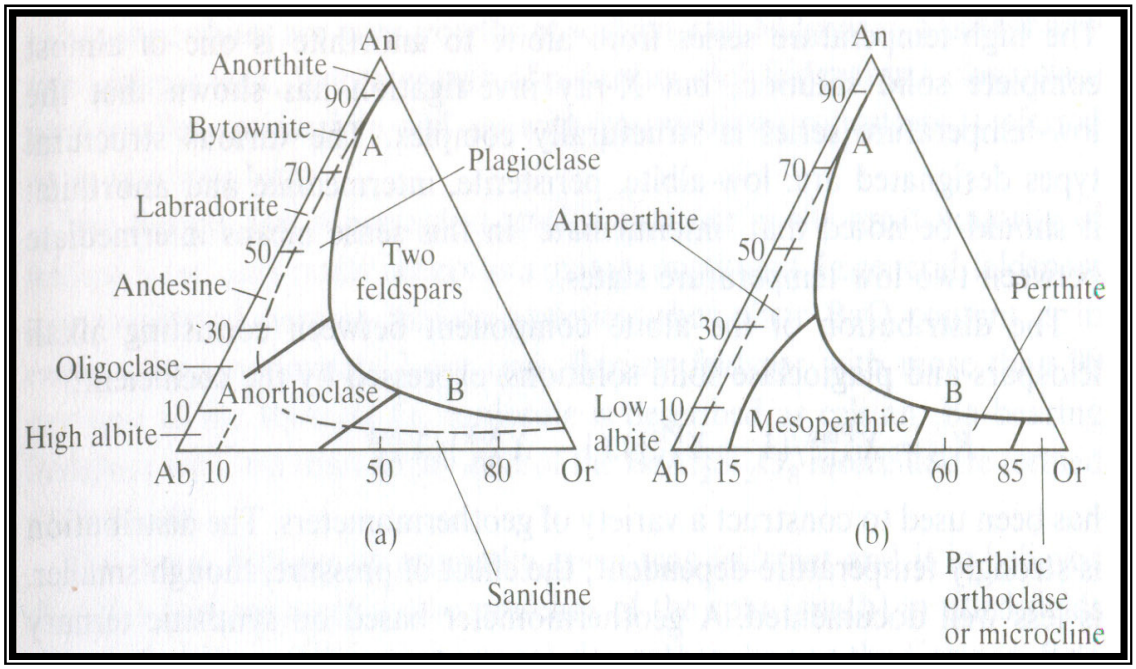

***Figure 1. The feldspar groupings: a) disordered feldspars and b) ordered feldspars. Composition in mol percent. Curve AB, limit of the ternary solid solution (From* Deer et al. 1997).**

Table 3. Summary of the uses of feldspar (after Harben 1995).

Uses	**Description**
Glass making source:	Source of Al_2O_3, Na_2O, K_2O and SiO_2
Glass making products:	Borosilicate glass, soda-lime flat and container glass, fibreglass, television tube glass
Alumina:	Workability of molten glass, increases resistance to chemical corrosion, improves hardness and durability
Alkalis:	Acts as a flux
Ceramics source:	Acts as a flux to form a glassy phase
Ceramics products:	Virtuous and semi-virtuous china, wall & floor tile, sanitaryware, electrical porcelain, glazes and enamels, pottery
Filler products:	Latex, exterior and interior paint, plastics, caulks, sealants, adhesives, mastics and elastomers
Mild abrasive:	Scouring powders, welding rod coating

1.2.3 Zirconium and Rare Earth Elements

The major source of zirconium is found in the minerals zircon and baddeleyite. Table *5* provides a summary of the uses of zircon.

Rare earth elements are being used in an increasing range of different applications. The mining of REE is of strategic importance to the economies of the developing world, because there is an increase in the demand for REE and REO (Kanazawa and Kamitani 2006; see Table 6).

Monazite [(Ce, La, Nd, Th) (PO_4, SiO_4)] and xenotime [Y(PO_4)] are phosphate minerals occurring in granites, metamorphic rocks, alkaline igneous rocks, and carbonates. Commonly, these minerals will be associated with placer deposits (Kanazawa and Kamitani 2006). Table 6 shows different applications for REE according to Griffiths (1984), Neary and Hihley (1984), and Harben (1995).

Table 4. Feldspar world production from 2004 to 2007 (modified after Potter 2007).

Country[3]	2004		2005		2006[e]		2007[e]	
Argentina	125,684	r	151,307	r	150,000		170,000	
Australia[e]	50,000		50,000	r	50,000		50,000	
Brazil	121,452	r	122,887	r	123,000	p	125,000	
Bulgaria	35,000	e	35,000		35,000		90,000	
Burma[e, 4]	10,000		10,000		10,000		10,000	
Chile	4,838		5,820	r	6,000		6,000	
China[e]	1,800,000		1,850,000		1,900,000		2,000,000	
Colombia[e]	100,000		100,000		100,000		100,000	
Cuba[e]	10,500	r	8,000	r	8,000		6,000	
Czech Republic	488,000	r	472,000	r	475,000		490,000	
Ecuador	53,469	r	38,250	r	40,000		68,000	
Egypt[e]	350,000		350,000		350,000		350,000	
Ethiopia[6]	361		445	r	478	5	480	
Finland	57,149		60,000		60,000		60,000	
France[e]	650,000		650,000		650,000		650,000	
Germany	182,842	r	168,640	r	167,332	5	171,303	6
Greece[e]	95,000		95,000		95,000		95,000	
Guatemala	4,473		3,808	r	4,000		17,200	
India[e]	150,000		150,000		160,000		160,000	
Iran	252,713		250,000		250,000		260,000	
Italy[e]	3,000,000	r	3,000,000	r	3,000,000		4,200,000	
Japan[e]	900,000		1,000,000		1,000,000		750,000	
Jordan	13,063	r	14,000		14,000		11,000	
Korea, Republic of	541,788		508,644	r	500,000		398,513	6
Macedonia[e]	20,000		20,000		20,000		40,000	
Malaysia	79,220		83,580	r	80,000		150,000	
Mexico	364,315		349,109		450,000		460,000	
Morocco[e]	20,000		20,000		20,000		20,000	
Nigeria[e]	1,700		1,700		1,700		1,700	
Norway[e]	75,000		76,000		75,000		75,000	
Pakistan	30,373	r	25,032	r	24,000		22,000	
Peru	6,005		6,000	r	6,500	p	6,050	
Philippines[e]	32,110	r, 5	11,850	r, 5	12,000		12,000	
Poland[7]	300,000	e	300,000		300,000		350,000	
Portugal	98,262	r	133,344	r	133,500	p	129,500	p,6
Romania	60,924	r	56,817	r	55,000		35,000	
Russia[e]	45,000		45,000		45,000		45,000	
Serbia and Montenegro[e, 8]	4,500		4,000		4,000		3,500	
Slovakia[e]	5,000		5,000		5,000		5,000	
South Africa	**53,721**	**r**	**57,534**	**r**	**76,000**		**90,232**	
Spain, includes pegmatite	552,507	r	580,000	r	580,000		600,000	
Sri Lanka	33,000	e	34,000		35,000		36,000	
Sweden	42,000		43,000		42,000		42,000	
Thailand	1,001,053		1,000,000		1,000,000		1,000,000	
Turkey	1,983,336		2,200,000		2,300,000		3,800,000	
United Kingdom, china stone	2,274	r	2,500	r	2,500		2,000	
United States	770,000		748,000		763,000	5	730,000	
Uruguay	2,450	r	2,150	r	2,200	p	2,500	
Uzbekistan[e]	4,300		4,300		4,300		4,300	
Venezuela	176,000		202,000	r	200,000		200,000	
Total	**14,800,000**	**r**	**15,100,000**	**r**	**15,400,000**		**18,100,278**	

The legend is on the next page

Table 4. Continued.

Legend
[e]Estimated. [p]Preliminary. [r]Revised. -- Zero.
[1]World totals, U.S. data, and estimated data are rounded to no more than three significant digits; may not add to totals shown.
[2]Table includes data available through April 24, 2007.
[3]In addition to the countries listed, China, Namibia, the United Arab Emirates, and Yemen may produce feldspar, but output is not officially reported; available general information is inadequate for the formulation of reliable estimates of output levels.
[4]Data are for fiscal years beginning April 1 of year stated.
[5]Reported figure.
[6]Data are for fiscal years ending July 7 of year stated.
[7]Of the amounts shown, the dedicated feldspar mine production accounts for only part of total feldspar production.
[8]In June 2006, Montenegro and Serbia formally declared independence from each other and dissolved their union. Mineral production data for 2006, however, still reflect the unified country.

Table 5. Different properties and uses of Zircon (after Harben 1995).

Uses	**Description**
Used in :	Refractories for ladle linings, continuous steel casting nozzles, refractory bricks for glass melting furnaces, ramming mixes, refractory cement & foundry sand (steel)
Ceramics:	Porcelain glazes, sanitaryware, wall tile, china ware, glazed brick & industrial tiles
Welding:	Welding rod coating

In South Africa, REE mineralitations occur in the Phalaborwa Complex, Glenover Complex, Pilansberg Complex, Kruidfontein Complex, and the Zandkops Drift Complex (Schürmann and Harmer 1998). These various complexes contain different quantities of REE and may be potential resources for the future.

Table 6. Summary of the uses of rare earth elements (after Griffiths (1984), Neary and Hihley (1984), and Harben (1995)).

Compound mixtures as in natural ores:	High strength micro alloyed steel
	Ductile iron and supper alloys
	Petroleum cracking catalyst
	Starting materials for mischmetal manufacture and rare earth silicides
	Mixed rare earth polishing compounds and carbon arcs used in fluorescent lights
Compound mixtures with 90 % of single REE:	Discolouration and polishing agents for glass
	Magnetic and electronic materials
	Hosts and activators in phosphors, lasers and lighting
	Neutron capture, super conductors, energy storage systems and fibre optics
Medical:	Cerium oxalate to counter seasickness
	Neodymium compounds for the treatment of thrombosis
Permanent magnets:	REE powder is milled and magnetically orientated, pressed at about 1150℃ and produces a magnet 2-5 times stronger than alnico magnets.
Other uses:	Computer disk drives, television screens, ceramics as sintering aid, synthetic garnet crystal production

1.3 Geography of Mamelodi Quarries

The privately owned Mamelodi Quarries have been in operation since the late 1980's. The mine is situated 25 km on the road leading to Cullinan, north east of Pretoria, South Africa (25° 41' 37.87" S; 28° 23' 52.30" E) (Figure 2). The focus of the mine is the production of an aggregate rock and crusher sand for the building industry. Attempts were made to produce a nepheline syenite product for the local glass and ceramics industry, but these were unsuccessful due to the high iron level in the concentrate.

The mining method used at Mamelodi Quarries is open pitting with off wall rock blasting (Figure 3). The size of the open pit is 330 m by 195 m and is approximately 25 m to 40 m deep. After blasting, the rock is moved by trucks to a primary jaw crusher. The rock is crushed and distributed by a conveyor belt system to secondary crushers to obtain different sizes for crusher sand and aggregate.

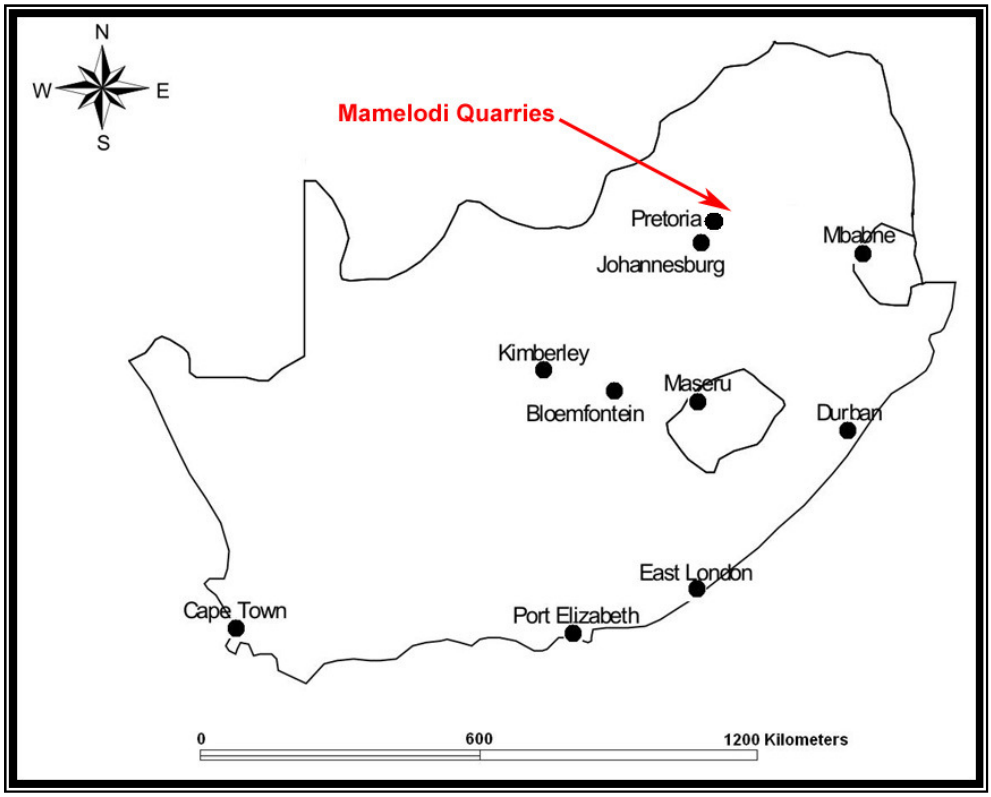

Figure 2. The location of Mamelodi Quarries.

Figure 3. Google earth image of the open cast mine of Mamelodi Quarries (from Terremetrica 2006).

2 REGIONAL GEOLOGY

2.1 Overview of geology of the Franspoort farm and the surrounding area

The Franspoort nepheline syenite intrusion is associated with other alkaline intrusions at Leeuwfontein, Wallmannsthal, and Leeuwkraal to form the Franspoort line (Shand 1922). The different alkaline intrusions are shown in Figure 4 (Frick & Malherbe 1986).The nepheline syenites were first discovered by A. L. Hall in 1903, and where then described in terms of geology and their formation (Shand 1922). The estimated age of the Franspoort nepheline syenite intrusions are 1 420 Ma (Snyman 1996).

Figure 5 shows a regional map of the geology found on Franspoort 332 JR farm. In the south, the Magaliesberg Quartzite (T3mQ) is exposed. Field observations by Toens (1952) indicates that most of the quartzite has been recrystallised. At the south border of the farm, a large nepheline syenite body (5sf) intruded and caused a dislocation of the quartzites (Shand 1922). The quartzite to the west of the body has a strike of east west; to the east, the strike changes to north east. To the west and east of the syenite intrusion there are two faults, which according to Shand (1922) were associated with dislocation of the Pretoria sedimentary beds during the intrusion. The southern part of the Franspoort farm forms part of the Mamelodi residential area and it is not possible to see the direct contact between the shale and the syenite intrusion. The nepheline syenite occurrences on the Franspoort farm consist of one large intrusive body to the south and two smaller intrusions in the middle of the farm. Mamelodi quarries are located on a smaller intrusion (Figure 5).

Trachy-andesites share a contact with the large nepheline syenite body to the south as well as the smaller syenite body of Mamelodi Quarries. According to Toens (1952), some of the trachy-andesites contain a number of dykes.

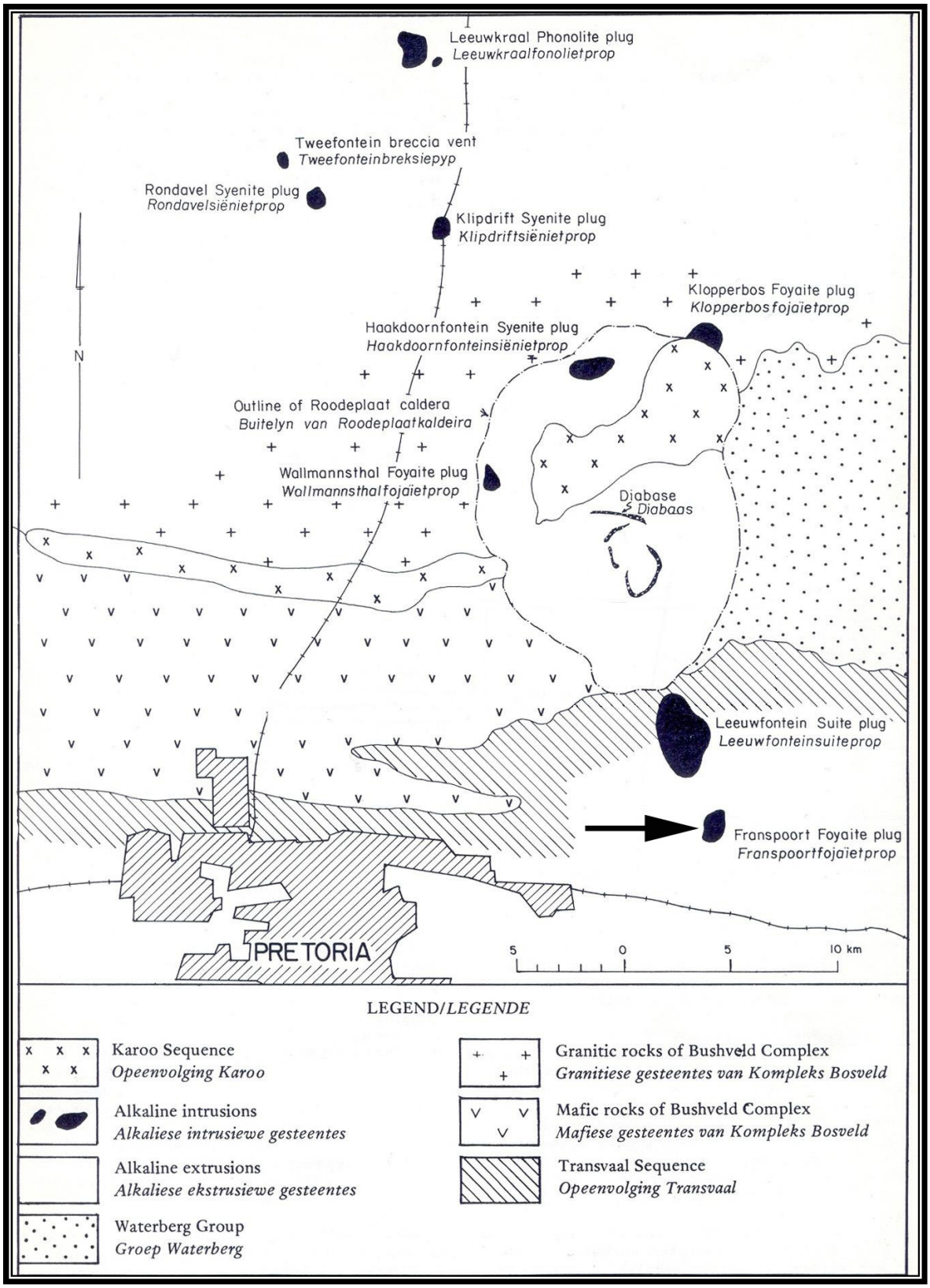

Figure 4. The different alkaline rocks north of Pretoria, South Africa (from Frick and Malherbe 1986).

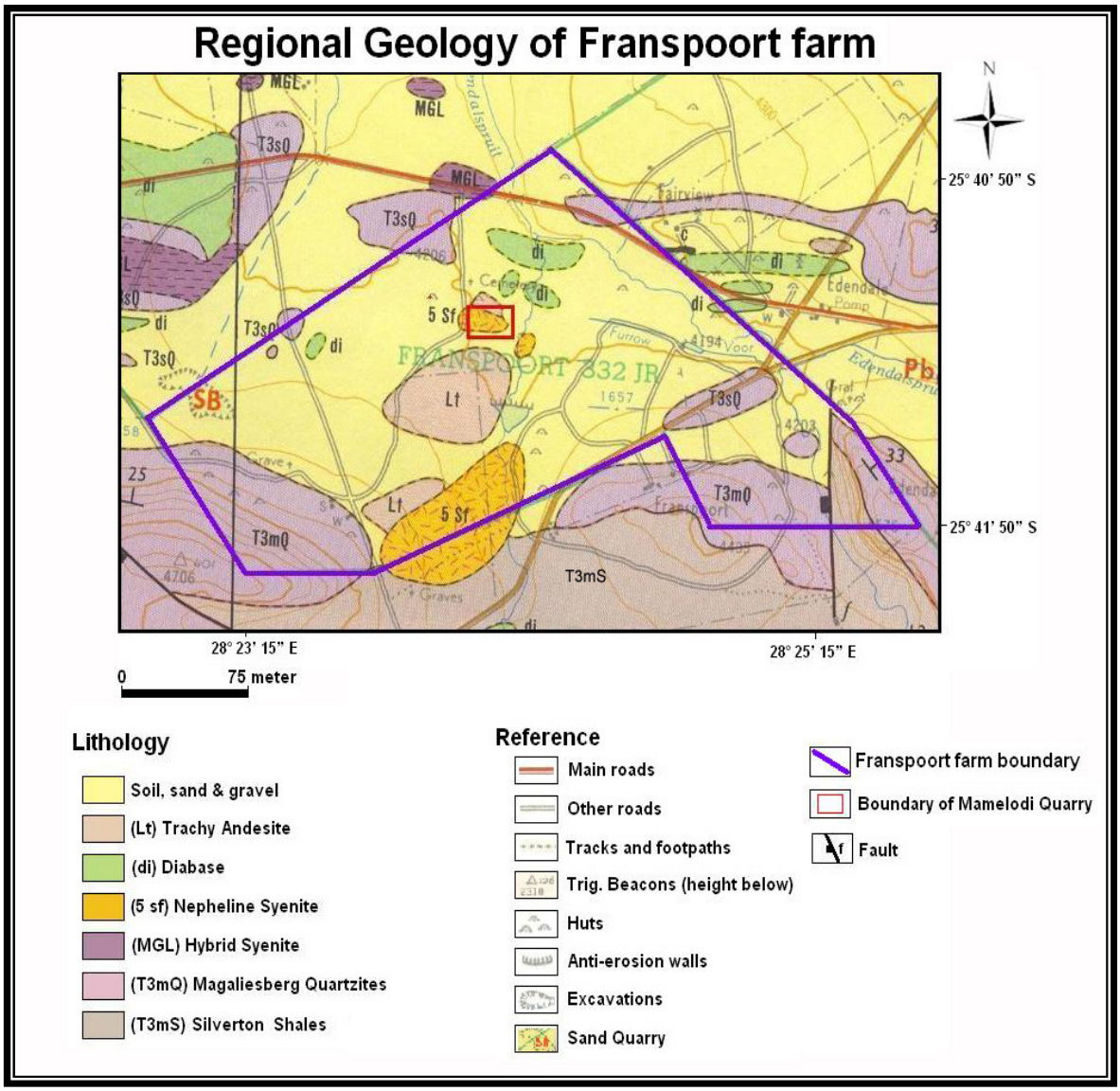

Figure 5. Regional geological map for Franspoort farm (modified after Besaans 1969).

A big part of the open pit is filled with water for most of the year and is mainly a reservoir of rainwater. During the annual rainy season, the groundwater level rises and mixes with the surface water in the quarry. The water is used for dust control, as the mine is located close to Mamelodi residential area. The management of the mine is planning to turn the quarry into a waste disposal site when the mining operation ends.

2.2 Geology of Mamelodi Quarries

Mapping the geology at Mamelodi Quarries is problematic, because the mine is covered with big boulders, which makes access to the rock face difficult (Figures 6 and 7).

The current mine records do not contain any geological information as records were only kept of the outline of the mine. The map presented in Figure 8 consequently only represents what could be observed in the quarry as independently mapped by the author. The following rock types were observed in the quarry: nepheline syenite, pegmatite, nepheline syenite containing xenoliths, and lamprophyre dykes. Two different types of nepheline syenite are distinguished based on a colour difference; a grey nepheline syenite and a red nepheline syenite.

The contact relationships between the different rock types are unclear, and the map (Figure 8) presents a possibility of how these contacts may have been before mining began. The largest part of the deposit consists of a grey nepheline syenite, which is the major product of the mine ("run of mine" [ROM]). On the north western side of the quarry, a red nepheline syenite is exposed, but is not currently mined.

Figure 6. A photo of the south eastern rock face at Mamelodi Quarries showing the large boulders scattered on the side of the mine. Width of view is ~ 200 m.

Figure 7. A photo of the open pit at Mamelodi Quarries. Width of view is ~ 600 m.

A large number of lamprophyre dykes, striking northeast to southwest, are exposed throughout the mine. In the southeast part of the mine, a pegmatite nepheline syenite rock occurs. Most of the outcrop has been destroyed during mining operations, and only a small area is left exposed.

Exposed on the northeast side of the mine is a small area of grey nepheline syenite with xenolith inclusions. The xenoliths are finer grained compared to the nepheline syenite and are dark grey to black in colour (Figure 9). For this study, only the grey nepheline syenite (referred to as Franspoort nepheline syenite [FNS] here after) was identified for use in the different separation tests. The petrographic results for the nepheline syenite rocks are presented in Chapter 6 since the focus of the project is on examining the different results obtained from the different separation techniques rather than on the genesis of the deposit.

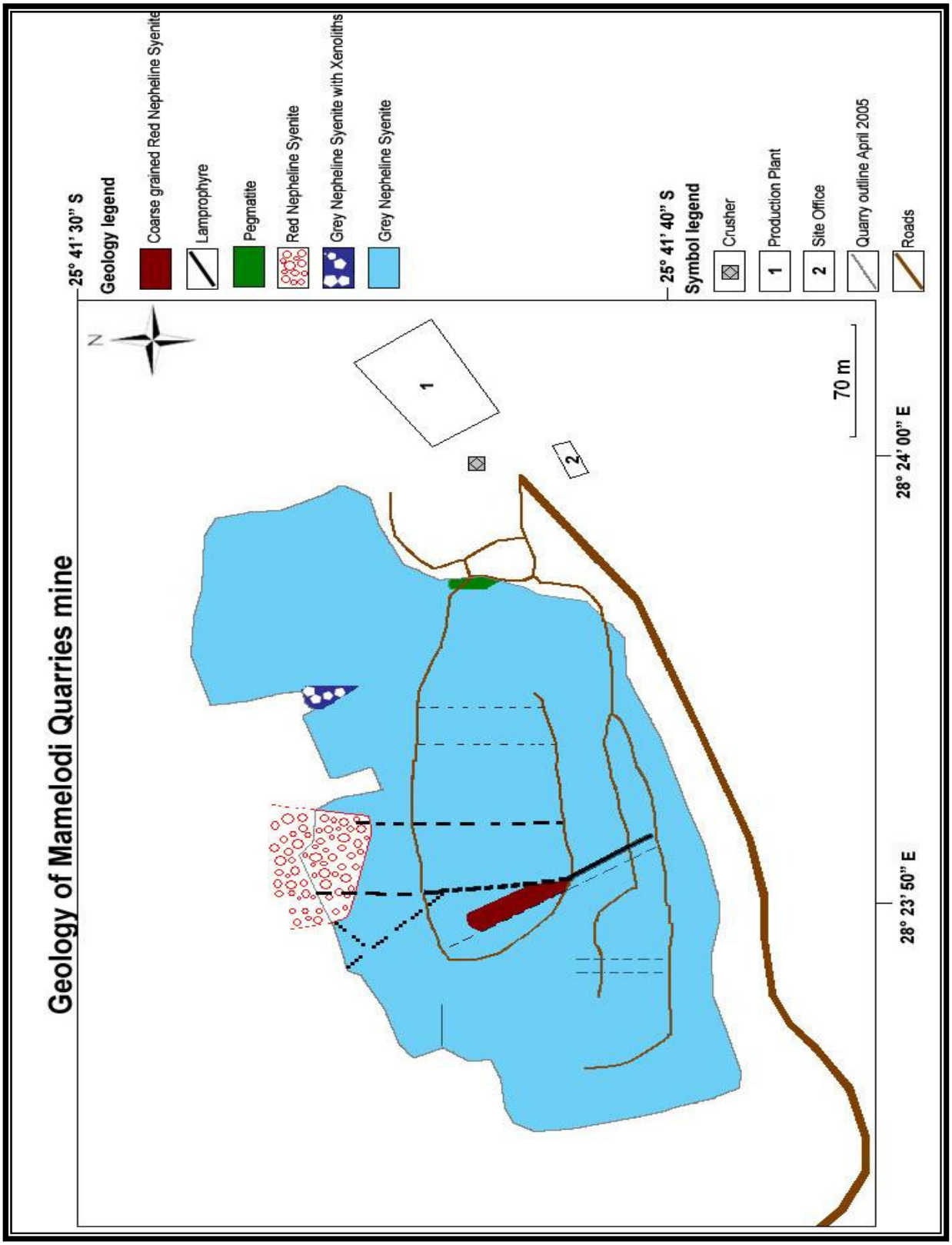

Figure 8. Geology as exposed at Mamelodi Quarries on Franspoort Farm (independently mapped by the author).

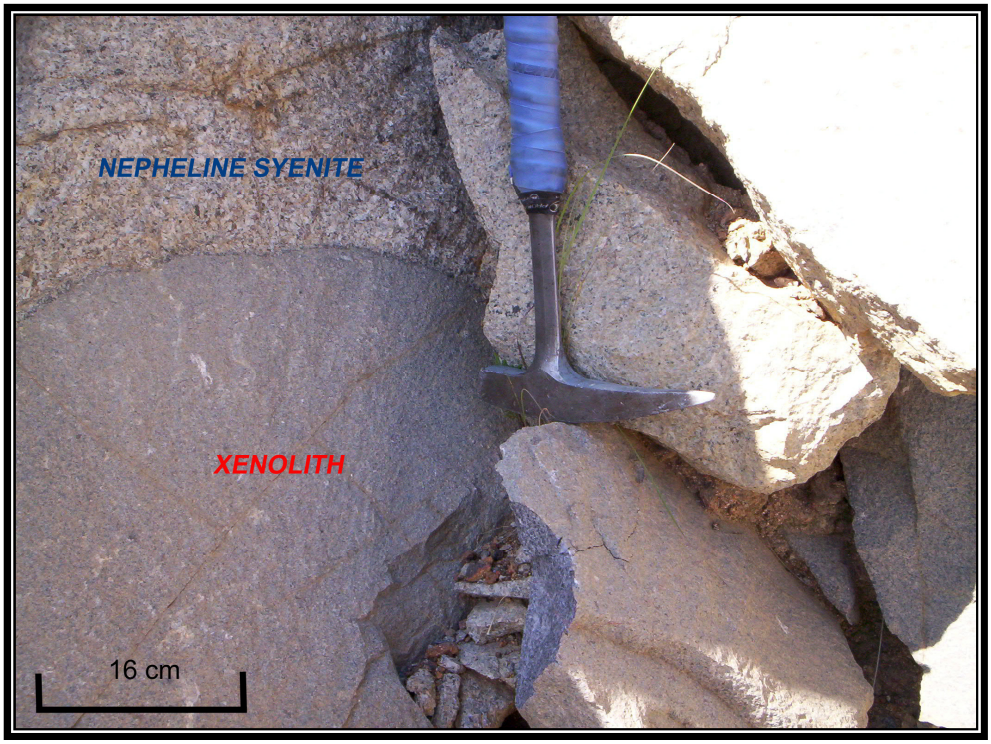

Figure 9. A photo of the grey nepheline syenite with xenolith inclusions. Hammer for scale.

3 MINERAL PROPERTIES AND EXPECTED BEHAVIOUR IN SEPARATION TECHNIQUES

Minerals have different physical and chemical properties that will influence the behaviour of the mineral in a specific separation process. The properties can be used to select a separation technique to concentrate or remove a specific mineral.

Magnetic separation was investigated for the removal of the minerals containing iron. "All materials are affected in some way when placed in a magnetic field, although with most substances the effect is too slight to be detected" (Wills 2006). Taking this onto account, minerals can be divided into two groups: diamagnetic minerals (the minerals, which are repelled away from the magnetic force to an area of low magnetic intensity, e.g., quartz) and paramagnetic minerals (the minerals, which are attracted to an area of large magnetic intensity, e.g., magnetite). High intensity magnetic separators can concentrate the paramagnetic minerals (e.g., rutile, pyrrhotite, and chromite) (Wills 2006).

Ferromagnetism is a special case of paramagnetism and applies to minerals that can be concentrated with low intensity magnetic separators (i.e. magnetite, hematite, and siderite) (Wills 2006). Therefore, minerals that contain iron in different concentrations with silica might be weakly magnetic. The magnetic properties of the mineral assemblage for the ROM sample are classified as: Non-magnetic minerals (diamagnetic minerals, i.e. nepheline), weakly magnetic minerals (silicate minerals containing iron, e.g. aegirine) and magnetic minerals (ferromagnetic minerals, i.e. magnetite). Low and high intensity magnetic separation were also investigated and the methods are described in detail in Chapter 4.

Minerals respond differently under the influence of gravity and separate due to the difference in specific gravity (density). Particle size has an important influence on density separation techniques that involves fluids (e.g. water), as larger particles will be affected much more than smaller particles (Wills 2006). The particles must therefore be sufficiently coarse to be affected by Newton's law, as surface friction forces will affect smaller particles (Wills 2006).

Table 7 provides data for the different minerals, their ideal chemical formulae, their expected magnetic behaviour, and densities.

Table 7. The different minerals in the ROM sample with ideal chemical formulae, expected magnetic behaviour, and density properties.

Mineral name	**Ideal chemical formula***	**Expected magnetic behaviour****	**Density (g/cm^3)***
Microcline	$KAlSi_3O_8$	Non-magnetic	2.56
Albite	$NaAlSi_3O_8$	Non-magnetic	2.62
Analcime	$NaAlSi_2O_6 \cdot (H_2O)$	Non-magnetic	2.30
Nepheline	$(Na,K)AlSiO_4$	Non-magnetic	2.59
Aegirine	$NaFe^{3+}Si_2O_6$	Weakly magnetic	3.57
Aegirine – augite	$(Na,Ca)(Fe^{3+},Fe^{2+},Mg)Si_2O_6$	Weakly magnetic	3.50
Sodalite	$Na_8Al_6Si_6O_{24}Cl_2$	Non-magnetic	2.29
Muscovite	$KAl_2(Si_3Al)O_{10}(OH,F)_2$	Non-magnetic	2.82
Fluorite	CaF_2	Non-magnetic	3.13
Chabazite	$(Ca_{0.5},Na,K)_4[Al_4Si_8O_{24}] \cdot 12H_2O$	Non-magnetic	2.09
Enstatite	$Mg_2Si_2O_6$	Non-magnetic	3.20
Actinolite	$Ca_2(Mg,Fe^{2+})_5Si_8O_{22}(OH)_2$	Weakly magnetic	3.04
Ilmenite	$Fe^{2+}TiO_3$	Magnetic	4.72
Magnetite	$Fe^{2+}Fe^{3+}{}_2O_4$	Magnetic	5.15
Pyrite	FeS_2	Magnetic	5.01
Zircon	$ZrSiO_4$	Non-magnetic	4.56

** Data from Deer et al. 1997, ** Observations from this study*

4 EXPERIMENTAL PROCEDURES FOR MINERAL SEPARATION

4.1 Introduction

The following separation tests were undertaken:

1. Milling tests at the University of Pretoria and Mamelodi Quarries
2. Screening
3. High-intensity wet magnetic separation at Mamelodi Quarries
4. Low-intensity dry magnetic separation at Outokumpu laboratory in Boksburg
5. Concentration of heavy minerals by means of heavy liquid gravity separation at the University of Pretoria
6. Spiral gravity separation at the University of Pretoria

The aim of the different separation tests is to produce a final concentrate that contains the lowest possible iron concentration for possible application in the glass and ceramic industry (nepheline product). The final concentrate for was:

- Magnetic separation tests = non-magnetic fraction of the final pass (see section 4.4 and 4.5 for details on the tests).
- Heavy liquid separation = the float fraction containing the low density minerals (see section 4.6 for details on the tests)
- Spiral separation = the light fraction (see section 4.7 for details on the tests)

4.2 Milling

Different milling and crushing tests were performed on the FNS (Franspoort nepheline Syenite) to determine the effect on the grain size distribution. A representative blast rock sample was collected from the primary jaw crusher at Mamelodi Quarries. This sample was crushed with a laboratory crusher at University of Pretoria, to produce smaller rock fragments. A swing mill with a carbon steel mill pot was used.

The sample was milled to particle sizes smaller that one millimetre. This material was used in a screening test to determine the particle size distribution.

At Mamelodi Quarries, a representative sample (two kilograms) was collected from a secondary crusher and milled in a ball mill (filled with alubit balls) for 5 hours. The particle size distribution was determined by a screening test.

4.3 Screening

Screening was used to determine the effect of the different milling tests on the grain size distributions. The grain size is important for the different separation methods investigated, because if the grain size is too large, the separation method could be ineffective. None of this material was used for chemical analyses.

The first tests were carried out at the University of Pretoria using a vibrating screen (Figure 10). A ro-tap screen shaker was used for the test at Mamelodi Quarries (Figure 11).

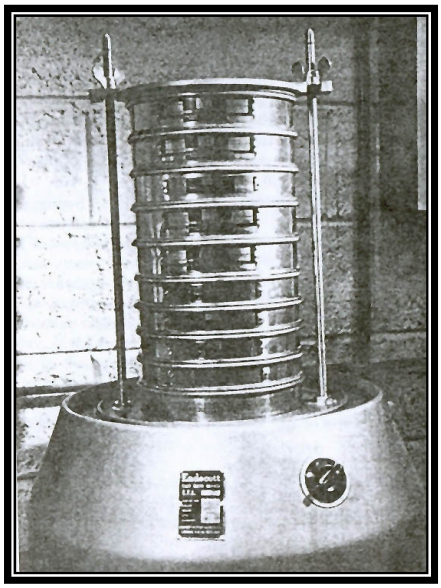

Figure 10. A photo of a vibrating screen shaker (from Wills 2006).

Due to the size of the mill pot at the University of Pretoria, a 1 kg sample of ROM was divided into ± 50 g fractions and these were milled for two minutes in a carbon steel milling pot. Table 8 represents the different screen sizes used for the test.

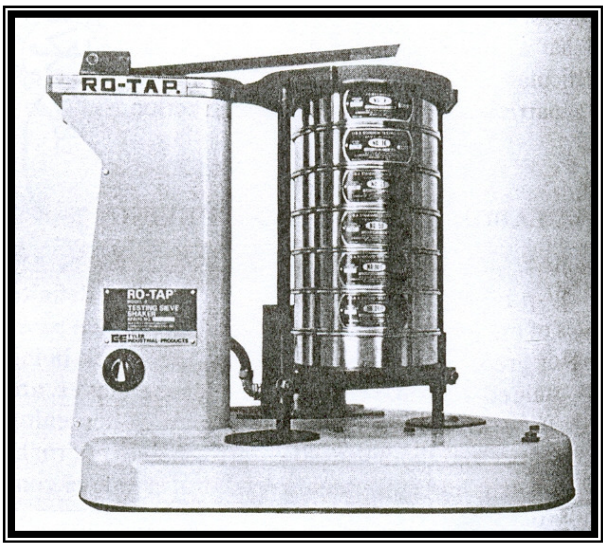

Figure 11. A photo of a ro-tap screen shaker (from Kelly and Spottiswood 1982).

Table 8. Screen sizes for the first screen test.

355 µm	125 µm
250 µm	75 µm
180 µm	53 µm
150 µm	25 µm

A 200 g sample of the grey nepheline syenite, with small rock fragments, was dry screened for 1 hour. Wet screening was applied after the dry screening step for the 75 to 25 µm size range. The second test was carried out at Mamelodi Quarries using the ROM crusher sand. Table 9 presents the different screen sizes used for the second test.

For this test 100 g of ROM was used and dry screened for 1 hour. After 1 hour the ROM material was separated into the different screen fractions. The results of both tests are described in Chapter 6.

Table 9. Screen sizes for second screen test.

425 µm	150 µm
300 µm	75 µm
212 µm	53 µm
180 µm	

4.4 High-intensity wet magnetic separation

High-intensity wet magnetic separation tests were performed on the ROM milled material. An Afmag PA 25 laboratory magnetic separator with a capacity of 230 000 Gauss was used. Based on previous experience, Carlos Martins (personal communication, geologist MQ) suggested that 160 000 Gauss can be used to achieve maximum separation after the fourth pass. The samples were mixed with water to give 25 % solid in water, i.e., ~ 250 g of the sample was mixed with 1 L of water and passed through the magnet (Figure 12). Before the separation process commenced, the magnet was cleaned with water. The 250 g sample was passed through the magnet four times and was split into magnetic and a non-magnetic fractions. The solid / water mixture was added to fill the feed hopper while closing the outlet with the magnet switched on.

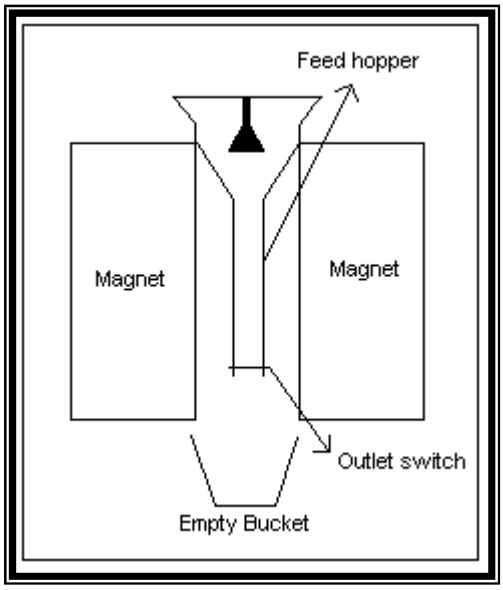

Figure 12. Cross-section of the magnetic separator.

After the feed hopper was filled, the outlet was opened and the non-magnetic material flowed out into a bucket. The magnet was switched off and cleaned with water. The non-magnetic material of the first pass was then again passed through the magnet in the same procedure as described above. The same step was applied for the non-magnetic fractions from passes two and three. Figure 13 shows a flow diagram for magnetic separation. The results are discussed in Chapter 6.

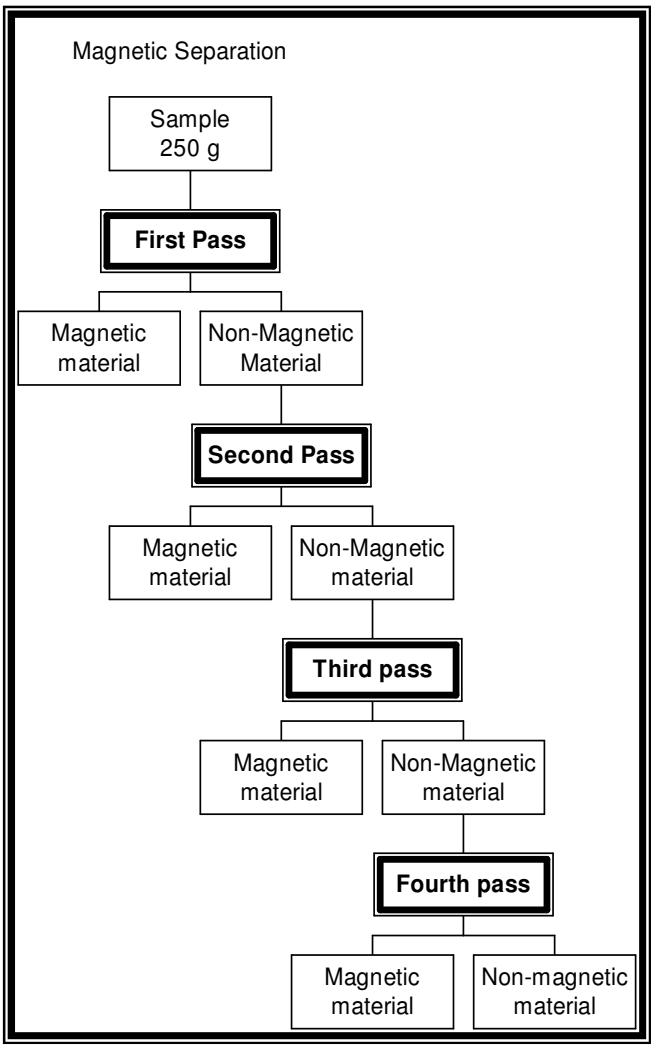

Figure 13. A flow diagram showing the different steps for the wet magnetic separation.

4.5 Low-intensity dry magnetic separation

The low-intensity dry magnetic separation test was preformed on the ROM material to ascertain whether more magnetic material could be recovered as compared to the wet magnetic separation technique. The aim was to concentrate the non-magnetic nepheline and alkali feldspar. The separation test took place at Outokumpu laboratory facilities in Boksburg. A modal 1994 international high force roller magnetic separator was used for the test.

Two different tests were carried out: the ROM sample was passed through the separator six times in the first test, and five times in the second. Figure 14 is an illustration of the test setup.

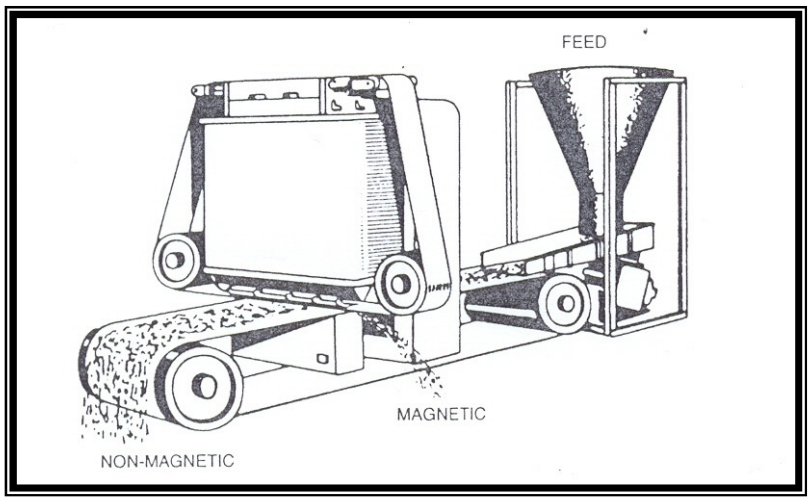

Figure 14. Example of roller magnetic separator (from Wills 2006).

A 1 kg sample was used and the sample was placed in a feeding chamber, which fed the material on a conveyor belt system to the magnet. A splitter at the one end of the magnet allowed different order settings to control the effect of the magnet for a larger feeding area. An ioniser was used to control the smaller dust particles. The different settings for test one and two are summarised in Tables 10 and 11.

After each step the non-magnetic portion was used as the feed for the next step. The final non-magnetic portion contained the highest concentration of nepheline and

alkali feldspars and hence the lowest iron content. The results are discussed in Chapter 6.

Table 10. Information from the dry magnetic separation test 1.

Product	Weight (g)	Mass %	Time (s)	RPM	Comments*
Feed	1106.00		27.28	350	4:4 Roll 0.65 Belt & No Ioniser
Mag 1	33.90	3.07			
Non Mag1	1072.00	96.93			
Feed	1072.00		27.00	240	6;2 & 0.25 & Ioniser
Mag 2	162.90	15.20			
Non Mag 2	899.30	83.89			
Lost	9.80	0.91			
Feed	899.30		27.00	200	4:1,3 & 0.13 & Ioniser
Mag 3	205.70	22.87			
Non Mag 3	685.70	76.25			
Lost	7.90	0.88			
Feed	685.70		27.00	150	4:1,3 & 0.13 & Ioniser
Mag 4	232.60	33.92			
Non Mag 4	450.10	65.64			
Lost	3.00	0.44			
Feed	450.10		27.00	120	4:1,3 & 0.13 & Ioniser
Mag 5	124.10	27.57			
Non Mag 5	324.80	72.16			
Lost	1.20	0.27			
Feed	324.80		27.00	100	4:1,3 & 0.13 & Ioniser
Mag 6	80.00	24.63			
Non Mag 6	244.40	75.25			
Lost	0.40	0.12			

**The first number is the size of the magnetic roller. The second number is the thickness of the rubber belt placed on the roller. The ioniser is a length of wire used to remove dust particles at the front of the roller.*

Table 11. Information from the dry magnetic separation test 2.

Product	Weight (g)	Mass %	Time (s)	RPM	Comments*
Feed	1115.00		27.00	200	4:4 Roll 0.65 Belt & No Ioniser
Mag 1	48.00	4.30			
Non Mag 1	1067.00	95.70			
Lost	0.00	0.00			
Feed	1067.00		27.00	190	6;2 & 0.25 & Ioniser
Mag 2	274.00	25.68			
Non Mag 2	793.00	74.32			
Lost	0.00	0.00			
Feed	793.00		27.00	150	4:1,3 & 0.13 & Ioniser
Mag 3	182.30	22.99			
Non Mag 3	600.10	75.67			
Lost	10.60	1.34			
Feed	600.10		27.00	120	4:1,3 & 0.13 & Ioniser
Mag4	159.10	26.51			
Non Mag 4	439.60	73.25			
Lost	1.40	0.23			
Feed	439.60		27.00	100	4:1,3 & 0.13 & Ioniser
Mag 5	118.30	26.91			
Non Mag 5	320.40	72.88			
Lost	0.90	0.20			

**The first number is the size of the magnetic roller. The second number is the thickness of the rubber belt placed on the roller. The ioniser is a length of wire used to remove dust particles at the in front of the roller.*

4.6 Gravity separation using heavy liquid

The ROM sample was screened with a size of ± 0.297 mm and washed to ensure that all dust particles were removed. The washed sand was dried.

Heavy liquid separation was applied to investigate the possibility of concentrating REE-containing minerals and zircon. The density of the liquid (tetrabromoethane) used was 2.96 g/cm^3. The light fraction of this separation should concentrate the nepheline and feldspars as their densities are smaller than 2.6 g/cm^3.

The schematic setup for the separation process is shown in Figure 15. A funnel with a rubber tube attached to the end (with a pinch clip in the closed position) was filled up with heavy liquid and the sample material added afterwards and stirred.

Tetrabromoethane was used for the separation. The detailed characteristics of tetrabromoethane are summarised in Table 12. Tetrabromoethane liquid is highly flammable and very toxic and care had to be taken not to inhale the fumes. In order to avoid this the experiment took place in a fume cabinet. A sample with weight between 20 g to 50g was used and added to 200 ml to 400 ml of tetrabromoethane. The sample was weighed and then added to the heavy liquid in the funnel whilst stirring. It was important to ensure that all the particles were coated with the liquid and to ensure that surface tension did not cause heavy particles to stay suspended (Allman and Lawrence 1972).

By using Stokes law it was possible to estimate the velocity of the different mineral particles and to calculate the time the particles need to settle to the bottom of the separation liquid or float to the top (Table 13). The reason for calculating the time for the different minerals was to obtain the best time for maximum separation of light from the dense minerals.

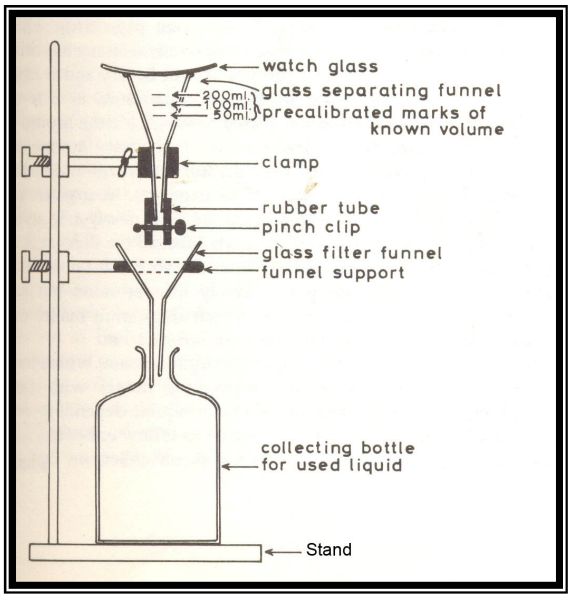

Figure 15. Equipment setup for the heavy liquid separation (from Allman and Lawrence 1972).

Table 12. Different properties of the heavy liquid tetrabromoethane (Hawley 1987).

Molecular weight:	345.65 g/mole
Chemical formula:	$C_2H_2Br_4$
Appearance:	Yellow to brown liquid
Odour:	Camphor and Iodoform
Solubility:	Insoluble in water and n-octanol, Soluble in methanol, diethyl-ether and acetone
Specific gravity:	2.967 @ 20℃
Boiling point:	240 ℃
Melting point:	0℃
Vapour density (air =1):	11.9
Vapour pressure (mm Hg):	<0.1mm of Hg @ 20℃

The equation for Stokes law is (Allman and Lawrence 1972):

$$V = \frac{2gr^2(d1 - d2)}{9\eta}$$

Where,

V = velocity of fall (cm sec^{-1}),

g = acceleration of gravity (cm sec^{-2}),

r = radius of particle (cm),

d1 = density of particle (g cm^{-3}),
d2 = density of medium (g cm^{-3}) and
ŋ = viscosity of liquid in poises (dyne sec cm^{-2}).

To calculate the time it will take for a particle of a specific mineral to settle, the following equation was used (Allman and Lawrence 1972):

$$t = D/V$$

Where,
t = time (min),
D = distance particle will travel (cm),
V = velocity of fall (cm sec^{-1}).

The negative values (V and t) calculated for specific minerals (Table 13) are an indication that these minerals will not settle, but float.

Different amounts of sample were mixed with different volumes of liquid and the ratio of heavy minerals to light minerals was calculated (Table 14). The reproducibility of the test results were evaluated by the variation of the sample weight.

The funnel opening was covered and the mixture was then left for a minimum of 30 minutes to allow the heavy particles to sink to the bottom of the funnel and the lighter particles to float to the surface. After 30 minutes, the mixture was again stirred and left for another 45 minutes to ensure that any agglomeration of particles was countered-acted to ensure maximum settling of the heavy minerals.

The pinch clip was opened to allow all the heavy minerals and liquid to pass through the filtration paper, before closing the pinch clip so that the lighter material did not fall into the funnel.

Table 13. Stokes law and estimated times for the settling of mineral particles in tetrabromoethane. (Note that the calculation was for settling and a negative number indicates the particle will float).

g = 980.62 (cm sec^{-1})	D =20 cm
r = 0.00002 (cm)	V =specific for each mineral
d2 = 2.947(g cm^{-3})	
ŋ = 0.09(dyne sec cm^{-2})	

Mineral	d1 (g cm^{-3})	d2 (g cm^{-3})	g (cm sec^{-1})	r (cm)	ŋ (dyne sec cm^{-2})	V (cm sec^{-1})	t (min)
Sodalite	2.29	2.947	980.62	0.00002	0.09	-0.02674	-12.47
Analcime	2.30	2.947	980.62	0.00002	0.09	-0.02633	-12.66
Microcline	2.56	2.947	980.62	0.00002	0.09	-0.01575	-21.16
Nepheline	2.60	2.947	980.62	0.00002	0.09	-0.01412	-23.60
Albite	2.62	2.947	980.62	0.00002	0.09	-0.01331	-25.04
Muscovite	2.83	2.947	980.62	0.00002	0.09	-0.00476	-70.00
Fluorite	3.13	2.947	980.62	0.00002	0.09	0.00745	44.75
Aegirine–augite	3.50	2.947	980.62	0.00002	0.09	0.02251	14.81
Ilmenite	4.70	2.947	980.62	0.00002	0.09	0.07135	4.67
Magnetite	4.30	2.947	980.62	0.00002	0.09	0.05507	6.05

Table 14. The different amounts of sample mixed with heavy liquid and the ratio of heavy minerals to lighter minerals.

	Initial weight (g)	Heavy part (g)	Light part (g)	Total (g)	Lost (g)	Heavy (%)	Light (%)	Lost (%)	Total (%)
1	40	7.50	32.40	39.90	0.10	18.75	81.00	0.25	100
2	50	9.89	39.90	49.79	0.21	19.78	79.80	0.42	100
3	40	7.40	31.20	38.60	1.40	18.50	78.00	3.50	100
4	50	10.00	38.20	48.20	1.80	20.00	76.40	3.60	100
5	40	8.00	31.90	39.90	0.10	20.00	79.75	0.25	100
6	30	6.00	23.40	29.40	0.60	20.00	78.00	2.00	100
7	30	5.50	23.00	28.50	1.50	18.33	76.67	5.00	100
8	20	3.80	15.50	19.30	0.70	19.00	77.50	3.50	100
9	30	6.20	23.00	29.20	0.80	20.67	76.67	2.67	100
10	30	5.90	23.40	29.30	0.70	19.67	78.00	2.33	100

The liquid passed through the filter paper and the heavy minerals were left behind. The sample was washed properly with ethanol to ensure that all the tetrabromoethane was removed and left to air dry. This procedure was also applied to the lighter mineral fraction. The process was repeated until the desired amount of sample for each fraction was collected for further analysis. The results are discussed in Chapter 6.

4.7 Gravity separating with the use of a spiral

Spiral tests were performed on the ROM using facilities of the Metallurgy Department of the University of Pretoria, with the assistance of Mr. P.C. W. Havemann. A spiral for material denser than 2 g/cm^3 was used (Figure 16).

Figure 16. A photo of the spiral used for gravity separation.

According to Wills (2006), particle sizes between 3 mm and 75 µm will deliver the best separation results when using spirals. The ROM sample was screened with a 425 µm screen. Unscreened ROM (particle sizes smaller than 2 mm) and screened ROM (particle size smaller than 425 µm) spiral tests were performed to compare the effect of particle size on the separation results.

Before the tests commenced, the spiral was cleaned with water. The tank of the spiral was filled with 32 litres of water. The initial spiral test was with screened ROM, with a 25 % solid in water pulp ratio, and failed due to a blockage by the solids. A new pulp with lower solid to water was calculated using the formula in Table 15. The correct ratio for the test setup was calculated to be 15.8 % solid in water. Six kilograms of solid material was added to the 32 litres of water, and was used for both screened ROM (test 1) and unscreened ROM (test 2).

Table 15. Summary of the amount of material needed for the spiral test.

X is the amount of material needed for test
A is the solid ratio = 0.25
B is the water ratio = 0.75
32 litres of water used
X = (A/B)*32
X = (0.25/0.75)*32
X = 10.67 kg material needed

The splitters of the spiral were changed and single samples of the dense (concentrate), medium (middling) and light (tailing) material was collected. After sampling of the first test was completed, 6 litres of water was added to the previous pulp, resulting in 11.1 % solid to water pulp and samples were collected. The same procedure was followed for the unscreened ROM sample.

The pulp was pumped to the top of the spiral. The feed flowed downwards in the spiral and the particles then separated due to the combined effects of centrifugal force, the differential settling rate of the particles, and the effect of interstitial trickling through the flowing of the particle bed. Figure 17 is a cross-section of a spiral stream (Wills 2006). The ports for removal of the higher specific gravity particles are located at the lowest points in the cross-section. Figure 18 is a flow diagram for the spiral tests. The results are discussed in Chapter 6.

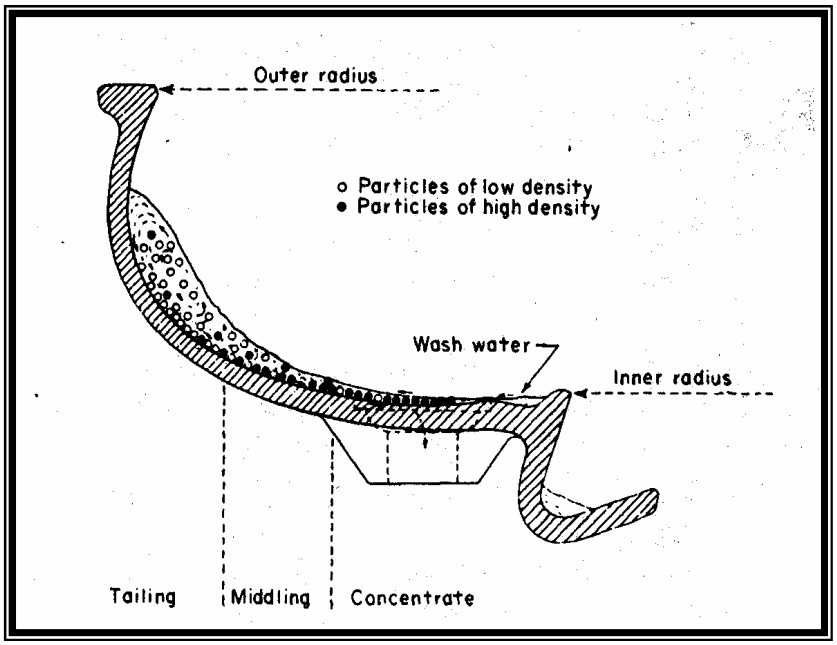

Figure 17. Cross-section of spiral streams (after Wills 2006).

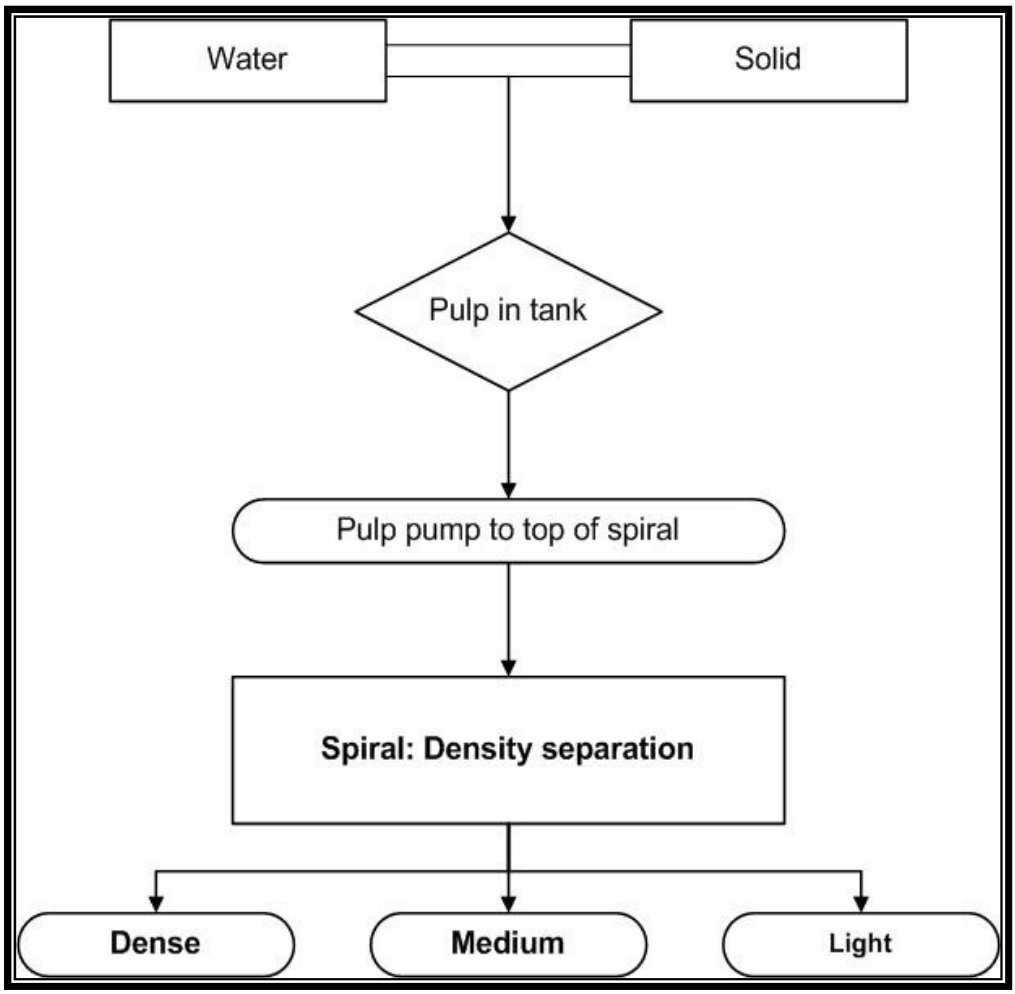

Figure 18. A flow diagram showing the different steps for the spiral separation test.

5 ANALYTICAL TECHNIQUES

For the different samples that were collected during the experimental procedures, X-ray diffraction (XRD) and X-ray fluorescence (XRF) analyses were performed to characterise these samples. It was important to prevent the samples from being contaminated with iron for the XRF major analysis and therefore the samples were milled using the following mill pots:

1. A tungsten carbide mill pot was used to mill samples to determine the major elements concentrations in XRF (to avoid contamination of the material with iron from the mill pot).
2. A carbon steel mill pot for the samples to be analysed by XRD and trace element analysis with XRF (to avoid contamination of the material with tungsten from the mill pot).

A riffle splitter was used to divide the samples into representative fractions to be used for the different analyses (Figure 19).

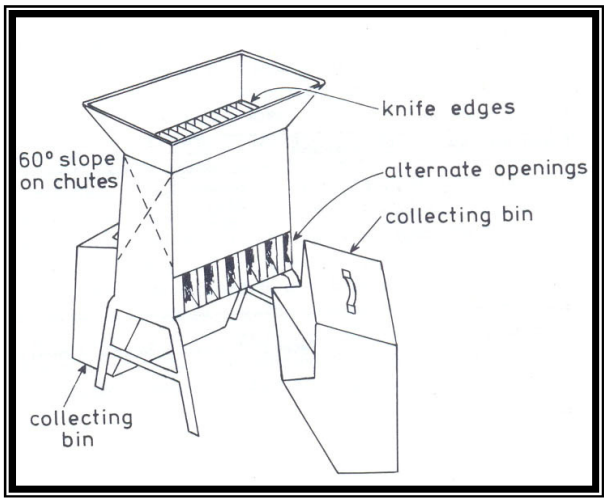

Figure 19. An example of a riffle splitter (from Allman & Lawrence 1972).

5.1 X-ray Diffraction

Selected samples were analysed by XRD at the University of Pretoria to confirm their mineral assemblages. The instrument conditions were as follows:

Instrument	:	Siemens D-501
Radiation	:	Cu Kα (λ = 1.5418 Å)
Power settings	:	40 kV, 40 mA

5.1.1 Sample preparation

For each of the milled samples approximately 10 g was milled in a micronizing mill to ensure that the particle sizes were evenly sized and smaller than 10 µm (Figure 20) Samples were prepared in a back loading sample holder (Figure 21). The sample holder was filled from the back and a cylinder was used to press the sample into place and the bottom plate was attached for analysis (Verryn 2005). For the quantitative analysis, the samples were placed into a front loading sample holder (Figure 22)

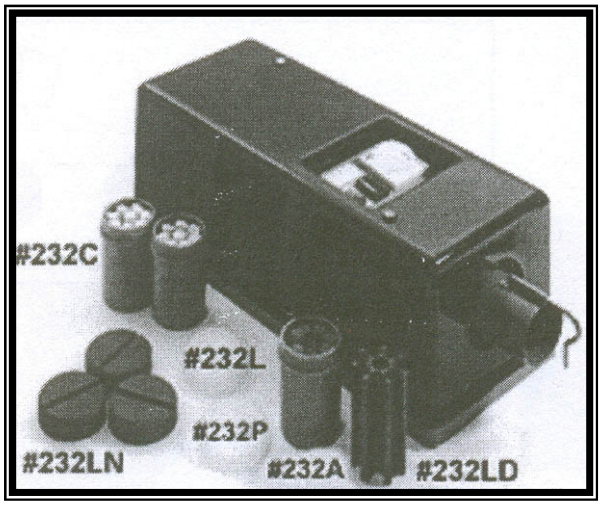

Figure 20. An annotated photo of an example of a micronising mill used in quantitative analysis sample preparation (from Verryn 2005).

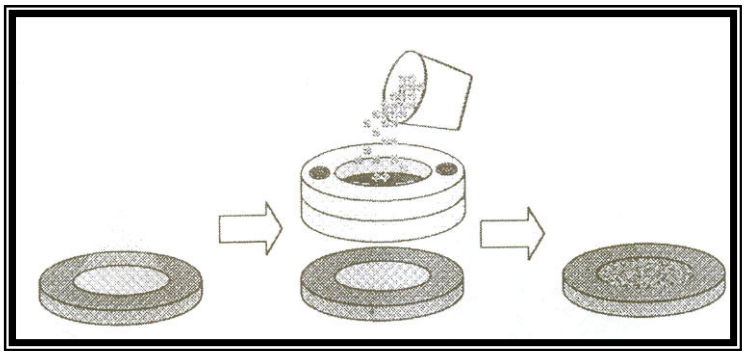

Figure 21. Diagram showing the Back loading sample holder (from Verryn 2005).

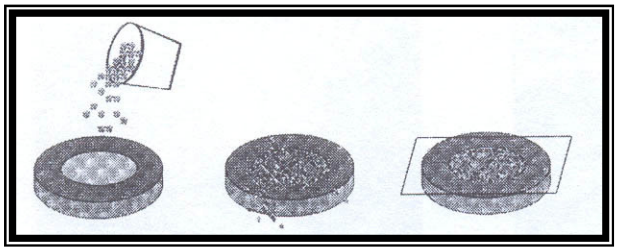

Figure 22. Diagram showing a front loading sample preparation method (from Verryn 2005).

5.1.2 Quantitative analysis using the Rietveld method

The Rietveld method is a computer based analytical process for calculating the quantities of different phases present in a mixture, by subtracting the calculated and unknown patterns from each other. By refinement of the scaling factor, and mathematical manipulation the weight percent of the phases present in the sample can be calculated (Verryn 2005).

According to Young 1993 “In the Rietveld method the least – squares refinements are carried out until the best fit is obtained between the entire observed powder diffraction pattern taken as a whole and the entire calculated pattern based on the simultaneously refined methods for the crystal structures, diffraction optics effects, instrumental factors, and other specimen characteristics as may be desired and can be modelled”.

The quantification values obtained by using this method are only as good as the quality of the calculated patterns of the unknown phases (Verryn 2005). The different

samples were analysed (ROM, xenolith, heavy liquid separation fractions), the raw data imported into Eva XRD evaluation program, and the different phases identified. The resulting diffraction pattern was imported into Topas (Brucker Rietveld software) and the quantities were calculated using the Rietveld method. For the detailed results for selected samples, see Appendix 1.

5.2 X-ray fluorescence

An ARL 9400XP+ Wavelength dispersive XRF Spectrometer with a rhodium tube was used for analysis. Major element analysis was performed on fused beads, while trace element analysis was perform from powder pellets. Tables 16 and 17 list the standard deviations, lower limits of detection (l.d) and 3σ values for ~ 250 XRF analyses of major and trace elements as determined on a geological standard reference material (GSN, granite, see Appendix 2 for certified and measured results). Detection limits were calculated from the calibration standard (information provided by Maggi Loubser 2006). The standard power setting of the X-ray tube is 30 kV, 80 mA for the elements Si, Al, Mg, Ca, Na, K, S and P and 50 kV, 50 mA for all other elements (heavy elements)

5.2.1 Pressed powders pellets for trace element measurements

For the trace element analysis, powder pellets were prepared. The pellets were prepared by mixing 10 g of powder with two drops of PVA (polyvininyl alcohol 40-88 % in saturated aqueous solution) as a binder in a plastic zip lock bag (Watson 1996). The mixture was placed in collapsible aluminium holder and pressed at 20 ton/cm^2 for two minutes using a polished piston and placed in a low temperature oven (below 100 ℃) to dry for 30 minutes.

The pressed pellet has a smooth surface in order to ensure precise and accurate results. The pellet was then analysed for trace elements (including REE) using the COLA algorithm with theoretical alphas from fundamental parameters (Lachance and Claisse 1980).

Table 16. Standard deviation, lower limits of detection (l.d) and 3 σ values for the XRF analyses of major element oxides.

	Standard deviation (wt %)	l.d (wt %)	3σ
SiO_2	0.4	0.02	1.2
TiO_2	0.03	0.0032	0.09
Al_2O_3	0.30	0.01	0.9
Fe_2O_3	0.30	0.0097	0.9
MnO	0.0065	0.0013	0.0195
MgO	0.1	0.0118	0.3
CaO	0.07	0.01	0.21
Na_2O	0.11	0.0265	0.33
K_2O	0.06	0.005	0.18
P_2O_5	0.08	0.01	0.24
Cr_2O_3	0.0053	0.0006	0.0159
NiO	0.01	0.0013	0.03
V_2O_5	0.0018	0.0008	0.0054
ZrO_2	0.005	0.0009	0.015
CuO	0.0037	0.0003	0.0111

5.2.2 Fused beads for major element measurements and the determination of loss on ignition

Preparation of samples in this study followed the standard procedure at the University of Pretoria. Representative aliquots of the samples were weighed into zirconia or porcelain crucibles and dried at 100℃ for 24 hours. The samples were removed from the furnace and left to cool in a desiccator, and then weighed and roasted at 1000℃ for 24 hours. Thereafter, the samples were removed from the furnace, left to cool in a desiccator, and weighed to determine the Loss on Ignition (LOI) and to ensure that all volatiles were removed from the sample. One gram of roasted sample was mixed with six grams of $Li_2B_4O_7$ flux (weighed to the fourth decimal place). The mixture was placed into a platinum crucible and melted at 1050℃ in a furnace for approximately 30 minutes. Following this step, the molten mixture was cast into a pre-heated casting dish and quenched in air.

The bottom side of the glass disc is analysed for major elements by XRF in order to obtain precise results (for detailed results see Appendix 2).

Table 17. Standard deviation, lower limits of detection and 3 σ values for XRF analyses of trace elements. Values for elements indicated with an * should be considered semi-quantitative.

	Standard deviation (ppm)	l.d (ppm)	3σ
As*	10	3	30
Cu	3	2	9
Ga	2	2	6
Mo	1	1	3
Nb	3	2	9
Ni	6	3	18
Pb	3	3	9
Rb	4	2	12
Sr	4	3	12
Th	2	3	6
U	2	3	6
W*	10	6	30
Y	4	3	12
Zn	4	4	12
Zr	6	10	18
Ba	14	5	42
Ce	14	6	42
Cl*	100	11	300
Co	6	3	18
Cr	40	15	120
F*	500	100	1500
La	24	5	72
S*	300	40	900
Sc	5	1	15
V	10	1	30

A problem was encountered during the roasting of the wet magnetic separation samples, especially the non-magnetic fractions thereof. The samples partially melted at 1000℃ and fused with the zirconia crucibles because the mixture of minerals caused a lowering in the eutectic melting point. The same problem was encountered when porcelain crucibles were used. It was not possible to separate the partially melted sample material from the crucibles without running the risk of sample contamination. To overcome this problem, the magnetic separation material was then roasted at a temperature of 850 ℃. This caused problems in determining the LOI. When roasting, not all the volatiles and crystal water were removed, and when fusions were prepared more of the volatiles were lost, causing low totals of the results. To overcome this problem, the material was roasted in old porcelain crucibles at 1000° C, LOI determined, and the crucibles with the material were discarded.

After the determination of the LOI, unroasted material was used for the fusion step to prevent contamination from the crucible. A correction for the loss of volatiles during the fusion process was applied by using the follow equation:

$$\text{sample} = (1x100)/(100 - \text{LOI})$$

The material from the dry magnetic, heavy liquid, and spiral separation tests were roasted in porcelain crucibles following the normal sample preparation method. For the samples that melted during roasting, unroasted material was used for fusing, with application of the correction equation.

5.2.3 Calibration of the XRF for rare earth elements measurement

The second aim of the different separation tests was to concentrate the REE and zirconium. To evaluate the success of each of the different separation tests, a cost effective method of analysis was needed. Therefore, the use of a semi-quantitative XRF method was investigated. The semi-quantitative method of calibration was chosen to evaluate the necessity of the more expensive methods to properly quantify the amount of REE in the FNS. Pressed powder samples were used for this analytical process.

The analytical software used was UniQuant®5. This software is used for samples where standards are not available (e.g., polymers). The results give the estimate correction (in wt%) with each elements estimated error (De Jong 2000). The spectrometer was calibrated using the method as described by De Jong (2000). The recommended background calculations and matrix corrections were followed.

Calibrating for REE is one of the most challenging areas in XRF, because of the multiple spectral overlaps of the different analyte K, L and M series lines (Willis 1997). The K excitation potentials for the different REE are 39 to 63 kV (Willis 1997).

Different X-ray spectrometers have different types of tubes used to generate X-rays (e.g. Rh or Au). Figure 23 presents a monazite scan comparison between Rh and Au tubes operating at 60 kV and 100 kV from Willis (1997). Better counts were obtained for the Au tube operation at 100 kV compared with the Rh tube, also operated at 100 kV.

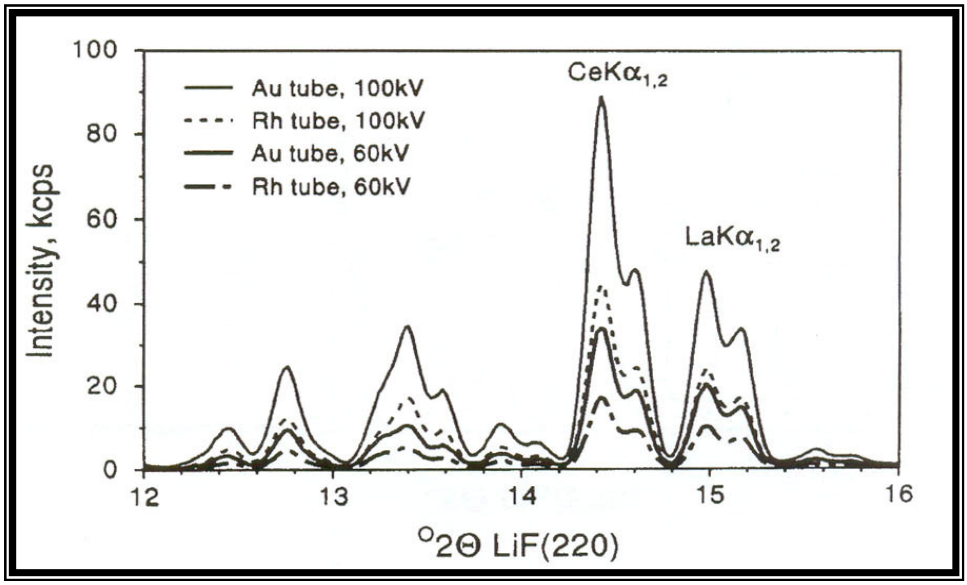

Figure 23. Wavelength scans of a monazite sample for an Rh tube and an Au tube for 60 kV and 100 kV (after Willis 1997).

In the case of an Au tube operating at 100 kV, the Au K lines will cause excitation of the REE K lines (Willis 1997). In Figure 24, a scan of a monazite sample with a Rh tube at 50 kV performed at the University of Pretoria is presented.

Spectral line overlap of the L series lines, together with absorption edges, was another problem to overcome. It was necessary to correct for the overlap from the K series lines of the transition elements like Cu, Ni, Fe, Mn, and Cr on the REE lines (Willis 1997) (Figure 25).

Because of the above-mentioned problems, the spectrometer was calibrated for REE using the L series lines, and corrected for interferences by the transition elements.

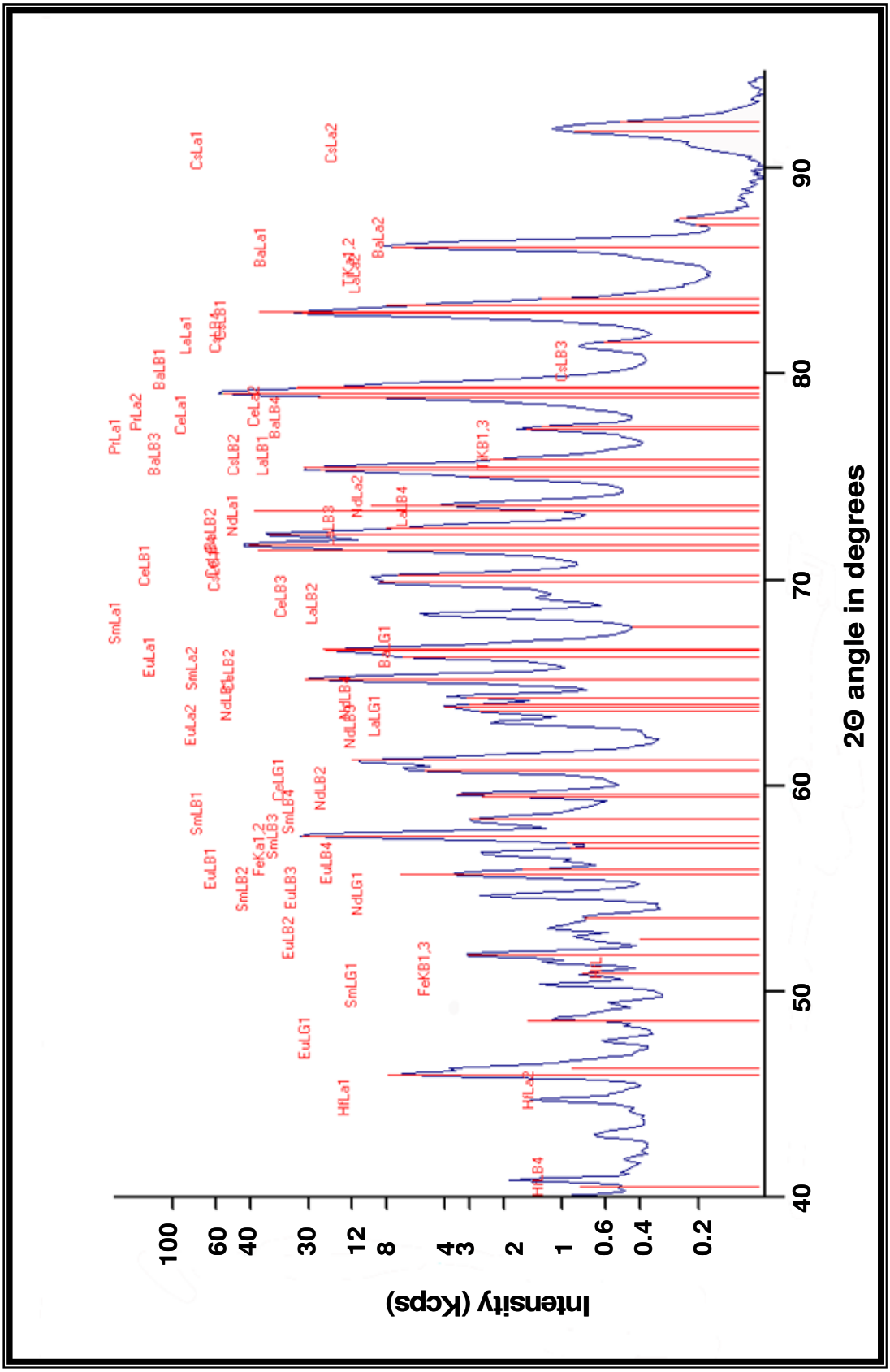

Figure 24. Wavelength scan of a monazite sample with an Rh tube at 50 KV at the University of Pretoria.

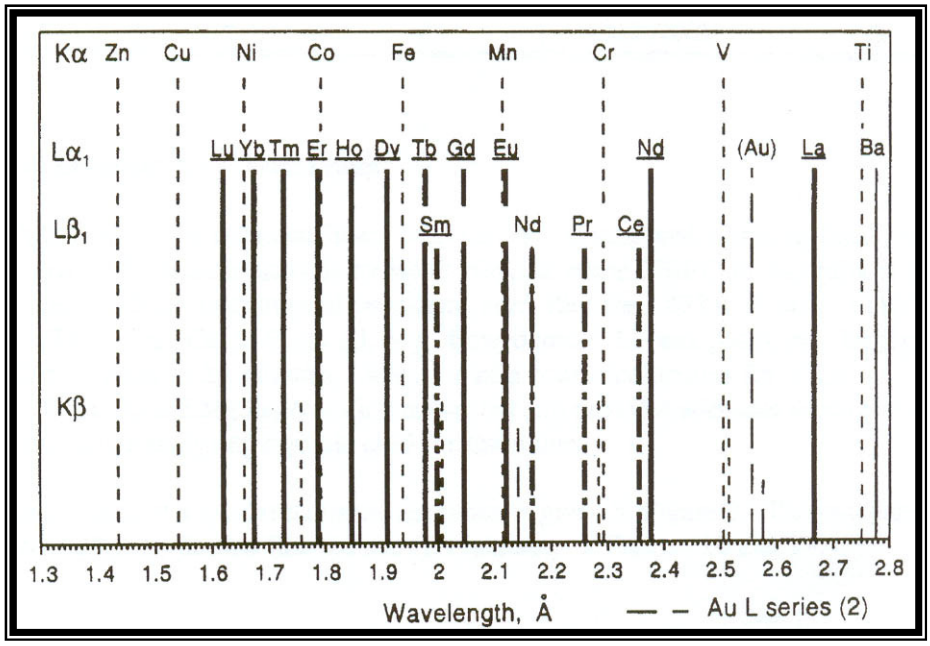

Figure 25. A wavelength plot of REE L series analyte lines with some Kα and Kβ of transition elements, which can cause spectral interference (Willis 1997).

5.2.4 Problems encountered with REE calibration methodology

It was necessary to see whether the calibration of UniQuant®5 was reliable. For this, the comparison of the certified values of standards (Std) were compared with the measured values (Msr) for the different standards. The standards used for calibration of selected oxides, with certified and measured values are shown in Table 18. The major element oxides and REE elements oxides were used to evaluate the calibration for the different standards (Figure 26 to 29). The different calibration curves for the major oxides of the data from UniQuant®5 looked promising, and the dry magnetic separation test material was selected for test analysis. The results are discussed in Chapter 6.

Table 18. Standard reference material used for calibration, with certified and measured values for selected oxides.

DC83610 (Rare earth element ore)*			
Oxide	Certified (Std) (wt%)	Measured (Msr) (wt%)	Standard error
Al_2O_3	14.69	19.19	0.18
CaO	0.03	0.02	0.00
CeO_2	0.00	0.00	0.00
Fe_2O_3	1.14	1.25	0.06
K2O	4.98	5.88	0.12
La_2O_3	0.00	0.00	0.00
Na_2O	0.16	0.18	0.01
SiO_2	74.55	73.11	0.15

DC83612 (Rare earth element ore)*			
Oxide	Certified (Std) (wt%)	Measured (Msr) (wt%)	Standard error
Al_2O_3	19.00	25.58	0.20
CaO	0.03	0.02	0.00
CeO_2	0.02	0.02	0.00
Fe_2O_3	3.46	3.68	0.10
K2O	2.11	2.61	0.08
La_2O_3	0.28	0.32	0.01
Na_2O	0.06	0.04	0.01
SiO_2	66.72	65.98	0.16

SY3 (Syenite rock)**			
Oxide	Certified (Std) (wt%)	Measured (Msr) (wt%)	Standard error
Al_2O_3	11.75	11.87	0.15
CaO	8.26	8.12	0.14
CeO_2	0.27	0.25	0.00
Fe_2O_3	6.48	6.12	0.12
K2O	4.23	4.16	0.10
La_2O_3	0.16	0.02	0.01
Na_2O	4.12	4.29	0.10
SiO_2	59.61	61.66	0.16

MSANT (Sea floor sediment)***			
Oxide	Certified (Std) (wt%)	Measured (Msr) (wt%)	Standard error
Al_2O_3	15.69	14.78	0.16
CaO	5.53	5.25	0.11
CeO_2	0.00	0.00	0.00
Fe_2O_3	8.06	7.65	0.14
K2O	1.40	1.31	0.06
La_2O_3	0.00	0.00	0.00
Na_2O	4.21	7.22	0.13
SiO_2	54.72	57.33	0.16

* Haizhou (1997), **Abbey (1981), *** Loubser 2006

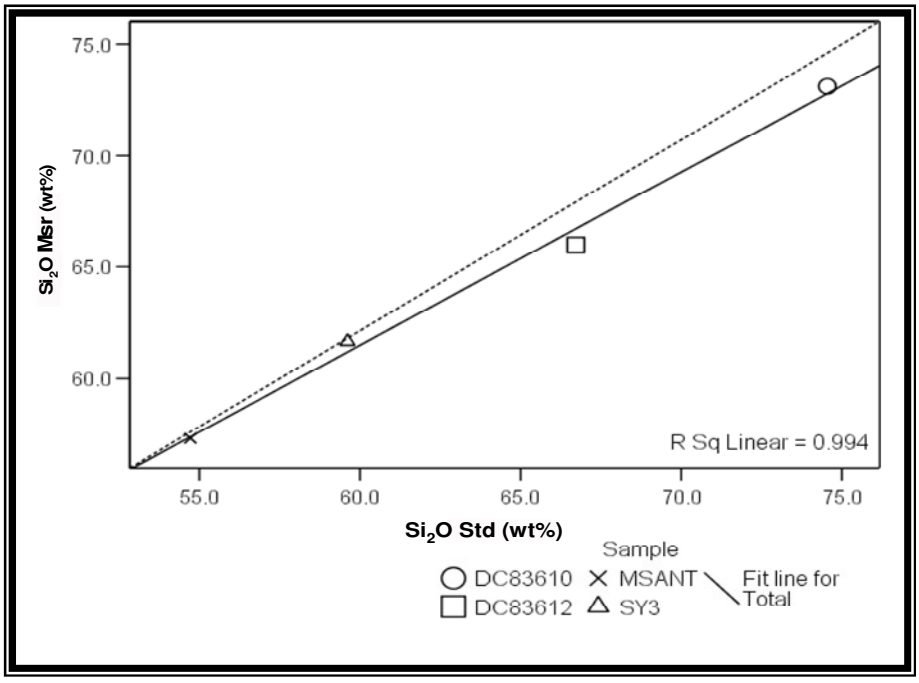

Figure 26. Comparison for UniQuant®5 calibration between measured (Msr) and certified (Std) values for SiO_2 (in wt%).

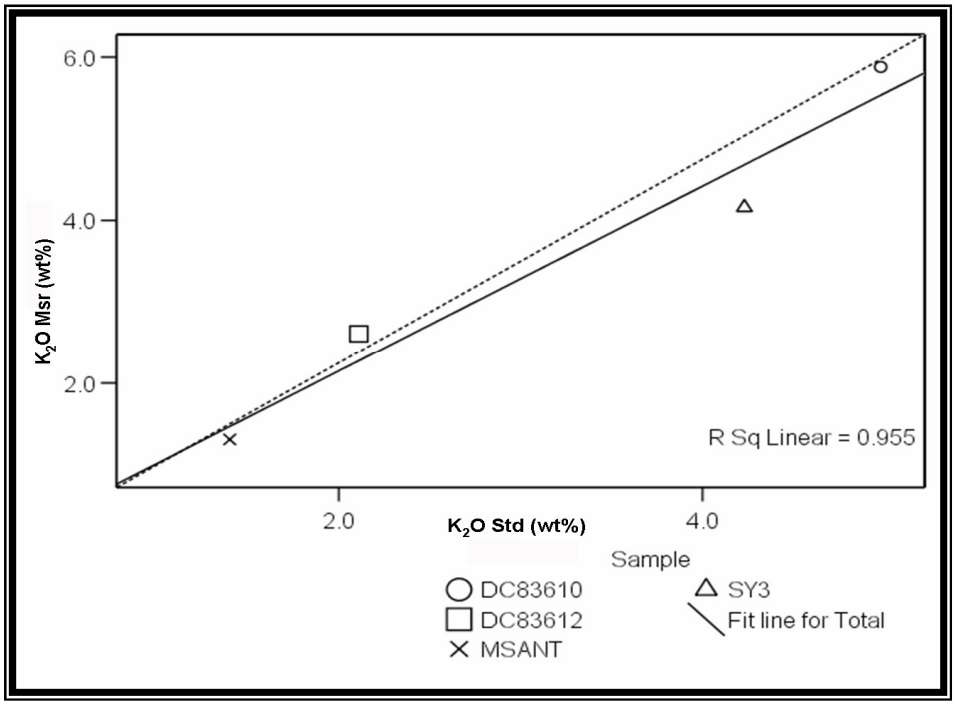

Figure 27. Comparison for UniQuant®5 calibration between measured (Msr) and certified values (Std) for K_2O (in wt%).

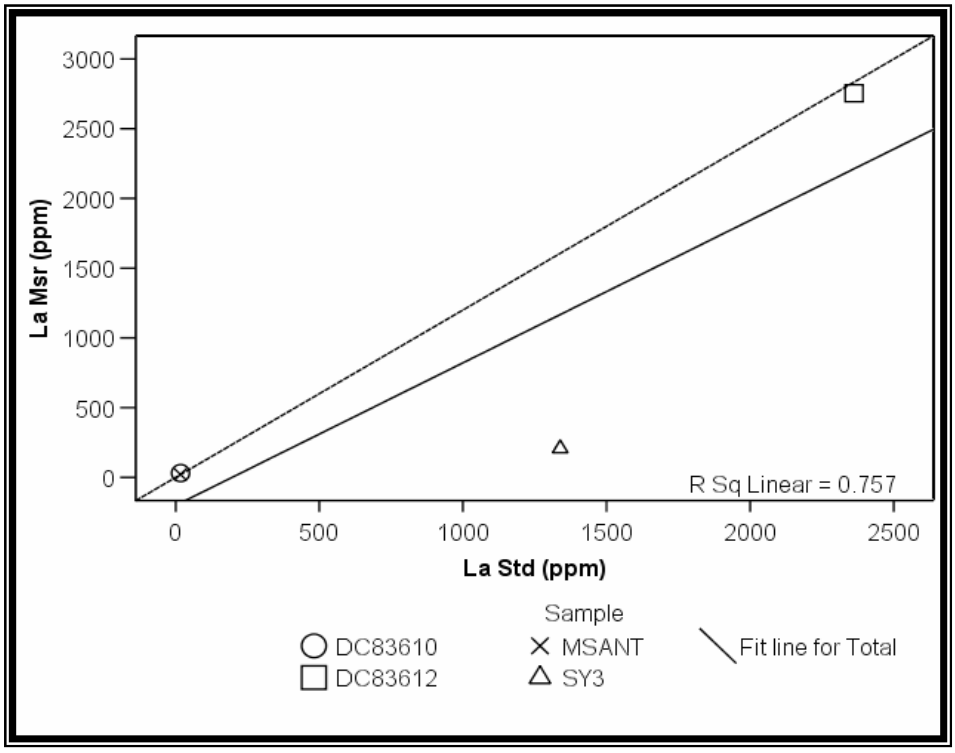

Figure 28. Comparison for UniQuant®5 calibration between measured (Msr) and certified values (Std) La (in ppm).

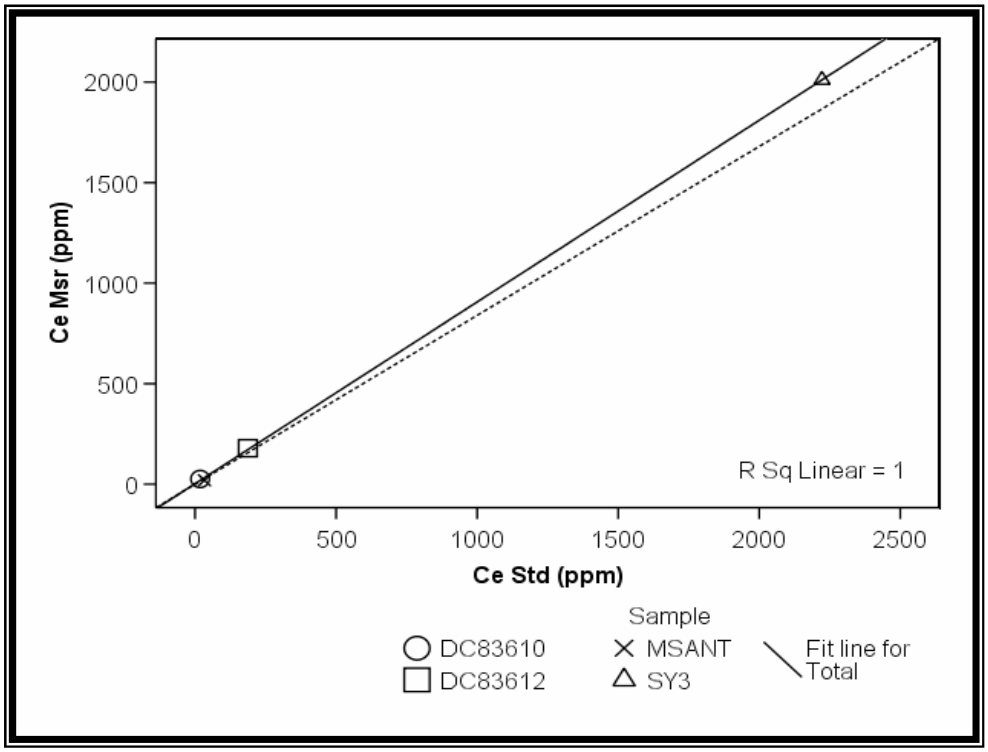

Figure 29. Comparison for UniQuant ® 5 calibration between measured (Msr) and certified values (Std) for Ce (in ppm).

5.3 Electron Microprobe Analyses

A Cameca SX50 electron microprobe was used to analyse minerals in the ROM sample, the light fraction of the screened spiral sample, and the final non-magnetic fraction of the wet magnetic separation at the Mineralogy Division of Mintek. The different elements analysed were Si, Fe, Al, Mg, Ca, Na, K and Cl. The light elements (Na, K, Cl) were analysed using wavelength dispersive spectroscopy (WDS) and the other elements with energy dispersive spectroscopy (EDS). Backscattered electron images were captured for visual confirmation of the different minerals and inclusions. The operating conditions for the microprobe are summarised in Table 19. The detailed results for the samples with mineral calculations are presented in Appendix 3.

Table 19. Standard operating conditions for the electron microprobe and standards used for calibration.

Acceleration potential	20 kV
Beam current	30 nA
Counting time	20 sec
Beam diameter	~ 1 µm
Standards	Hematite for Fe
	Jadeite for Na and Al
	Halite for Cl
	Orthoclase for K
	Periclase for Mg
	Rutile for Ti
	Wollastonite for Ca and Si

6 EXPERIMENTAL RESULTS

The results for the different separation steps are divided into the following sections:

- Petrographic results
- The results for the screening tests
- The magnetic separation results with a focus on the recovery of magnetic and non-magnetic material
- The density separation
- The geochemical results (XRD, XRF, and electron microprobe analysis).

6.1 Petrographic results

The petrographic study focused on the grey nepheline syenite, the nepheline pegmatite, and the xenolith inclusion in the grey nepheline syenite, which are exposed at the north eastern face of the Quarry and a thin section of each of these rock types were described. Tables 20 and 21 provide a summary of the minerals observed with transmitted and reflected light microscopy. X-ray diffraction analysis (Rietveld technique) was used to confirm the minerals identified in the thin sections and to quantify the proportions of the minerals (Appendix 1).

Table 20. Main minerals present in the different rocks of Mamelodi Quarries with ideal formula.

Mineral name	**Ideal chemical formula***
Microcline	$KAlSi_3O_8$
Albite	$NaAlSi_3O_8$
Analcime	$NaAlSi_2O_6{\cdot}(H_2O)$
Nepheline	$(Na,K)AlSiO_4$
Aegirine	$NaFe^{3+}Si_2O_6$
Aegirine – augite	$(Na,Ca)(Fe^{3+}, Fe^{2+},Mg)Si_2O_6$
Sodalite	$Na_8Al_6Si_6O_{24}Cl_2$
Muscovite	$KAl_2(Si_3Al)O_{10}(OH,F)_2$
Fluorite	CaF_2
Chabazite	$Ca_2[Al_4Si_8O_{24}]{\cdot}12H_2O$
Enstatite	$Mg_2Si_2O_6$
Actinolite	$Ca_2(Mg,Fe^{2+})_5Si_8O_{22}(OH)_2$
Ilmenite	$Fe^{2+}TiO_3$
Magnetite	$Fe^{2+}Fe^{3+}{}_2O_4$
Zircon	$ZrSiO_4$

** Data from Deer et. al. 1997*

6.1.1 Grey nepheline syenite

Hand specimens of the grey nepheline syenite (FNS) contain white feldspar laths (average length ~ 5 mm), with grey and red nepheline crystals (average length ~ 1 to 3 mm), and black aegirine crystals. In transmitted light, the following minerals were identified: nepheline, microcline, albite, aegirine, aegirine – augite, sodalite, fluorite, mica, chabazite, and analcime (Figure 30). Aegirine and aegirine – augite crystals are interstitial to nepheline and feldspar.

Fluorite (Figure 31) is recognized by its purple colour, isotropic nature, and perfect cleavage. The purple colouration is due to the presence of U and Th (Deer et. al. 1997). Ilmenite and magnetite are present in small quantities. The only sulphide observed is pyrite (Figure 32). The degree of alteration in the FNS is significant, as many nepheline crystals contain fibrous zeolite crystals (chabazite). The feldspar was identified as microperthite (with albite and microcline in equal amounts as detected with XRD), and is partially altered to zeolite.

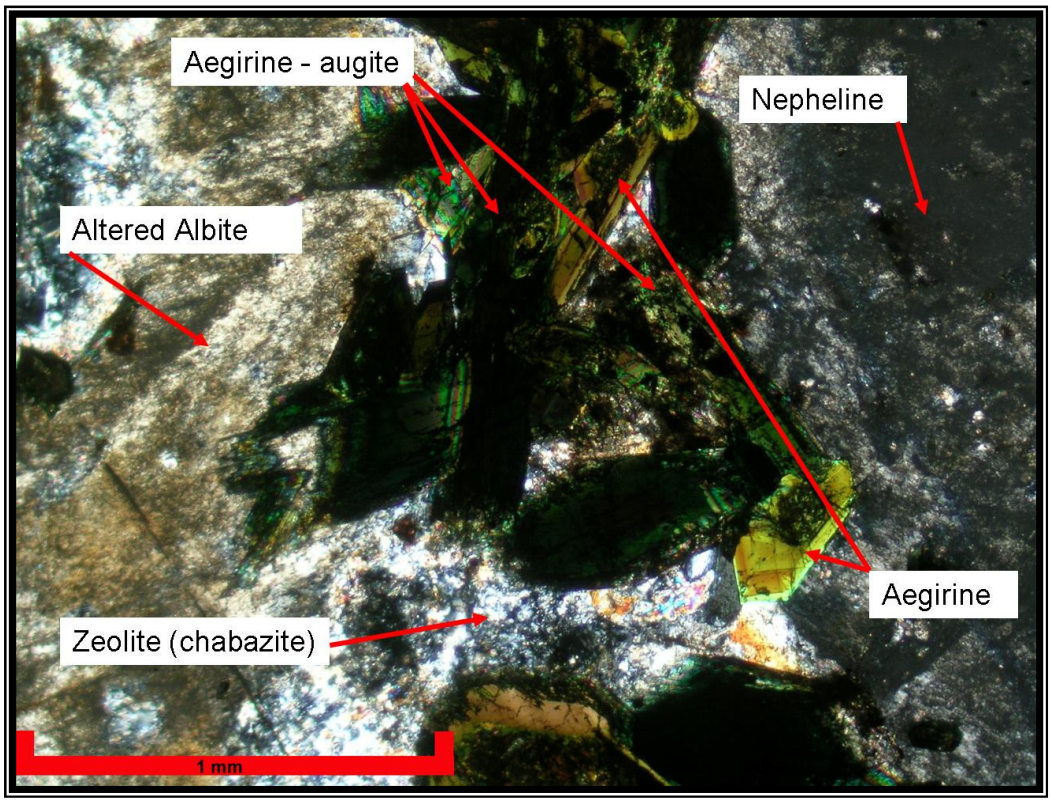

Figure 30. Photomicrograph of the grey nepheline syenite; crossed polars; width of scale bar = 1 mm.

Table 21. **Comparison of the different minerals observed using transmitted and reflected light microscopic with the X-ray diffraction quantities for 1 sample for each rock type (— *indicates mineral identified with different microscopy methods).***

Rock type:	**Grey nepheline syenite**		
Minerals identified	**Transmitted microscopy**	**Reflected microscopy**	**XRD quantities**
Microcline	—		22.73
Albite	—		22.76
Analcime	—		23.75
Nepheline	—		7.63
Aegirine – Augite, Aegirine	—		4.97
Sodalite	—		4.84
Muscovite	—		5.61
Fluorite	—		1.08
Chabazite	—		0.68
Enstatite	—		4.24
Actinolite	—		0.75
Ilmenite		—	0.43
Magnetite		—	0.35
Pyrite		—	not detected
Rock type:	**Pegmatite**		
Minerals identified	**Transmitted microscopy**	**Reflected microscopy**	**XRD quantities**
Microcline	—		29.64
Albite	—		31.52
Analcime	—		20.46
Nepheline	—		not detected
Aegirine – Augite, Aegirine	—		1.16
Sodalite	—		not detected
Muscovite	—		13.08
Fluorite	—		0.58
Chabazite			not detected
Enstatite	—		1.89
Actinolite	—		not detected
Ilmenite		—	0.84
Magnetite		—	0.82
Pyrite		—	not detected
Rock type:	**Xenolith**		
Minerals identified	**Transmitted microscopy**	**Reflected microscopy**	**XRD quantities**
Microcline	—		32.79
Albite	—		21.37
Analcime	—		19.51
Nepheline	—		5.65
Aegirine – Augite, Aegirine	—		7.31
Sodalite	—		5.99
Muscovite	—		4.04
Fluorite	—		0.92
Chabazite			1.93
Enstatite	—		0.48
Actinolite	—		not detected
Ilmenite		—	not detected
Magnetite		—	not detected
Pyrite		—	not detected

Pyroxene, feldspar, and nepheline are present as larger crystals (> 1 mm) compared to the smaller biotite and fluorite crystals. Zircon is present in small amounts as an accessory mineral. In the mining operation, the grey nepheline syenite is crushed for aggregate and building sand, is referred to as crushed ROM, and has the same mineral composition as the grey nepheline syenite rock.

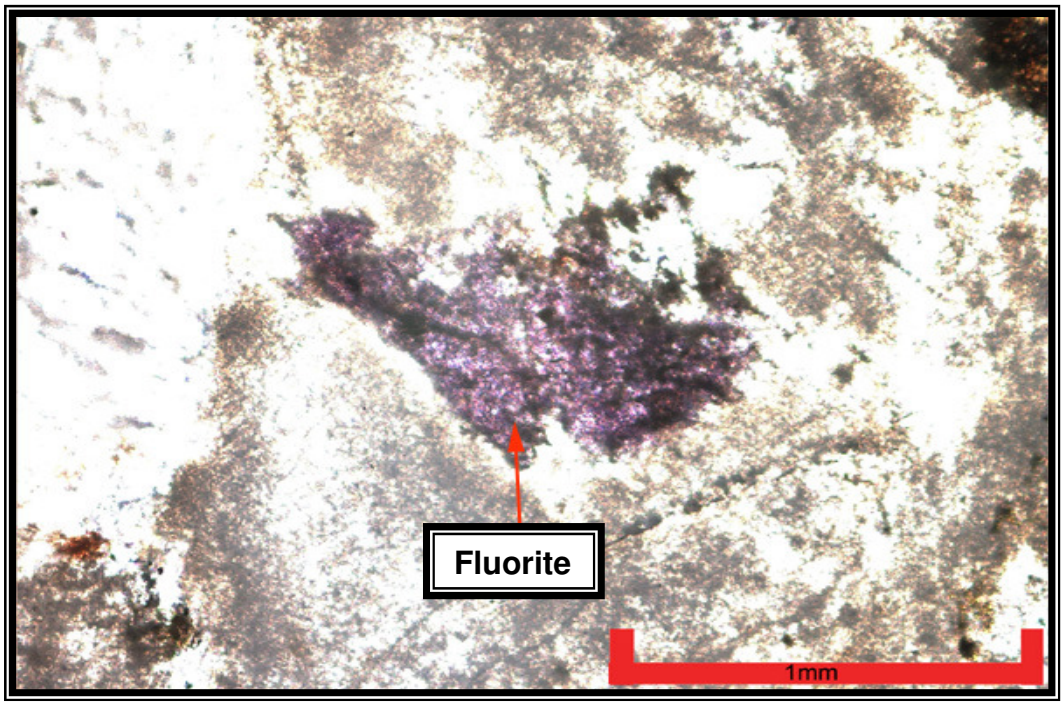

Figure 31. Photomicrograph of the fluorite; uncrossed polars; width of scale bar = 1 mm.

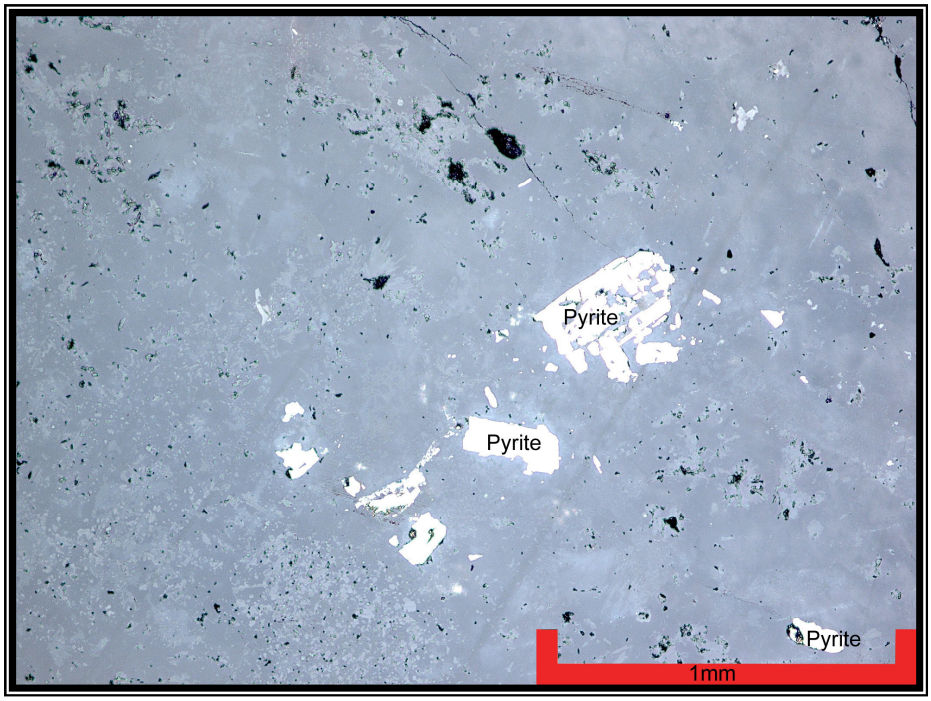

Figure 32. Photomicrograph of the grey nepheline syenite; reflected light; width of scale bar = 1 mm.

6.1.2 Pyroxenitic pegmatite

The pegmatite is darker then the nepheline syenite, and exhibits crystal sizes between 5 and 8 mm. In hand specimen, grey feldspar laths (average length greater than 5 mm) are recognisable. Referring to the XRD analysis in Table 21 shows nepheline was not detected. Albite, zeolite, and microcline are present in larger quantities than in FNS (Figure 33). Aegirine – augite and enstatite occur in lower amounts compared to FNS (see table 21 for XRD values).

The higher proportion of analcime in the pegmatite, and the absence of nepheline could be due to the alteration of nepheline to analcime and sodalite. Ilmenite and magnetite are more abundant compared to FNS.

Pyrite is the only sulphide mineral observed under reflected light (Figure 34). The concentration of pyroxene quantified with XRD is less than in the FNS (Table 21). Crystals of pyroxene (aegirine-augite and enstatite) are coarser in the pegmatite than in the FNS (average size in pegmatite 5 mm and for FNS 3 mm).

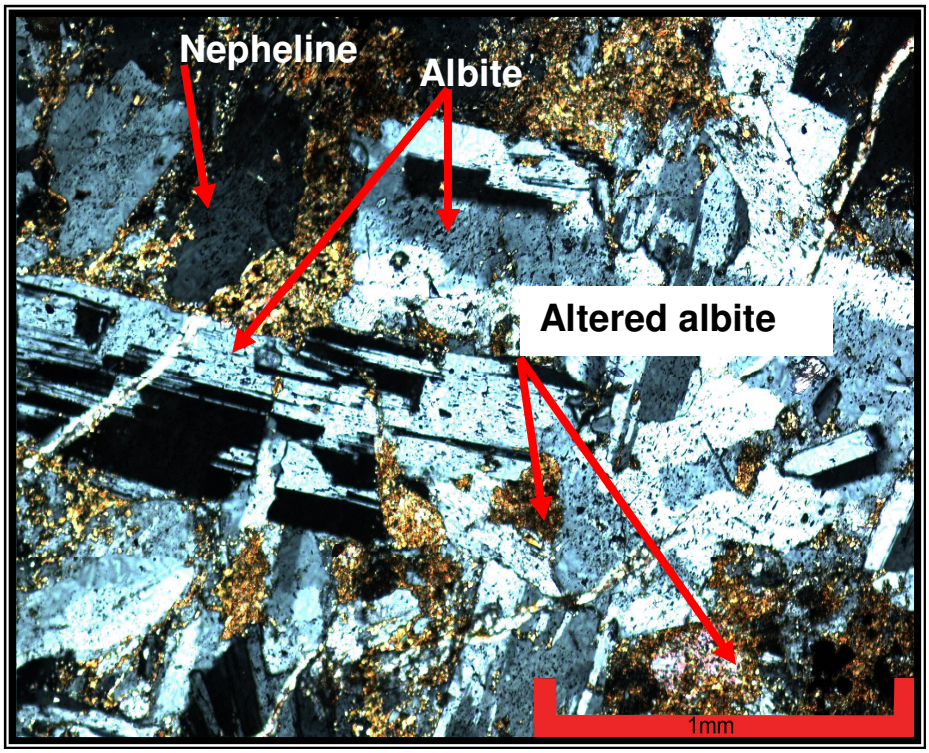

Figure 33. Photomicrograph of the pegmatite; crossed polars; width of scale bar = 1 mm.

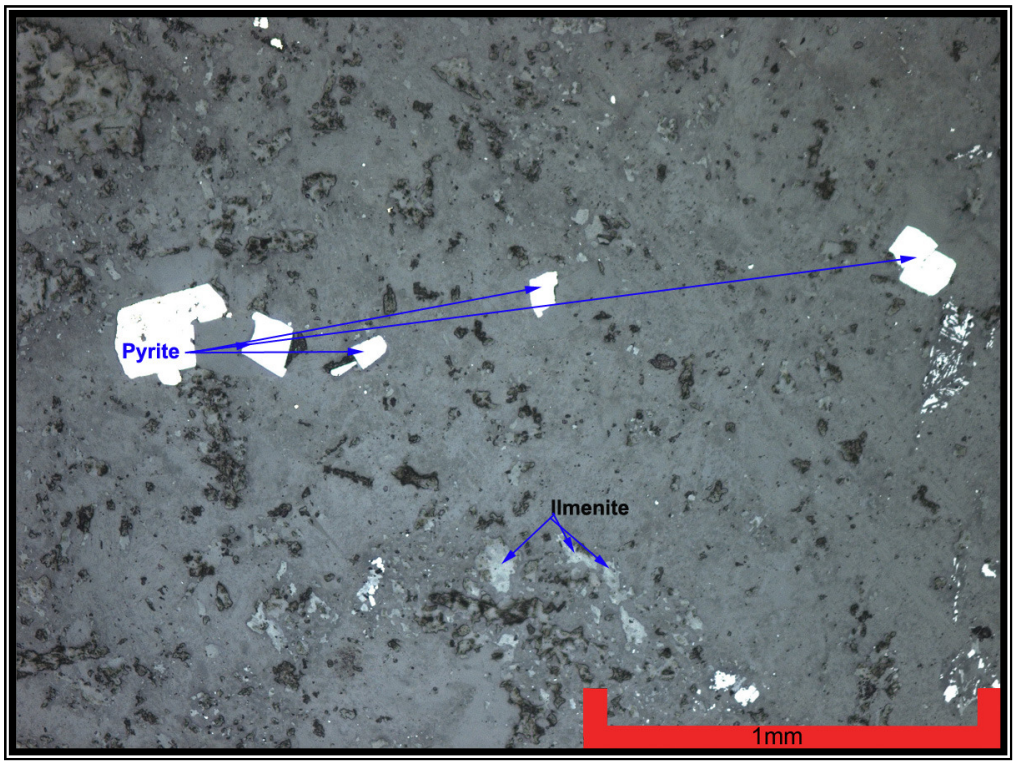

Figure 34. Photomicrograph of a section of pegmatite; reflected light; width of scale bar = 1 mm.

6.1.3 Xenolith

In hand specimen white feldspar laths (average length ~ 3 mm) with grey and red nepheline crystals (average length ~ 1 mm) and black aegirine crystals are present. The xenolith contains more microcline, aegirine – augite, sodalite, and chabazite than the FNS. Figure 35 shows a photomicrograph of the xenolith under crossed polarised light. Euhedral aegirine – augite crystals and plagioclase groundmass form the main mineral assemblage.

The crystal size of the minerals for the xenolith is smaller than the FNS (on average 1 mm in the xenolith compared to 3 mm in the FNS). The aegirine – augite crystals are more needle-like and microcline is more abundant than albite in the xenolith (see Table 21 for XRD values). The alteration products are analcime, sodalite, and chabazite. Figure 36 shows a photomicrograph of the xenolith in reflected light, showing the presence of pyrite, ilmenite, and magnetite.

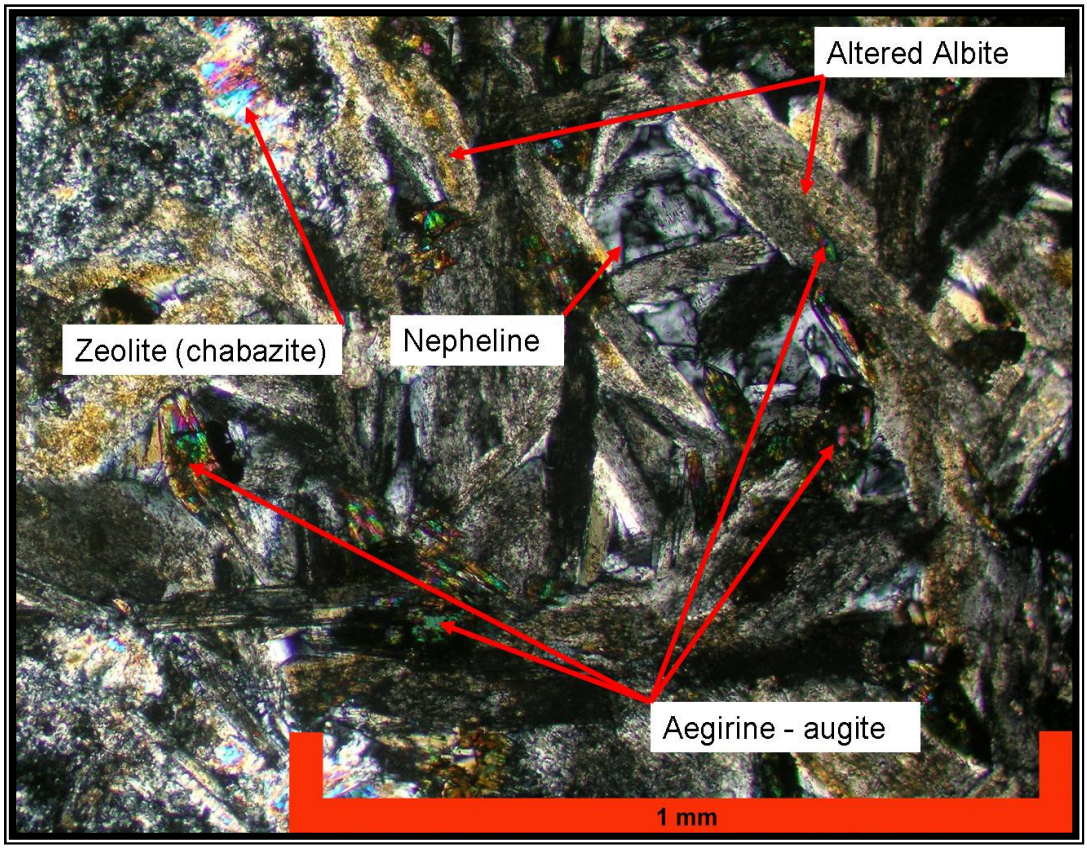

Figure 35. Photomicrograph of the xenolith; crossed polars; width of scale bar = 1 mm.

6.1.4 Crushed nepheline syenite (ROM)

The crushed ROM was used as the starting material for all the different separation methods. The mineral assemblage described for the grey nepheline syenite is also applicable to the ROM sample. Figure 37 shows a photomicrograph of the crushed ROM sample with albite, aegirine – augite, magnetite, sodalite, analcime, and chabazite.

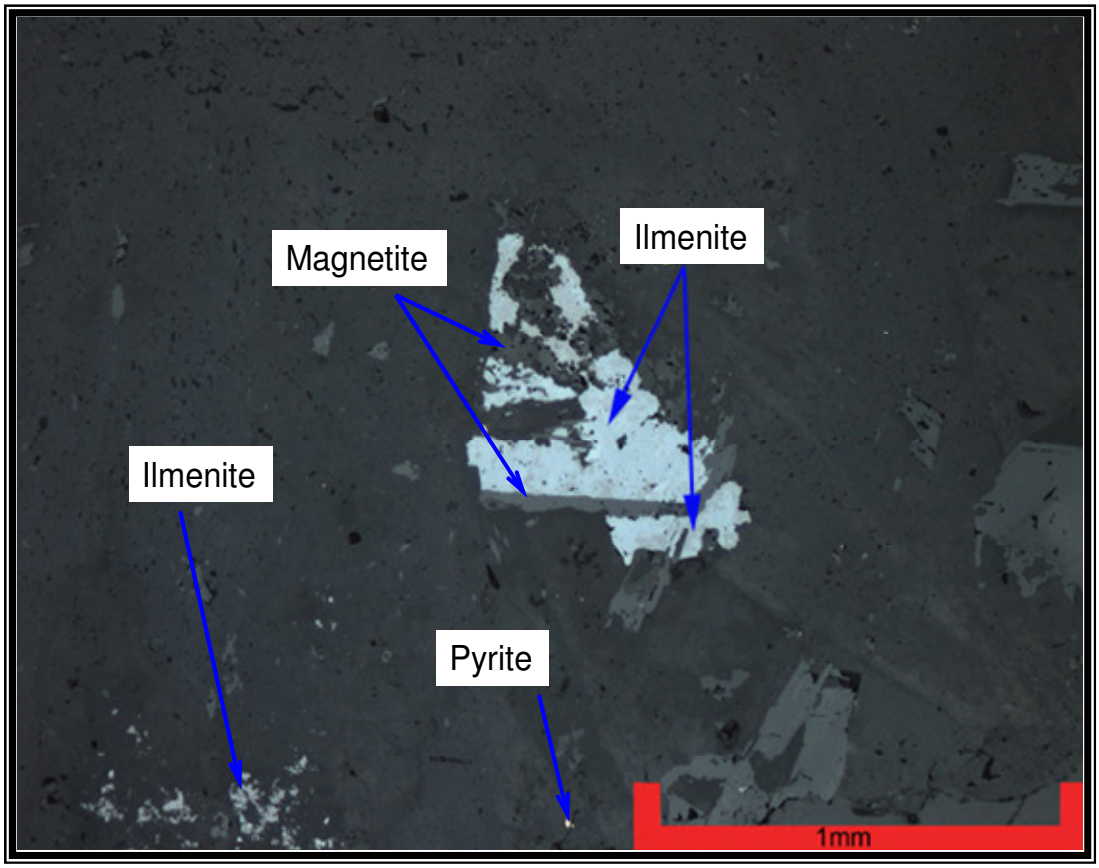

Figure 36. Photomicrograph of the xenolith; reflected light; width of scale bar = 1 mm.

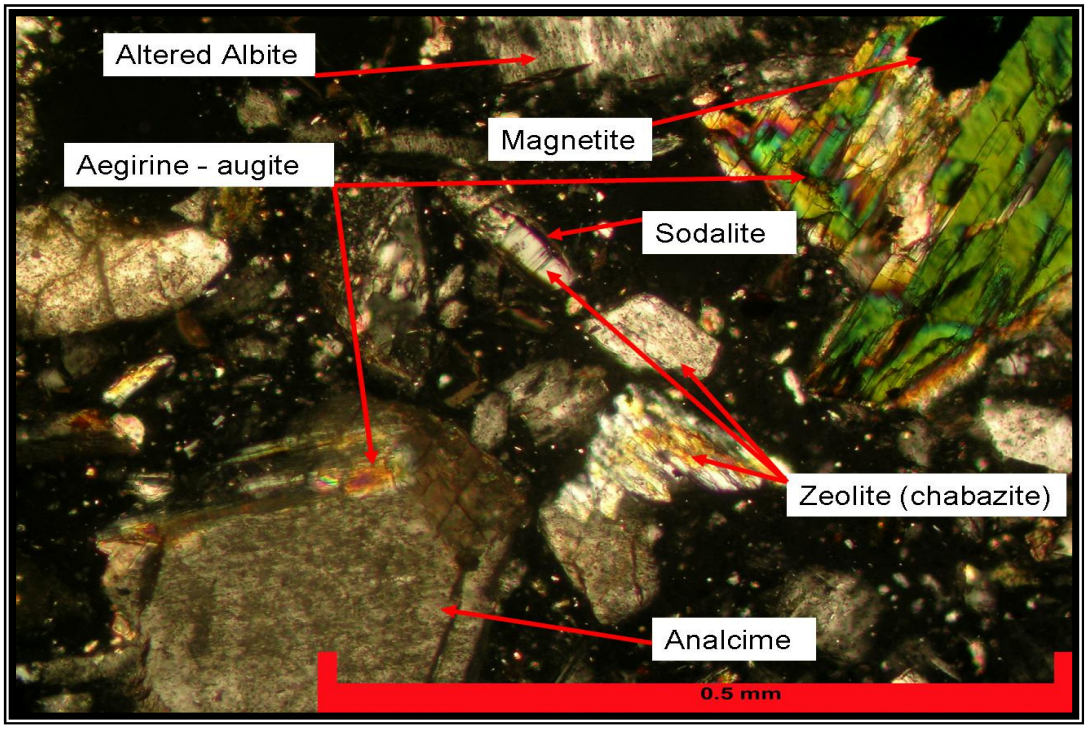

Figure 37. Photomicrograph of the ROM crusher sand; crossed polars, width of scale bar = 0.5 mm.

6.2 Screening tests

The reason that the screening tests were preformed was to determine the effect of different milling methods on the grain size distributions. The grain sizes are important for the different separation methods, because if the grain sizes are too large, the separation of the minerals will not be effective. The different test results are summarised in Table 22. The sample used for the screen test result at the University of Pretoria was milled using a laboratory swing mill, whereas a ball mill was used to mill the sample at Mamelodi Quarries (see section 4.2).

Table 22. The screening test results for ROM samples, performed at the University of Pretoria and Mamelodi Quarries.

ROM sieve test at University of Pretoria for a 200g sample					ROM sieve test at Mamelodi Quarries for 100g sample			
Sieve size (µm)	**Sample weight (g)**	**Mass %**	***Cum %**		**Sieve size (µm)**	**Sample weight (g)**	**Mass %**	***Cum %**
355	0	0	0		**425**	32.5	33	33
250	2	1	1		**300**	22.5	23	55
180	69	34	35		**212**	13.0	13	69
150	19	10	45		**180**	5.0	5	74
125	5	2	47		**150**	4.5	5	78
75	44	22	69		**75**	11.0	11	89
53	0	0	69		**53**	5.0	5	94
25	17	9	77		**<50**	6.0	6	100
< 25	46	23	100		**Total**	99.5	100.0	
Total	200	100			**Lost sample**	0.5		

*Cum = Cumulative

The results for the screen test at the University of Pretoria indicate that most of the material concentrated in the size fraction 250 - 180 µm (34 mass %). This was nearly equal to the size fraction of less than 53 µm (32 mass %; Figure 38).

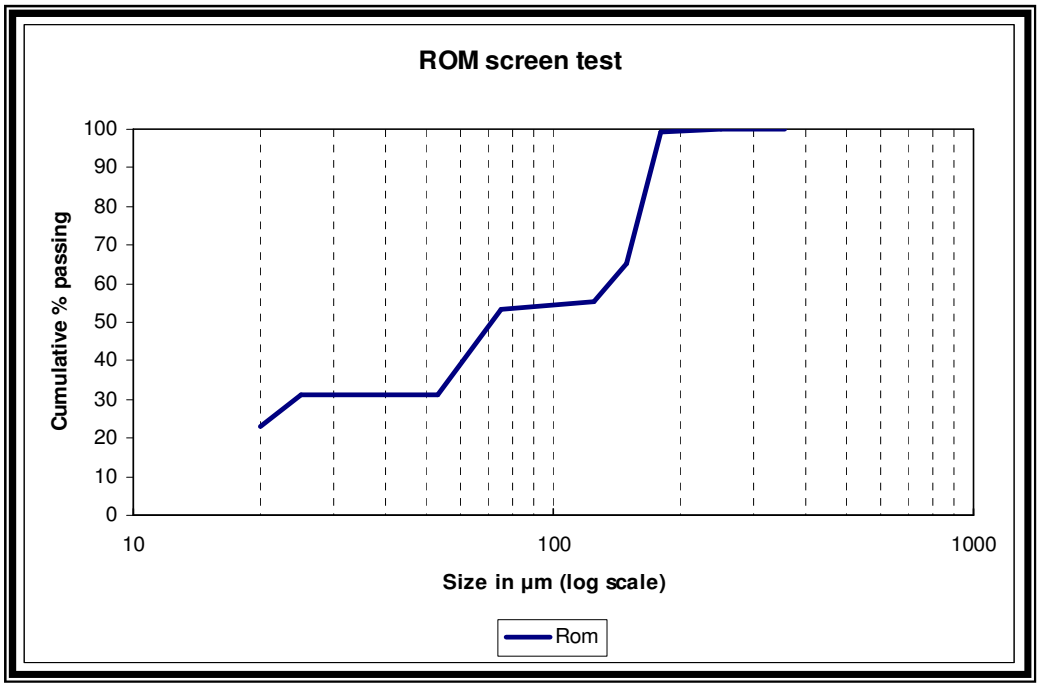

Figure 38. Graph of screen test performed on the ROM sample milled at the University of Pretoria.

The results for the screen test at Mamelodi Quarries indicate the most common size fraction was 500 - 425 µm (33 mass %). Equal amounts of material concentrated in size fractions 75 µm and 53 µm (11 mass %; Figure 39).

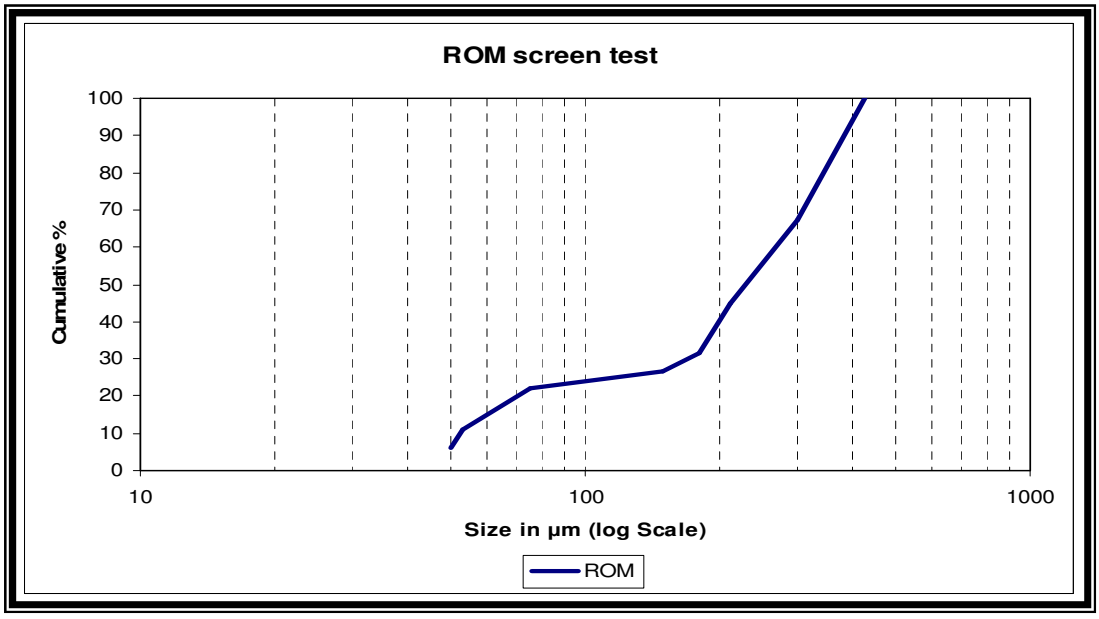

Figure 39. Graph of screen test performed on the ROM sample milled at Mamelodi Quarries.

A similar screen test was performed by Martins (1999) using crusher sand ROM and the following screen sizes: 4750 µm, 2360 µm, 1180 µm, 600 µm, 425 µm, 300 µm, and 150 µm (Table 23). The results for the screen test performed by Martins (1999) indicate that most of the material concentrated in the size fraction 1180 - 600 µm (30 mass %). Equal amounts concentrated in size fractions 300 µm and 425 µm (17 mass %; Figure 40).

In Figure 41, the different screen tests on a ROM sample from this study and that of Martins (1999) are plotted together. The comparison shows that the sample screened at the UP was the fines of the three, whereas the crusher sand used by Martins (1999) was the coarsest.

Table 23. Screen test results for ROM sample from Martins (1999).

ROM screen test results of 100g sample			
Sieve size (µm)	**Sample weight (g)**	**Mass %**	***Cum %**
4750	0.0	0	0
2360	9.0	9	9
1180	17.2	17	26
600	29.7	30	56
425	10.9	11	67
300	16.5	17	84
150	14.1	14	98
120	1.9	2	100
Total	99.3	100	

*Cum = Cumulative

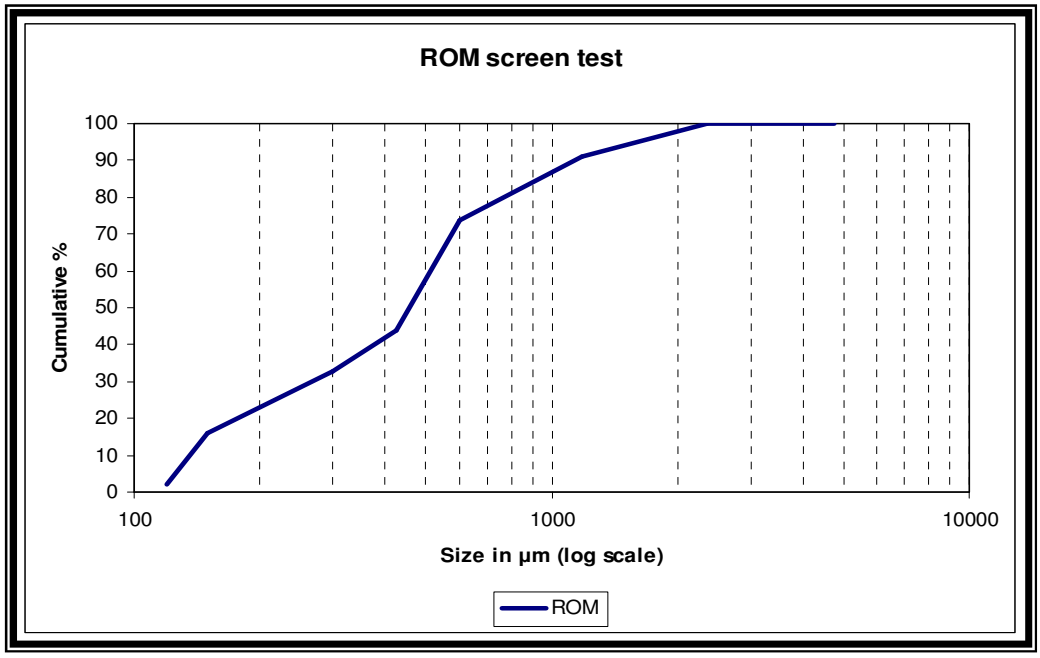

Figure 40. Graph of screen test performed on the ROM sample by Martins (1999).

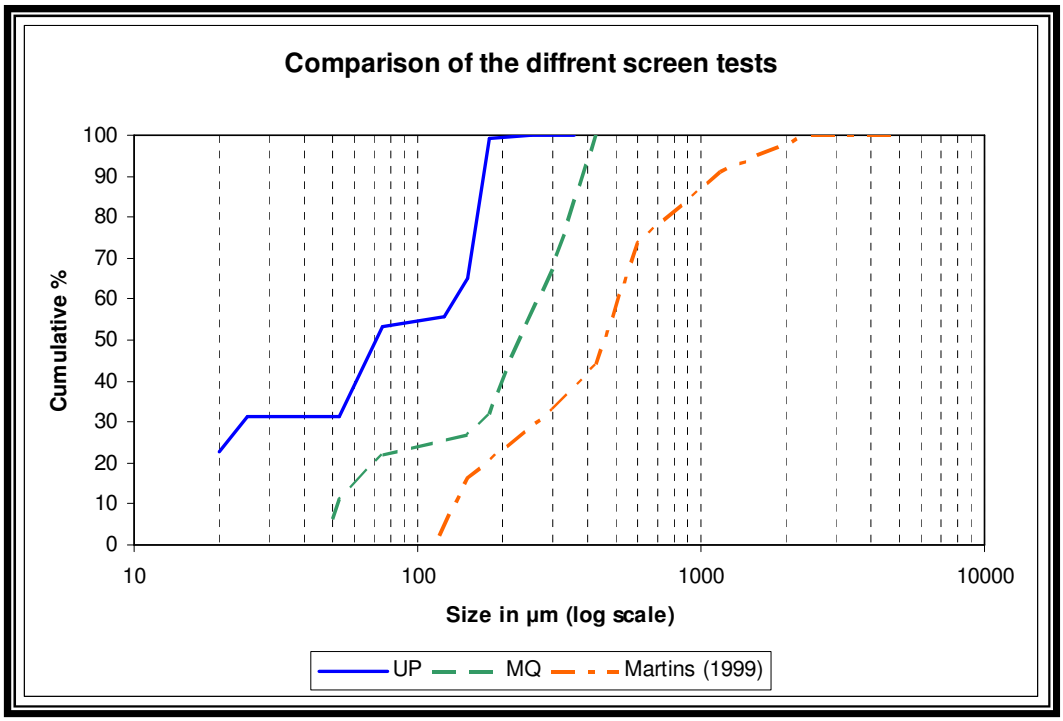

Figure 41. Comparison of the different screen tests on ROM samples performed in this study and by Martins (1999).

The reason for the variation in the particle sizes is the different time periods the samples in this study were milled compared to the crushed sample of Martins (1999). The ROM sample milled at UP is more fine-grained than the sample milled at MQ. The different grain sizes for the different milling steps are important for the different separation tests that were used. In wet magnetic separation it is important that the material is not too coarse or too fine, otherwise some of the magnetic minerals will pass through together with non-magnetic minerals. In the case of dry magnetic separation, all grain sizes smaller than 30 µm cause too much dust during the separation (loss to air); thus representative results will not be obtained. In the case of spiral separation, coarse grains of the light minerals will end up with the heavy minerals.

By knowing the grain size distribution of the crusher sand as produced by MQ, the appropriate screening could be applied to provide material best suited for the specific separation step. The different separated portions were milled at UP to obtain the correct particle size for XRF and XRD analyses.

6.3 Magnetic separation recovery of magnetic and non-magnetic material

The results of the mass fractions of the wet magnetic separation tests on ROM rock are presented in Table 24. The ROM contains ~90 % non-magnetic minerals and ~10% magnetic minerals. The weight percentage of sample is plotted against the passes for the magnetic and non-magnetic fractions in Figure 42. Four passes were performed on the sample. The graph clearly indicates that highest proportion of the magnetic minerals was separated out after the first pass.

Table 24. Results of the wet magnetic separation test for the ROM sample.

Wet magnetic separation of ROM					
ROM	**Non-magnetic (g)**	**Magnetic (g)**	**Total**	**Non-magnetic (mass %)**	**Magnetic (mass%)**
Pass 1	133.00	53.50	186.50	71.31	28.69
Pass 2	198.00	11.00	209.00	94.74	5.26
Pass 3	187.50	6.00	193.50	96.90	3.10
Pass 4	177.50	5.00	182.50	97.26	2.74
Total	696.00	75.50	771.50		
Percentage	90.21	9.79			

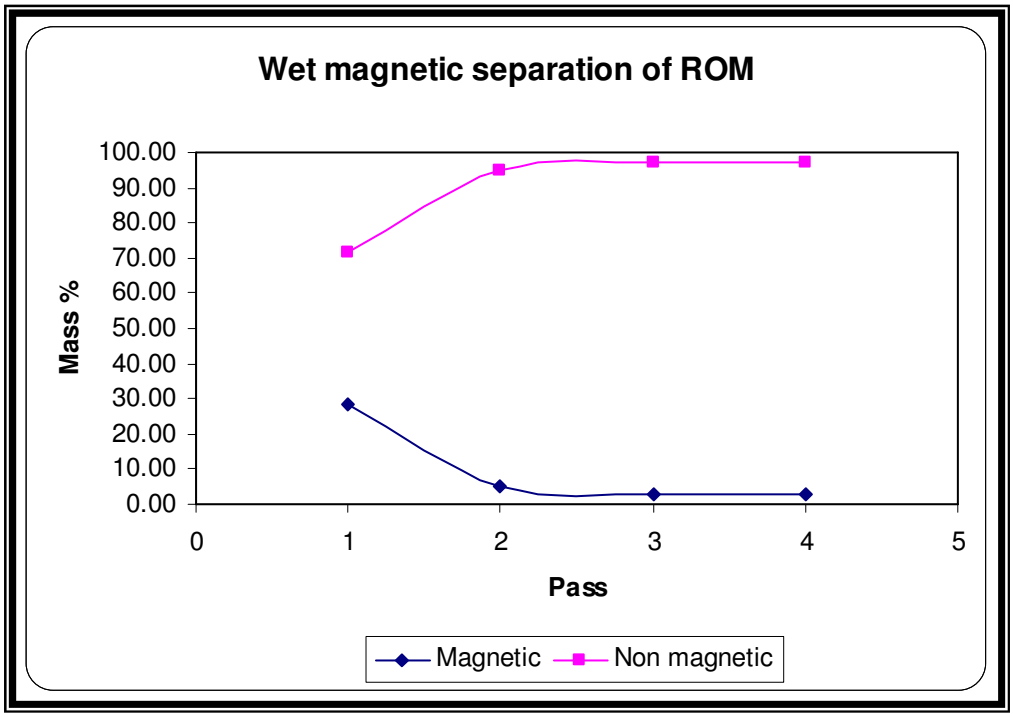

Figure 42. Graph showing the wet magnetic separation results of the ROM sample.

Dry magnetic separation tests (for methodology see section 4. 5) were also performed on the ROM. Two test were preformed: The first test (Test 1) used six passes; the second (Test 2) used only five. Table 25 presents the results of the weight fractions of the dry magnetic separation tests on ROM sample. In Figures 42 and 43, the mass percentage of the samples is plotted against the passes for the non-magnetic and magnetic fractions for tests 1 and 2. The two different tests clearly indicate that changing the rolls per minute (RPM) had a noticeable effect on extracting the magnetic minerals (see Tables 10 and 11 section 4.5). During the first test, pass 4 shows that the highest proportion of the magnetic minerals was concentrated (Figure 43), in contrast to test 2, whereas pass 2 concentrated the highest proportion of magnetic minerals (Figure 44).

Table 25. Results of the dry magnetic separation for ROM sample.

Test 1							
Pass	**Magnetic (g)**	**Non-magnetic (g)**	**Lost (g)**	**Total (g)**	**Magnetic (Mass %)**	**Non-magnetic (Mass%)**	**Lost (Mass%)**
1	34	1072		1106	3	97	
2	162	899	10	1071	15	84	1
3	206	686	8	899	23	76	1
4	233	450	3	686	34	66	0
5	124	325	1	450	28	72	0
6	80	244	0	325	25	75	0
Test 2							
Pass	**Magnetic (g)**	**Non-magnetic (g)**	**Lost (g)**	**Total (g)**	**Magnetic (Mass %)**	**Non-magnetic (Mass%)**	**Lost (Mass%)**
1	48	1067		1115	4	96	0
2	274	793		1067	26	74	0
3	182	600	11	793	23	76	1
4	159	440	1	600	27	73	0
5	118	320	1	440	27	73	0

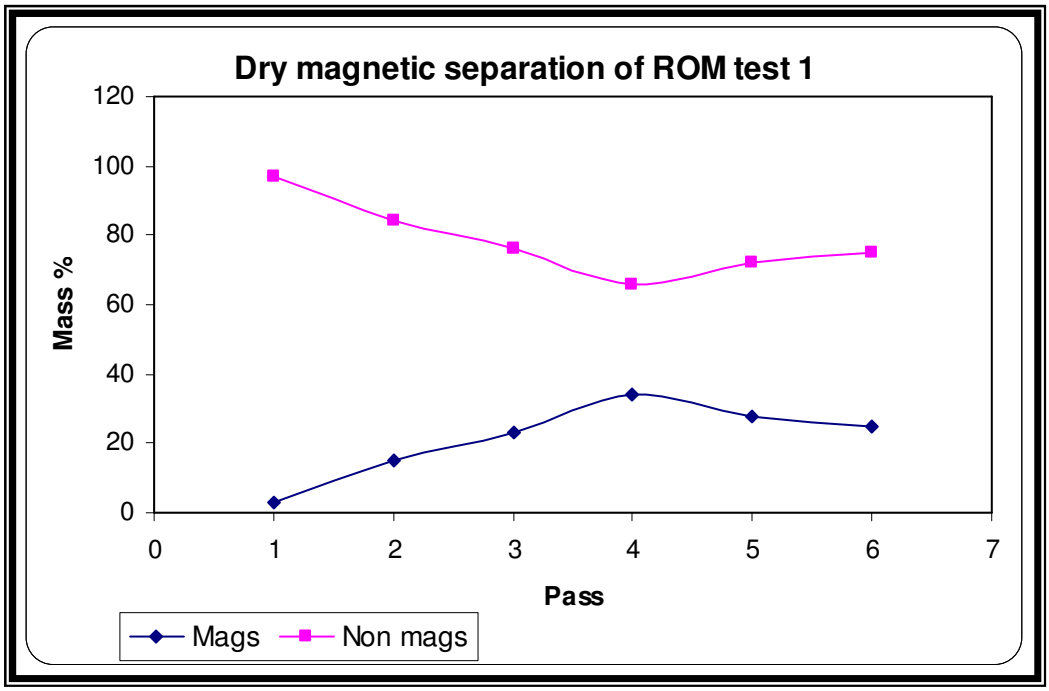

Figure 43. Graph showing the dry magnetic separation results of the ROM sample for test 1.

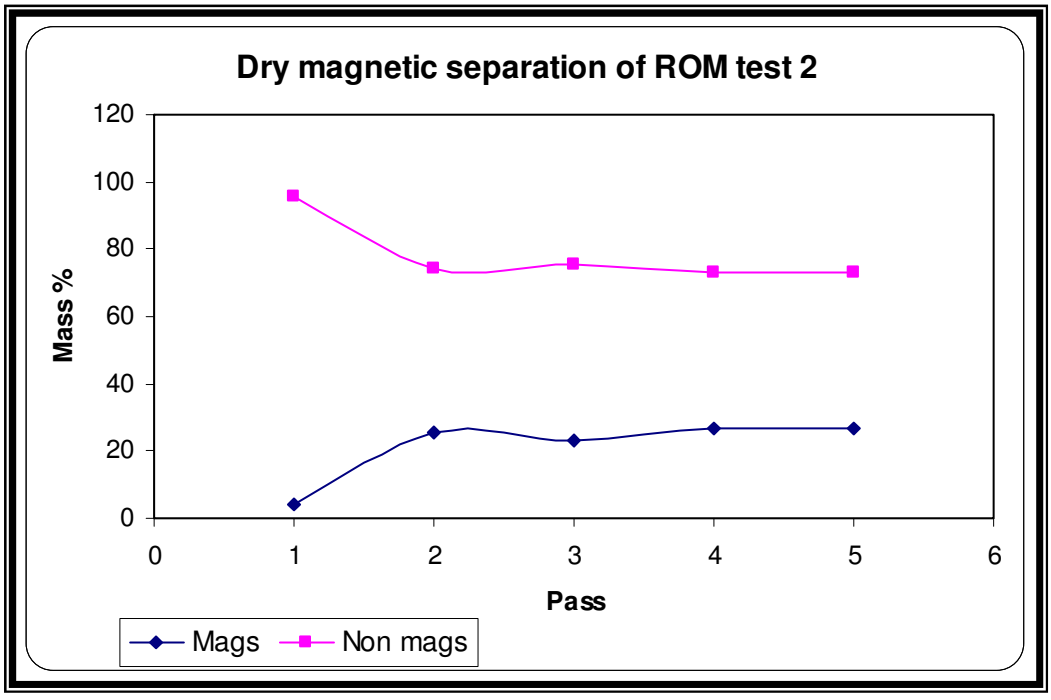

Figure 44. Graph showing the dry magnetic separation results of the ROM sample for test 2.

6.4 XRF results for the different tests

The separated fractions from the different tests were analysed using XRF for major and trace elements. Different abbreviations are used to identify the different fractions from the separation methods and are reported in Table 26. The major oxides of importance are Al_2O_3, Fe_2O_3 (reflecting total iron), Na_2O, and CaO, and are reported in weight percent (wt %). The trace elements of interest are Zr, Cl, F, Ba, La, and Ce, and these are reported in parts per million (ppm). Detailed results are presented in Appendix 2. The results will be interpreted and discussed in Chapter 7 for all the separation tests.

6.4.1 XRF results for high-intensity wet magnetic separation

The XRF results (major and trace elements) for the high-intensity wet magnetic separation are plotted in Figure 45. Concentration variation for TiO_2, Fe_2O_3, MnO, MgO, and CaO display similar trends (Figure 45 a). These elements were concentrated in the magnetic fractions of the separation, relative to the non-magnetic fractions. The concentrations of TiO_2, MnO, and MgO decreased to below 0.9 wt %, and for Fe_2O_3 and CaO the concentrations decreased to 0.78 wt % and 0.75 wt % respectively in the non-magnetic fraction (Figure 45 a). SiO_2, Al_2O_3 and K_2O display similar trends to each other and concentrated slightly more in the non-magnetic fractions than in the magnetic fractions of the separation test, whereas Na_2O values were higher in the magnetic fraction as compared to the non-magnetic fractions (Figure 45 a). The trace elements that share a similar trend are Th, U, Y, Sr, Ce, and La, which concentrated in the first two magnetic fractions of the test and decreased in the non-magnetic fractions (Figure 45 b). Rubidium contents vary slightly but do not display a clear trend (Figure 45 b). The trace element Ba is seemingly constant in all the magnetic and non-magnetic fractions.

The trace elements F, Cl and Zr are present in higher concentrations than the above-mentioned trace elements and are plotted separately in Figure 45 c. Fluorine is not clearly affected by magnetic separation, whereas Cl decreased and Zr increased in the first two magnetic fractions and stayed constant in the non-magnetic fraction.

Table 26. Different abbreviations used to identify the different fractions from the separation methods in this study.

Sample abbreviation	Description	Sample abbreviation	Description
ROM 1	Run of mine 1	RNMP3	Wet magnetic test non-magnetic pass 3
ROM 2	Run of mine 2 (second analysis of ROM material)	RNMP4	Wet magnetic test non-magnetic pass 4
RNMAGS6T1	Dry magnetic test 1 non-magnetic pass 6	SRD1	Spiral test screened dense material 1
RMAGS1T1	Dry magnetic test 1 magnetic pass 1	SRD2	Spiral test screened dense material 2
RMAGS2T1	Dry magnetic test 1 magnetic pass 2	SRL1	Spiral test screened light material 1
RMAGS3T1	Dry magnetic test 1 magnetic pass 3	SRL2	Spiral test screened light material 2
RMAGS4T1	Dry magnetic test 1 magnetic pass 4	SRM1	Spiral test screened medium material 1
RMAGS5T1	Dry magnetic test 1 magnetic pass 5	SRM2	Spiral test screened medium material 2
RMAGS6T1	Dry magnetic test 1 magnetic pass 6	URD1	Spiral test unscreened dense material 1
RNMAGS5T2	Dry magnetic test 2 non-magnetic pass 5	URD2	Spiral test unscreened dense material 2
RMAGS1T2	Dry magnetic test 2 magnetic pass 1	URL1	Spiral test unscreened light material 1
RMAGS2T2	Dry magnetic test 2 magnetic pass 2	URL2	Spiral test unscreened light material 2
RMAGS3T2	Dry magnetic test 2 magnetic pass 3	URM1	Spiral test unscreened medium material 1
RMAGS4T2	Dry magnetic test 2 magnetic pass 4	URM2	Spiral test unscreened medium material 2
RMAGS5T2	Dry magnetic test 2 magnetic pass 5	HLRH	Heavy liquid test on ROM dense material
RMP1	Wet magnetic test magnetic pass 1	HLRSM	Heavy liquid test on ROM starting material
RMP2	Wet magnetic test magnetic pass 2	HLRL	Heavy liquid test on ROM light material
RMP3*	Wet magnetic test magnetic pass 3		
RMP4*	Wet magnetic test magnetic pass 4		
RNMP1	Wet magnetic test non-magnetic pass 1		
RNMP2	Wet magnetic test non-magnetic pass 2		

* Samples not analysed for traces owing to a lack of sample material

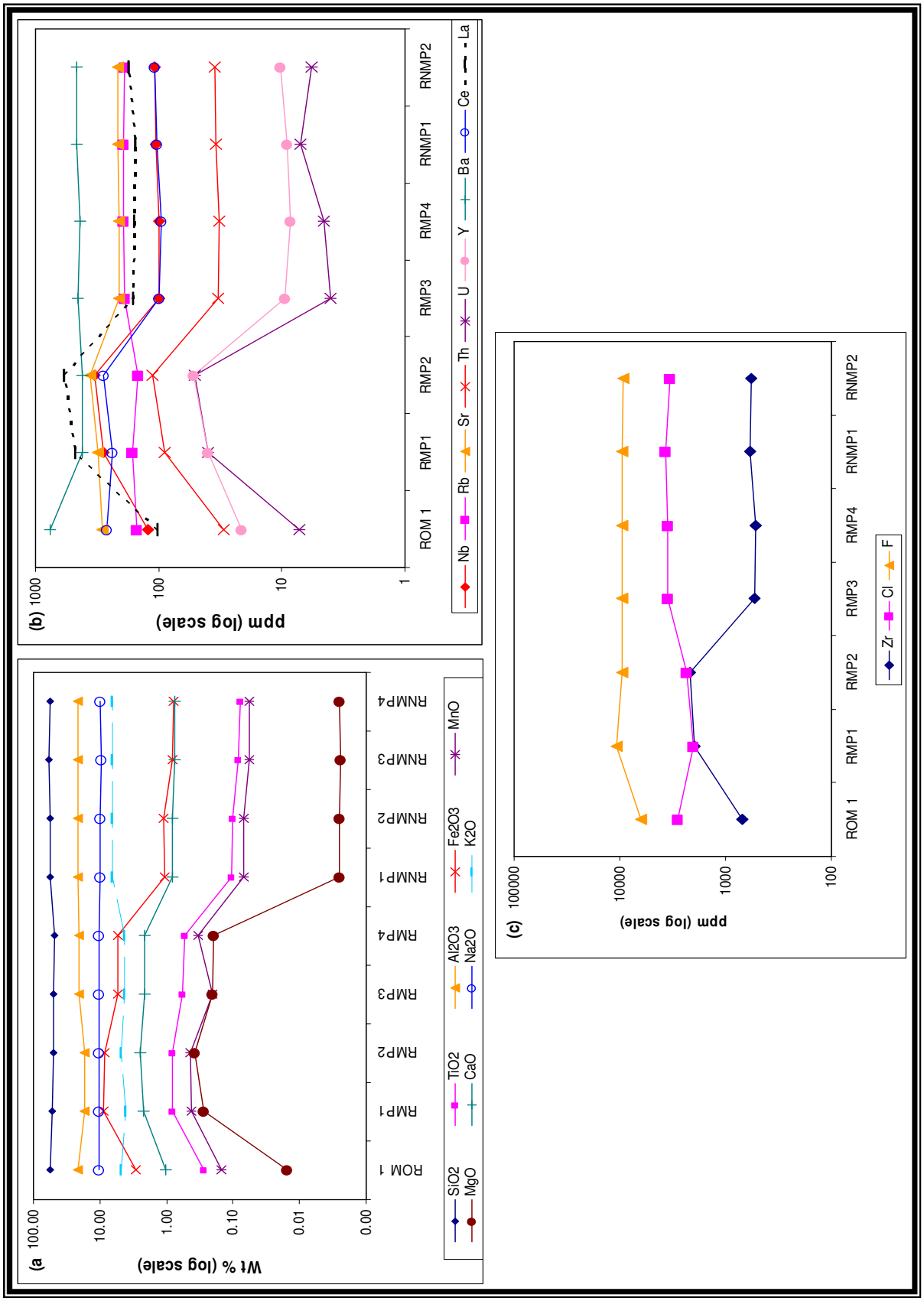

Figure 45. XRF results for the high-intensity wet magnetic separation. (a) Major element concentrations, (b) trace elements with low concentrations and (c) trace elements with higher concentrations (Cl, Zr and F). For abbreviations see Table 26.

6.4.2 XRF results for low-intensity dry magnetic separation

Two tests were carried out for the low-intensity dry magnetic separation and only one non-magnetic fraction produced. The difference between the two tests was the change in the number of times the material was subjected to magnetic separation, to produce a single non-magnetic fraction (test 1 used 6 passes and test 2 used 5 passes). The XRF results are plotted in Figures 47 and 48.

The trends for both tests are similar and only small variations in concentration are observed. The same trends are observed for TiO_2, Fe_2O_3, MnO, MgO, and CaO concentrations for both tests (Figure 46 a and b). In the non-magnetic fraction of test 1, TiO_2, MnO, and MgO decreased to below 0.05 wt % and Fe_2O_3 and CaO concentrations decrease to 0.68 wt % and 0.35 wt % respectively. Similar results are seen in test 2. These elements concentrated more in the first magnetic fraction (RMAGS1T1 and RMAGS1T2) than in the other fractions. SiO_2, Al_2O_3, K_2O, and Na_2O contents decreased in small amounts in the first magnetic fraction (RMAGS1T1 and RMAGS1T2) and increased in concentration in the non-magnetic fraction (RNMAGS6T1 and RNMAGS5T1) (Figure 46 a and b).

The trace elements Nb, Th, U, Y, and La displayed similar trends in that they concentrated in the first two magnetic fractions (RMAGS1 and RMAGS2), and decreased thereafter. Barium and Sr displayed higher values in the second magnetic fractions of both tests (RMAGS2) and stayed constant for the remainder of the fractions thereafter, whereas Ce showed a sharp increase in the second magnetic fraction and sharply decreased in the remainder of the fractions with approximately 100 ppm left in the non-magnetic fraction (RNMAGS6T1 and RNMAGS5T2).

The trace elements F, Cl, and Zr are plotted in Figure 47 a and b. Fluorine decreases in concentration after the second magnetic fraction (RMAGS2) and shows an even decline thereafter for both tests, whereas Cl concentrations sharply decline in the first magnetic fraction with steady increase thereafter. Zirconium contents concentrated in the first magnetic fractions and decreased in the non-magnetic fraction (see Chapter 7 for interpretation and discussion of the results).

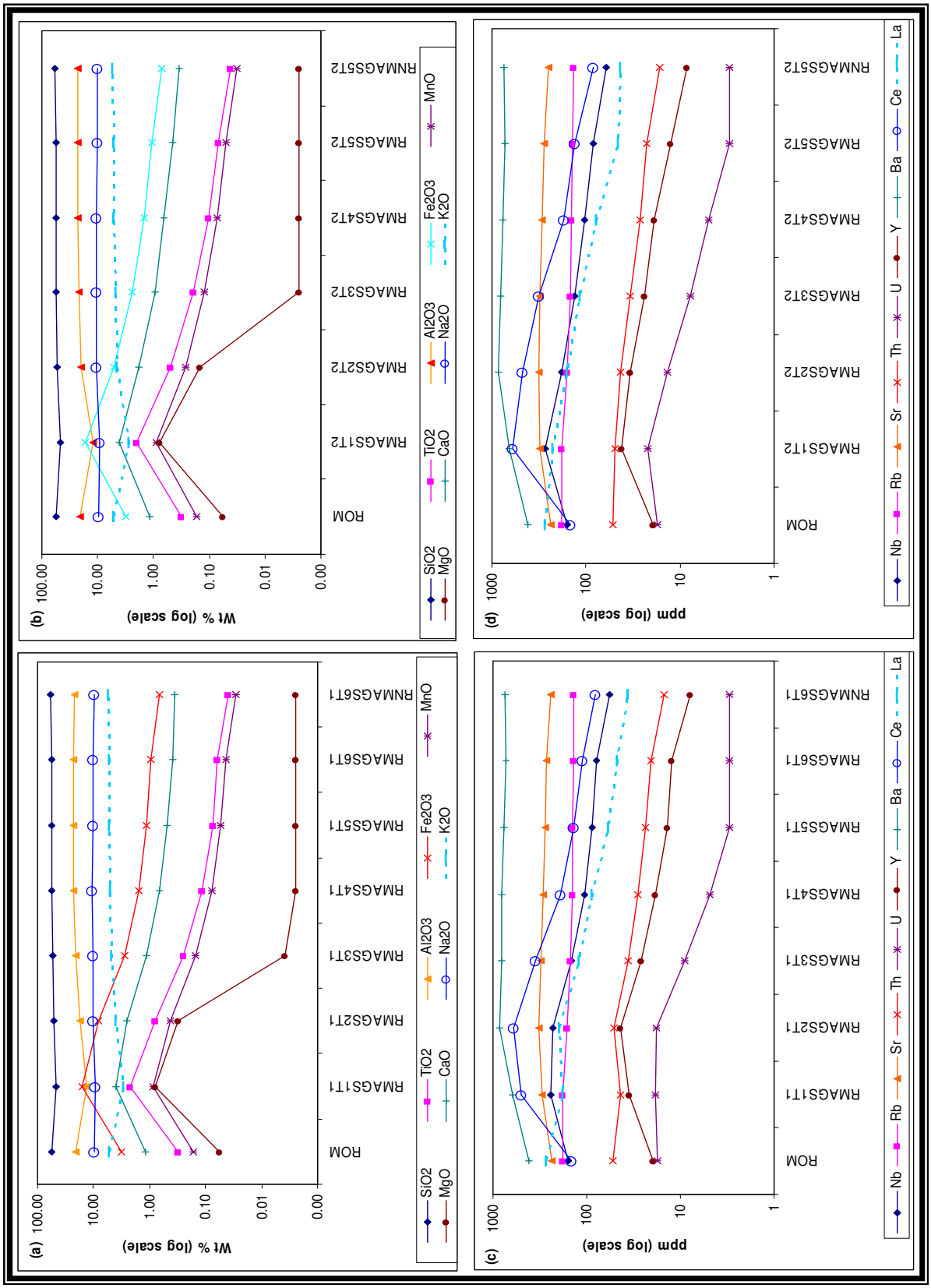

Figure 46. XRF results for the low-intensity dry magnetic separation. (a) Major elements concentration for test 1, (b) major elements concentration for test 2, (c) trace element concentrations for test 1, and (d) trace element concentrations for test 2. For abbreviations, see Table 26.

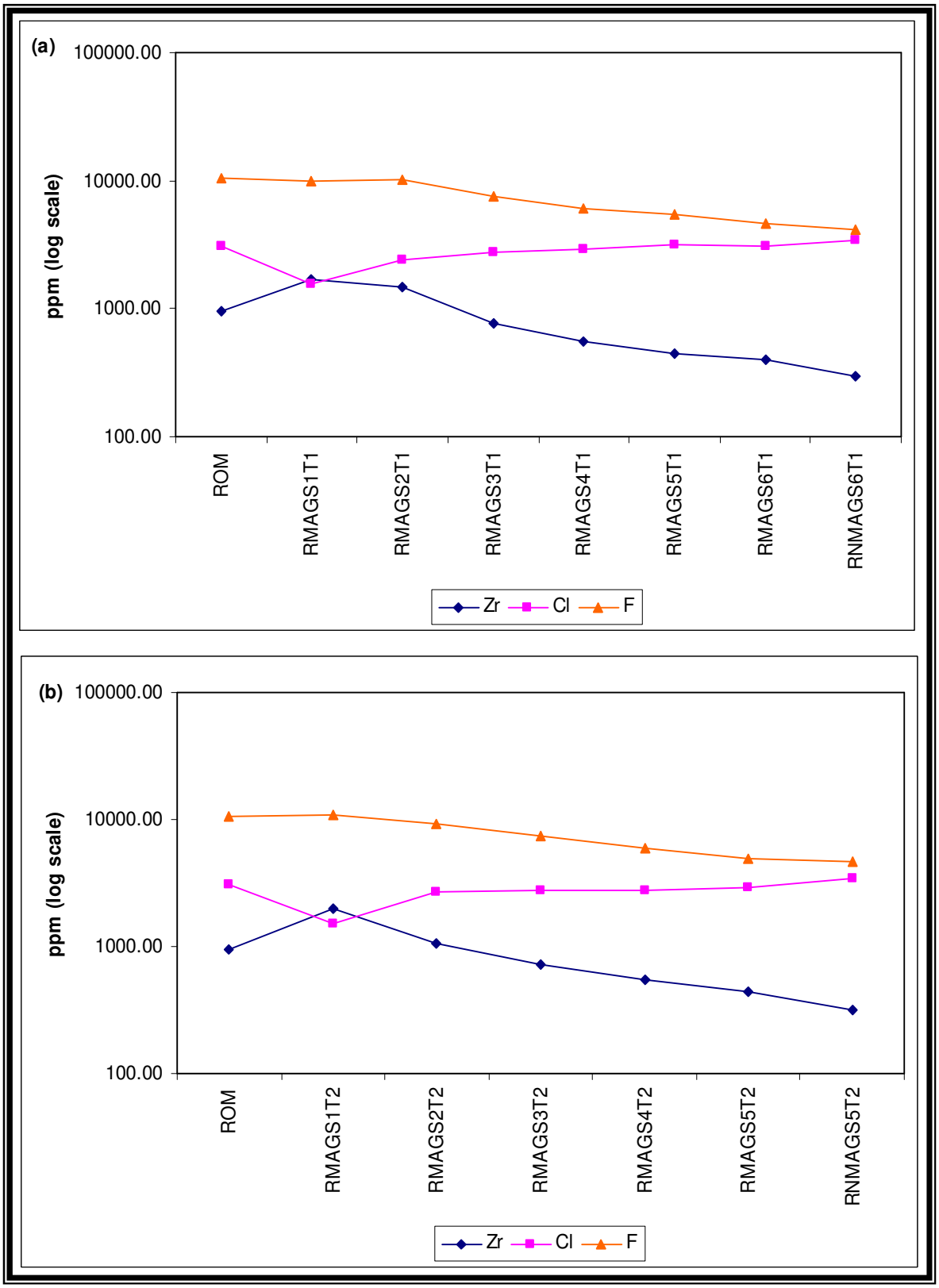

Figure 47. XRF results for the low-intensity dry magnetic separation. (a) trace elements with higher concentrations (Cl, Zr and F) for test 1 and (b) trace elements with higher concentrations (Cl, Zr and F) for test 2. For abbreviations, see Table 26.

6.4.3 XRF results for gravity separation using heavy liquid

Heavy liquid with a density of 2.96 g/cm^3 was used to separate the lighter minerals from the denser minerals (see Chapter 4.6 for details on the methodology). The XRF results for the different fractions are plotted in Figure 48. The same behaviour is observed for concentrations of TiO_2, Fe_2O_3, MnO, MgO, and CaO whereby the highest concentrations are in the heavy fraction of the separation test (HLRH) (Figure 48 a). Al_2O_3 and K_2O concentrations are lower in the heavy fraction of the separation, whereas for SiO_2 and Na_2O amounts are constant throughout with slight decreases in the heavy fraction (HLRH) of the separation (Figure 48 a).

The trace elements concentrations that show similar trends are Nb, Sr, Th, U, Y, Ce, and La, which are higher in the HLRH of the separation (Figure 48 b). Barium, is more abundant in the lighter fraction (HLRL) of the separation test, whereas Rb displays no preference for the different separation fractions (Figure 48 b).

The trace elements F, Cl, and Zr are plotted in Figure 48 c. Fluorine and Zr were concentrated in the HLRH compared to that of Cl which was depleted in the heavy fraction and more concentrated in the HLRL (Figure 48 c; see Chapter 7 for interpretation and discussion of the results).

6.4.4 XRF results for gravity separation using a spiral

Two tests were carried out for both the screened and unscreened ROM sample. The only difference between the two tests was that for the first test solid 15.8 % to water was used and this was 11.1 % in the second test. Figures 49 and 50 are the different plots for the two tests for the major and trace elements.

The trends observed for the major and trace elements are similar for both the screened and unscreened ROM samples for test 1. SiO_2 and Na_2O do not display changes in concentration from the dense (SRD and URD) to the lighter (SRL and URL) fractions of the separation test (Figure 49 a and b). K_2O and Al_2O_3 are more concentrated in the medium (SRM and URM) and light fractions of the separation test than in the denser fraction (Figure 49 a and b).

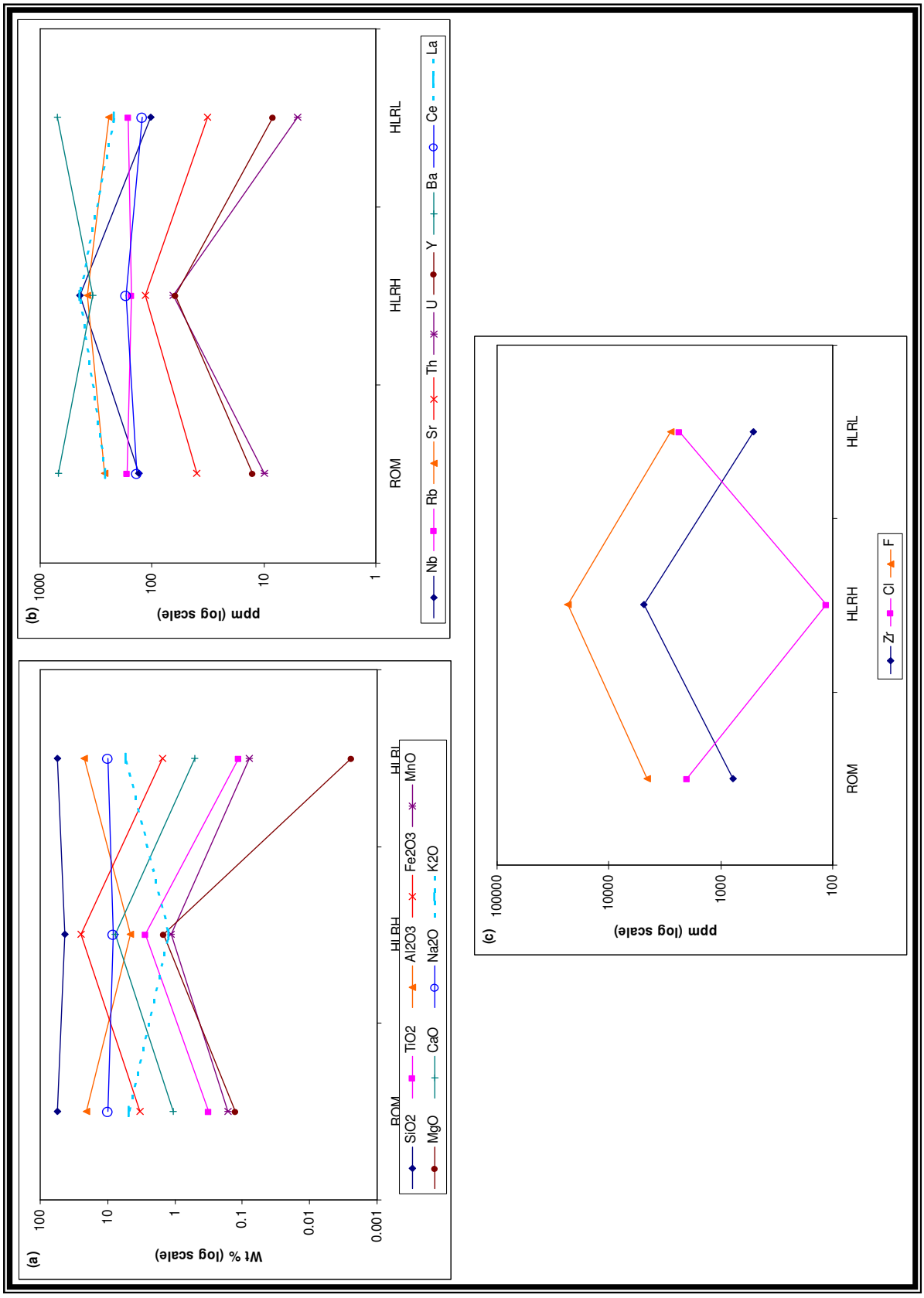

Figure 48. XRF results for gravity separation using a heavy liquid. (a) Major element concentration,(b) trace elements with low concentrations and (c) trace elements with higher concentrations (Cl, Zr and F). For abbreviations, see Table 26.

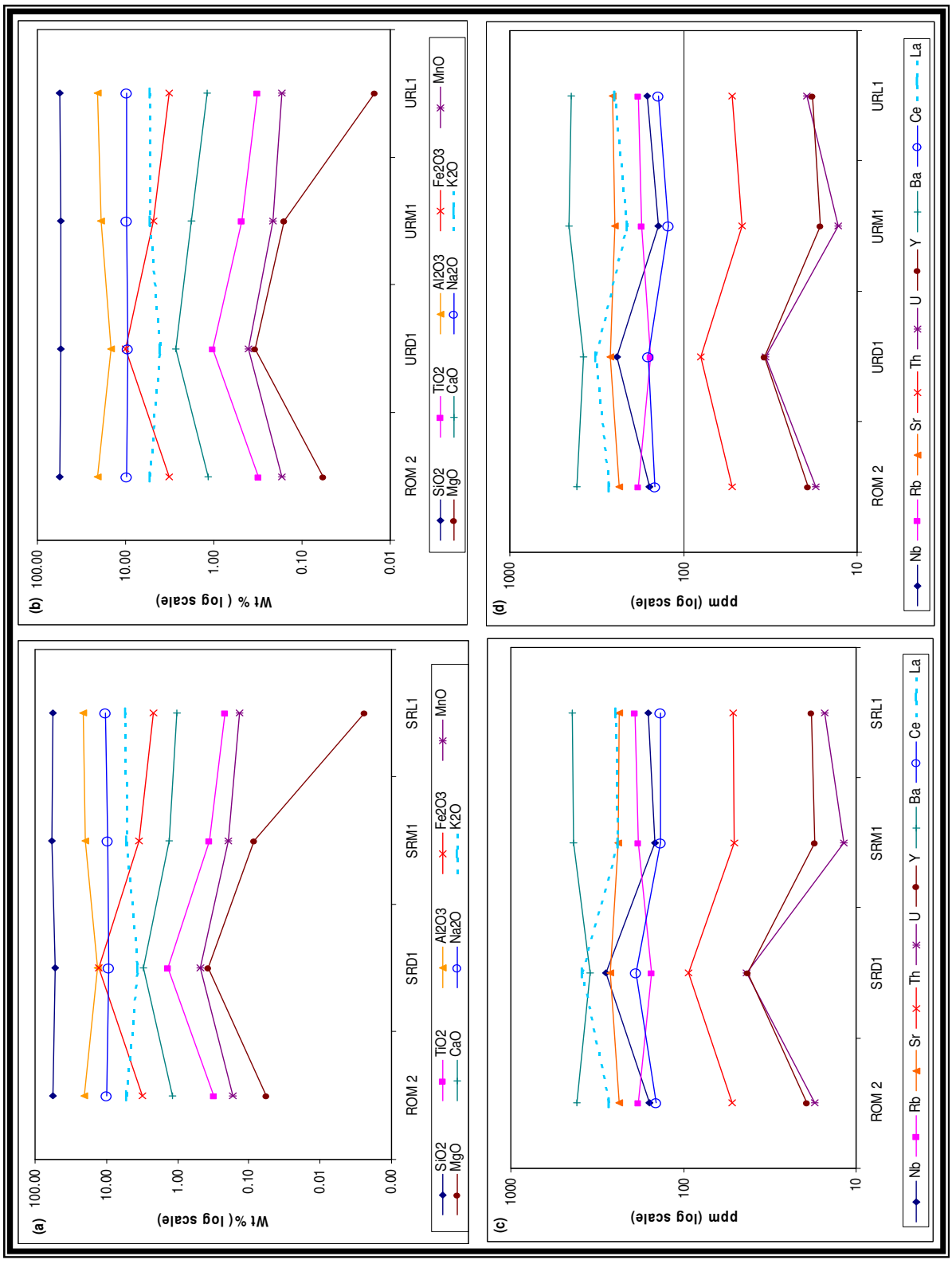

Figure 49. XRF results for the spiral separation test 1. (a) Major element concentration for screened ROM, (b) major element concentration for unscreened ROM, (c) trace element concentrations for screened ROM and (d) trace element concentrations for unscreened ROM. For abbreviations, see Table 26.

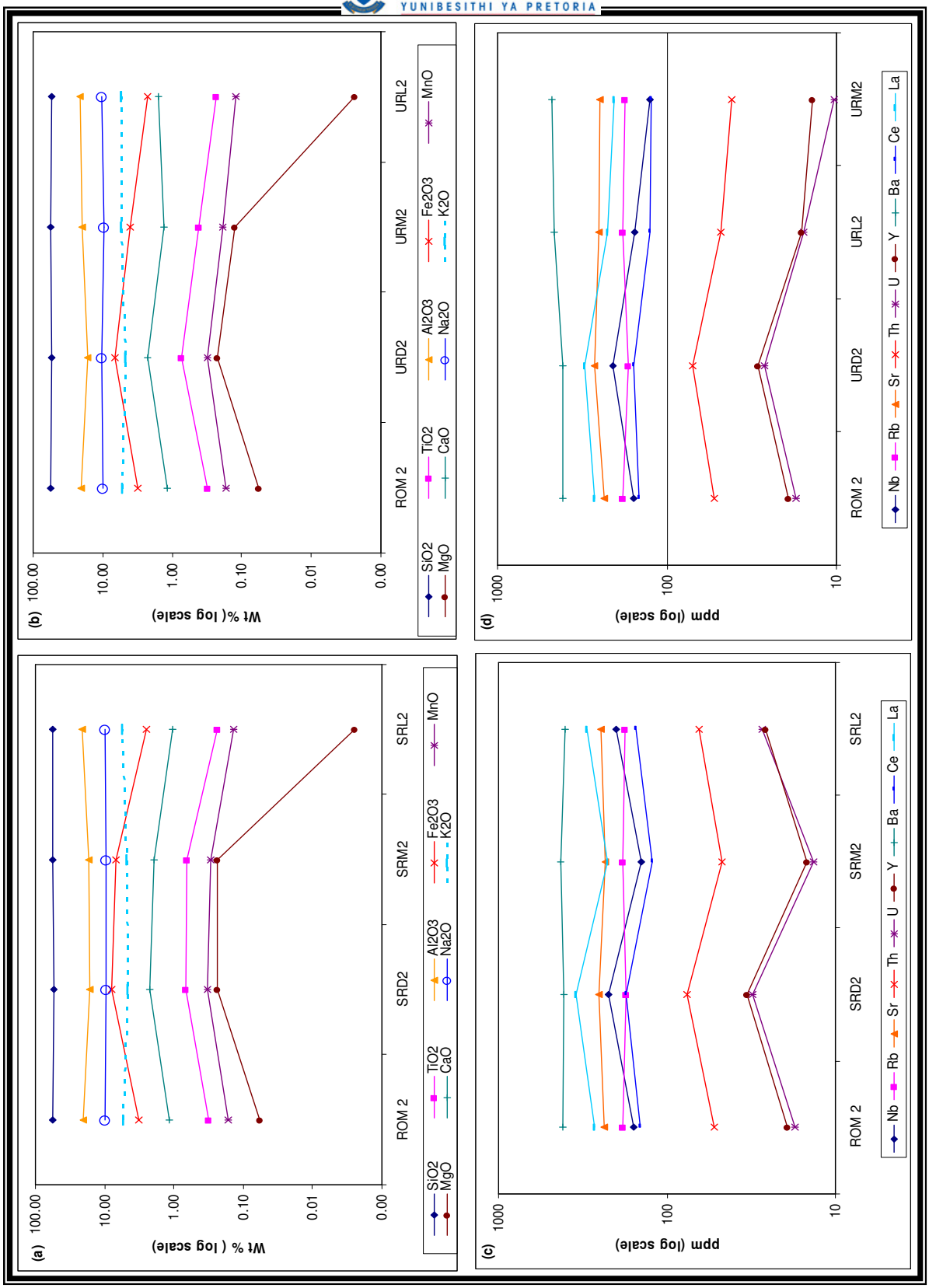

Figure 50. XRF results for the spiral separation test 2. (a) Major element concentration for screened ROM, (b) major element concentration for unscreened ROM, (c) trace element concentrations for screened ROM and (d) trace element concentrations for unscreened ROM. For abbreviations, see Table 26.

The same trend is observed for TiO_2, Fe_2O_3, MnO, MgO, and CaO whereby the highest concentrations of these elements are in the dense fraction of the separation test (Figure 49 a and b).

The trends observed in the second test are different to those from the first test but there is no significant difference between the screened and unscreened ROM sample (Figure 50 a and b). The elements TiO_2, Fe_2O_3, MnO, MgO, and CaO decreased in concentration from the denser to lighter fractions, whereas SiO_2, Al_2O_3, Na_2O and K_2O contents remained constant in all of the different fractions for both the screened and unscreened ROM (Figure 50 a and b). The trace elements show the same trend as observed for the first test (Figure 50 c and d).

Trace elements F, Cl, and Zr are plotted in Figures 51 and 52. Fluorine and Zr concentrations in both the screened and unscreened ROM sample, for test 1, are higher in the dense fraction, whereas Cl concentrated in the medium fraction (SRM and URM) of the separation (Figure 51 a and b). The same observations are made for the results of the second test as for the first test (Figure 52 a and b; see Chapter 7 for interpretation and discussion of the results).

6.4.5 XRF UniQuant©5 results for the low-intensity dry magnetic separation tests

The focus of the UniQuant©5 investigation was to examine the trace elements Ba, Ce and La. The variation in major and trace elements are different compared to conventional XRF analyses, because the analyses were done on a powder pellet and the values normalized without considering LOI. The trace elements concentrations were changed from the reported oxides to elements for comparisons in the Discussion chapter (Chapter 7).The detailed results are presented in Appendix 2. The results are plotted in Figures 53 and 54. Similar data trends are observed in both tests, and only small variations in concentration are observed. TiO_2, Fe_2O_3, and CaO are concentrated more in the first magnetic fraction for both tests (RMAGS1; Figure 53 a and b).

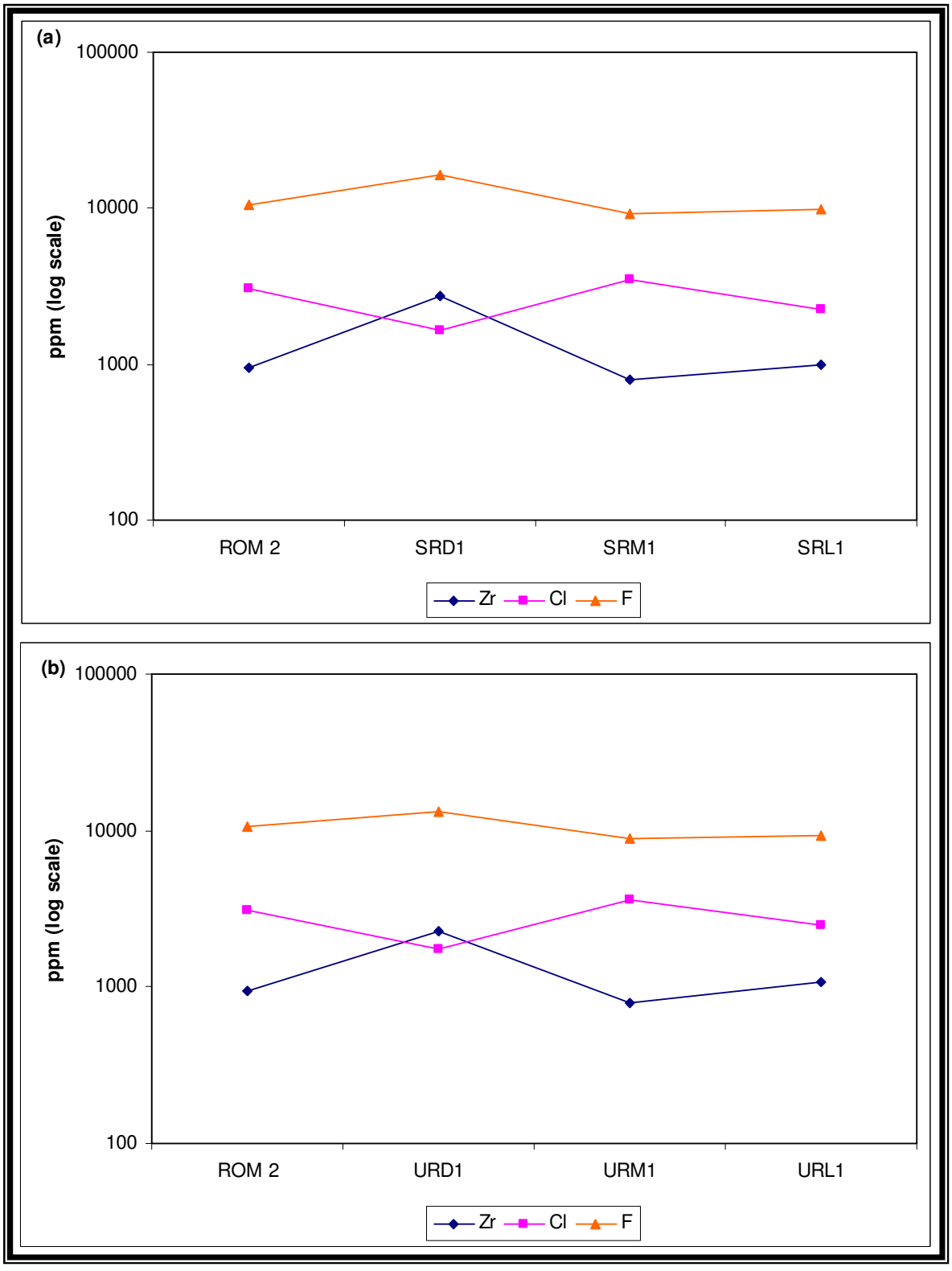

Figure 51. XRF results for the spiral separation for test 1. (a) trace elements with higher concentrations (Cl, Zr, and F) for screened ROM, (b) trace elements with higher concentrations (Cl, Zr, and F) for unscreened ROM. For abbreviations, see Table 26.

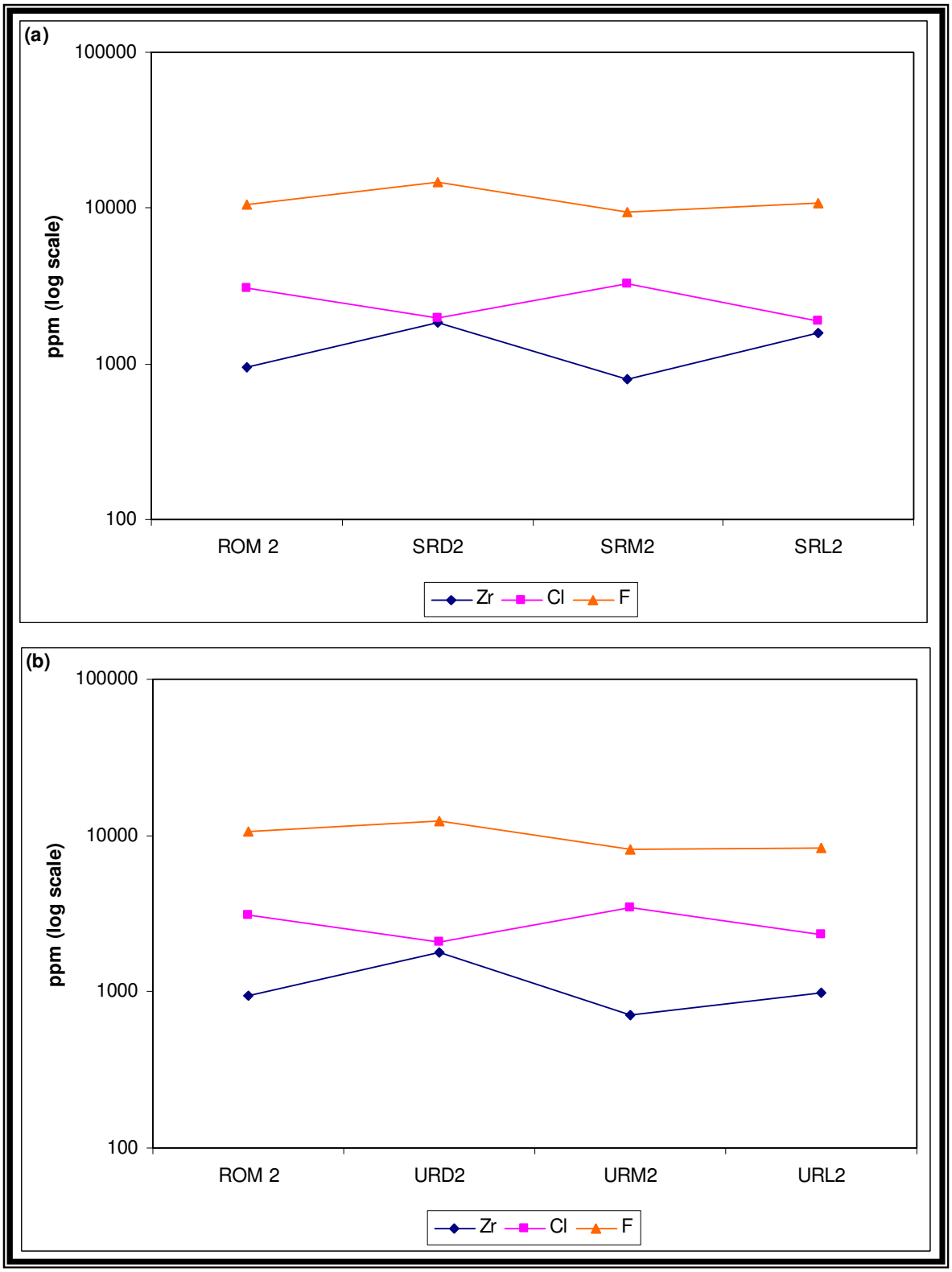

Figure 52. XRF results for the spiral separation for test 2, (a) trace elements with higher concentrations (Cl, Zr, and F) for screened ROM, (b) trace elements with higher concentrations (Cl, Zr, and F) for unscreened ROM. For abbreviations, see Table 26.

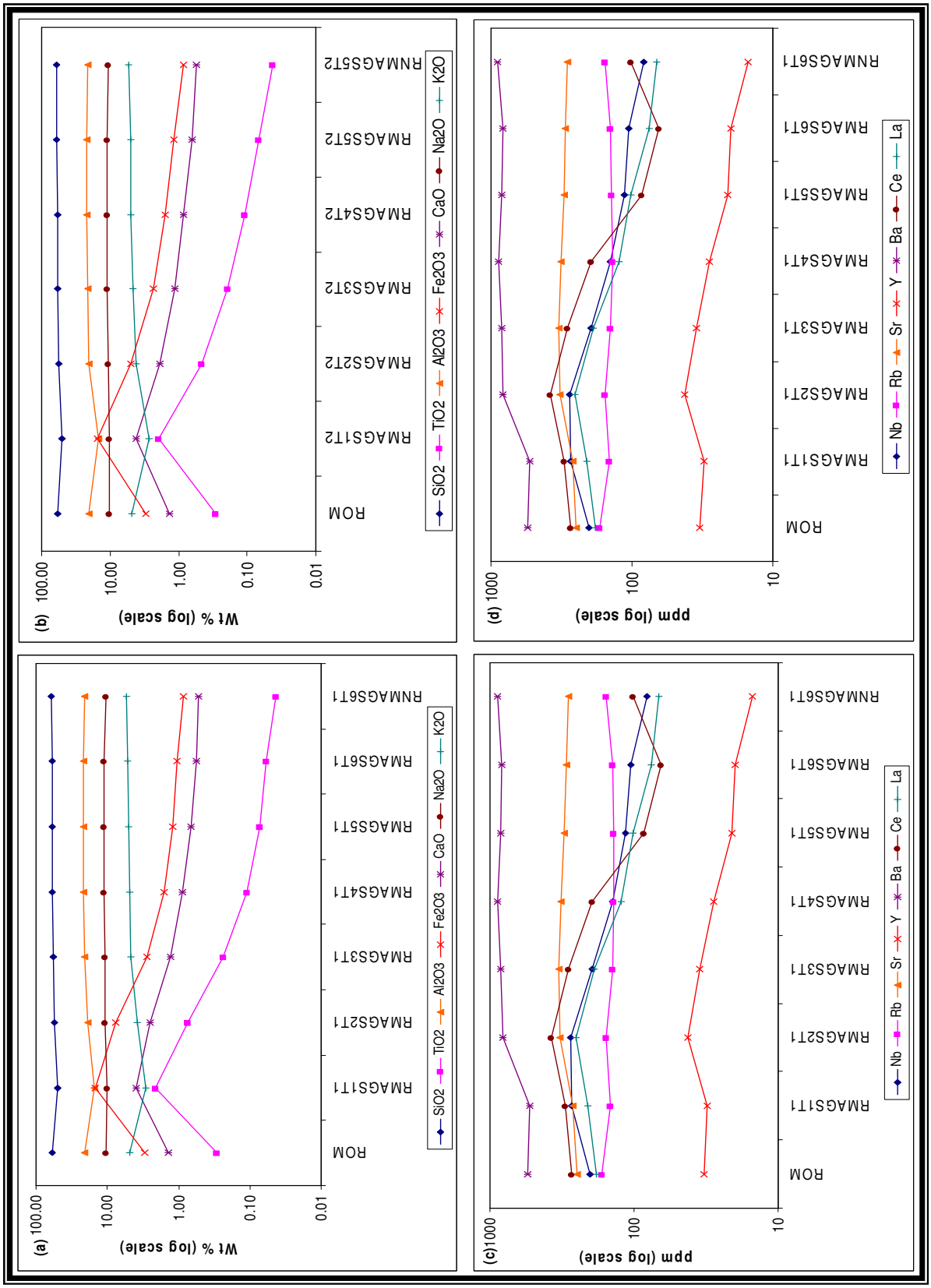

Figure 53. UniQuant©5 results for the low-intensity dry magnetic separation. (a) major element concentrations for test 1, (b) major element concentrations for test 2, (c) trace element concentrations for test 1 and (d) trace element concentrations for test 2. For abbreviations, see Table 26.

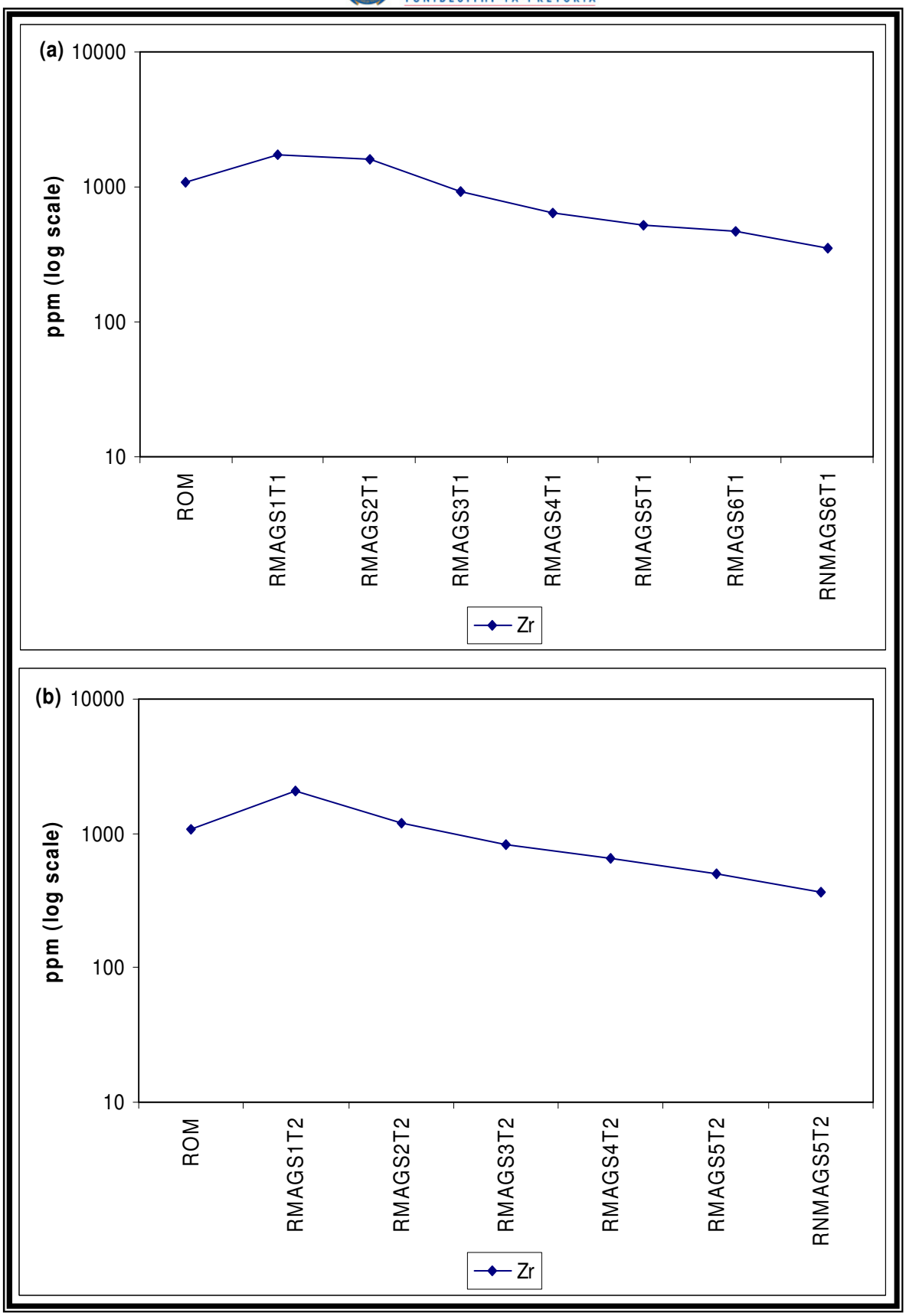

Figure 54. UniQuant©5 results for the low-intensity dry magnetic separation. (a) Zr concentrations for test 1 and (b) Zr concentrations for test 2. For abbreviations, see Table 26.

The concentration of these elements in the non-magnetic fraction decreased to 0.04 wt % (TiO_2), 0.85 wt % (Fe_2O_3), and 0.55 wt % (CaO). SiO_2, Al_2O_3, K_2O, and Na_2O contents decreased in small amounts in the first magnetic fraction and concurrently increased in concentration in the non-magnetic fraction (RNMAGS6T1 and RNMAGS5T1) (Figure 53 a and b)

Niobium, Y, Ce, and La concentration patterns are similar in that they concentrated in the first two magnetic fractions (RMAGS1 and RMAGS2), and decreased thereafter (Figure 53 c and d). Barium and Sr showed higher values in the second magnetic fractions (RMAGS2) and stay constant for the fractions thereafter, whereas Rb only changed slightly for the different fractions (Figure 53 c and d).

Zirconium concentrated in the first and second magnetic fraction for the first test with a steady decrease in the non-magnetic fraction (Figure 54 a). In the second test, Zr concentrated in the first magnetic fraction and decreased in the remainder of the fractions (Figure 54 b; see Chapter 7 for interpretation and discussion of the results).

6.4.6 Variation of total iron content in the Franspoort Nepheline syenite

The nepheline syenite deposit at Mamelodi Quarries as mentioned in Section 2.2 2, contains different nepheline syenites. Analytical data was obtained from an unpublished source from the University of Pretoria (Kgwakgwe 2004). Detailed results are presented in Appendix 2. The total iron content in the red nepheline syenite is higher than that in the grey nepheline syenite (Figure 55). The grey nepheline syenite has an average Fe_2O_3 content of 3.50 wt % compared to 4.83 wt % for the red nepheline syenite (see Chapter 7 for interpretation and discussion of the results).

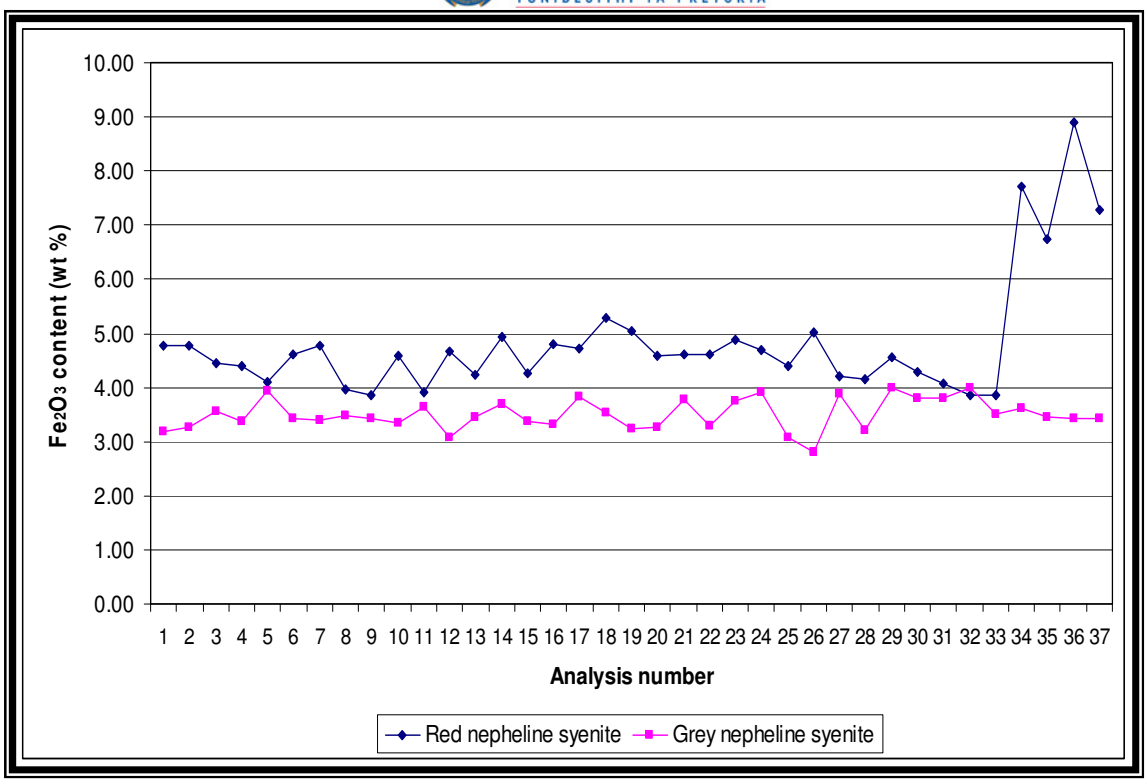

Figure 55. Variation of Fe_2O_3 content of the nepheline syenites at Mamelodi Quarries.

6.5 Electron microprobe analysis

The electron microprobe analysis (EMPA) was focused on analysing the following elements: Si, Fe, Al, Mg, Ca, Na, K, and Cl. Three samples were analysed to evaluate the mineral concentrations for the nepheline concentrate from the non-magnetic fraction of the wet magnetic separation (RNMP4), the light fraction (nepheline concentrate) of the screened ROM sample (SRL1), and the starting material for all the different separation tests (ROM 1).

The minerals analysed with the EMPA were aegirine, albite, microcline, nepheline, and sodalite (for detailed microprobe results see Appendix 3). Backscattered electron images of the different minerals (obtained using the SEM) provided additional spatial information of the iron mineral inclusions in nepheline, albite, and microcline. Only mineral totals between 97 wt % and 102 wt % were used. All the mineral analyses from the different samples (RNMP4, SRL1, and ROM 1) were very similar to each other and are thus plotted together. The elemental wt % is used for

ternary plots and is normalised to 100. Cations calculated for mineral formulas are normalised to 100 for ternary plots.

For comparison of the results, mineral compositions from two other nepheline syenites (Woolley et al. 1995; Nude et al. 2009) are used here, in order to test whether the values obtained in this study are comparable to EMPA data from other similar deposits.

6.5.1 Aegirine

Aegirine was analysed to provide information on the iron concentration, as well as Na content in this mineral. The average formula for the composition of the aegirine analyses is: $Na_{0.960}Fe_{1.022}Si_{2.029}O_6$ compared to the ideal formula of Deer et al. (1997) which is $NaFe[Si_2O_6]$ (Figure 56). Figure 57 provides a ternary plot of Fe, Na and (K+Ca). The different analyses indicate that the aegirine compositions do not show much variance. There is a close relationship between published data for aegirines from Deer et al. (1978) and the analyses of this study (Figure 57). Plotting Fe+Ca versus Al+Na, using data from Deer et al. (1978) and aegirine from the ROM, results in a negative correlation, which implies partial coupled substitution between Al and Fe. However, other analyses of the ROM sample do not follow this trend. This implies that a more complex relationship between Al and Fe exists, possibly reflecting different assemblages or stages in the crystallisation of the nepheline syenite or that the Fe occurs in different oxidation states (i.e., only some of the Fe can be replaced by Al). Figure 58 presents a binary plot of Al+Na against Fe+Ca. The scatter possibly implies that both Fe^{2+} and Fe^{3+} occur in the aegirine.

The presence of Ca in minor amounts is expected, as Ca can substitute for Na, probably in coupled substitution with Al for Fe (Figures 58 and 59). The aegirine analysed in this study contains slightly higher Fe contents as compared to the published data from Deer et al. (1978) (see Appendix 3 for the Al, Fe and Ca contents).

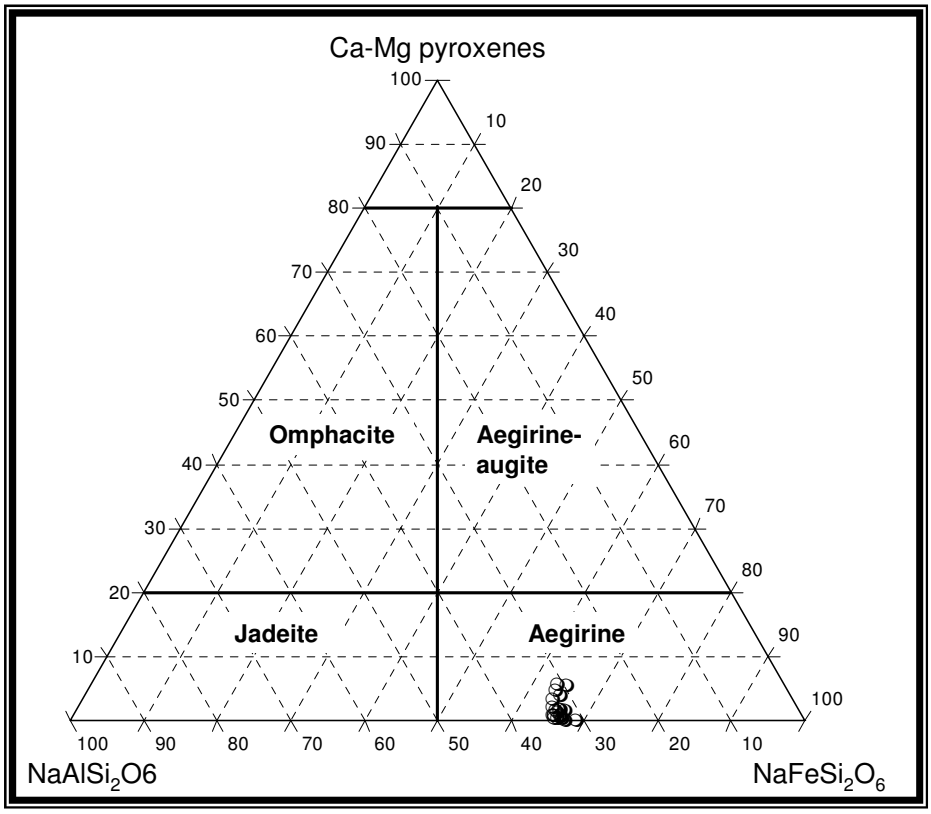

Figure 56. Ternary diagram of Ca-Mg pyroxenes - NaAlSi2O6 – NaFeSi2O6 containing the cations calculated from the EMPA data for aegirine in this study.

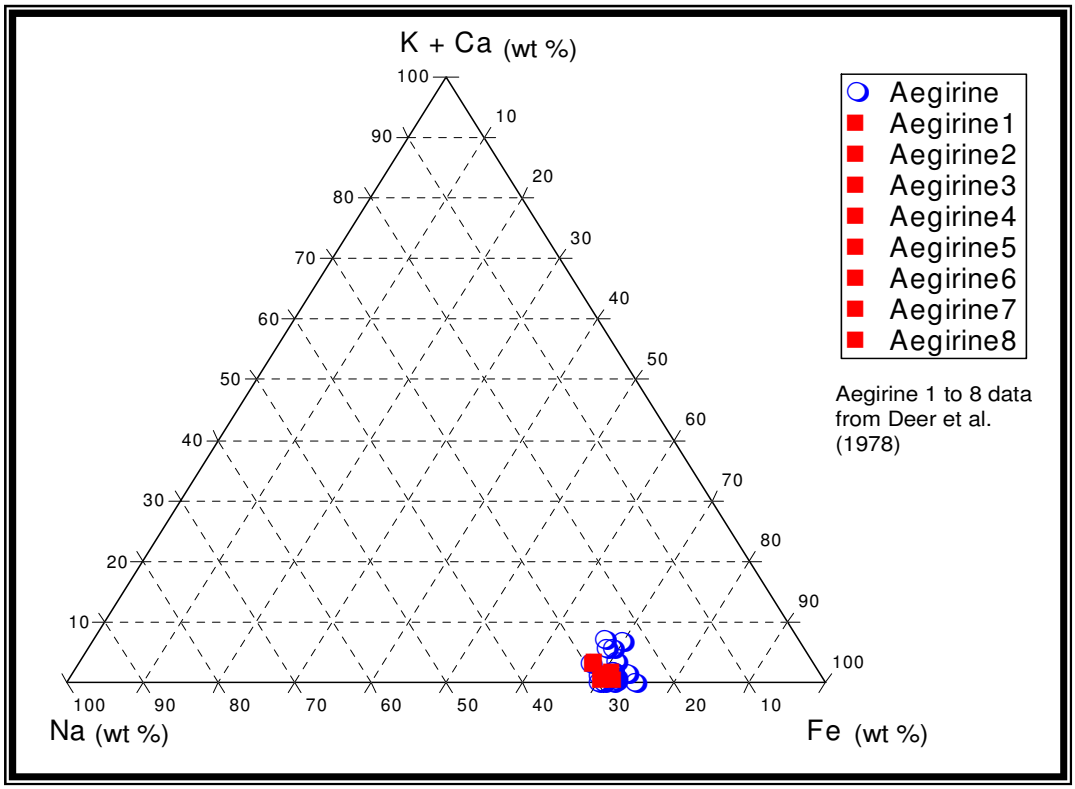

Figure 57. Ternary diagram of (K+Ca)-Na-Fe showing the composition of aegirine as determined by EMPA in this study as well as published data for aegirine by Deer et al. (1978).

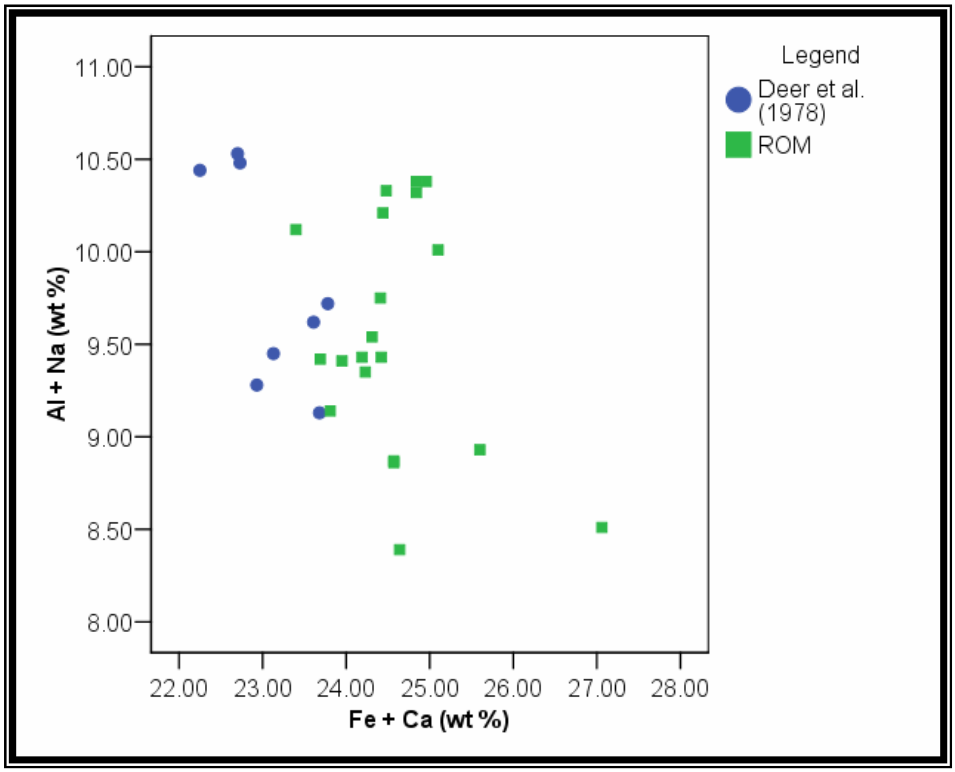

Figure 58. Binary diagram of Al+Na versus Fe+Ca for the aegirine analyses as determined by EMPA as well as published data by Deer et al. (1978).

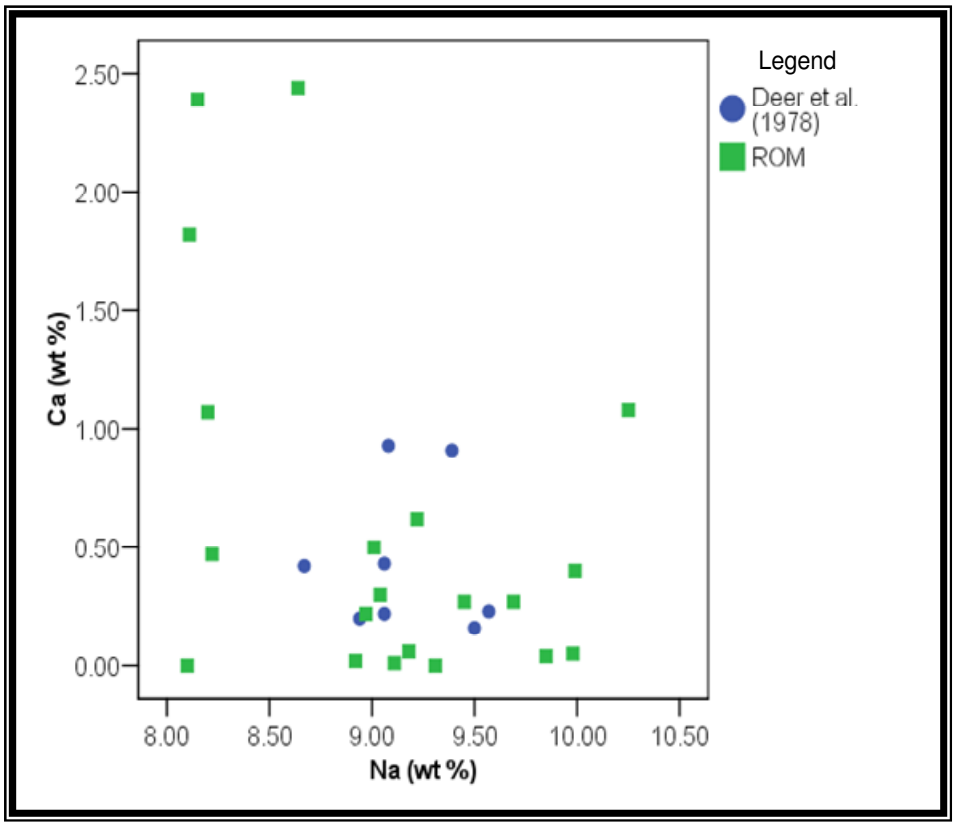

Figure 59. Binary diagram of Ca versus Na for the aegirine analyses as determined by EMPA as well as published data by Deer et al. (1978).

6.5.2 Albite and Microcline

The two feldspars analysed in the sample are albite and microcline. The calculated cations for the mineral formulae for albite and microcline are plotted in Figure 60. The comparison of elemental wt % for both feldspar minerals and data from Deer et al. (1997) are plotted in Figure 61. Albite and microcline occur in solid solution (Deer et al. 1997). The Na contents in microcline range from a minimum of 0.03 wt % to a maximum of 0.96 wt %, whereas albite contains K in the range of 0.11 wt % to 1.08 wt %. The maximum Fe content observed in the feldspar minerals is 0.3 wt %. This will influence the Fe concentration in the final nepheline concentrate. As with the aegirine compositions, the compositions of the feldspars from other nepheline syenites (Woolley et al. 1995; Nude et al. 2009) are similar to those in this study (Figure 61).

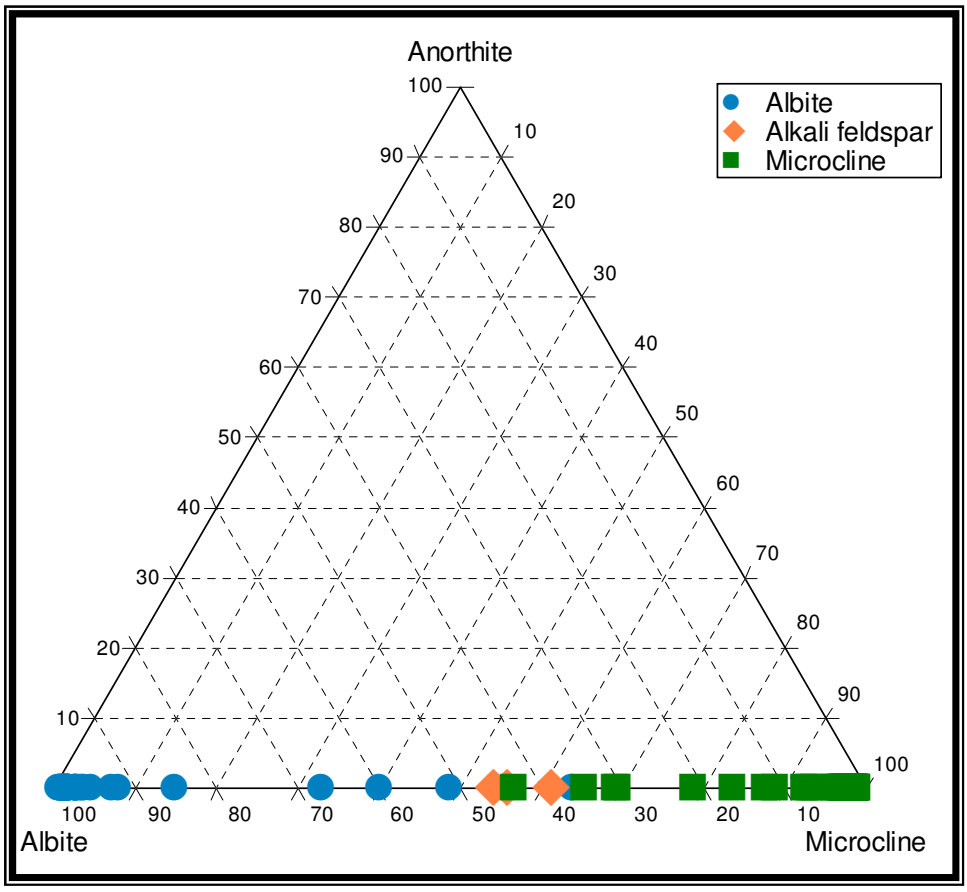

Figure 60. Ternary diagram of anorthite – albite – microcline showing cation proportions for albite and microcline compositions in this study calculated from the EMPA data.

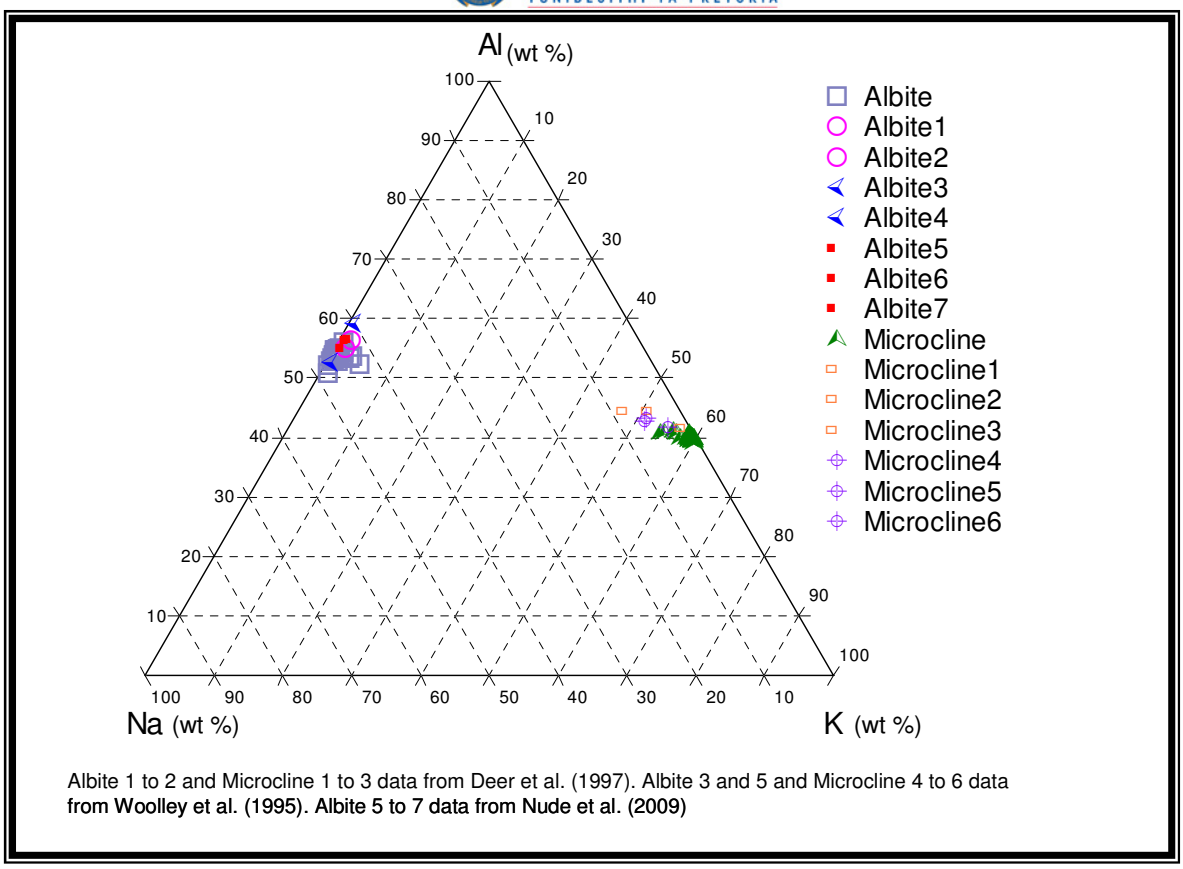

Figure 61. Ternary diagram of Al-Na-K showing the comparison of albite and microcline as determined by EMPA in this study as well as published data by Deer et al. (1997), Woolley et al. (1995) and Nude et al. (2009).

6.5.3 Nepheline

The EMPA analyses for nepheline are reported in Appendix 3. A ternary plot using normalised Na, Fe, and K is shown in Figure 62. All the nepheline analyses contained Fe in minor amounts (ranging from 0.28 wt % to 0.94 wt %; see Appendix 3 for values). The Fe content in the nepheline is high and thus will influence the total iron content in the final nepheline concentrate.

6.5.4 Sodalite

A normalised ternary plot of Al, Na, and Cl is shown in Figure 63. The composition of the analysed sodalite does not vary greatly and compares well with the published data (Figure 63).

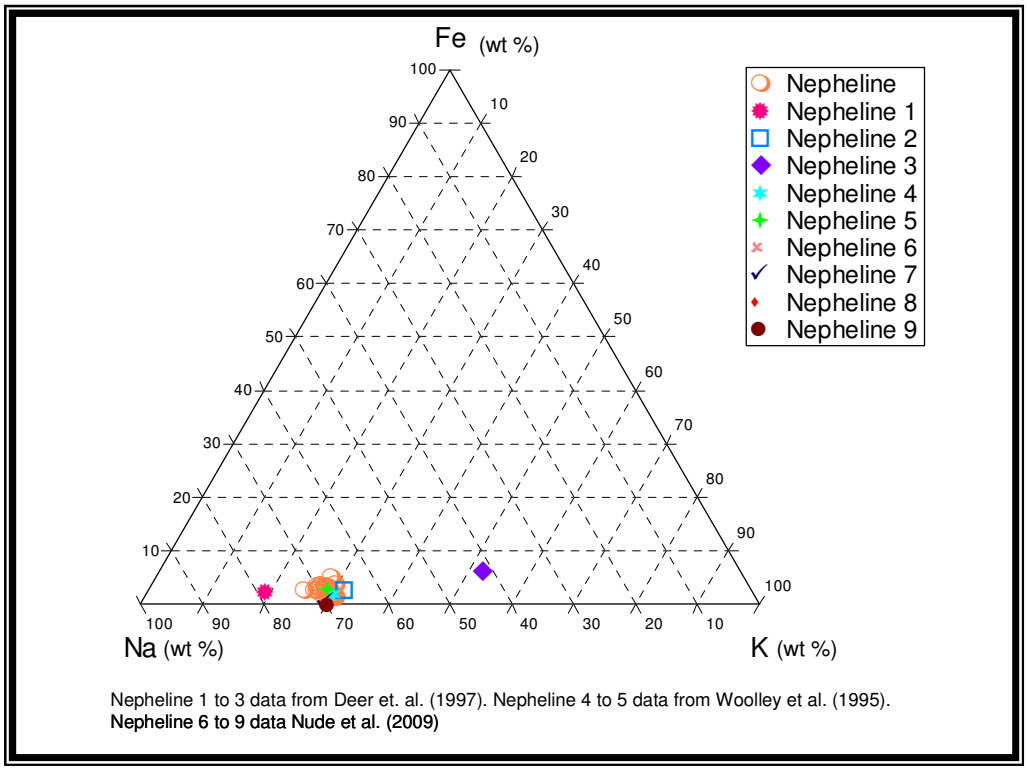

Figure 62. Ternary diagram of Fe-Na-K showing the composition of nepheline as determined by EMPA in this study as well as published data by Deer et al. (1997), Woolley et al. (1995), and Nude et al. (2009)data.

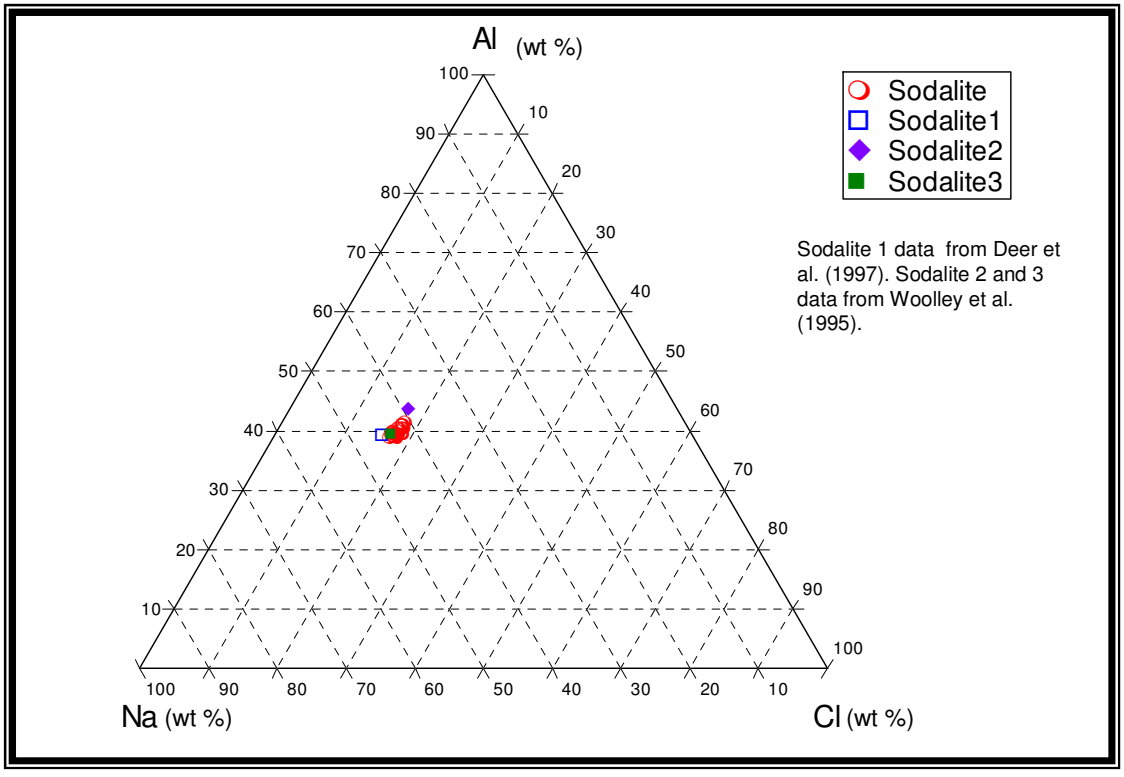

Figure 63. Ternary diagram of Al-Na-Cl showing the composition of sodalite as determined by EMPA in this study as well as published data by Deer et al. (1997) and Woolley et al. (1995).

6.5.5 Backscattered electron images

Figures 64 to 66 present backscattered electron images of two selected samples used for the EMPA for the ROM crusher sand (ROM1) and the light fraction of the screened ROM spiral test (SRL1). The important observation for both samples is the occurrence of small inclusions of ilmenite, zircon, and aegirine in the feldspar minerals and nepheline (Figures 64 to 66). Analcime is mostly associated with nepheline, albite, and microcline. Analcime occurs in two textural settings:

a) rare monomineralic grains
b) common intergrowths with nepheline, albite and microcline

Sodalite commonly occurs as monomineralic grains. Iron-rich minerals inclusions are observed in albite, microcline, and nepheline. Aegirine, occurs as needle-like to bleb-like inclusions locked in albite, microcline, and nepheline crystals, and as discrete mineral grains (Figures 64 to 66).

Ilmenite ($FeTiO_3$) mostly occurs as small inclusions (µm scale) in albite, microcline, and nepheline, but also as discrete grains (indicated in the petrographic study). The implications of these inclusions in the Na, K, and Al-rich minerals will be discussed in Chapter 7.

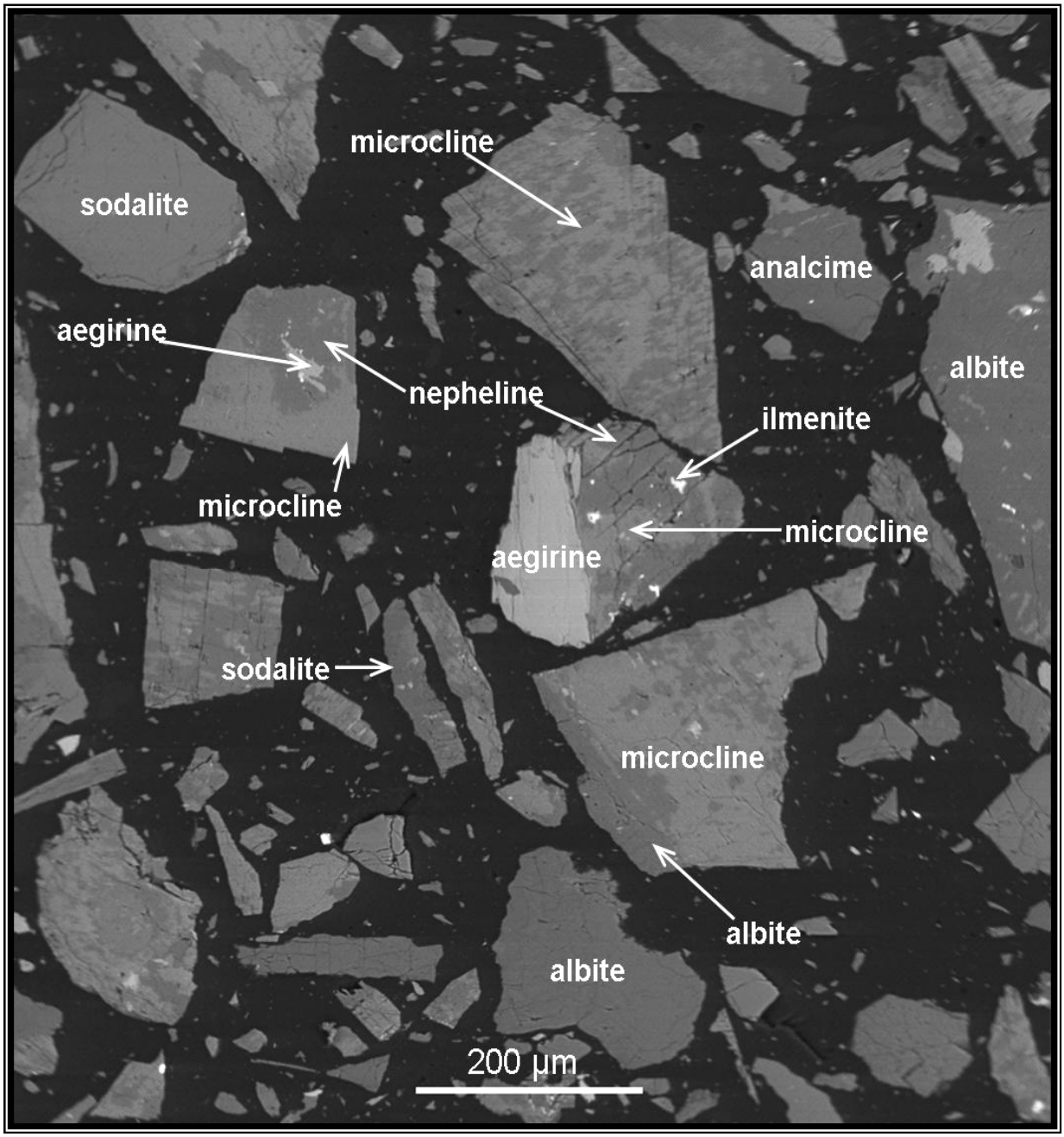

Figure 64. Backscattered electron image showing the different minerals within the ROM crusher sand (ROM 1) used for the microprobe analysis. Width of scale bar = 200 µm.

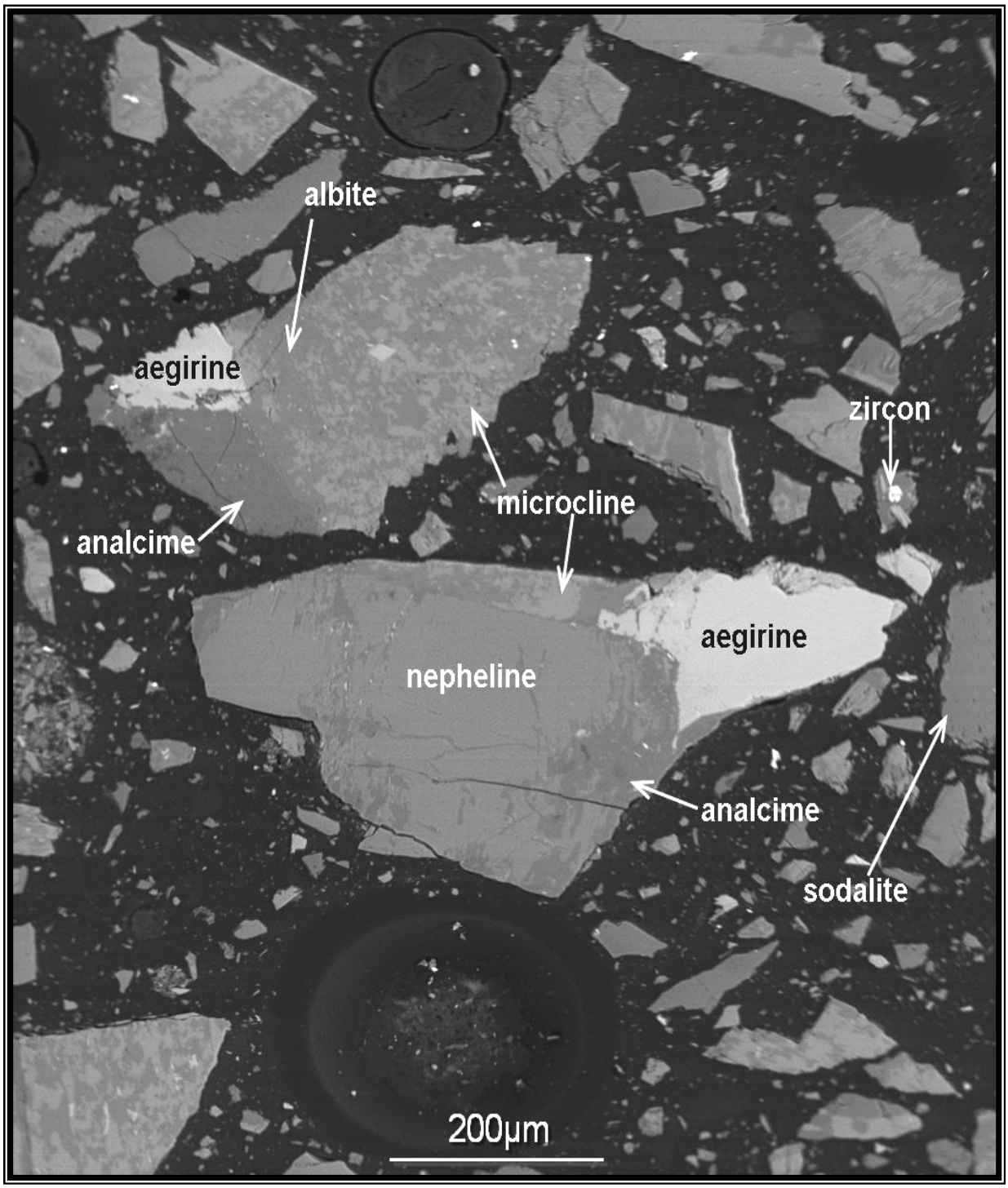

Figure 65. Backscattered electron image showing the different minerals for the light fraction of the screened ROM spiral test (SRL1) used for the microprobe analysis. The holes observed are due to polishing effects; width of scale bar = 200 µm.

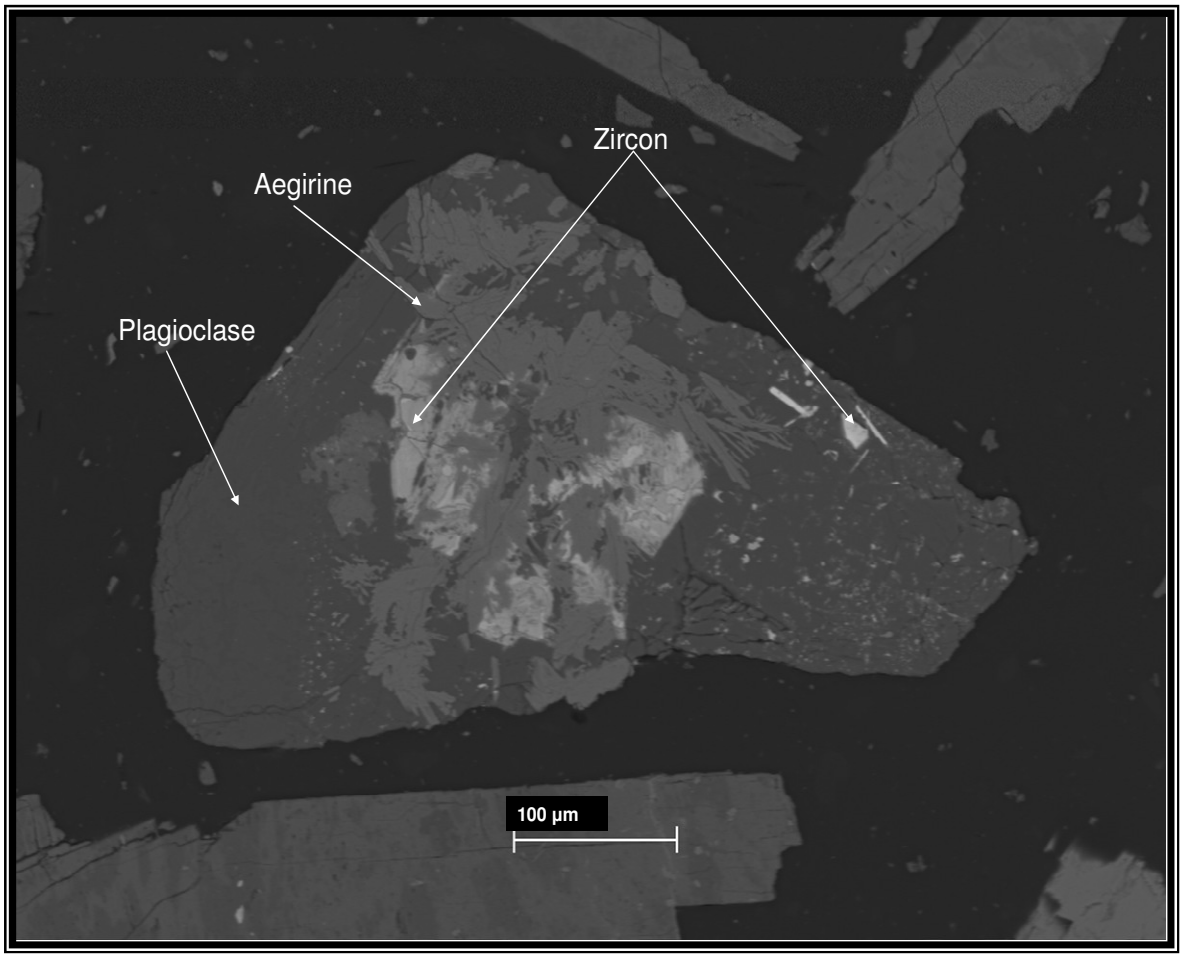

Figure 66. Backscattered electron image of albite mineral grains with aegirine and zircon intergrowths (ROM1 sample). Width of scale bar = 100 µm.

7 INTERPRETATION AND DISCUSSION

7.1 Petrographic results - alteration

Only the grey nepheline syenite (crushed ROM, ROM-1 and ROM-2) will be discussed as it is the focus of this study. In the nepheline syenite the mineral assemblage includes albite, microcline, and nepheline. These minerals are most susceptible to hydrothermal alteration. Therefore, the presence of sodalite and zeolite (chabazite) is an indication that alteration took place. The quantities detected by XRD for these minerals are 4.84 wt % for sodalite and 0.68 wt % for chabazite (Table 21). The formation of sodalite can take place from albite and nepheline in the presence of NaCl-containing fluids (Drüppel et al. 2005). The two reactions that occur according to Drüppel et al. (2005) are:

$$6Na[AlSi_3O_8] + 2NaCl \rightarrow Na_8[Al_6Si_6O_{24}]Cl_2 + 12SiO_2 \text{ (aqueous solution)}$$
albite sodalite

$$6Na_4[Al_4Si_4O_{16}] + 8NaCl \rightarrow 4Na_8[Al_6Si_6O_{24}]Cl_2$$
nepheline sodalite

The quantity of analcime as detected by XRD is 23.75 wt %. Analcime (analcite) is chemically a zeolite but is the only zeolite to crystallize as a primary mineral in igneous rocks, and therefore has a paragenesis similar to that of the feldspathoids (Passaglia and Sheppard 2001). This indicates that analcime probably formed as a primary mineral, but can also be a product of alteration of nepheline (i.e., a secondary product). The distinction between magmatic and hydrothermal analcime cannot easily be made when analcime occurs as interstitial grains (Deer et al. 1997). The backscattered electron images (Figures 64 to 66) clearly show both large crystals of analcime (Figure 64), but also grains where it is associated with nepheline (Figure 65). Therefore, analcime is considered both a primary mineral phase, as well as the product of hydrothermal alteration of nepheline. Textural differences between the primal and alteration analcime is easily distinguished.

Alteration analcime would occur on the edges of grains together with nepheline and where it replaces nepheline the original crystal structure of nepheline is retained as seen in (Figure 37).

Actinolite, as detected by quantitative XRD in amounts of 0.75 wt % (Table 21), has also been identified as an alteration product of the pyroxene minerals (Deer et al. 1997).

7.2 Variation of total iron content in the Franspoort Nepheline syenite

The concentration of Fe_2O_3 varies across the nepheline syenite deposit mined at Mamelodi Quarries (Figure 55). The high Fe_2O_3 (ranging from 3.85 wt % to 8.90 wt %) content in the red nepheline syenite is due to an increase of pyrite and iron containing silicates. The variation is large and eliminates the red nepheline syenite as material for the glass and ceramic industry. The variation in the grey nepheline syenite (ranging from 2.80 wt % to 3.99 wt %) is more reasonable for attempting to lower the Fe_2O_3 content.

7.3 Petrographic results – iron mineral inclusions in the different alkali-containing minerals

The different minerals that carry iron in the grey nepheline syenite are: aegirine ($NaFeS_2iO_6$), aegirine – augite ($(NaCa)(FeMg)Si_2O_6$), ilmenite ($FeTiO_3$), magnetite (Fe_3O_4) and pyrite (FeS_2). These minerals occur as discrete crystals, but also as inclusions in albite, microcline and nepheline (evidenced in both the photomicrographs and SEM images; Figures 30, 32, 64 - 66). The size of these inclusions varies from ~1 µm up to ~1 mm (Figures 30, 32, 64 - 66). The size of these inclusions does not allow them to be separated from the host minerals, even with fine milling, and this will cause the iron content in the final nepheline product to be always above 0.05 wt %. The feldspar and nepheline minerals also contribute to

the iron budget. The iron concentration for nepheline products as produced by the different tests is thus undesirable for the glass and ceramic industry.

7.4 Size distribution and influence of different milling tests

The size distribution of the minerals is important, as the different separation tests require specific size ranges to obtain optimum separation conditions. Therefore, the sizing results for the three milling methods were of importance to select a starting material for use in all of the separation tests.

The laboratory mill used at UP to mill a ROM sample produced a size distribution with top size of 250 µm (1 mass %) and 52 mass % of the material was smaller than 75 µm. The ROM sample milled with a ball mill at Mamelodi Quarries had a top size of 425 µm (33 mass %) and 22 mass % of the material was smaller than 75 µm. The coarser crusher sand used by Martins (1999) had a top size of 2360 µm (9 mass %) and only 16 mass % of the material was smaller than 150 µm.
Table 27 provides the different size requirements for each of the different separation tests performed. The particle size requirements for each of the separation tests are important in selecting the appropriate starting material. The particle size range produced with the laboratory mill at UP, and the ball mill at MQ, were too fine, and therefore not suitable as a starting material. The coarse crusher sand produced by MQ and used by Martins (1999), consists of coarser material and not as much fines and was thus chosen as the starting material for the different tests, because it met more of the size requirements for the different separation tests.

Table 27. Size requirements of material used for the different separation tests.

Separation method	Maximum size (top size)*	Minimum size (bottom size)*
High-intensity wet magnetic separation	5 mm	20 µm
Low-intensity dry magnetic separation	2 mm	75 µm
Heavy liquid separation	4 mm	50 µm
Spiral separation	3 mm	75 µm

* Wills (1997)

7.5 Geochemistry: Major and trace element analyses (Determined by X-ray fluorescence)

As the same material was used in all the separation tests, it is possible to examine all the geochemical data together. The correlation matrix is used to confirm the trends observed in the geochemical data for each test and to confirm the element associations for the different minerals.

The two correlation coefficients described are the Pearson product moment coefficient of correlations (r) and Spearman's rank correlation coefficient (r_s). "Pearson is a measurement of the strength of the linear relationship between two variables x and y" (McClave and Sincich 2003) and is used to describe the correlation for normally distributed data.

The coefficient is calculated for a sample with *n* data points for variables x and y as follows :

$$r = \frac{\sum XY - \frac{\sum X \sum Y}{n}}{\sqrt{(\sum X^2 - \frac{(\sum X)^2}{n})(\sum Y^2 - \frac{(\sum Y)^2}{n}}}$$

The Spearman's rank correlation coefficient r_s provides a measure of correlation between ranks and is used for correlation between any pair of variables and the observation is done on the ranking of the pair (McClave and Sincich 2003). The coefficient is calculated (McClave and Sincich 2003) as follows:

$$r_s = 1 - \frac{6\sum (X_i - Y_i)^2}{n(n^2 - 1)}$$

The correlation coefficient is scale-less and assumes a value between -1 and +1 (McClave and Sincich 2003). A coefficient value of 0 is an indication that there is no

linear relationship between the x and y variables. The closer the coefficient value is to +1 indicates a direct or positive correlation between the variables, whereas -1 indicates an inverse or negative correlation.

The dataset produced in this study is not normally distributed and consists of a small amount of data points (n = 37) and, therefore, the non-parametric statistical correlation matrix (Spearman (r_s)) was calculated for the complete XRF dataset (see Appendix 4 for the correlation matrix).

The major elements of interest are Fe, Ti, Al, Mg, Ca, Na, and K. The nepheline concentrate should contain the elements Al, Ca, Na, and K. Therefore, the relationship between these elements was investigated, because Fe and Ti are undesired elements in the nepheline product. Pearson correlation coefficients (r) and Spearman correlation coefficients (r_s) are provided for the different graphs plotted in Figures 67 and 68, and include the upper and lower 95 % confidence limits for the mean of the data points. It should be noted that for the dataset in this study r_s is more reliable than r.

Iron content is positively correlated with TiO_2, MgO, and CaO, whereas Fe_2O_3 shows a negative relationship with Al_2O_3 and K_2O. The relationship between Fe_2O_3 and Na_2O is slightly negative (Figure 67). The correlation graph of Al_2O_3 with MgO, CaO, Na_2O, and K_2O is plotted in Figure 68. A strong negative relationship is observed between Al_2O_3 and MgO, as well as CaO, whilst there is a positive correlation between Al_2O_3, Na_2O, and K_2O. The Spearman correlation coefficient values are plotted in Figures 69 and 70. The correlation coefficient values are only an indication of a positive or negative relationship between different elements and confirm the relationships observed in Figures 67 and 68.

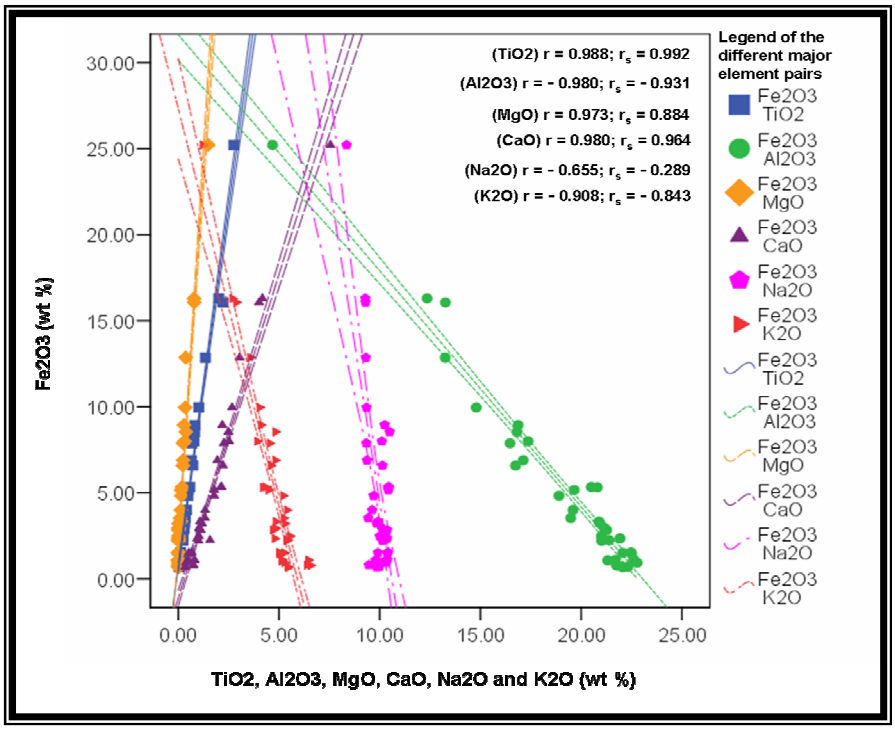

Figure 67. The correlation graph for Fe_2O_3 with TiO_2, MgO, CaO, Na_2O and K_2O; r and r_s are indicated for each element pair, include the upper and lower 95 % confidence limits for the mean of the data points.

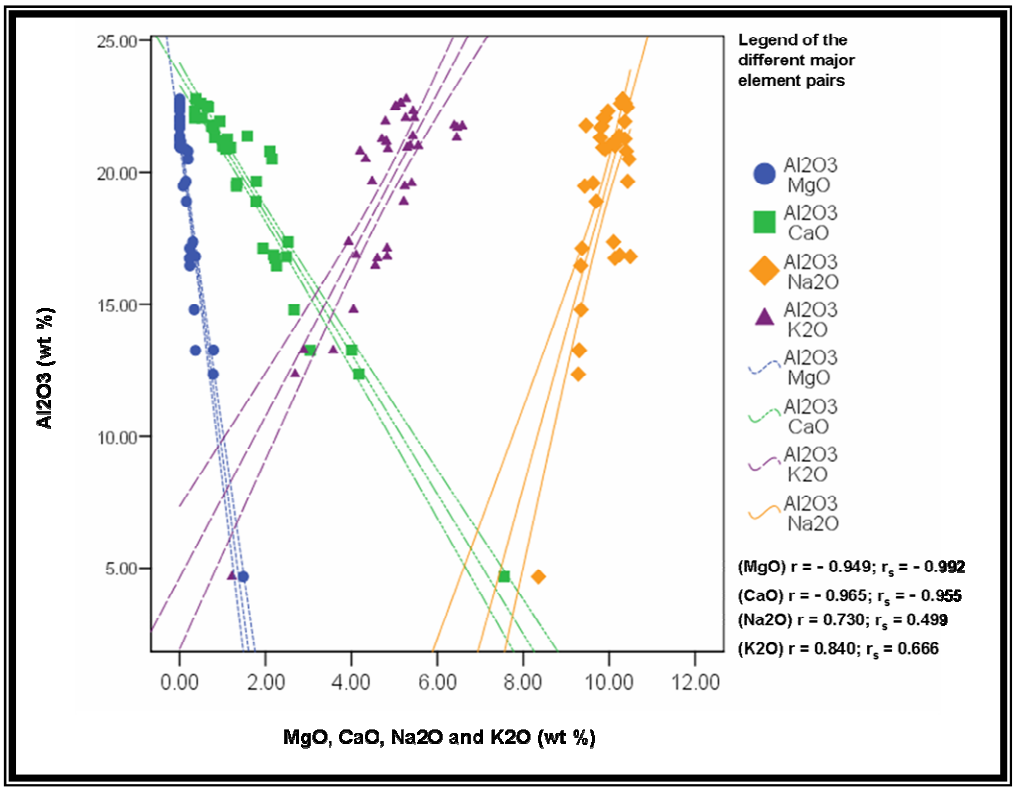

Figure 68. correlation graph for Al_2O_3 with MgO, CaO, Na_2O, and K_2O; r and r_s are indicated for each element pair, include the upper and lower 95 % confidence limits for the mean of the data points.

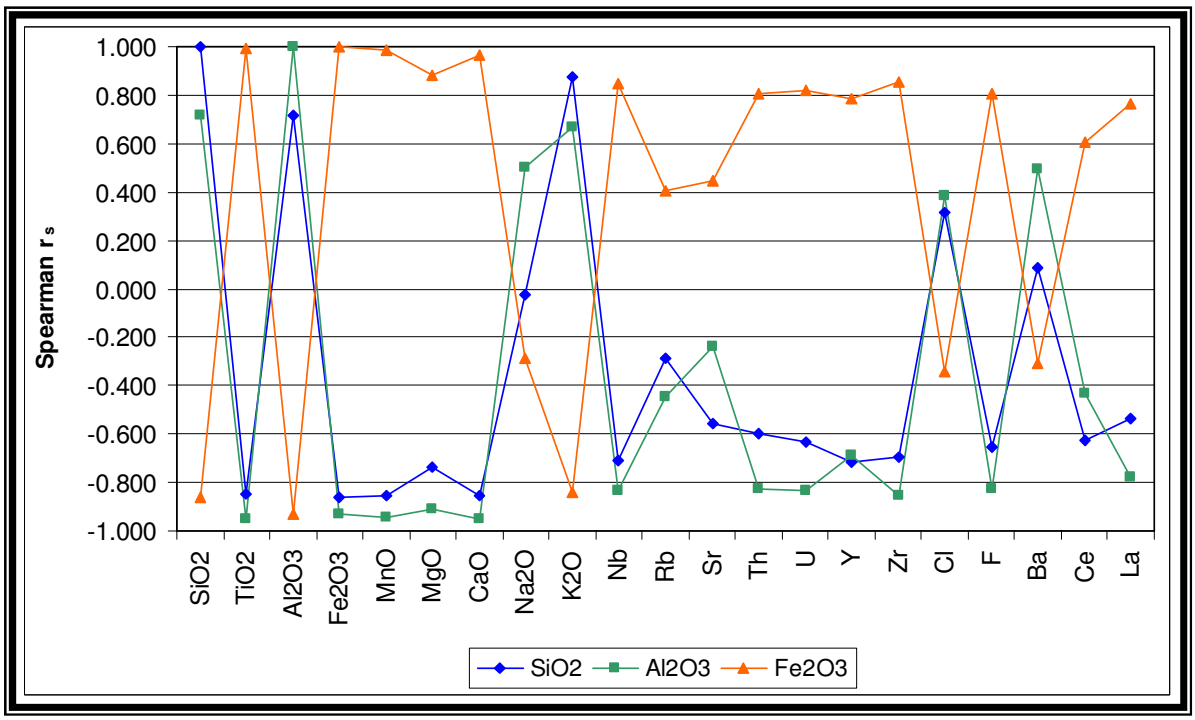

Figure 69. Binary graph showing the Spearman correlation coefficients for SiO_2, Al_2O_3, and Fe_2O_3 with all other elements.

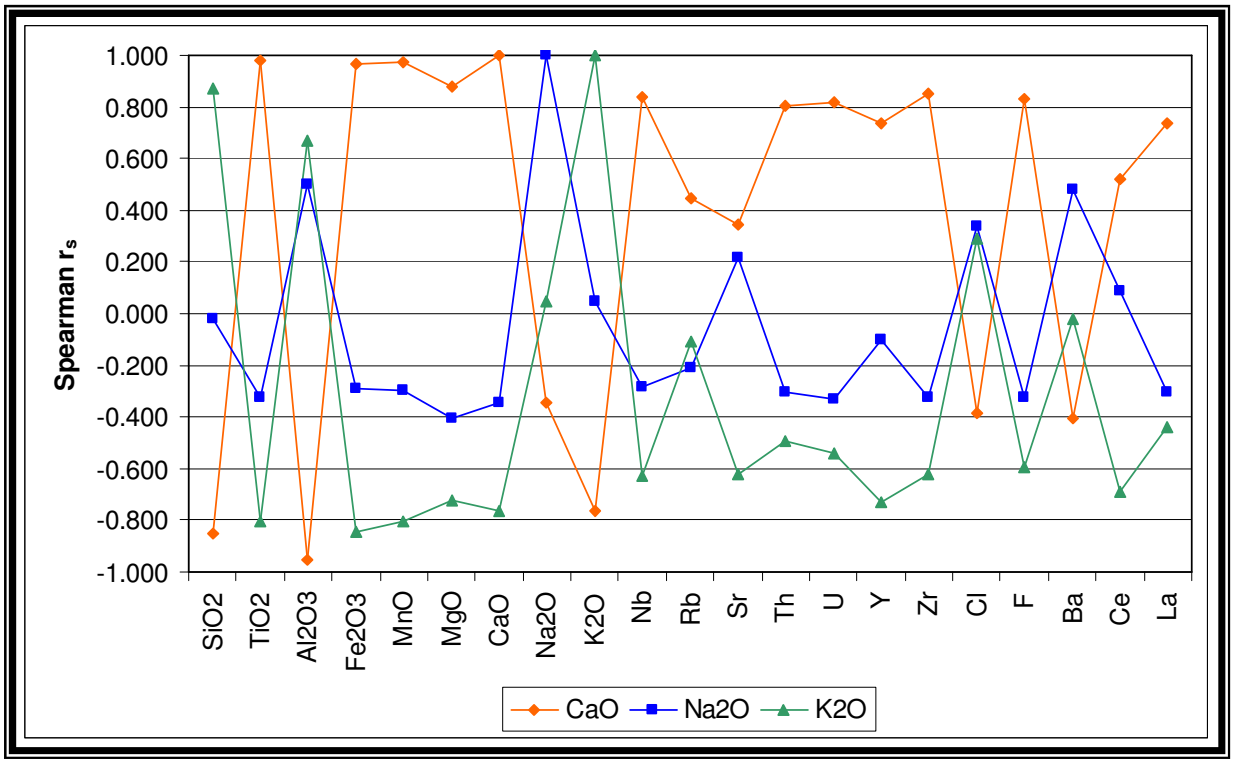

Figure 70. Binary graph showing the Spearman correlation coefficients for CaO, Na_2O, and K_2O with all other elements.

The correlations observed between the different elements are an indication that specific minerals are controlling the occurrence of the different elements. A binary plot representing the relative importance of ilmenite and aegirine is presented in Figure 71. Titanium are controlled by aegirine, with a smaller effect from ilmenite (Figure 71). Ilmenite and aegirine are concentrated in the heavy fraction (HLRH) of the heavy liquid separation, the first magnetic fractions (RMAGS1T1 and RMAGS1T2) for both the dry magnetic test and the dense fractions of the spiral separation for the screened (SRD1) and unscreened tests (URD 1; Figure 71).

The relationship of Fe with Ca is controlled by both aegirine and aegirine – augite, which occur as a solid solution series (Deer et al. 1997; Figure 72). Based on this diagram, aegirine and aegirine – augite contribute to roughly equal amounts to this relationship between Ca and Fe.

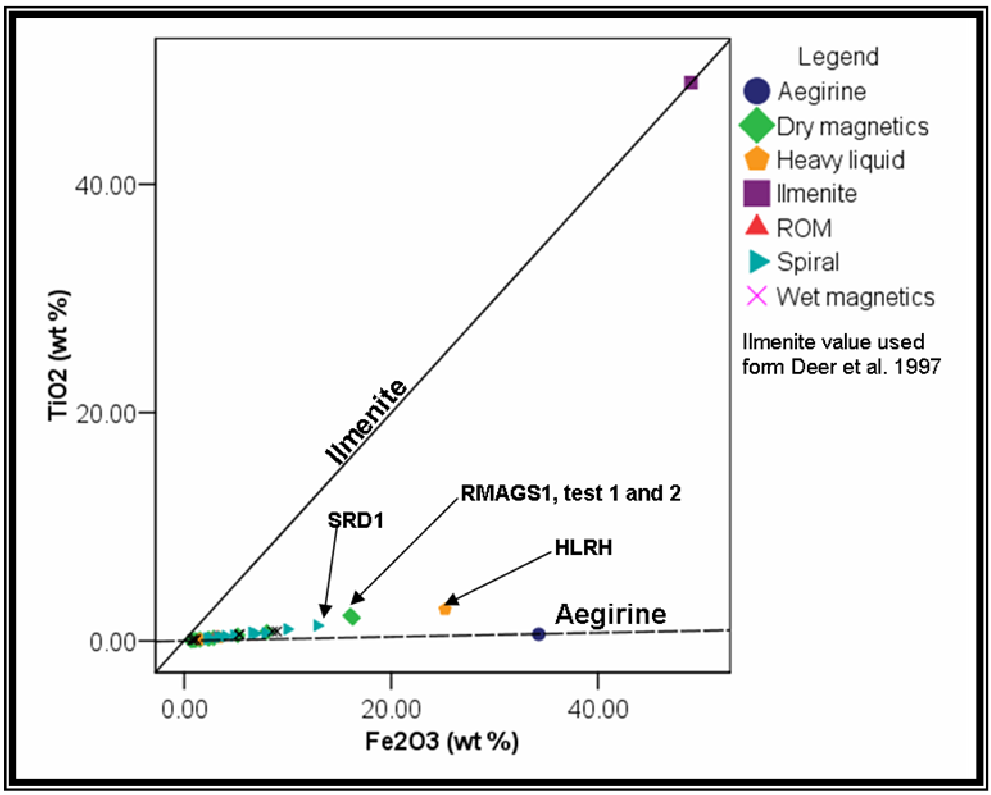

Figure 71. Binary graph showing the influence of ilmenite and aegirine on the relationship between TiO_2 and Fe_2O_3. For abbreviations, see Table 26.

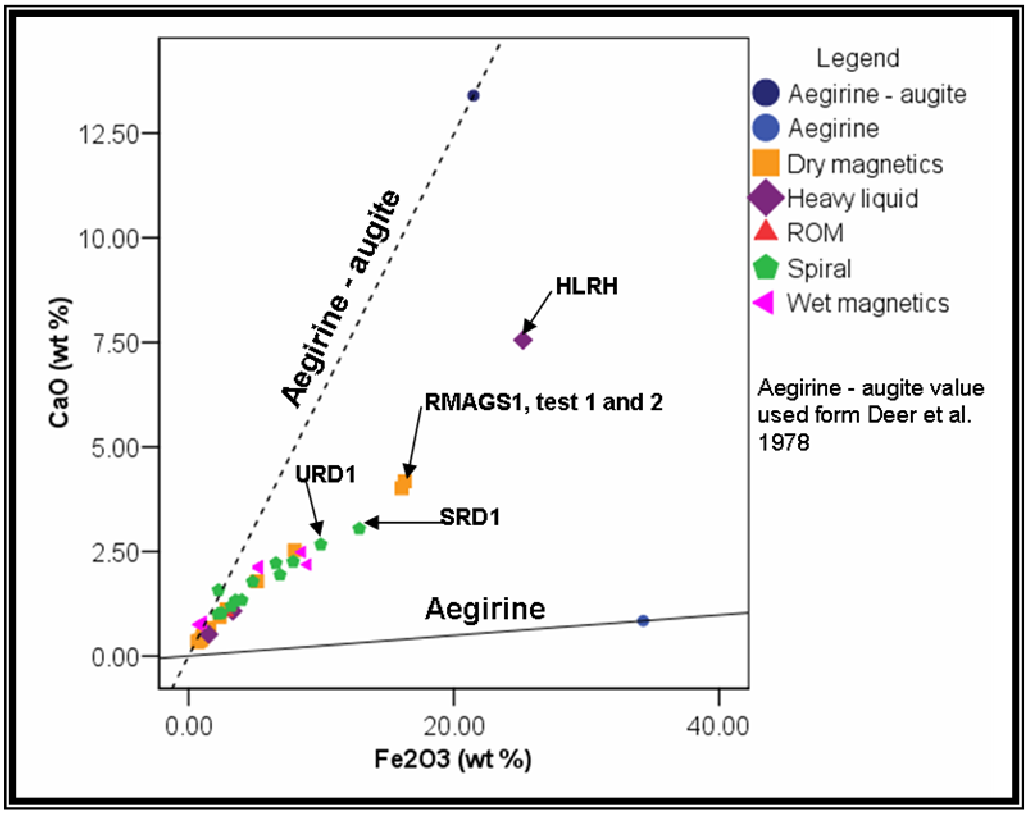

Figure 72. Binary graph showing the influence of aegirine – augite and aegirine on the relationship between CaO and Fe_2O_3. For abbreviations, see Table 26.

A binary plot for Na_2O and Fe_2O_3 is presented in Figure 73. If a specific mineral controlled Na, it would follow that mineral trend, but the graph reflects the occurrence of complex mixtures (Figures 67 and 69). The relationship between Na_2O and Al_2O_3 provides a explanation of the controlling minerals of Na_2O (Figure 74). It is clear that Na_2O contents are controlled by a combination of nepheline, albite, and sodalite (Figure 74), whereas K_2O contents are strongly controlled by microcline and predominantly nepheline (Figure 75) in accordance with the XRD data (Table 21).

The observation made with regard to the controlling minerals for the major elements is applied to the trace elements to determine the occurrence of the different trace elements in the different minerals. The trace elements Nb, Rb, and Sr were added together and compared with the different major elements (Figure 76). A positive correlation is observed between the trace elements Nb+Rb+Sr and CaO, as well as Fe_2O_3 which are the controlling elements for aegirine and aegirine – augite, whereas there is a negative correlation between Nb+Rb+Sr and Al_2O_3 as well as K_2O which reflects the feldspars.

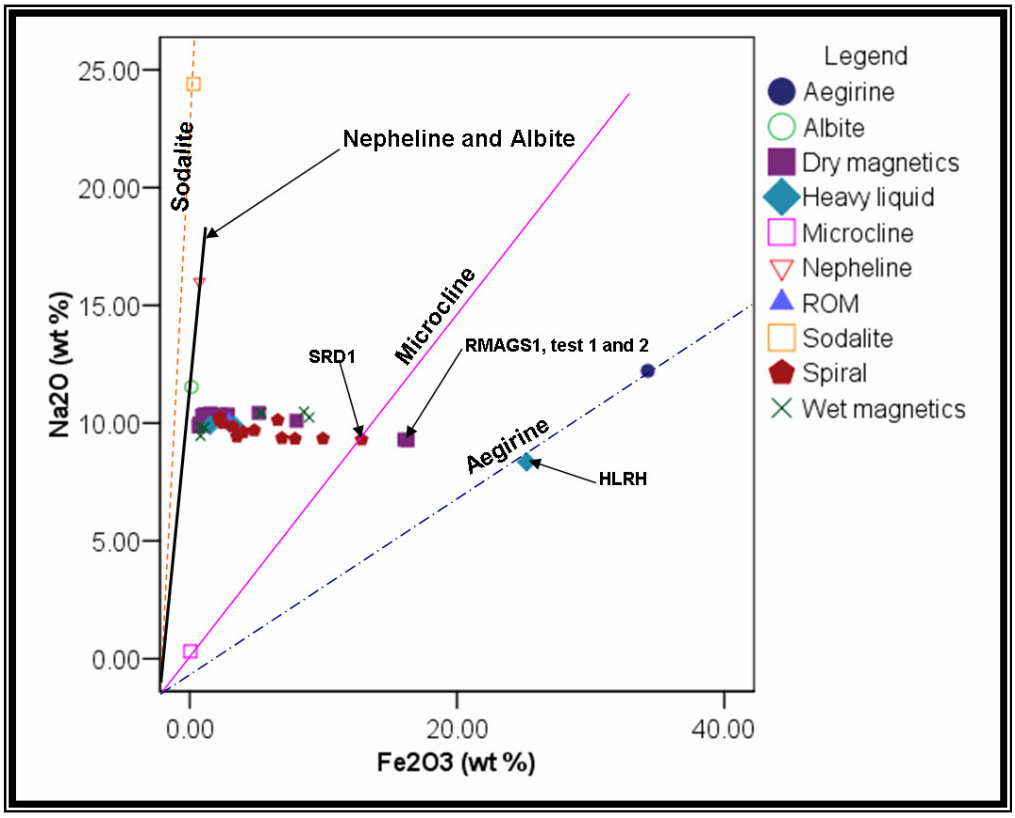

Figure 73. Binary graph showing the influence of aegirine, microcline, nepheline, albite and sodalite on the relationship between Na_2O and Fe_2O_3. For abbreviations, see Table 26.

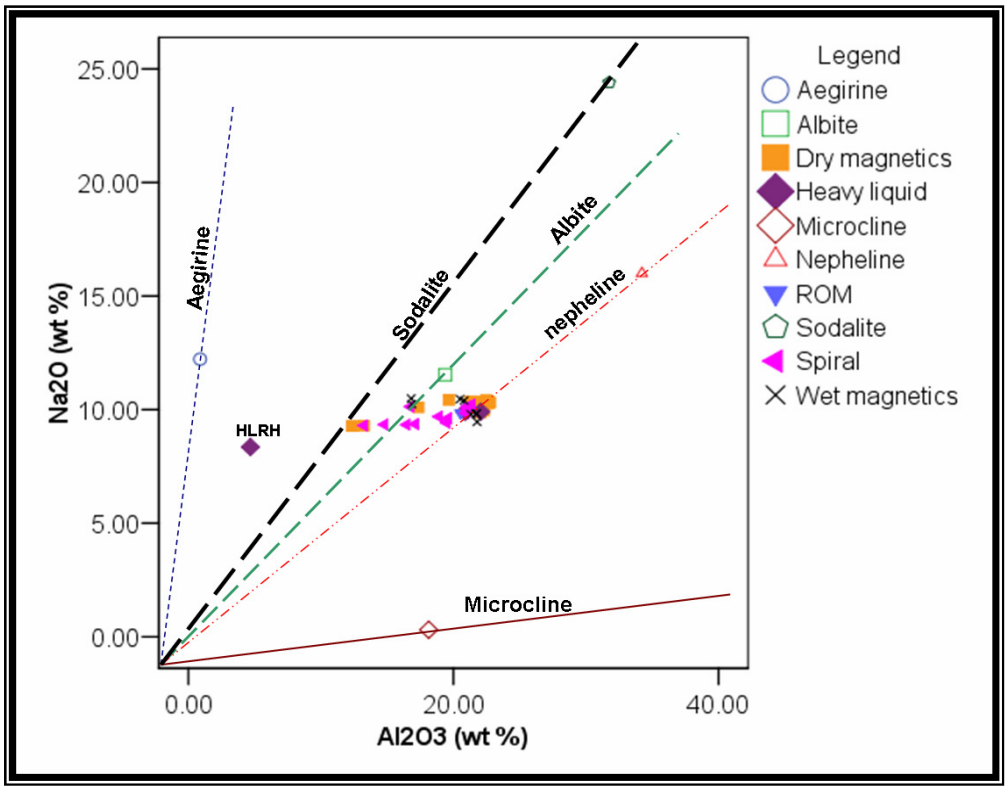

Figure 74. Binary graph showing the influence of aegirine, microcline, nepheline, albite, and sodalite on the relationship between Na_2O and Al_2O_3. For abbreviations, see Table 26.

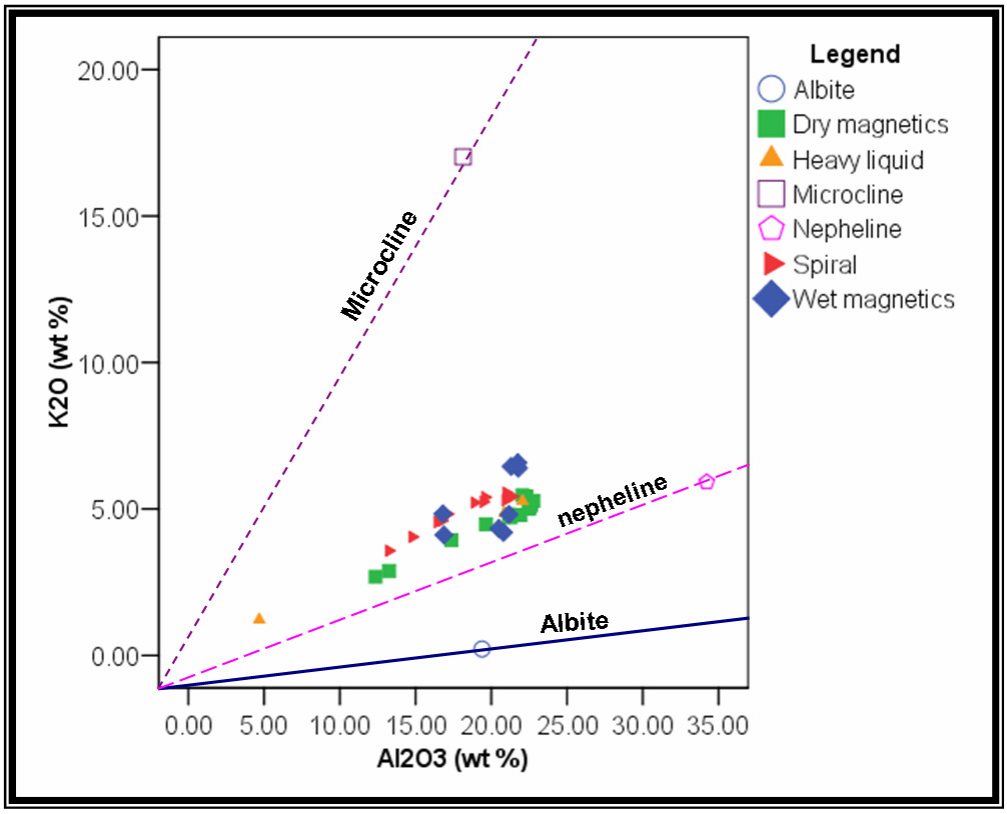

Figure 75. Binary graph showing the influence of aegirine, microcline, nepheline, albite, and sodalite on the relationship between K_2O and Al_2O_3.

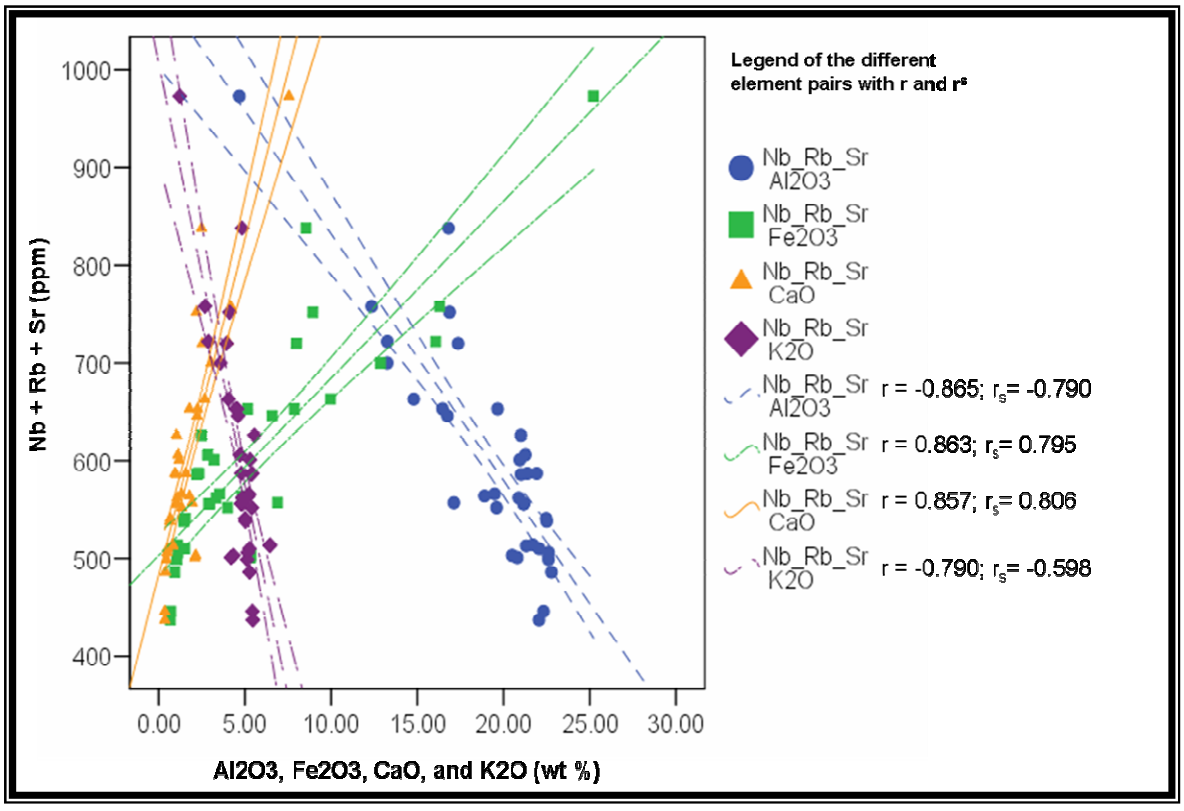

Figure 76. Binary graph showing the influence of the different relationships of selected major elements with Nb+Rb+Sr. See text for explanation.

Thorium, U, and Y occur in zircon and fluorite (Figure 77). A positive correlation is observed with Zr and F and this indicates that Th, U and Y substitute for other elements in trace amount. The two data points (RMP1 and RMP2 from the wet magnetic separation) imply intergrowths of zircon and fluorite with a magnetic host.

The trace element Ba is present in small quantities (less than 2 wt %) in the majority of feldspars (Deer et al. 1997). The binary plot presented in Figure 78 does not indicate this clearly, although there is a slight positive correlation with Na_2O and Al_2O_3 (see Appendix 4 for correlation matrix values) and can be an indication that Ba in this study can occur in albite.

Cerium and La provide proxy elements for the behaviour of the rare earth elements in the different minerals. The Spearman correlation values for these two elements are plotted in Figure 79. A binary plot of Ce with the selected major elements CaO, Na_2O and K_2O is presented in Figure 80.

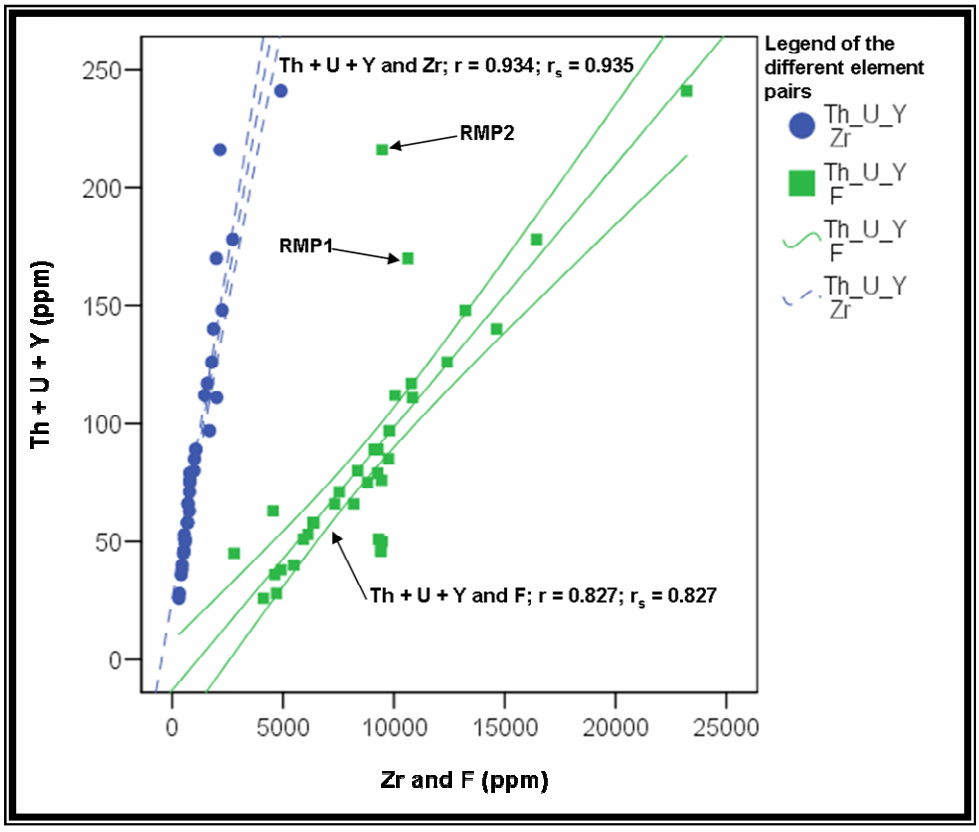

Figure 77. Binary graph showing the influence of the different relationships of Zr and F with Th + U + Y. See text for explanation. For abbreviations, see Table 26.

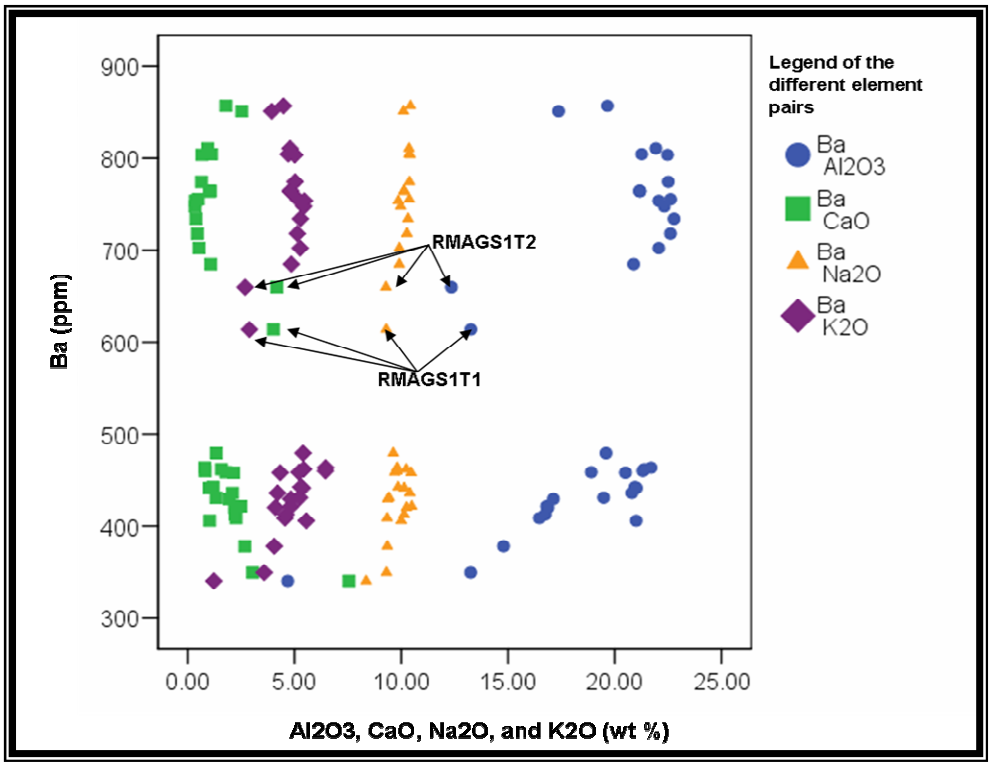

Figure 78. Binary graph showing the influence of the different relationships of selected major elements with Ba. See text for explanation. For abbreviations, see Table 26.

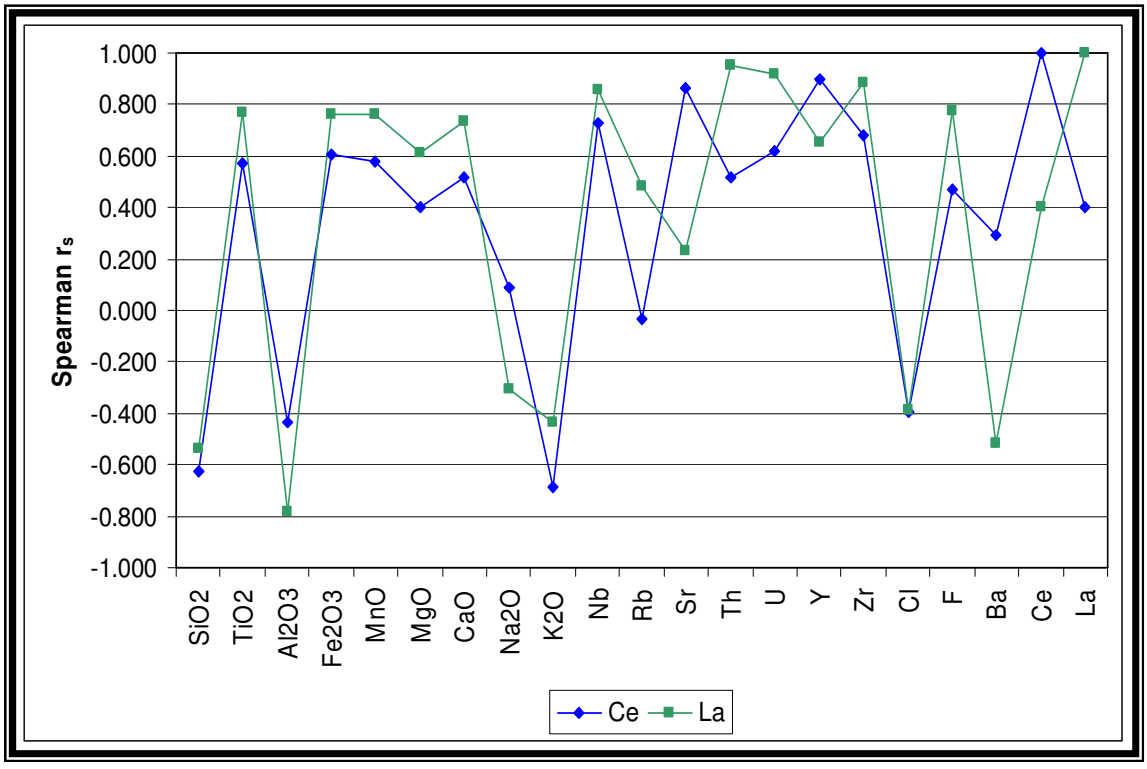

Figure 79. Binary graph showing the Spearman correlation coefficients for Ce and La with all other elements.

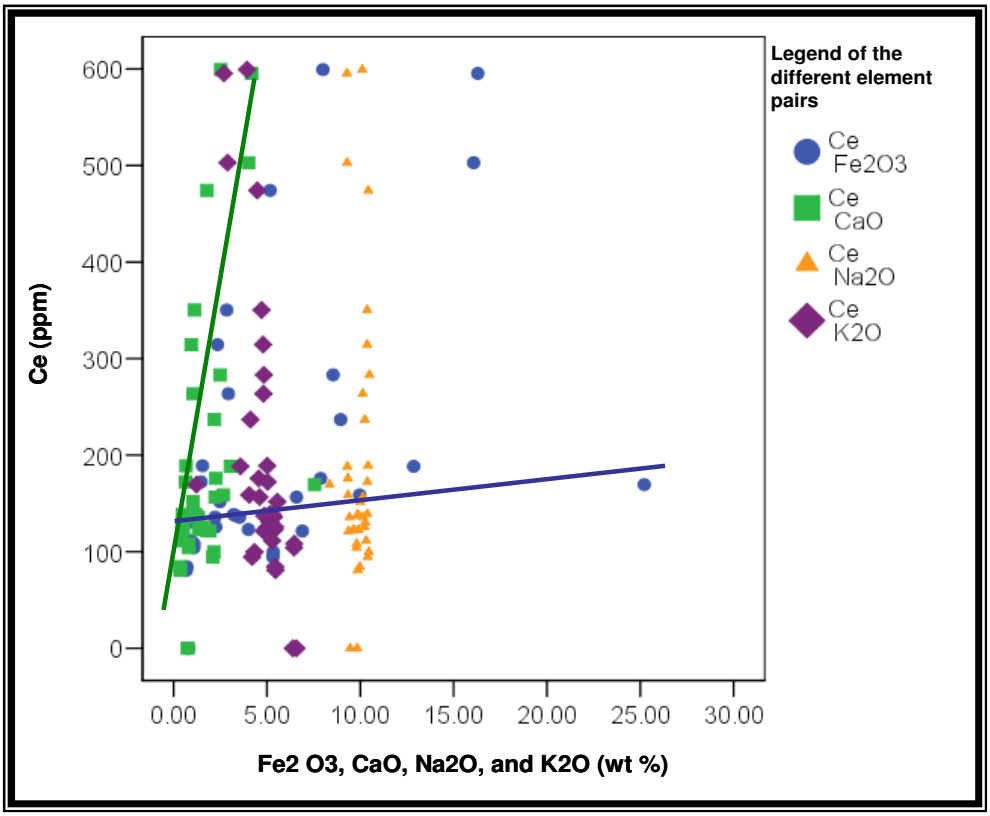

Figure 80. Binary graph showing the influence of the different relationships of selected major elements with Ce. See text for explanation. For abbreviations, see Table 26.

The Spearman correlation coefficient indicate a positive correlation with Fe_2O_3 and CaO. Cerium is known to occur in trace amounts in aegirine (Deer et al. 1978) The two solid lines on the graph indicates two different trends with CaO and Fe_2O_3 with Ce and indicates that Ce probably occurs in both aegirine and aegirine - augite. The binary plot for the correlation between Ce with Zr and F is plotted in Figure 81. There is a slight positive correlation between these elements. The relationship between Ce and F shows two distinct trends and properly indicate two populations of fluorite.

Lanthanum shows good correlations with Zr and F (Figures 79 and 82) and therefore is associated with zircon and fluorite. Fluorite is known for the substitution of Ca with Ce and La and a weak correlation is observed between Ce, La and F (Figures 80, 81 and 82). Consequently, they cannot be easily extracted from the host minerals. The relationship between La and Ce is plotted in Figure 83. Two trends of different La/Ce ratios is observed indicating the occurrence of two different fluorite minerals, but without a detailed geochemical evaluation of the fluorite, this problem can not be resolved.

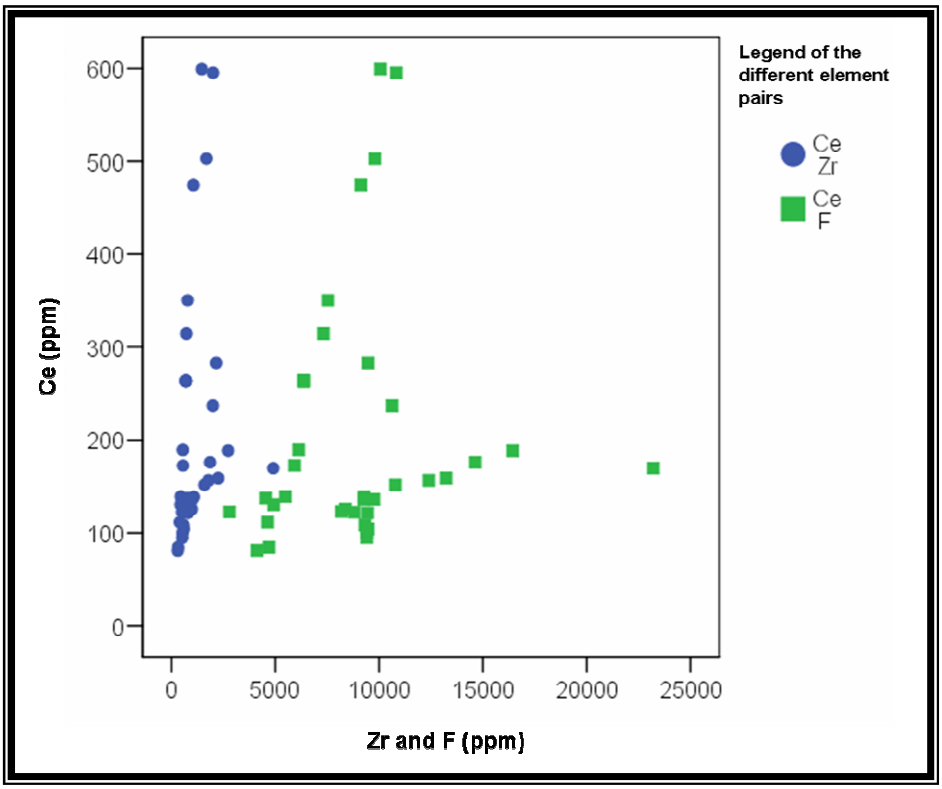

Figure 81. Binary graph showing the influence of the different relationships of Zr and F with Ce. See text for explanation. For abbreviations, see Table 26.

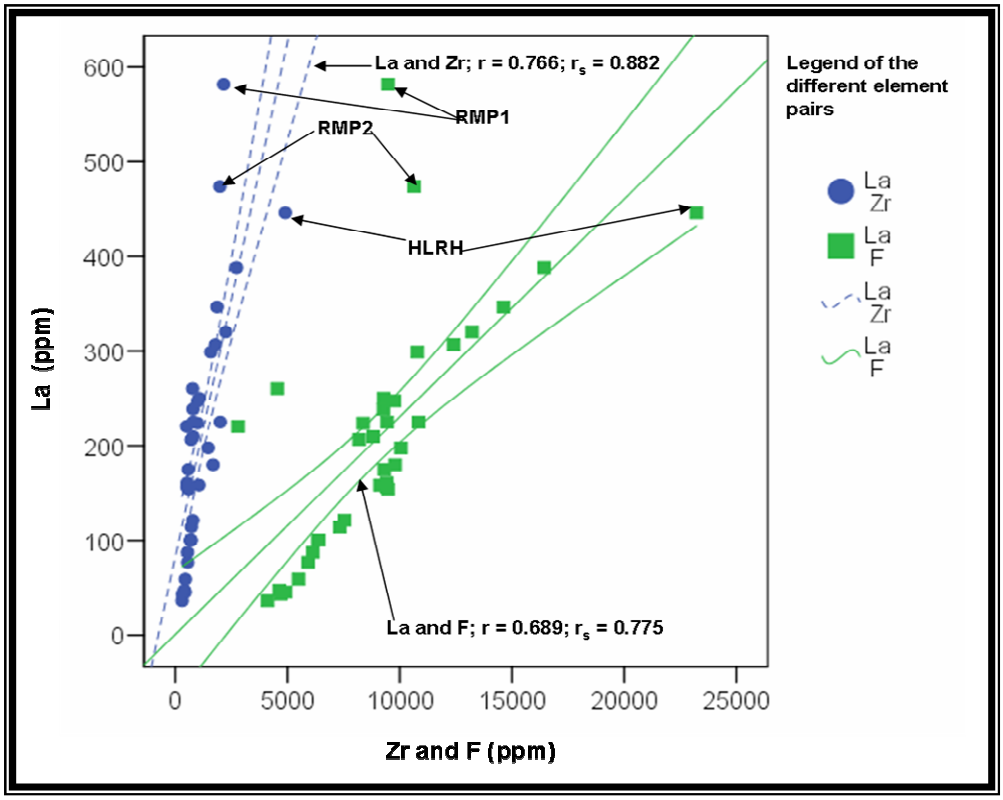

Figure 82. Binary graph showing the influence of the different relationships of Zr and F with La. See text for explanation. For abbreviations, see Table 26.

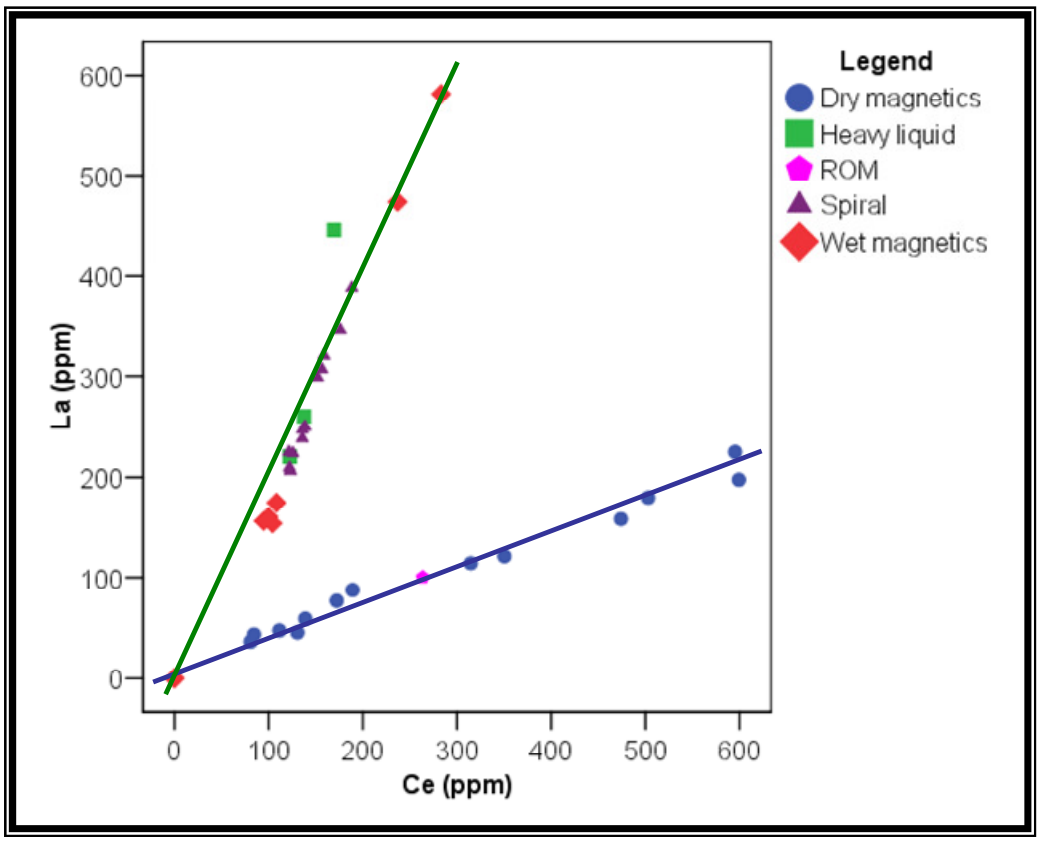

Figure 83. Binary graph showing the relationship between La and Ce. See text for explanation

7.6 Geochemistry: Major and trace element concentrations (Determined by Uniquant®5)

The 14 dry magnetic separation samples were analysed using XRF UniQuant®5 calibration as described in Chapter 5. The accuracy of UniQuant®5 was tested by comparing these results with results obtained using the traditional XRF methods described in Chapter 5 (WinXRF refers to routine analysis of major and trace elements). A Spearman correlation matrix was calculated using the same definitions as described in section 7.4 (see Appendix 5 for the correlation matrix).

The major element correlations are plotted in Figures 84 and 85. The stippled line in all the graphs represents the 1:1 ratio. The major elements correlate strongly (r_s larger than 0.9). This is a good indication that the data produced by the UniQuant®5 for the major elements are very close to the data that one can obtain by using the conventional glass disk major element determination by XRF.

The trace element correlations are plotted in Figures 86 and 87. The variation of Rb is too small and therefore displays only weak correlation between UniQuant®5 and WinXRF. The other trace elements are relatively strongly correlated (Figures 86 and 87). The larger range of the trace elements indicates there is not much difference between the two XRF techniques for detecting trace elements. The correlation is, however, not as strong as with the major elements and can be an indication that the calibration for these elements will need more refining. The correlation for Zr for both methods is very strong with a r_s value of +1 (Figure 88). From the graphs (Figures 86 and 87) UniQuant®5 over estimated the trace element values compared with WinXRF and therefore, the data points do not plot on the 1:1 ratio line.

The data presented here indicate that UniQuant®5 shows promise of being both a precise and accurate analytical method to provide information on major and trace element concentrations, but refinement is needed of the calibration for the trace and rare earth elements.

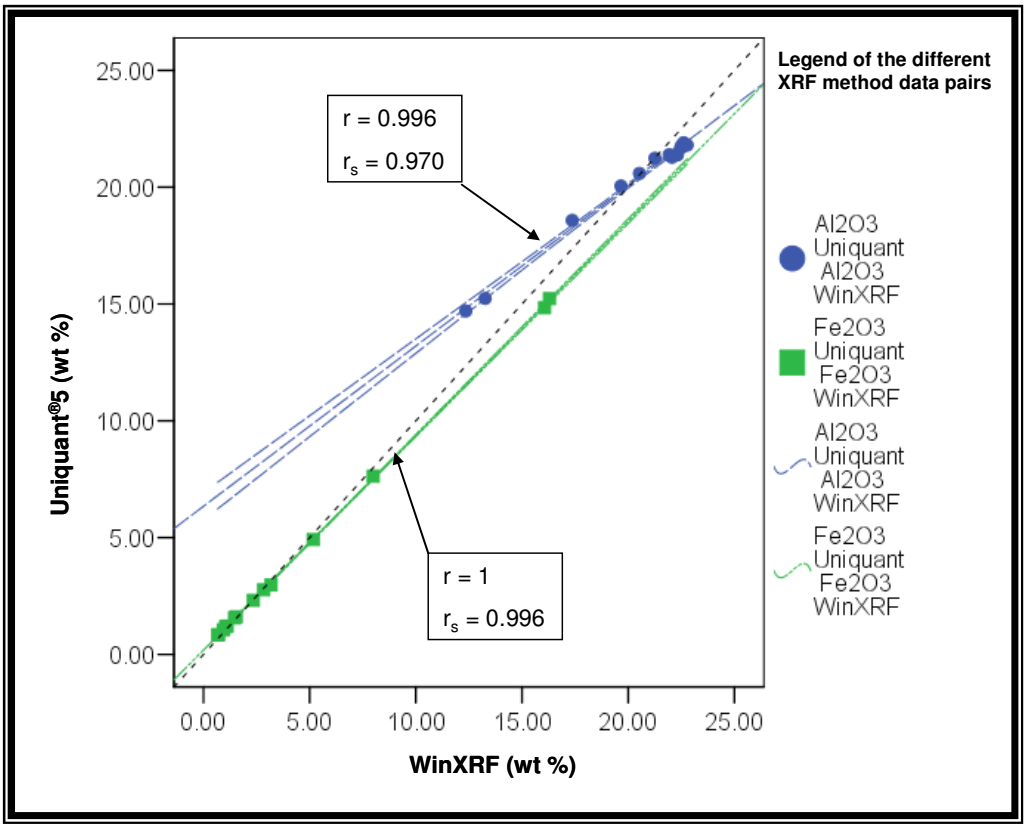

Figure 84. The correlation graph ccomparing Uniquant®5 data with WinXRF data for Al_2O_3 and Fe_2O_3; r and r_s are indicated for each pair of data. The stipple line represents the 1:1 ratio.

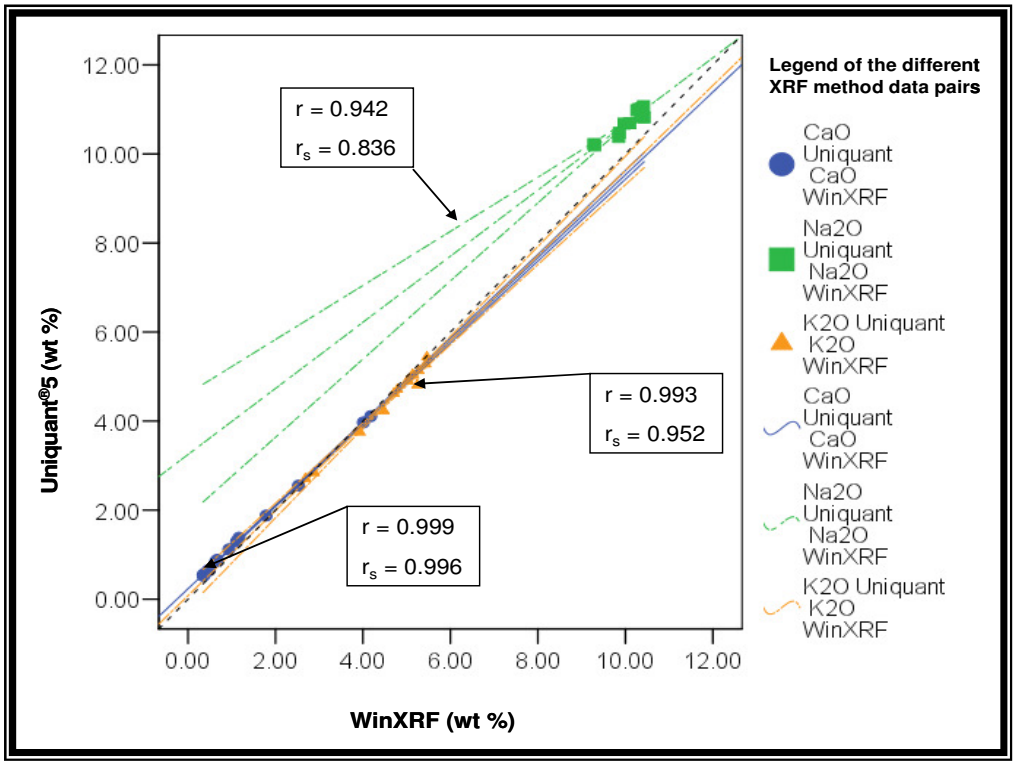

Figure 85. The correlation graph ccomparing Uniquant®5 data with WinXRF data for CaO, Na_2O and K_2O; r and r_s are indicated for each pair of data. The stipple line represents the 1:1 ratio.

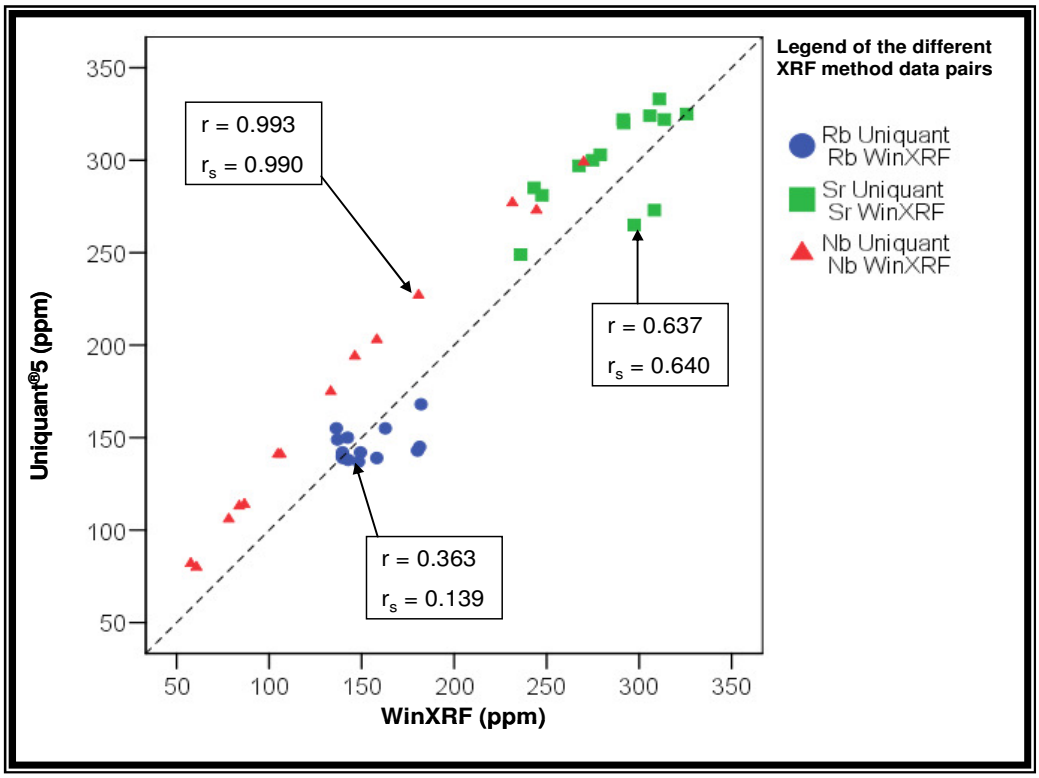

Figure 86. The correlation graph ccomparing Uniquant®5 data with WinXRF data for Rb, Sr, and Nb; r and r_s are indicated for each pair of data. The stipple line represents the 1:1 ratio.

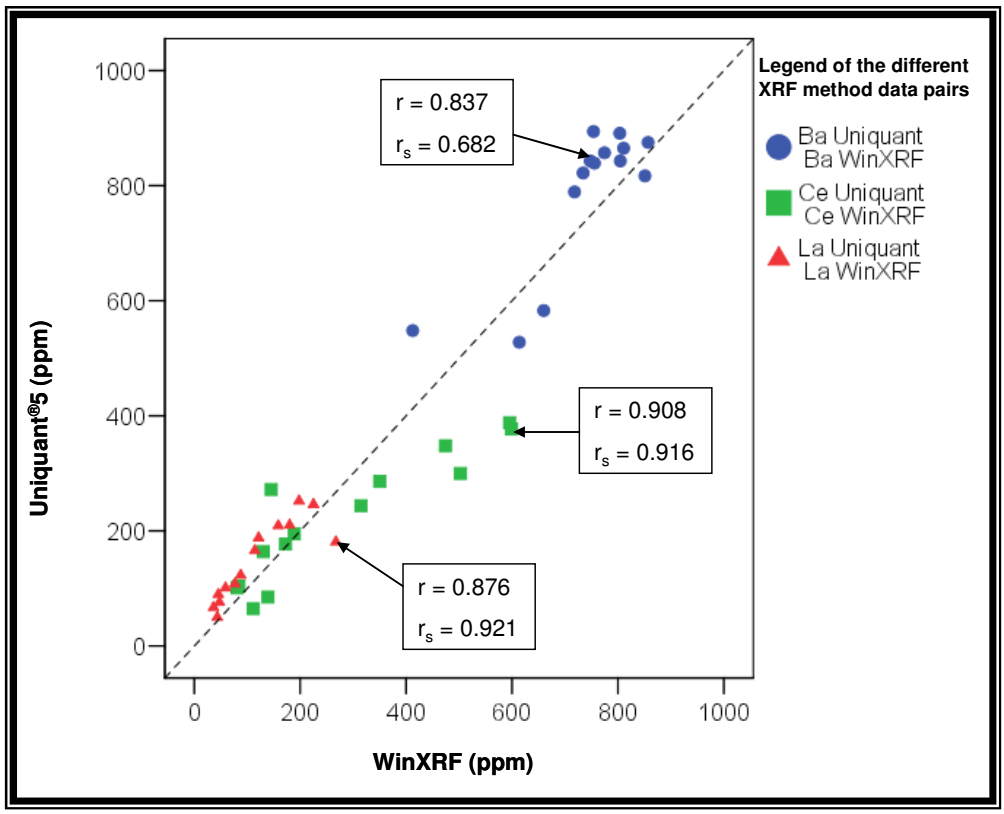

Figure 87. The correlation graph ccomparing Uniquant®5 data with WinXRF data for Ba, Ce, and La; r and r_s are indicated for each pair of data. The stipple line represents the 1:1 ratio.

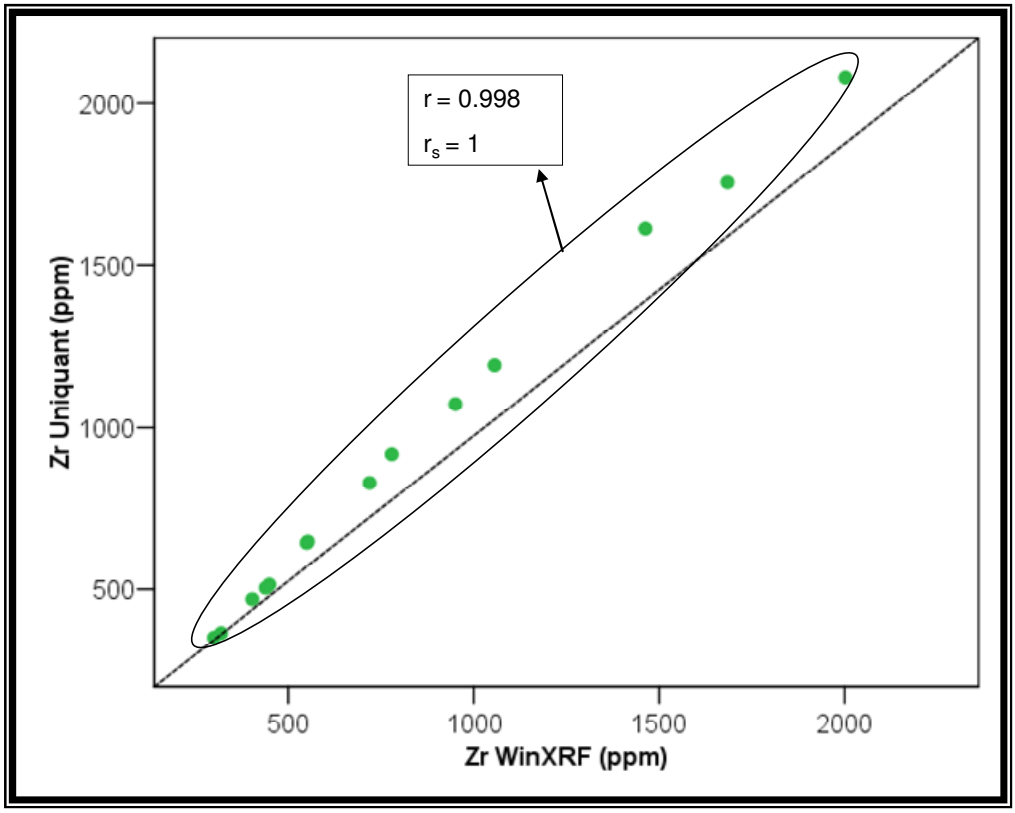

Figure 88. The correlation graph comparing Uniquant®5 data with WINXRF data for Zr; r and r_s are indicated. The stipple line represents the 1:1 ratio.

7.7 Evaluation of the different separation methods for producing a low iron-containing nepheline product

An important factor to consider in evaluating nepheline syenite, for economic application, is the total iron content left in the final nepheline products, after the process of extracting the iron-rich minerals. The FNS contains high aluminium and alkali contents, which would make it a good source to be used as a flux for the ceramics and glass industry. To evaluate the success of the different separation techniques, Fe_2O_3, Al_2O_3, Na_2O, and K_2O contents will be the main elements of consideration. Table 28 summarise the different important element concentrations as required by the glass and ceramic industry, as compared with the product obtained for each of the different separation tests.

Table 28. Summary of the major elements considered for glass and ceramic industries compared with the different products of the different separation tests.

	Glass Industry*	**Ceramics Industry***	**Dry magnetic separation****	**Wet magnetic separation****	**Spiral separation****	**Heavy liquid Separation****
Fe_2O_3 (wt %)	***0.4 - 0.07***	***0.05 - 0.07***	0.68 - 0.70	0.78 - 0.80	2.22 - 3.21	1.51
Al_2O_3 (wt %)	***22.50 - 23.80***	***22.50 - 23.80***	22.06 - 22.32	21.25 - 21.78	20.00 - 21.57	22.06
Na_2O (wt %)	***7.50 - 10.4***	***7.80 - 9.80***	9.86 - 9.97	9.80 - 9.83	9.85 - 10.23	9.91
K_2O (wt %)	***5.00 - 9.00***	***4.6 - 9.10***	5.43 - 5.46	5.83 - 5.98	5.29 - 5.55	5.26

* Harben (1995), ** Data from XRF results

Sodium and K_2O are associated with Al_2O_3: albite, microcline, analcime, nepheline, and sodalite. These minerals have lower densities than iron-rich minerals and are non-magnetic. Thus, all of these minerals will concentrate in the light and non-magnetic fractions of the different separation methods used.

The elements Al_2O_3, Na_2O and K_2O falls into the ranges acceptable for the glass and ceramic industry. The ROM sample used has on average an initial iron content of 3.37 wt %. The dry magnetic separation after six passes produced the best non-magnetic material separate with the lowest iron content of 0.68 wt % (Table 28).

7.7.1 Possible alternatives for separation

The combination of different separation techniques might deliver better results than the methods used alone. Two different alternative models combining a number of the separation techniques, are presented in Figures 86 and 87. However, these modals would require testing within a pilot plant setup that is beyond the scope of this study. The nepheline concentrate will contain albite, microcline, and nepheline and from the EMPA results of this study, it is known that iron is contained in the crystal structures of these minerals. The combination models can reduce the amounts of unwanted ilmenite, aegirine, and aegirine – augite and thus will lower the final iron content, but might not bring it into acceptable ranges for application in the glass and ceramic industry.

For both alternative models, the first step would be to mill the sample to a fineness of 70 % passing 1 mm. The fines would then be deslimed (screening the sample to remove the finest fraction below 75 µm). For the first proposed model (Figure 86), dry magnetic separation could then be performed. The best results for dry magnetic separation was obtained for the first test (see section 6.3), where the final nepheline concentrate (RNMAGS6T1) contained 0.68 wt % Fe, but only 22 mass % of the initial material was left. Following the dry magnetic separation, the non-magnetic material could then be added to water, and spiral separation could take place for the removal of iron-containing silicates that are non-magnetic (Figure 86). This could produce, in theory, a final nepheline product with the lowest possible iron-content. The final yield will even be lower that 20 mass % after the spirals separation is complete (Figure 86).

Alternatively, the same initial steps (up to the desliming stage), but instead of dry magnetic separation, spiral separation would be performed first, followed by wet magnetic separation of the lighter material (Figure 87). The use of a spiral will reduce costs because lower amounts of electricity are needed for initial separation compared to magnetic separation.

The yield of light to dense material form the spiral separation was not determined in this study, but from the XRD results the heavy minerals is less than 10 mass % and

the light fraction should contain ~ 90 mass % light material. The wet magnetic separation produced a non-magnetic yield of ~ 90 mass %. The final yield expected from this method is higher than for the dry magnetic separation modal (Figure 87).

Another separation technique not investigated is flotation. Burat et al. (2006) produced a nepheline syenite product with Fe_2O_3 content below 0.1 wt % with the combination of dry magnetic separation and flotation. Further investigation would be necessary to evaluate the benefit of floatation for the FNS.

The price for low iron-containing nepheline syenite was constant over 2008 to 2009 at ~ 32 Canadian dollars per ton (Tran 2009). The nepheline syenite concentrate from the different tests is above the acceptable levels and therefore the price per ton will be lower than that quoted above, should a market for the product be found.
A full cost/benefit analysis goes beyond the scope of this study, but if attempted, the following aspects need to be taken into account:

- Plant establishment costs (for one of the two methods proposed above). This includes equipment costs; e.g., should ball milling be used ceramic balls (rather than steel balls due to Fe contamination) will be used for this process. The equipment will have an influence on the factors such as electric use; e.g., should ceramic balls used, an increase in the amount of and therefore electricity to mill the material to the desired size will occur (as opposed to steel balls).
- The cost and availability of electricity. Currently, South Africa is facing supply problems, and increases in the tariffs (by 30 %) have taken place in 2009 and more are predicted.
- Labour costs
- Identification and availability of a market for the nepheline product produced.

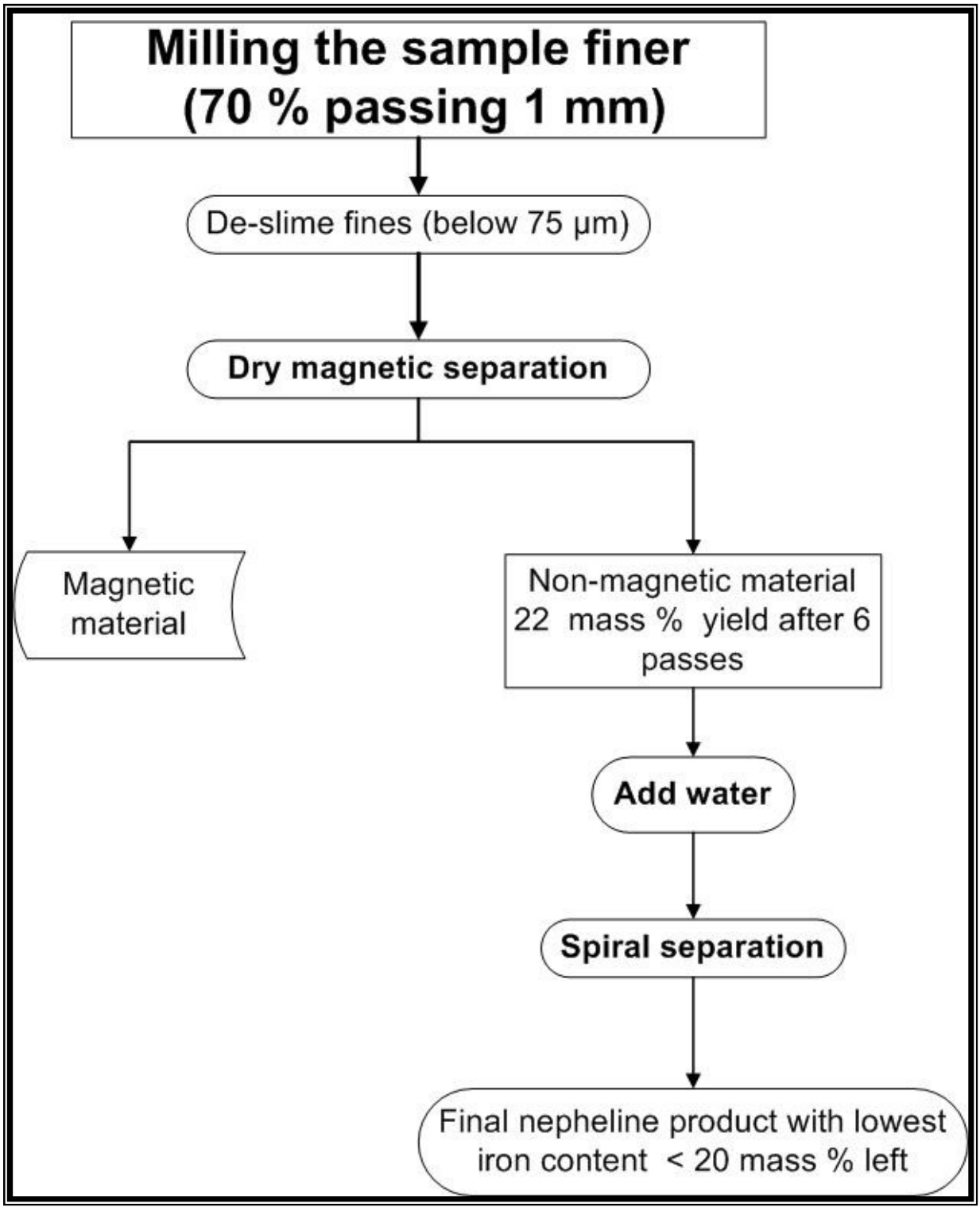

Figure 89. Flow diagram showing the combination of dry magnetic and spiral separation to remove Fe_2O_3 from Franspoort nepheline syenite (FNS).

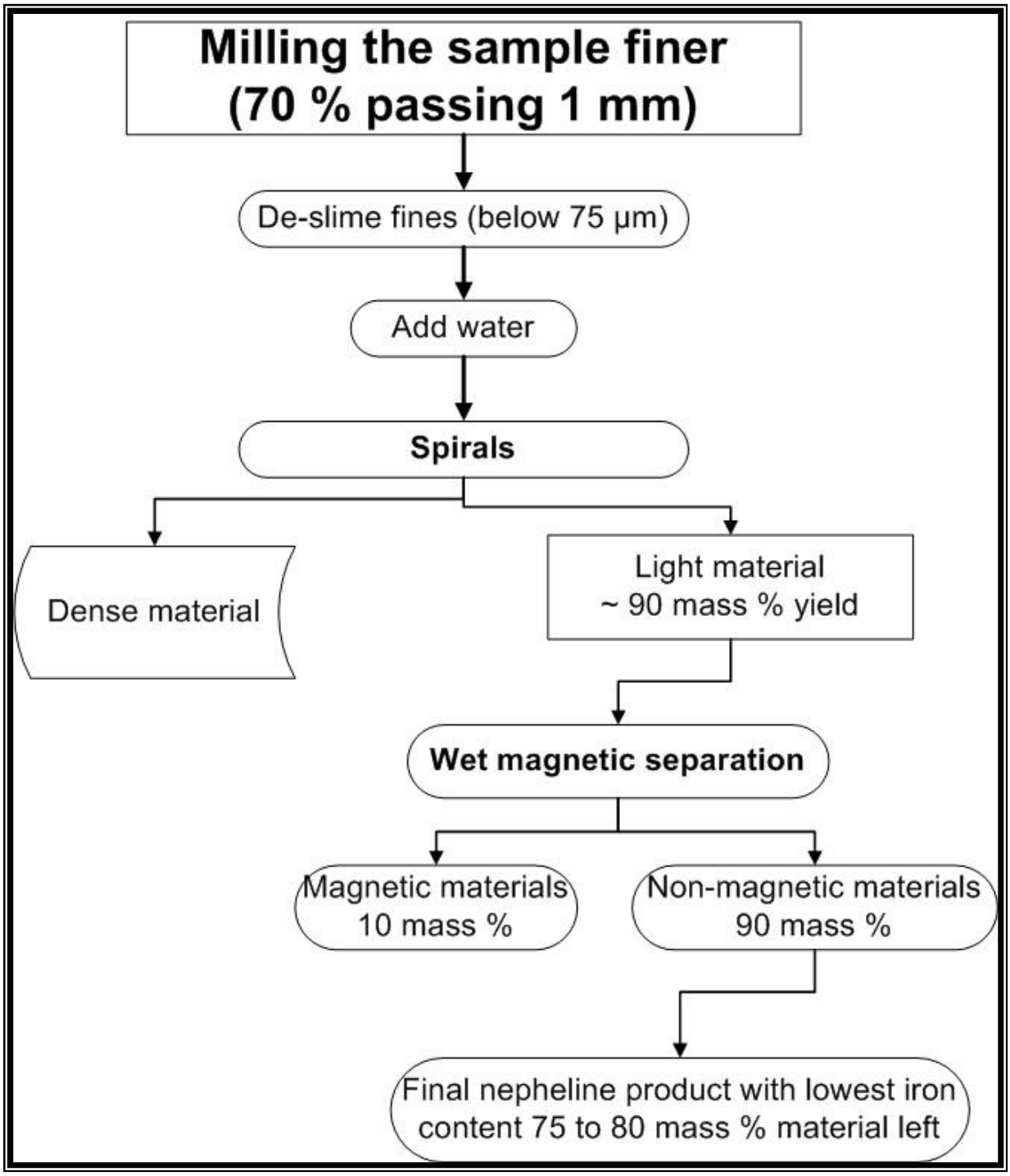

Figure 90. Flow diagram for spiral separation combined with wet magnetic separation to remove Fe_2O_3 from Franspoort nepheline syenite (FNS).

7.8 Evaluation of the different separation methods for concentrating zircon and rare earth elements as by-products

The most important trace element for MQ is Zr, which could lead to a by-product (section 1.2.3, Table 5). Properties that could be used to separate Zr include the density of zircon (4.56 g/cm^3 Deer et al. 1997), particle size, and magnetic properties. The density of zircon causes it to concentrate with other dense minerals (so heavy liquid and spiral separation would be options of concentration). Zircon is slightly magnetic; therefore, magnetic separation would not be successful.

The particle size of the Zr-containing minerals is important, as the glass industry requires a product with the particle size of Zr to be below 0.25 mm (Harben 1995). Although zircon was not detected with XRD, it was identified in the petrographic study and SEM imagery (Figures 62 and 63). Zircon occurred mostly as inclusions in nepheline and albite. The size of the Zr grains range from ~10 µm to 200 µm (Figures 62 and 63).

The best results for Zr separation were obtained using heavy liquid separation which resulted in a Zr content of 4900 ppm. This could be used for beneficiation in theory, but because of the textural settings of the zircon in the material (as interlocked crystals in nepheline and albite) this is not possible at MQ.

Lanthanum and Ce were used as proxies for the rare earth elements. Geochemical results indicate that these elements occur in trace amounts as element substitutions in the different minerals (e.g., zircon and fluorite, Ce in aegirine; section 7.4). They are not concentrated in large amounts in any specific mineral (e.g., monazite) that could be separated for beneficiation.

8 CONCLUSIONS AND RECOMMENDATIONS

Mamelodi Quarries mine the Franspoort nepheline syenite deposit for aggregate and crusher sand. They were interested in an evaluation of different separation methods to produce a nepheline product for use in the South African glass and ceramic industry (i.e., one that has a low iron content).

The petrographic and XRD results indicate that the following minerals are present in the nepheline syenite: nepheline, microcline, albite, aegirine, aegirine – augite, sodalite, fluorite, mica, chabazite, actinolite, and analcime.

The starting composition of the Franspoort nepheline syenite is iron-rich (3.37 wt %) in comparison to other commercially mined nepheline syenites (> 0.40 wt %). The different separation tests evaluated to obtain a nepheline product were high-intensity wet magnetic separation, low-intensity dry magnetic separation, gravity separation using heavy liquid separation, and spiral gravity separation.

ROM was used for the different separation tests. Different milling methods were investigated and screening tests performed to determine the size distribution in the starting material. Each of the separation tests require a minimum and maximum size to obtain optimized separation. The coarse crusher sand produced by Mamelodi Quarries was selected for all tests.

The best results to produce a clean nepheline product were obtained from the low-intensity dry magnetic separation with final iron content of 0.68 wt %. Aegirine and aegirine - augite, magnetite, ilmenite, and pyrite contain most of the iron (confirmed by the petrographic, XRD, and microprobe results). The nepheline product mostly contains nepheline, microcline, albite, sodalite, and analcime.

The iron-rich minerals occur as discrete crystals, but are also locked within albite, microcline, and nepheline as small inclusions from 1 µm to 1 mm. Some of the iron-containing minerals can be liberated by fine milling, however, fine intergrowths will not be liberated with this technique. In addition the milling of the material to finer

grind sizes will not separate as well as the coarser material it will be below the optimum sizes for the separation steps.

Nepheline, albite, and microcline all contain Fe_2O_3 in their crystal structure in concentrations above 0.5 wt % and this is the major cause for the final nepheline product to have too high iron concentrations, which make it unsuitable for use in the glass and ceramic industry.

The study indicates that the final nepheline product produced will not meet the standard of the glass and ceramic industry and beneficiation would be unsuccessful.

The concentration of zircon and the rare earth elements was a secondary aim of the project. Zircon was mostly locked in host minerals and heavy liquid separation produced results of 4900 ppm. The size of the inclusions ranged from approximately 10 µm to 100 µm. Lanthanum and Ce were used as proxies for the rare earth elements. They have substituted for other elements in some of the minerals present especially in fluorite and zircon. Therefore, zircon and the rare earth elements cannot be beneficiated as a by-product for Mamelodi Quarries as they cannot be separated from their host minerals.

Acknowledgements

The following people are acknowledged for their contribution to the project. Without their help, I would not have succeeded.

- Prof. Roland Merkle for project co-ordination and being the promoter and supervisor for this project.
- Mr. Anton von Willich and Tom Ferguson for financial support.
- Carlos Martins for advice and help with wet magnetic separation.
- Mr. P.C. W. Havemann of the Department of Metallurgy, and Peter Gräser for assistance in spiral tests.
- Marco Claasen for helping with screen tests at the University of Pretoria.
- Maggie Loubser for being a mentor in questions concerning XRF methods and analysis.
- Dr Sabine Verryn for XRD analysis.
- Mintek Mineralogy Division for sponsoring the electron microprobe analyses and moral support.
- Archie Corfield for electron microprobe analyses.
- Dr Louise Coney for proof reading and support in writing and finalising the thesis.
- Wendy Thompson for proof reading of the thesis
- Gryffenberg family for financial and emotional support to complete the project

References

Abbey, S. (1981) The search for "best values". A study of three Canadian rocks. *Geostandards Newsletter* **5,** 13-26

Allman, M. and Lawrence, D. F. (1972). *Geological laboratory techniques*, 1st edition. Blandford press, London. 335pp.

Besaans, A.J. (1969). Stratigraphic map of Silverton (1:50 000 geological map). *Department of Mines, Geological survey of South Africa*, South Africa, (One sheet).

Boelema, R. (1998). Feldspar. In: Wilson, M. G. C. and Anhaeusser, C.R. (Editors), *The mineral resources of South Africa*, 6th Edition, CTP book printers, Pretoria, 267 – 268.

Burat. F., Kangal. O. and Onal. G. (2006). An alternative mineral in the glass and ceramic industry: Nepheline syenite. *Minerals Engineering*, **19**, 370 - 371.

De Jong, W. J. (2000). *Uniquant®5 a unique concept in XRF analysis.* Omega data Systems, Veldhoven. 20pp.

Deer, W.A., Howie, R. A. and Zussman, J. (1978). *Rock-forming minerals,* Volume 2A Single-chain silicates, 2nd edition. Longman, London. 668 pp.

Deer, W.A., Howie, R. A. and Zussman, J. (1997). *An introduction to the rock forming minerals*, 2nd edition. Longman, Hong Kong. 696 pp.

Frick, C. and Malherbe, S. J. (1986). The geology of the Roodeplaat caldera, north-east of Pretoria. Government Printer, Pretoria. 79pp.

Griffiths, J. (1984). Rare earths attracting increase attention. *Industrial Minerals* April, 19 – 37.

Haizhou, W. (1997). Certificate of Certified Reference Material, NCS DC 86309 – NCS DC86312, Rare Earth Ore. China National Analysis Centre for Iron and Steel, Beijing, 4pp

Harben, P. W. (1995). *The industrial minerals handybook a guide to markets, specifications and prices*, 2nd edition, Warwick Printing , London. 254pp.

Hawley, G.G. (1987). The condensed chemical dictionary, 11th edition. Van Nostrand Reinold, New York. pp 779. Material Safety Data Sheet available from: *http://www.sciencelab.com/xMSDS-1_1_2_2_Tetrabromoethane-9927415*

Kanazawa, Y., and Kamitani, M. (2006). Rare earth minerals and resources in the world. *Journal of Alloys and Compounds*. 1339-1343.

Kelly, E.G and Spottiswood, D.J. (1982). *Introduction to Mineral Processing*, John Wiley and Sons, New York. 491pp

Kgwakgwe, P. (2004) Unpublished X-ray fluorescence data. University of Pretoria. 4pp

Lachance, G. R. and Claisse, F (1980). A comprehensive Alpha Coefficient Algorithm. *Advances in X-Ray Analysis* **23**, 87

Lapidus, D. F. (1990). *Collins dictionary of geology*, 1st Edition. HarperCollins Publishers, Glasglow. 565pp

Loubser, M. (2006). X-Ray Fluorescence Spectroscopy Analysis. Unpublished laboratory notes, 11p

Martins, C. (1999). The *Franspoort alkali complex on farm Franspoort 332JR*. Unpublished mine report. 50pp

McClace, J. T. and Sincich, T. Statistics, 9th Edition. Prentice Hall, New York. 850pp

Neary, C.R. and Hihley, D.E. (1984). The economic importance of the Rare Earth Elements. In: Henderson, P. (Editor). *Rare earth element geochemistry*, Elsevier, New York, pp. 423 – 466.

Nockolds, S.R., Knox, R.W.O'B. and Chinner, G.A. (1978). *Petrology for students.* Cambrige University press, London. 435pp.

Nude. P.M., Shervais. J.W., Attoh. K., Vetter, S.K. and Barton, C. (2009). Petrology and geochemistry of nepheline syenite and related carbonate-rich rocks in the Pan-African Dahomeyide orogen, southeastern Ghana, West Africa. Article in press for Journal of African Earth Science. 11pp.

Passaglia, E. and Sheppard, R.A. (2001). The crystal chemistry of zeolites. In Bish, D.L. and Ming D.W. (Editors). *Natural Zeolites: occurrence, properties, applications.* The Mineralogical Society of America, Washington DC. **45**, 69-116

Potter, M.J. (2007). Feldspar and nepheline syenite. (Internet), 12pp. Available from: *http://minerals.usgs.gov/minerals/pubs/commodity/feldspar/myb1-2007-felds.pdf*

Shand, S.J. (1922). The alkaline rocks of the Franspoort line. *Transvaal Geological Society of South Africa*. **25**, 81 -100.

Schürmann, L. W. and Harmer, R. E. (1998). Rare earth elements. In: Wilson, M. G. C. and Anhaeusser, C.R. (Editors). *The Mineral Resources of South Africa*, 6th Edition, CTP book printers, Pretoria, 569 – 573.

Snyman. C. P. (1996). *Geologie van Suid Afrika in twee volumes*. Department of Geology, Universiteit van Pretoria, South Africa. Volume 1, 473pp.

Terremetrica, *Satellite image of Mamelodi Quarries.* (Google earth modified 17 November 2005). (Published by Europe Technologies). Available from *http://www.earth.google.com/download-earth.html*

Toens, P.D. (1952). *The geology around Leeuwfontein north-east of Pretoria.* MSc. Thesis (unpublished) University of Pretoria. Pretoria, South Africa, 126pp.

Tran, A., (editor), (2009). Minerals price watch. January 2009, **169**, 14

Verryn, S. M. C. (2005). *Introduction to X-ray powder diffraction.* Short course. University of Pretoria, South Africa. 96pp.

Watson, J.S. (1996). Fast simple methods of powder pellet preparation for X-ray Fluorescence analysis. *X-ray Spectrometry* **25** 173 -174

Wills, B.A. (2006). *Wills' Mineral processing technology. An Introduction to the Practical Aspects of Ore Treatment and Mineral Recovery, 7th* edition. Butterworth - Heinemann. Oxford. 444pp

Willis, J.P. (1997) An evaluation of the analysis of Monazite and REE compounds by WDXRFS: a spectroscopist's nightmare (or challenge?). *Denver X-ray Conference Proceedings*. **41**. 829 - 842.

Woolley, A. R. Williams, C. T., Wall, F., Garcia, D., and Moutez, J. (1995). The Bingo carbonatite-ijolite-nepheline syenite complex, Zaire: geology, petrography, mineralogy and petrochemistry. *Journal of African Earth Sciences,* **21**, 329-348.

Young, R. A. (1993). Introduction to the Rietveld method. In: R.A. Young (Editor), *The Rietveld method*. Oxford University press, Oxford, 1 - 40.

Appendix 1. Geochemical Results: X-ray Diffraction

Diffraction pattern of ROM sample.

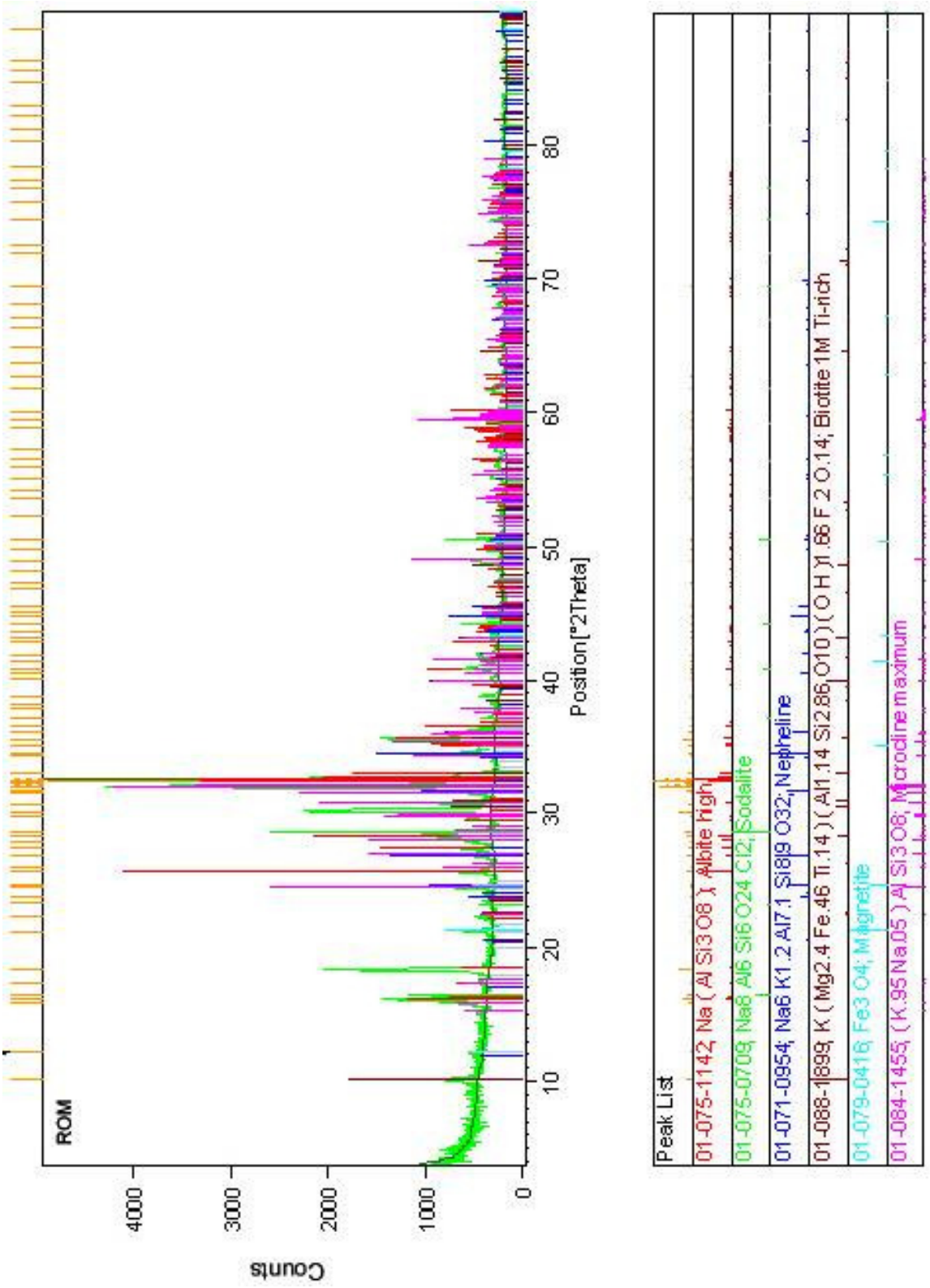

Quantification results of ROM sample.

Autoquan - Results

University of Pretoria, MINERAL SCIENCE
MATERIAALKUNDE EN METALLURGIES

ROM

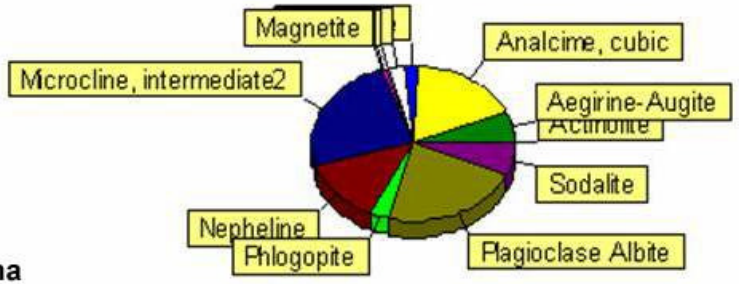

Mineral	Weight %	2 sigma
Actinolite	0.49 %	+- 0.54 %
Aegirine-Augite	6.10 %	+- 1.71 %
Analcime, cubic	17.70 %	+- 1.50 %
Chabazite	2.08 %	+- 1.44 %
Enstatite	2.46 %	+- 2.61 %
Fluorite	0.56 %	+- 0.33 %
Ilmenite	0.71 %	+- 0.54 %
Magnetite	0.00 %	+- 0.00 %
Microcline, intermediate2	24.78 %	+- 2.49 %
Nepheline	13.03 %	+- 1.59 %
Phlogopite	3.09 %	+- 1.11 %
Plagioclase Albite	22.31 %	+- 2.34 %
Sodalite	6.69 %	+- 0.72 %

Diffraction pattern of pegmatite rock sample.

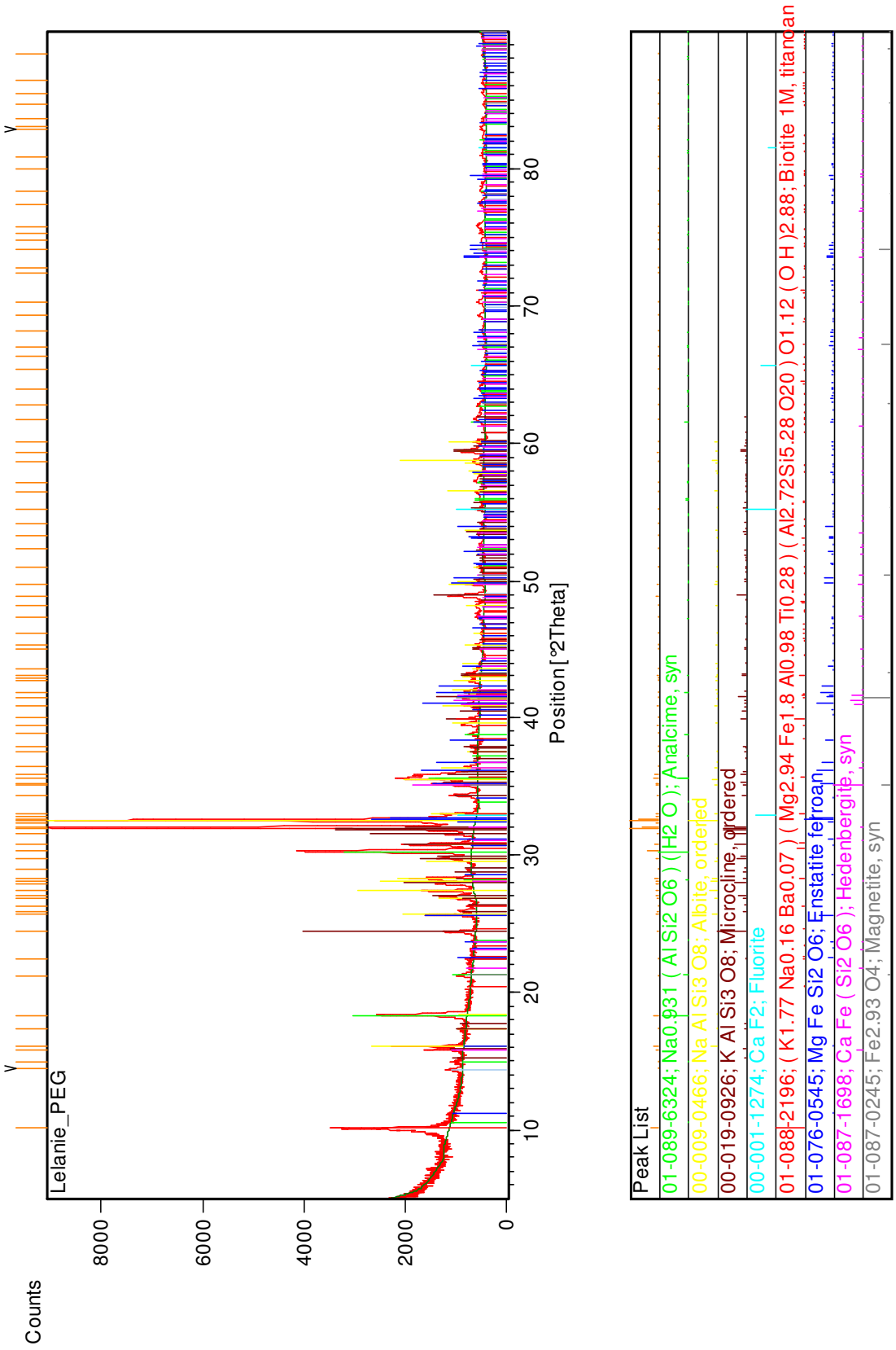

Autoquan - Results

University of Pretoria, MINERAL SCIENCE
MATERIAALKUNDE EN METALLURGIES

2006/06/20

PEG

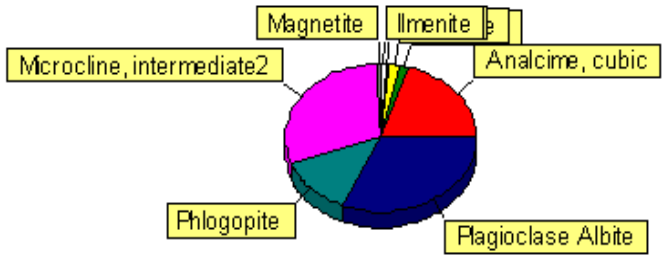

Analcime, cubic	20.46 +- 0.72 %
Diopside	1.16 +- 0.39 %
Enstatite	1.89 +- 1.59 %
Fluorite	0.58 +- 0.16 %
Ilmenite	0.84 +- 0.23 %
Magnetite	0.82 +- 0.23 %
Microcline, intermediate2	29.64 +- 1.02 %
Phlogopite	13.08 +- 0.72 %
Plagioclase Albite	31.52 +- 1.14 %

Quantification results of pegmatite rock sample.

Diffraction pattern of xenolith (MQ1) sample.

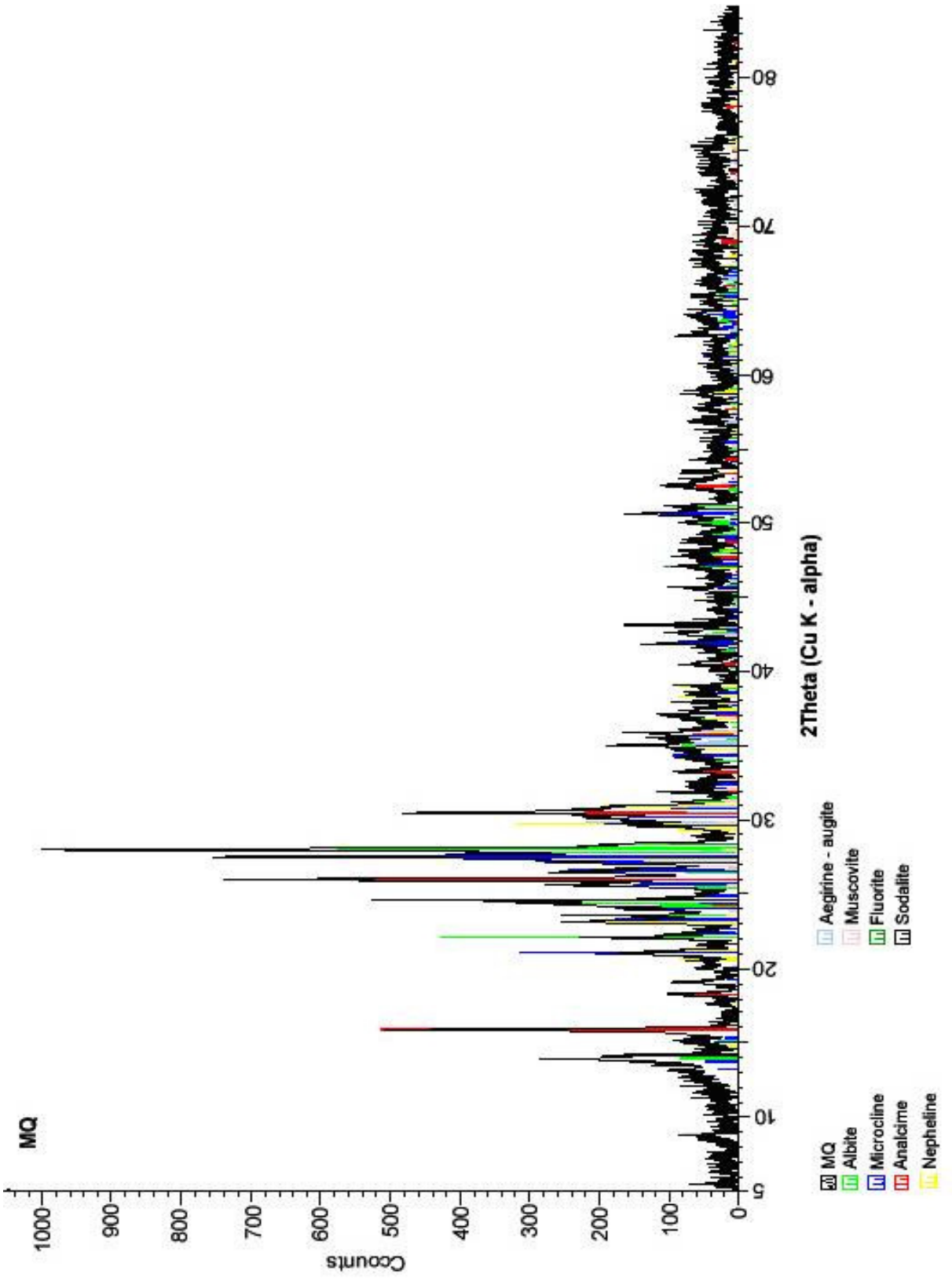

Autoquan - Results

University of Pretoria, MINERAL SCIENCE
MATERIAALKUNDE EN METALLURGIES

MQ sample

(Xenolith)

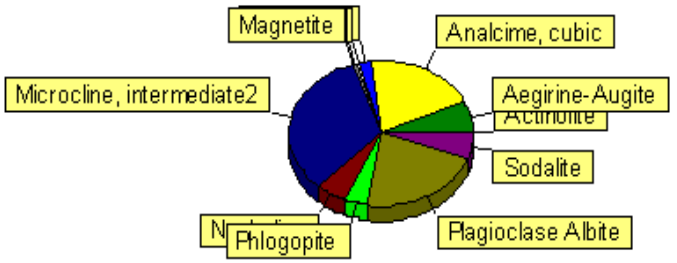

Actinolite	0.00 +- 0.00 %
Aegirine-Augite	7.31 +- 1.80 %
Analcime, cubic	19.51 +- 1.50 %
Chabazite	1.93 +- 1.50 %
Enstatite	0.48 +- 1.17 %
Fluorite	0.92 +- 0.33 %
Ilmenite	0.00 +- 0.00 %
Magnetite	0.00 +- 0.00 %
Microcline, intermediate2	32.79 +- 2.43 %
Nepheline	5.65 +- 1.53 %
Phlogopite	4.04 +- 1.50 %
Plagioclase Albite	21.37 +- 2.22 %
Sodalite	5.99 +- 0.72 %

Quantification results of xenolith (MQ1) sample.

Diffraction pattern of heavy liquid separation ROM starting material sample (HLRSM).

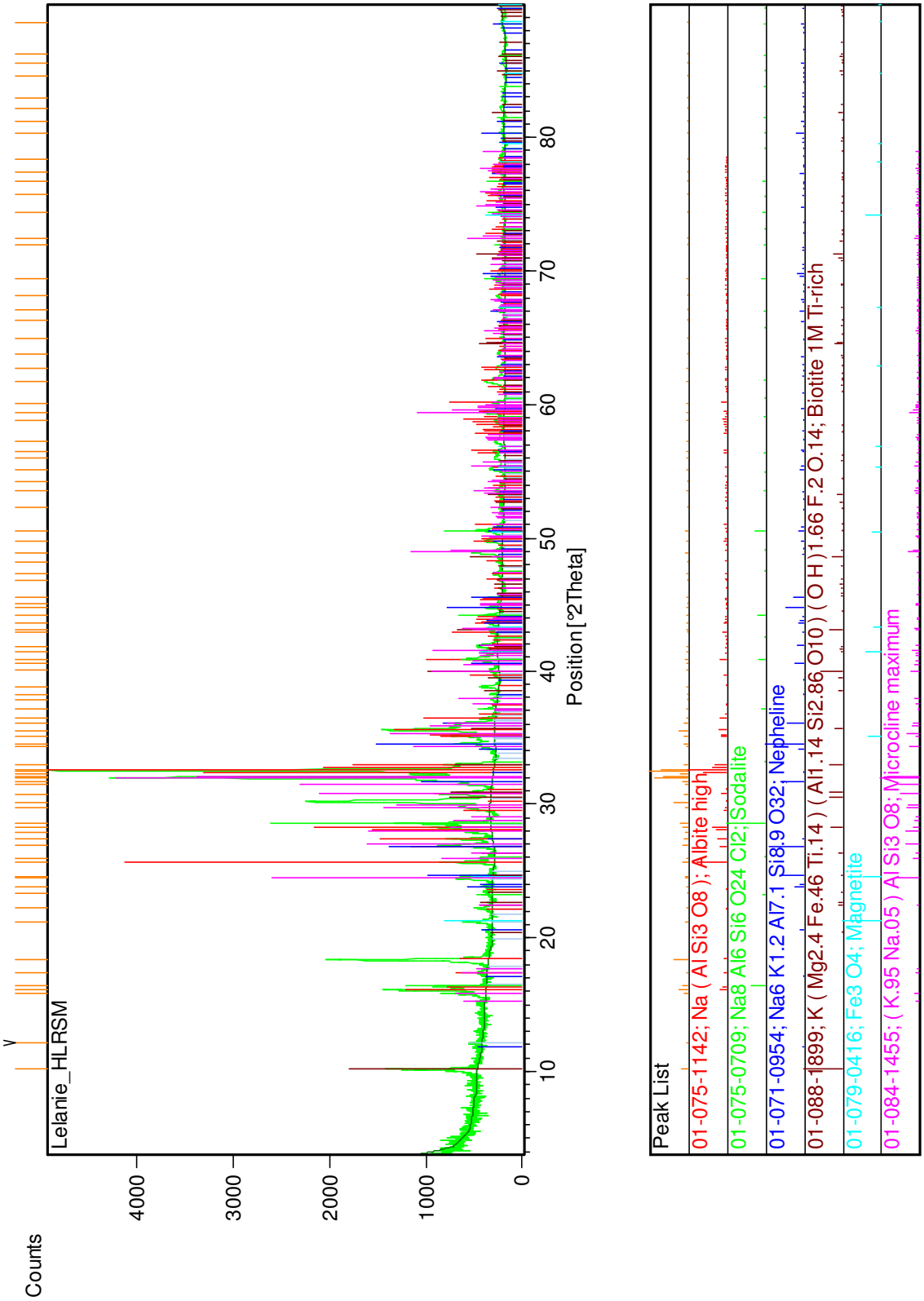

Quantification results of heavy liquid separation ROM starting material sample (HLRSM).

Autoquan - Results

University of Pretoria, MINERAL SCIENCE
MATERIAALKUNDE EN METALLURGIES

HLRSM

	Weight %	2 sigma
Actinolite	0.75	+- 0.26 %
Analcime, cubic	23.75	+- 0.69 %
Augite	4.97	+- 0.90 %
Chabazite	0.86	+- 0.45 %
Enstatite	4.24	+- 1.38 %
Fluorite	1.08	+- 0.18 %
Ilmenite	0.43	+- 0.24 %
Magnetite	0.35	+- 0.21 %
Microcline, intermediate2	22.73	+- 0.93 %
Nepheline	7.63	+- 0.54 %
Phlogopite	5.61	+- 0.78 %
Plagioclase Albite	22.76	+- 0.90 %
Sodalite	4.84	+- 0.27 %

Diffraction pattern of heavy liquid separation of ROM heavy portion sample (HLRH).

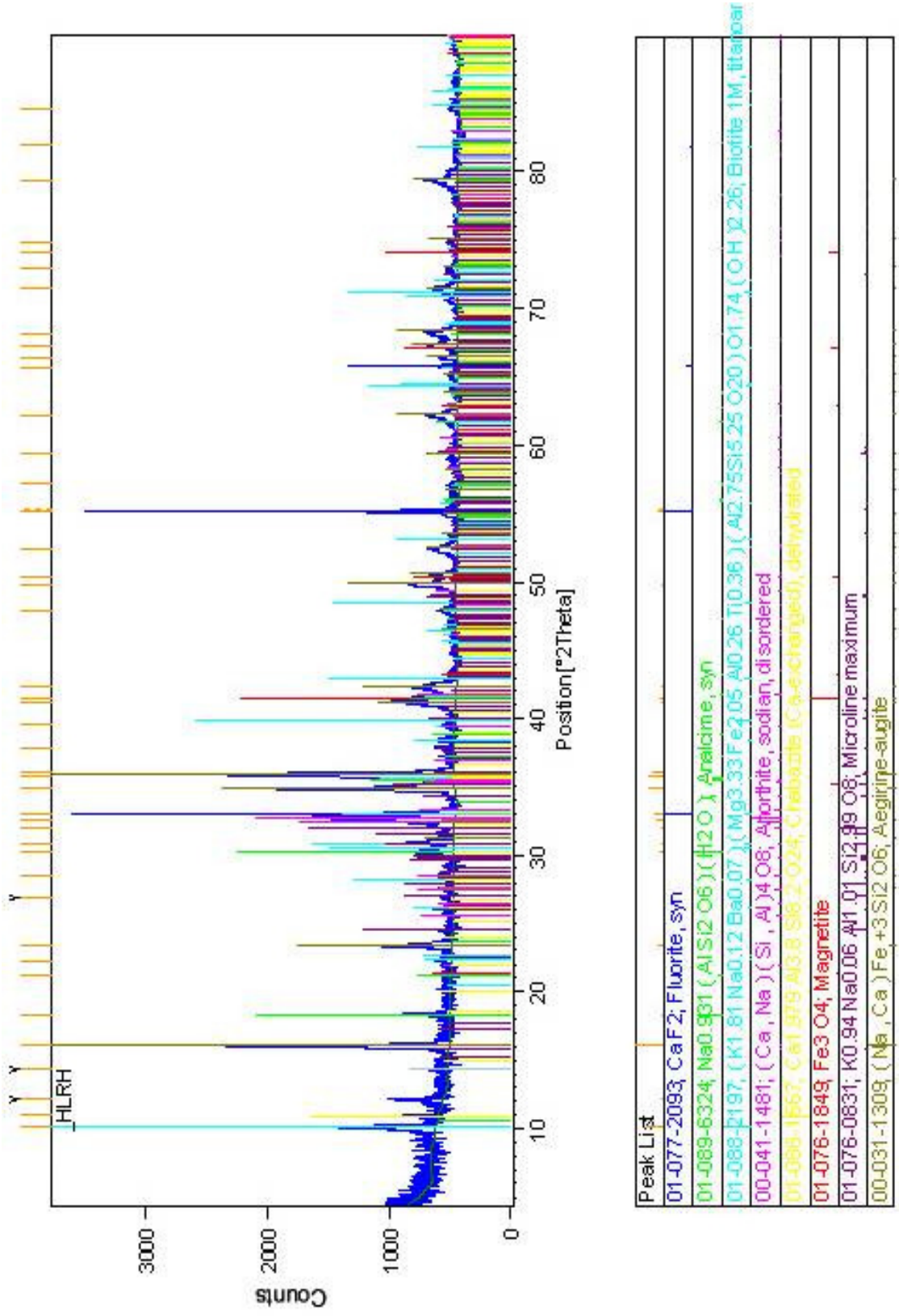

Quantification results of heavy liquid separation of ROM heavy portion sample (HLRH).

Autoquan - Results

University of Pretoria, MINERAL SCIENCE
MATERIAALKUNDE EN METALLURGIES

HLRH

	Weight %	2 sigma
Actinolite	2.52	+- 0.66 %
Aegirine-Augite	59.11	+- 1.89 %
Analcime, cubic	5.60	+- 0.75 %
Chabazite	1.83	+- 0.84 %
Enstatite	5.94	+- 1.41 %
Fluorite	3.82	+- 0.30 %
Ilmenite	2.39	+- 0.36 %
Magnetite	0.00	+- 0.00 %
Microcline, intermediate2	3.85	+- 0.87 %
Nepheline	1.00	+- 0.66 %
Phlogopite	10.15	+- 1.02 %
Plagioclase Albite	3.26	+- 0.81 %
Sodalite	0.54	+- 0.30 %

Quantification results of heavy liquid separation of ROM light portion sample (HLRL).

Autoquan - Results

University of Pretoria, MINERAL SCIENCE
MATERIAALKUNDE EN METALLURGIES

HLRL

	Weight %	2 sigma
Actinolite	0.00	+- 0.00 %
Analcime, cubic	23.49	+- 0.66 %
Augite	2.24	+- 0.69 %
Chabazite	0.79	+- 0.30 %
Enstatite	4.87	+- 1.14 %
Fluorite	0.66	+- 0.14 %
Ilmenite	0.45	+- 0.26 %
Magnetite	0.06	+- 0.08 %
Microcline, intermediate2	26.47	+- 0.93 %
Nepheline	8.09	+- 0.45 %
Phlogopite	2.40	+- 0.45 %
Plagioclase Albite	25.24	+- 0.87 %
Sodalite	5.24	+- 0.25 %

Appendix 2: Geochemical Results: X-Ray Fluorescence

Standard deviation, lower limits of detection (l.d) and 3σ values

	Standard deviation (wt %)	l.d (wt %)	3σ
SiO_2	0.4	0.02	1.2
TiO_2	0.03	0.0032	0.09
Al_2O_3	0.3	0.01	0.9
Fe_2O_3	0.3	0.0097	0.9
MnO	0.0065	0.0013	0.0195
MgO	0.1	0.0118	0.3
CaO	0.07	0.01	0.21
Na_2O	0.11	0.0265	0.33
K_2O	0.06	0.005	0.18
P_2O_5	0.08	0.01	0.24
Cr_2O_3	0.0053	0.0006	0.0159
NiO	0.01	0.0013	0.03
V_2O_5	0.0018	0.0008	0.0054
ZrO_2	0.005	0.0009	0.015
CuO	0.0037	0.0003	0.0111
As*	10	3	30
Cu	3	2	9
Ga	2	2	6
Mo	1	1	3
Nb	3	2	9
Ni	6	3	18
Pb	3	3	9
Rb	4	2	12
Sr	4	3	12
Th	2	3	6
U	2	3	6
W*	10	6	30
Y	4	3	12
Zn	4	4	12
Zr	6	10	18
Ba	14	5	42
Ce	14	6	42
Cl*	100	11	300
Co	6	3	18
Cr	40	15	120
F*	500	100	1500
La	24	5	72

Values for elements indicated with an * should be considered semi-quantitative.

Sample Data for XRF (l.d. = lower limit of detection. * indicates sample not analysed for trace elements and given value = 0)

Sample	SiO_2	TiO_2	Al_2O_3	Fe_2O_3	MnO	MgO	CaO	Na_2O
GSN certified	65.80	0.68	14.67	3.75	0.06	2.30	2.50	3.77
GSN measured	65.68	0.65	14.64	3.66	0.05	2.22	2.99	3.76
ROM 1	55.24	0.28	21.16	2.93	0.15	0.02	1.04	10.13
ROM 2	55.40	0.31	20.53	3.18	0.17	0.06	1.17	9.85
RNMAGS6T1	57.72	0.04	22.06	0.68	0.03	0.00	0.35	9.86
RMAGS1T1	46.31	2.22	13.26	16.07	0.89	0.79	4.01	9.29
RMAGS2T1	50.95	0.78	17.36	7.99	0.42	0.31	2.52	10.10
RMAGS3T1	53.97	0.25	21.26	2.84	0.15	0.00	1.11	10.36
RMAGS4T1	55.91	0.12	22.47	1.54	0.08	0.00	0.67	10.42
RMAGS5T1	56.19	0.07	22.61	1.11	0.05	0.00	0.49	10.38
RMAGS6T1	56.97	0.06	22.78	0.93	0.04	0.00	0.38	10.31
RNMAGS5T2	57.96	0.04	22.32	0.70	0.03	0.00	0.35	9.97
RMAGS1T2	46.65	2.01	12.35	16.29	0.87	0.78	4.18	9.28
RMAGS2T2	53.05	0.50	19.65	5.17	0.27	0.15	1.79	10.43
RMAGS3T2	55.15	0.20	21.92	2.35	0.12	0.00	0.94	10.36
RMAGS4T2	55.87	0.10	22.50	1.46	0.07	0.00	0.64	10.38
RMAGS5T2	56.07	0.07	22.61	1.05	0.05	0.00	0.45	10.26
RMP1	51.58	0.82	16.87	8.94	0.42	0.28	2.19	10.24
RMP2	49.68	0.82	16.81	8.54	0.44	0.37	2.49	10.49
RMP3*	46.50	0.57	20.50	5.34	0.33	0.20	2.15	10.68
RMP4*	49.00	0.53	20.80	5.99	0.33	0.20	2.10	10.40
RNMP1	56.64	0.11	21.31	1.08	0.07	0.00	0.81	9.80
RNMP2	56.00	0.10	21.69	1.09	0.07	0.00	0.80	9.81
RNMP3	57.25	0.08	21.78	0.80	0.06	0.00	0.76	9.46
RNMP4	57.14	0.08	21.75	0.78	0.06	0.00	0.75	9.83
SRD1	52.82	1.35	13.25	12.86	0.48	0.37	3.04	9.30
SRD2	54.58	0.68	16.46	7.88	0.33	0.24	2.26	9.34
SRL1	56.13	0.22	21.01	2.22	0.14	0.00	1.00	10.13
SRL2	56.55	0.24	21.00	2.48	0.14	0.00	1.03	10.00
SRM1	57.42	0.35	19.48	3.53	0.19	0.08	1.33	9.43
SRM2	55.37	0.64	17.12	6.89	0.29	0.24	1.94	9.37
URD1	53.46	1.02	14.79	9.96	0.41	0.34	2.67	9.34
URD2	54.39	0.73	16.74	6.58	0.31	0.23	2.22	10.13
URL1	55.26	0.32	20.94	3.21	0.17	0.02	1.19	9.85
URL2	55.08	0.24	21.38	2.25	0.12	L.D.	1.58	10.23
URM1	54.81	0.48	18.90	4.83	0.22	0.16	1.78	9.70
URM2	56.33	0.41	19.59	4.00	0.19	0.12	1.33	9.62
HLRH	43.63	2.75	4.68	25.21	1.12	1.48	7.55	8.35
HLRSM	55.05	0.32	20.88	3.33	0.16	0.13	1.08	9.91
HLRL	56.63	0.11	22.06	1.51	0.08	**l.d.**	0.52	9.91

Continued on next page

Sample	K_2O	P_2O_5	ZrO_2	LOI	Total	As	Cu	Ga
GSN certified	4.63	0.28	0.03	1.32	99.82	**l.d.**	20	22
GSN measured	4.72	0.29	0.03	1.29	100.01	**l.d.**	24	21
ROM 1	4.81	**l.d.**	0.11	3.04	98.91	17	8	26
ROM 2	5.24	0.02	0.11	3.49	99.52	17	9	29
RNMAGS6T1	5.46	**l.d.**	0.04	2.74	98.98	9	7	24
RMAGS1T1	2.89	0.08	0.28	2.07	98.15	31	17	29
RMAGS2T1	3.93	0.03	0.23	3.02	97.65	28	12	27
RMAGS3T1	4.71	**l.d.**	0.14	3.30	98.09	20	9	26
RMAGS4T1	5.01	**l.d.**	0.09	3.13	99.43	16	8	27
RMAGS5T1	5.16	**l.d.**	0.07	2.99	99.13	15	7	27
RMAGS6T1	5.28	**l.d.**	0.06	2.82	99.65	10	7	26
RNMAGS5T2	5.43	**l.d.**	0.05	2.74	99.60	10	6	24
RMAGS1T2	2.69	0.07	0.34	2.04	97.56	29	15	27
RMAGS2T2	4.48	0.02	0.18	3.15	98.82	25	11	28
RMAGS3T2	4.79	**l.d.**	0.12	3.29	99.23	16	9	27
RMAGS4T2	5.03	**l.d.**	0.09	3.28	99.43	13	7	27
RMAGS5T2	5.13	**l.d.**	0.07	3.61	99.38	11	8	26
RMP1	4.07	0.04	0.29	2.97	98.71	23	14	31
RMP2	3.53	0.05	0.25	4.76	98.23	25	14	31
RMP3*	6.99	0.04	0.29	4.23	97.81	0	0	0
RMP4*	5.10	0.04	0.24	4.65	99.38	0	0	0
RNMP1	5.94	0.02	0.08	2.57	98.43	8	101	28
RNMP2	5.90	0.02	0.08	3.47	99.05	7	8	29
RNMP3	5.83	0.02	0.07	3.33	99.44	8	8	29
RNMP4	5.98	0.02	0.07	3.21	99.67	5	15	29
SRD1	3.58	0.04	0.32	2.54	99.94	33	16	30
SRD2	4.55	0.03	0.21	2.81	99.36	24	13	30
SRL1	5.37	0.02	0.09	3.71	100.03	16	10	29
SRL2	5.55	0.02	0.11	2.55	99.66	19	11	30
SRM1	5.24	0.03	0.13	2.92	100.14	13	23	30
SRM2	4.83	0.03	0.18	2.81	99.70	15	11	29
URD1	4.05	0.03	0.27	2.58	98.93	30	17	28
URD2	4.60	0.03	0.21	2.75	98.93	20	36	29
URL1	5.29	0.02	0.12	3.55	99.93	16	11	29
URL2	5.43	0.02	0.09	3.44	99.84	10	14	29
URM1	5.22	0.02	0.13	3.04	99.29	13	15	29
URM2	5.40	0.02	0.11	2.99	100.13	14	15	29
HLRH	1.22	0.06	0.76	1.48	99.79	100	29	26
HLRSM	4.85	0.02	0.12	3.24	99.08	15	9	28
HLRL	5.26	**l.d.**	0.08	3.13	99.29	15	9	28

Continued on next page

Sample	Mo	Nb	Ni	Pb	Rb	Sr	Th	U
GSN certified	**l.d.**	21	34	53	185	570	42	8
GSN measured	**l.d.**	22	38	48	181	577	44	6
ROM 1	11	122	8	37	150	284	30	7
ROM 2	16	158	7	44	182	236	52	17
RNMAGS6T1	8	58	7	24	136	243	15	3
RMAGS1T1	13	244	12	56	181	297	43	19
RMAGS2T1	14	231	9	55	163	326	51	18
RMAGS3T1	12	146	7	48	149	311	36	9
RMAGS4T1	10	106	8	38	143	292	29	5
RMAGS5T1	9	87	8	35	140	279	23	**l.d.**
RMAGS6T1	9	78	7	28	140	268	21	**l.d.**
RNMAGS5T2	8	61	7	24	137	248	16	**l.d.**
RMAGS1T2	13	270	11	47	180	308	48	22
RMAGS2T2	13	181	9	51	158	314	43	13
RMAGS3T2	11	133	8	40	148	306	34	8
RMAGS4T2	10	105	7	33	142	291	27	5
RMAGS5T2	9	84	7	30	140	275	22	3
RMP1	21	281	9	72	162	309	90	40
RMP2	30	329	10	86	146	363	113	51
RMP3*	0	0	0	0	0	0	0	0
RMP4*	0	0	0	0	0	0	0	0
RNMP1	14	107	5	52	192	214	34	7
RNMP2	15	108	7	44	189	217	35	6
RNMP3	13	100	6	39	191	212	33	4
RNMP4	13	99	6	42	193	209	32	5
SRD1	17	282	9	159	153	265	93	43
SRD2	15	223	9	94	176	254	76	31
SRL1	15	159	7	38	192	235	52	15
SRL2	15	201	9	44	178	247	64	27
SRM1	15	146	7	40	182	238	50	12
SRM2	14	141	7	37	184	232	47	14
URD1	16	243	10	294	155	265	80	34
URD2	16	209	10	311	170	267	71	26
URL1	15	163	9	49	183	255	52	19
URL2	15	154	8	48	181	252	48	16
URM1	16	139	7	101	175	250	46	13
URM2	15	126	6	68	177	249	42	10
HLRH	24	443	23	120	153	377	115	64
HLRSM	14	131	8	44	166	265	40	10
HLRL	11	102	7	26	164	244	32	5

Continued on next page

Sample	W	Y	Zn	Zr	Cl	Cr	F	S
GSN certified	450	19	48	235	450	55	1050	140
GSN measured	455	13	52	237	605	59	2199	538
ROM 1	14	21	99	691	2833	32	6376	74
ROM 2	7	19	111	950	3076	30	10607	51
RNMAGS6T1	9	8	72	300	3443	32	4115	**l.d.**
RMAGS1T1	16	35	270	1684	1539	55	9797	161
RMAGS2T1	15	43	159	1463	2379	34	10054	214
RMAGS3T1	10	26	111	779	2775	31	7537	98
RMAGS4T1	7	19	91	550	2884	29	6128	103
RMAGS5T1	10	14	84	449	3126	30	5490	198
RMAGS6T1	6	12	83	403	3067	31	4630	108
RNMAGS5T2	6	9	71	319	3461	31	4702	41
RMAGS1T2	12	41	251	2002	1505	40	10839	167
RMAGS2T2	10	33	130	1056	2701	33	9120	145
RMAGS3T2	9	24	103	719	2776	32	7330	154
RMAGS4T2	9	19	91	553	2726	30	5920	60
RMAGS5T2	8	13	87	439	2945	30	4916	74
RMP1	**l.d.**	40	184	1992	2042	37	10635	143
RMP2	13	52	266	2156	2333	49	9476	549
RMP3*	0	0	0	0	0	0	0	0
RMP4*	0	0	0	0	0	0	0	0
RNMP1	**l.d.**	9	80	589	3666	34	9473	**l.d.**
RNMP2	**l.d.**	10	76	577	3397	33	9313	**l.d.**
RNMP3	**l.d.**	9	72	532	3544	32	9414	**l.d.**
RNMP4	**l.d.**	9	69	519	3521	30	9419	**l.d.**
SRD1	10	42	260	2729	1664	49	16436	192
SRD2	8	33	160	1861	1982	38	14633	93
SRL1	**l.d.**	18	111	999	2236	37	9761	37
SRL2	7	26	150	1586	1868	38	10785	77
SRM1	**l.d.**	17	155	791	3514	32	9270	**l.d.**
SRM2	**l.d.**	15	107	795	3281	32	9441	**l.d.**
URD1	14	34	325	2251	1754	426	13228	201
URD2	6	29	407	1786	2074	222	12403	152
URL1	9	18	144	1073	2480	43	9282	62
URL2	8	16	138	983	2303	50	8369	49
URM1	**l.d.**	16	244	794	3599	37	8815	79
URM2	7	14	179	705	3484	37	8191	**l.d.**
HLRH	17	62	410	4900	113	79	23211	767
HLRSM	**l.d.**	13	100	771	2028	**l.d.**	4550	123
HLRL	**l.d.**	8	63	507	2344	**l.d.**	2795	**l.d.**

Continued on next page

Sample	V	Ba	Ce	La
GSN certified	65	1400	75	135
GSN measured	57	1417	60	138
ROM 1	17	764	264	100
ROM 2	26	412	145	267
RNMAGS6T1	17	754	81	36
RMAGS1T1	56	614	503	180
RMAGS2T1	24	851	599	198
RMAGS3T1	17	804	350	121
RMAGS4T1	17	804	189	88
RMAGS5T1	17	755	139	59
RMAGS6T1	17	734	111	47
RNMAGS5T2	17	748	84	43
RMAGS1T2	52	660	595	225
RMAGS2T2	17	857	474	159
RMAGS3T2	17	811	315	114
RMAGS4T2	17	774	172	77
RMAGS5T2	17	718	131	45
RMP1	39	420	237	474
RMP2	35	422	283	582
RMP3*	0	0	0	0
RMP4*	0	0	0	0
RNMP1	17	460	104	154
RNMP2	17	464	108	175
RNMP3	17	458	100	161
RNMP4	17	436	95	157
SRD1	33	350	188	388
SRD2	25	409	176	347
SRL1	21	442	136	247
SRL2	26	406	152	299
SRM1	18	431	136	239
SRM2	26	430	121	225
URD1	33	378	159	320
URD2	34	413	157	307
URL1	19	443	139	250
URL2	20	462	126	224
URM1	17	459	122	210
URM2	18	479	123	206
HLRH	69	340	170	446
HLRSM	17	685	137	260
HLRL	17	702	123	220

UniQuant®5 results for Low-intensity dry magnetic separation.

UniQuant results for dry magnetic separation samples

Sample	SiO_2	TiO_2	Al_2O_3	Fe_2O_3	MnO	CaO	Na_2O	K_2O
RMAGS1T1	49.31	2.09	15.24	14.84	0.70	3.97	10.19	2.84
RMAGS2T1	54.83	0.74	18.58	7.63	0.34	2.55	10.69	3.75
RMAGS3T1	58.19	0.23	21.24	2.77	0.13	1.30	10.83	4.62
RMAGS4T1	59.04	0.11	21.67	1.61	0.07	0.89	11.07	4.90
RMAGS5T1	59.55	0.07	21.77	1.22	0.05	0.66	11.01	5.03
RMAGS6T1	59.76	0.06	21.80	1.05	0.05	0.56	11.01	5.13
RNMAGS6T1	60.83	0.04	21.28	0.85	0.03	0.52	10.47	5.44
RMAGS1T2	49.53	1.92	14.70	15.23	0.69	4.11	10.22	2.71
RMAGS2T2	56.63	0.47	20.05	4.92	0.23	1.88	10.82	4.23
RMAGS3T2	58.47	0.19	21.39	2.32	0.11	1.12	11.00	4.71
RMAGS4T2	59.09	0.11	21.77	1.57	0.07	0.85	11.03	4.91
RMAGS5T2	59.57	0.07	21.90	1.19	0.05	0.64	10.98	5.04
RNMAGS5T2	60.65	0.04	21.38	0.84	0.04	0.55	10.68	5.28

Sample	ZnO	P_2O_5	ZrO_2	SO3	Cl	Ga_2O_3	Rb_2O	SrO
RMAGS1T1	0.03	0.09	0.24	0.10	0.11	0.00	0.02	0.03
RMAGS2T1	0.02	0.04	0.22	0.14	0.15	0.00	0.02	0.04
RMAGS3T1	0.01	0.02	0.12	0.09	0.18	0.00	0.02	0.04
RMAGS4T1	0.01	0.02	0.09	0.10	0.19	0.00	0.02	0.04
RMAGS5T1	0.01	0.02	0.07	0.14	0.20	0.00	0.02	0.04
RMAGS6T1	0.01	0.01	0.06	0.10	0.20	0.00	0.02	0.04
RNMAGS6T1	0.01	0.01	0.05	0.04	0.23	0.00	0.02	0.03
RMAGS1T2	0.03	0.08	0.28	0.09	0.10	0.00	0.02	0.03
RMAGS2T2	0.02	0.04	0.16	0.10	0.18	0.00	0.02	0.04
RMAGS3T2	0.01	0.02	0.11	0.12	0.18	0.00	0.02	0.04
RMAGS4T2	0.01	0.02	0.09	0.08	0.18	0.00	0.02	0.04
RMAGS5T2	0.01	0.02	0.07	0.07	0.19	0.00	0.02	0.04
RNMAGS5T2	0.01	0.01	0.05	0.06	0.23	0.00	0.02	0.03

Sample	Y_2O_3	Nb_2O_5	BaO	La_2O_3	CeO_2	Total
RMAGS1T1	0.00	0.04	0.06	0.02	0.04	99.18
RMAGS2T1	0.01	0.04	0.09	0.03	0.05	99.12
RMAGS3T1	0.00	0.03	0.09	0.02	0.04	99.31
RMAGS4T1	0.00	0.02	0.10	0.01	0.02	99.36
RMAGS5T1	0.00	0.02	0.09	0.01	0.01	99.37
RMAGS6T1	0.00	0.02	0.09	0.01	0.01	99.42
RNMAGS6T1	0.00	0.01	0.10	0.01	0.01	99.47
RMAGS1T2	0.00	0.04	0.07	0.03	0.05	99.11
RMAGS2T2	0.01	0.03	0.10	0.02	0.04	99.22
RMAGS3T2	0.00	0.03	0.10	0.02	0.03	99.31
RMAGS4T2	0.00	0.02	0.10	0.01	0.02	99.40
RMAGS5T2	0.00	0.02	0.09	0.01	0.02	99.44
RNMAGS5T2	0.00	0.01	0.09	0.01	0.01	99.46

Unpublished results of the major elements from (Kgwakgwe 2004).

XRF data from unpublished results of the Major elements from (Kgwakgwe 2004).

	SiO_2	TiO_2	Al_2O_3	Fe_2O_3	MnO	MgO	CaO	Na_2O	K_2O	LOI	Total
Grey nepheline1	55.44	0.75	20.04	4.55	0.16	0.53	2.13	9.00	3.90	2.49	99.08
Grey nepheline2	53.52	0.38	20.37	4.76	0.27	0.45	1.55	8.80	3.64	5.27	99.04
Grey nepheline3	57.21	0.28	21.14	3.08	0.15	0.09	1.13	7.97	4.58	3.71	99.34
Grey nepheline4	56.26	0.28	20.63	3.46	0.14	0.14	1.21	8.68	5.26	3.28	99.36
Grey nepheline5	56.17	0.35	21.02	3.70	0.19	0.28	1.38	9.07	4.58	3.06	99.86
Grey nepheline6	56.01	0.33	21.18	3.38	0.16	0.16	1.21	10.16	4.93	2.24	99.78
Grey nepheline7	55.92	0.31	21.36	3.32	0.16	0.15	1.18	10.42	4.99	2.06	99.90
Grey nepheline8	55.54	0.32	20.69	3.83	0.19	0.17	1.29	9.46	4.76	3.46	99.73
Grey nepheline9	56.54	0.30	21.11	3.52	0.18	0.15	1.22	8.59	4.75	3.50	99.88
Grey nepheline10	57.30	0.31	20.92	3.23	0.16	0.03	1.05	8.86	4.92	3.07	99.88
Grey nepheline11	56.41	0.38	20.54	4.29	0.21	0.25	1.47	7.72	4.60	3.93	99.83
Grey nepheline12	57.45	0.30	20.56	3.25	0.18	0.17	1.25	9.19	4.08	3.32	99.80
Grey nepheline13	56.12	0.35	20.71	3.77	0.21	0.17	1.26	10.20	4.75	2.44	100.01
Grey nepheline14	56.74	0.29	21.26	3.28	0.14	0.12	1.01	9.77	4.90	2.48	99.99
Grey nepheline15	56.18	0.49	20.55	3.75	0.16	0.37	1.79	7.69	4.70	4.22	99.93
Grey nepheline16	55.51	0.49	20.48	3.92	0.18	0.41	1.60	8.37	4.72	4.11	99.81
Grey nepheline17	57.15	0.32	20.68	3.08	0.15	0.11	1.02	9.61	5.00	2.67	99.79
Grey nepheline18	56.85	0.28	21.17	2.80	0.13	0.11	0.98	8.61	4.97	4.19	100.12
Grey nepheline19	55.20	0.48	20.08	3.88	0.18	0.32	1.52	8.58	4.57	5.09	99.95
Grey nepheline20	54.43	0.54	19.63	4.31	0.22	0.41	1.68	10.03	4.57	3.86	99.71
Grey nepheline21	57.00	0.29	20.99	3.20	0.15	0.11	0.92	8.50	5.17	3.55	99.88
Grey nepheline22	56.00	0.37	20.81	3.98	0.20	0.19	1.16	9.33	4.78	3.11	100.11
Grey nepheline23	55.73	0.37	20.39	3.80	0.20	0.19	1.35	9.60	4.68	3.45	99.86
Grey nepheline24	55.74	0.44	20.18	4.19	0.23	0.15	1.30	9.84	4.64	3.16	99.99
Grey nepheline25	55.95	0.34	20.41	3.80	0.19	0.14	1.31	10.07	4.64	3.15	100.01
Grey nepheline26	56.04	0.42	20.44	4.11	0.20	0.05	1.32	9.57	5.13	2.76	100.05
Grey nepheline27	54.94	0.39	19.56	4.28	0.23	0.23	1.54	9.61	4.51	4.55	99.88
Grey nepheline28	55.94	0.37	20.35	3.99	0.21	0.15	1.33	10.08	4.45	3.23	100.12
Grey nepheline29	56.18	0.33	20.85	3.51	0.16	0.15	1.27	10.33	4.91	2.30	100.01
Grey nepheline30	56.10	0.35	20.89	3.61	0.17	0.16	1.31	10.06	4.55	2.75	99.98
Grey nepheline31	56.56	0.36	21.08	3.46	0.17	0.15	1.29	10.27	4.44	2.25	100.05
Grey nepheline32	56.09	0.34	20.96	3.43	0.17	0.15	1.22	10.34	4.81	2.44	99.97
Grey nepheline33	56.81	0.37	20.96	3.41	0.16	0.17	1.33	10.17	4.79	1.70	99.90
Grey nepheline34	55.86	0.37	20.57	3.25	0.20	0.00	0.79	9.87	5.07	3.45	99.44
Grey nepheline35	54.69	0.35	20.71	3.56	0.21	0.04	1.12	10.63	4.95	2.92	99.17
Grey nepheline36	54.71	0.33	20.79	3.38	0.16	0.03	1.11	10.26	4.76	3.35	98.89
Grey nepheline37	55.45	0.38	20.80	3.92	0.23	0.07	1.24	9.28	4.86	3.37	99.59
Grey nepheline38	53.78	0.32	20.48	3.43	0.16	0.04	1.14	9.91	4.65	4.69	98.60

Continued on next page

	SiO_2	TiO_2	Al_2O_3	Fe_2O_3	MnO	MgO	CaO	Na_2O	K_2O	LOI	Total
Red nepheline1	55.76	0.37	20.39	3.95	0.18	0.40	1.47	8.37	4.30	4.60	99.82
Red nepheline2	56.65	0.51	19.78	4.78	0.24	0.11	1.10	7.75	4.71	3.67	99.30
Red nepheline3	56.37	0.34	20.12	3.50	0.16	0.84	2.17	6.18	5.58	4.32	99.61
Red nepheline4	56.89	0.41	20.20	4.78	0.21	0.29	1.01	7.90	4.45	3.85	100.03
Red nepheline5	56.21	0.46	20.07	4.46	0.18	0.34	1.07	7.93	4.09	4.86	99.87
Red nepheline6	56.65	0.47	20.21	4.40	0.19	0.29	1.04	7.44	5.09	3.76	99.54
Red nepheline7	54.42	0.30	20.64	4.10	0.18	0.92	2.62	5.65	5.39	5.05	99.27
Red nepheline8	55.22	0.53	19.85	4.62	0.24	0.38	1.32	8.89	4.51	4.19	99.78
Red nepheline9	55.27	0.51	19.93	4.78	0.23	0.39	1.21	8.74	3.55	4.46	99.07
Red nepheline10	56.53	0.32	20.73	3.97	0.19	0.28	1.20	7.28	5.25	3.99	99.78
Red nepheline11	56.30	0.35	20.07	3.85	0.20	0.21	1.27	8.27	3.90	4.86	99.31
Red nepheline12	56.86	0.39	20.06	4.59	0.21	0.24	1.08	7.86	4.46	4.21	100.02
Red nepheline13	56.92	0.32	20.57	3.90	0.18	0.21	1.25	7.32	4.96	4.23	99.90
Red nepheline14	56.86	0.34	20.38	4.65	0.21	0.41	1.20	6.07	5.62	3.79	99.61
Red nepheline15	57.54	0.34	20.06	4.24	0.25	0.21	1.10	7.10	4.75	4.41	100.02
Red nepheline16	56.56	0.50	19.92	4.93	0.22	0.39	1.23	6.88	4.93	4.34	99.91
Red nepheline17	57.04	0.38	20.30	4.26	0.19	0.20	1.00	7.16	4.75	4.40	99.69
Red nepheline18	56.34	0.34	19.42	4.81	0.23	0.36	1.66	7.44	4.18	5.07	99.89
Red nepheline19	58.48	0.40	19.54	4.73	0.20	0.40	1.08	5.85	5.79	3.48	99.99
Red nepheline20	58.14	0.34	19.60	5.28	0.20	0.42	1.15	6.16	5.21	3.19	99.69
Red nepheline21	56.76	0.50	19.41	5.04	0.24	0.35	1.37	6.82	4.71	4.64	99.86
Red nepheline22	58.73	0.37	18.95	4.57	0.25	0.33	1.82	6.04	5.53	3.07	99.72
Red nepheline23	56.84	0.51	19.70	4.62	0.23	0.36	1.04	7.58	4.52	4.43	99.85
Red nepheline24	57.10	0.47	19.89	4.60	0.19	0.26	1.19	7.53	4.35	4.40	100.01
Red nepheline25	56.66	0.50	19.92	4.87	0.24	0.30	1.06	7.23	5.08	3.97	99.84
Red nepheline26	57.16	0.44	20.20	4.69	0.20	0.25	0.96	7.90	4.89	3.33	100.03
Red nepheline27	57.63	0.48	20.14	4.40	0.22	0.33	1.30	7.72	3.81	3.99	100.04
Red nepheline28	56.79	0.46	19.47	5.01	0.24	0.32	1.14	8.24	4.31	3.99	99.97
Red nepheline29	57.36	0.36	20.60	4.20	0.21	0.15	0.84	7.64	5.19	3.34	99.88
Red nepheline30	56.95	0.38	20.42	4.14	0.20	0.18	1.23	7.43	5.12	3.91	99.99
Red nepheline31	57.20	0.55	20.29	4.55	0.22	0.34	1.39	9.42	4.95	1.02	99.95
Red nepheline32	55.11	0.50	19.76	3.88	0.22	1.02	1.54	6.79	5.07	5.96	99.88
Red nepheline33	66.83	0.62	13.17	7.70	0.12	2.27	2.48	1.57	2.77	2.22	99.90
Red nepheline34	52.46	1.50	18.76	6.75	0.21	1.41	4.15	8.28	3.72	1.51	99.12
Red nepheline35	50.31	2.31	17.54	8.90	0.25	2.16	6.29	5.80	3.13	2.28	99.47
Red nepheline36	53.26	1.63	18.99	7.29	0.27	1.27	4.72	6.38	3.93	1.66	99.61
Red nepheline37	50.04	0.44	22.12	3.86	0.20	0.20	1.05	11.47	2.13	7.92	99.43
Red nepheline38	54.77	0.33	20.71	3.65	0.20	0.07	1.18	7.97	4.45	4.67	98.01

Appendix 3. Geochemical Results: Electron Microprobe Analysis

Microprobe conditions and lowest limits of detection

Acceleration potential	20 kV
Beam current	30 nA
Counting time	20 sec
Beam diameter	~ 1 micron
Standards	Hematite for Fe
	Jadeite for Na and Al
	Halite for Cl
	Orthoclase for K
	Periclase for Mg
	Rutile for Ti
	Wollastonite for Ca and Si
Limits of detection Element %	
Na	0.041
Mg	0.026
Al	0.022
Si	0.037
Cl	0.031
K	0.023
Ca	0.022
Ti	0.026
Fe	0.120

Reference analyses of standards used for calibration of microprobe. (l.d. = lowest limit of detection, n.d. = not detected)

Reference	**Hematite**	Hematite	Hematite	Hematite	**Jadeite**	Jadeite	Jadeite	Jadeite
PHASE	**Expected**	1	2	3	**Expected**	1	2	3
Na	**n.d.**	l.d.	l.d.	l.d.	**11.2800**	11.2871	11.2316	11.2240
Mg	**n.d.**	l.d.	l.d.	l.d.	**0.0600**	0.0515	0.0659	0.0639
Al	**n.d.**	0.0054	0.0043	0.0043	**13.3300**	13.3172	13.2918	13.3834
Si	**n.d.**	0.0271	0.0280	0.0263	**27.7900**	27.5901	27.7015	27.5861
Cl	**n.d.**	l.d.	l.d.	l.d.	**n.d**	l.d.	l.d.	l.d.
K	**n.d.**	l.d.	l.d.	l.d.	**n.d**	0.0033	0.0041	0.0063
Ca	**n.d.**	l.d.	l.d.	l.d.	**0.0400**	0.0447	0.0427	0.0472
Ti	**n.d.**	l.d.	l.d.	l.d.	**n.d**	l.d.	0.0048	l.d.
Fe (as Fe_2O_3)	**69.9400**	69.6387	69.7140	69.6971	**0.1000**	0.0939	0.1516	0.0940
O	**30.0500**	29.9562	29.9891	29.9801	**47.5313**	47.2890	47.4108	47.3312
Total	**99.9900**	99.6275	99.7370	99.7114	**100.1313**	99.6768	99.9048	99.7373
Reference	**Halite**	Halite	Halite	Halite	**Orthoclase**	Orthoclase	Orthoclase	Orthoclase
PHASE	**Expected**	1	2	3	**Expected**	1	2	3
Na	**39.3400**	39.3540	39.3889	39.4588	**1.0100**	1.0152	1.0123	0.9848
Mg	**n.d.**	n.d.	n.d.	n.d.	**n.d.**	n.d.	n.d.	n.d.
Al	**n.d.**	n.d.	n.d.	n.d.	**9.8200**	9.7380	9.7577	9.7767
Si	**n.d.**	0.0045	0.0039	0.0046	**30.4500**	30.3420	30.3091	30.3864
Cl	**60.6600**	60.4455	60.5458	60.4351	**0.0000**	n.d.	l.d.	l.d.
K	**n.d.**	0.0132	0.0090	0.0138	**12.2000**	12.1444	12.2138	12.2314
Ca	**n.d.**	n.d.	n.d.	n.d.	**0.0100**	0.0140	0.0155	0.0225
Ti	**n.d.**	0.0065	0.0082	0.0050	**n.d**	0.0039	0.0040	0.0093
Fe (as Fe_2O_3)	**n.d.**	0.0777	0.0828	0.0746	**l.d.**	l.d.	l.d.	l.d.
O	**n.d.**	n.d.	n.d.	n.d.	**46.2769**	46.0841	46.0706	46.1662
Total	**n.d.**	99.9014	100.0386	99.9919	**99.7869**	99.3813	99.4082	99.5803
Reference	**Periclase**	Periclase	Periclase	Periclase	**Rutile**	Rutile	Rutile	Rutile
PHASE	**Expected**	1	2	3	**Expected**	1	2	3
Na	**n.d.**	n.d.	n.d.	n.d.	**n.d.**	0.0066	0.0074	n.d.
Mg	**60.3000**	59.9010	59.9521	59.8332	**n.d.**	0.0028	0.0041	n.d.
Al	**n.d.**	n.d.	n.d.	n.d.	**n.d.**	0.0079	0.0146	n.d.
Si	**n.d.**	0.0235	0.0210	0.0312	**n.d.**	0.0598	0.0709	0.0430
Cl	**n.d.**	l.d.	l.d.	l.d.	**n.d.**	n.d.	n.d.	n.d.
K	**n.d.**	n.d.	n.d.	n.d.	**n.d.**	0.0032	l.d.	0.0047
Ca	**n.d.**	0.0047	0.0049	0.0058	**n.d.**	0.0029	0.0047	n.d.
Ti	**n.d.**	l.d.	l.d.	l.d.	**59.9500**	59.7042	59.7460	59.8410
Fe (as Fe_2O_3)	**n.d.**	l.d.	l.d.	l.d.	**n.d.**	l.d.	l.d.	l.d.
O	**39.6856**	39.4687	39.5018	39.4286	**40.0677**	39.9946	40.0378	40.0710
Total	**99.9856**	99.4359	99.5246	99.3294	**100.0177**	99.8054	99.8993	100.0207

Continued on next page

Reference	**Wollastonite**	Wollastonite	Wollastonite	Wollastonite
PHASE	**Expected**	1	2	3
Na	**0.0100**	0.0069	l.d.	l.d.
Mg	**0.0100**	0.0178	0.0083	0.0160
Al	**n.d.**	n.d.	n.d.	n.d.
Si	**23.9900**	23.8825	23.8931	23.8850
Cl	**n.d.**	n.d.	n.d.	n.d.
K	**n.d.**	n.d.	n.d.	n.d.
Ca	**34.1700**	34.0328	34.0285	34.1540
Ti	**0.0100**	n.d.	0.0027	l.d.
Fe (as Fe_2O_3)	**0.1500**	0.1454	0.1372	0.1450
O	**41.0455**	40.8637	40.8643	40.9132
Total	**99.3855**	98.9491	98.9358	99.1182

Microprobe results elements calculated to oxides (l.d. = lower limit of detection)

Analysis	**1**	**2**	**3**	**4**	**5**	**6**	**7**	**8**
Sample	**HLRL**	**HLRL**	**RNMP4**	**HLRL**	**HLRL**	**HLRL**	**HLRL**	**RNMP4**
Mineral	Aegirine	Aegirine	Aegirine	Aegirine	Aegirine	Aegirine	Aegirine	Aegirine
Na	8.102	8.971	8.200	9.853	9.177	9.305	10.255	8.222
Mg	l.d.	l.d.	0.232	0.105	l.d.	l.d.	l.d.	0.140
Al	0.288	0.565	0.938	0.265	0.242	0.121	0.128	0.646
Si	24.254	23.746	23.413	23.967	24.239	24.425	23.328	24.194
Cl	0.035	l.d.	0.081	l.d.	l.d.	l.d.	l.d.	0.050
K	0.030	0.071	0.068	l.d.	0.368	l.d.	0.036	0.072
Ca	l.d.	0.218	1.074	0.039	0.062	l.d.	1.084	0.466
Ti	l.d.	l.d.	0.930	0.372	0.208	l.d.	l.d.	0.373
Fe	24.636	24.087	22.736	23.355	23.634	24.193	23.879	24.103
O	41.294	41.126	41.340	41.335	41.414	41.573	40.953	41.891
Total	98.643	98.791	99.011	99.310	99.347	99.662	99.671	100.156
Analysis	**9**	**10**	**11**	**12**	**13**	**14**	**15**	**16**
Sample	**ROM 1**	**ROM 1**	**RNMP4**	**RNMP4**	**RNMP4**	**ROM 1**	**HLRL**	**HLRL**
Mineral	Aegirine	Aegirine	Aegirine	Aegirine	Aegirine	Aegirine	Aegirine	Aegirine
Na	8.925	9.008	9.040	9.687	8.108	8.149	9.451	9.979
Mg	l.d.	0.143	0.180	0.112	0.231	0.152	0.059	0.078
Al	0.491	0.422	0.705	0.632	0.745	0.361	0.934	0.234
Si	24.805	24.216	23.983	23.657	23.618	23.631	23.949	24.482
Cl	l.d.	l.d.	l.d.	l.d.	l.d.	l.d.	l.d.	l.d.
K	0.100	0.112	0.049	l.d.	0.044	l.d.	l.d.	l.d.
Ca	l.d.	0.499	0.303	0.274	1.823	2.392	0.268	0.047
Ti	l.d.	0.335	0.413	0.207	1.791	0.424	0.297	0.329
Fe	23.932	23.920	24.115	24.569	22.751	24.671	24.570	24.391
O	42.107	41.911	41.977	41.757	42.246	42.011	42.302	42.336
Total	100.388	100.568	100.776	100.906	101.383	101.793	101.857	101.881
Analysis	**17**	**18**	**19**	**20**	**1**	**2**	**3**	**4**
Sample	**HLRL**	**ROM 1**	**HLRL**	**RNMP4**	**RNMP4**	**RNMP4**	**RNMP4**	**HLRL**
Mineral	Aegirine	Aegirine	Aegirine	Aegirine	Albite	Albite	Albite	Albite
Na	9.216	8.636	9.112	9.991	8.621	8.504	8.193	8.395
Mg	0.094	0.217	l.d.	0.052	l.d.	l.d.	l.d.	l.d.
Al	0.788	0.293	0.235	0.342	10.046	10.252	10.007	10.188
Si	24.049	24.194	24.401	24.567	30.758	30.901	31.045	31.037
Cl	l.d.	l.d.	l.d.	l.d.	l.d.	l.d.	l.d.	l.d.
K	l.d.	l.d.	2.002	l.d.	0.246	0.044	0.322	0.075
Ca	0.618	2.440	l.d.	0.401	l.d.	l.d.	l.d.	0.025
Ti	0.314	0.633	l.d.	0.230	l.d.	l.d.	l.d.	l.d.
Fe	24.475	23.164	24.219	24.076	0.204	0.003	0.206	0.035
O	42.337	42.317	41.998	42.456	47.111	47.294	47.266	47.377
Total	101.905	101.905	101.987	102.130	96.999	97.013	97.055	97.166

Continued on next page

Analysis	5	6	7	8	9	10	11	12
Sample	ROM 1	ROM 1	ROM 1	HLRL	HLRL	ROM 1	ROM 1	ROM 1
Mineral	Albite	Albite	Albite	Albite	Albite	Albite	Albite	Albite
Na	8.522	9.443	8.518	8.430	8.414	8.339	8.802	9.176
Mg	l.d.	l.d.	l.d.	l.d.	l.d.	l.d.	l.d.	l.d.
Al	10.254	10.009	10.306	10.228	10.273	10.309	10.168	10.116
Si	30.919	30.410	30.922	31.123	31.100	31.146	30.945	30.839
Cl	l.d.	0.051	l.d.	l.d.	l.d.	l.d.	l.d.	l.d.
K	0.107	0.208	0.110	0.031	0.069	0.071	0.121	0.043
Ca	l.d.	0.028	l.d.	l.d.	l.d.	l.d.	l.d.	l.d.
Ti	l.d.	l.d.	l.d.	l.d.	l.d.	l.d.	l.d.	l.d.
Fe	l.d.	0.173	l.d.	l.d.	l.d.	l.d.	l.d.	l.d.
O	47.347	46.954	47.395	47.503	47.518	47.584	47.421	47.349
Total	97.204	97.278	97.308	97.357	97.422	97.508	97.567	97.583

Analysis	13	14	15	16	17	18	19	20
Sample	HLRL	RNMP4	ROM 1	RNMP4	RNMP4	HLRL	ROM 1	HLRL
Mineral	Albite	Albite	Albite	Albite	Albite	Albite	Albite	Albite
Na	8.307	8.577	8.437	8.493	8.413	8.516	8.992	8.819
Mg	l.d.	l.d.	l.d.	l.d.	l.d.	l.d.	l.d.	l.d.
Al	10.169	10.158	10.175	10.107	10.211	10.266	10.165	10.295
Si	31.051	31.012	31.140	31.160	31.120	31.208	31.057	30.947
Cl	l.d.	l.d.	l.d.	l.d.	l.d.	l.d.	l.d.	l.d.
K	0.515	0.118	0.172	0.114	0.068	0.105	0.072	0.109
Ca	l.d.	l.d.	0.053	l.d.	l.d.	l.d.	l.d.	l.d.
Ti	l.d.	l.d.	l.d.	l.d.	l.d.	l.d.	l.d.	l.d.
Fe	l.d.	0.246	0.124	0.211	0.262	l.d.	l.d.	0.208
O	47.453	47.482	47.563	47.559	47.595	47.686	47.580	47.596
Total	97.599	97.621	97.671	97.681	97.703	97.842	97.919	98.001

Analysis	21	22	23	24	25	26	27	28
Sample	HLRL	RNMP4	ROM 1	RNMP4	ROM 1	RNMP4	ROM 1	RNMP4
Mineral	Albite	Albite	Albite	Albite	Albite	Albite	Albite	Albite
Na	8.663	8.631	8.424	8.016	8.618	8.609	8.561	8.722
Mg	l.d.	l.d.	l.d.	l.d.	l.d.	l.d.	l.d.	l.d.
Al	10.193	10.337	10.387	10.450	10.301	10.219	10.376	10.259
Si	31.089	31.185	31.155	31.498	31.138	31.356	31.345	31.376
Cl	0.051	l.d.	l.d.	l.d.	l.d.	l.d.	l.d.	0.039
K	0.181	0.081	0.280	0.109	0.217	0.053	0.078	0.034
Ca	l.d.	l.d.	l.d.	0.023	l.d.	l.d.	l.d.	l.d.
Ti	l.d.	l.d.	l.d.	l.d.	l.d.	l.d.	l.d.	l.d.
Fe	0.202	l.d.	l.d.	l.d.	0.160	0.129	l.d.	l.d.
O	47.620	47.753	47.733	48.004	47.748	47.869	47.955	47.941
Total	98.011	98.029	98.034	98.143	98.198	98.274	98.402	98.458

Continued on next page

Analysis	29	30	31	32	33	34	35	36
Sample	HLRL	RNMP4	ROM 1	HLRL	RNMP4	RNMP4	HLRL	HLRL
Mineral	Albite	Albite	Albite	Albite	Albite	Albite	Albite	Albite
Na	8.379	8.470	8.490	8.470	8.772	8.408	8.347	8.457
Mg	l.d.	l.d.	l.d.	l.d.	l.d.	l.d.	l.d.	l.d.
Al	10.387	10.470	10.435	10.416	10.329	10.485	10.335	10.394
Si	31.222	31.378	31.422	31.487	31.389	31.637	31.315	31.713
Cl	l.d.	l.d.	l.d.	l.d.	l.d.	l.d.	l.d.	l.d.
K	0.601	0.092	0.087	0.110	0.087	0.087	0.958	0.087
Ca	0.023	l.d.	l.d.	l.d.	l.d.	l.d.	l.d.	l.d.
Ti	l.d.	l.d.	l.d.	l.d.	l.d.	l.d.	l.d.	l.d.
Fe	l.d.	l.d.	l.d.	l.d.	l.d.	l.d.	l.d.	l.d.
O	47.856	48.047	48.062	48.114	48.030	48.308	47.988	48.349
Total	98.486	98.538	98.549	98.639	98.666	98.935	99.014	99.058

Analysis	37	38	39	1	2	3	4	5
Sample	RNMP4	HLRL	HLRL	ROM 1	ROM 1	HLRL	ROM 1	RNMP4
Mineral	Albite	Albite	Albite	Microcline	Microcline	Microcline	Microcline	Microcline
Na	8.542	8.955	8.549	0.553	0.587	0.339	0.277	0.179
Mg	l.d.	l.d.	l.d.	l.d.	l.d.	l.d.	l.d.	l.d.
Al	10.486	10.443	10.547	9.329	9.480	9.449	9.413	9.436
Si	31.588	31.562	32.011	29.449	29.854	29.680	29.704	29.792
Cl	l.d.	l.d.	l.d.	l.d.	l.d.	l.d.	l.d.	l.d.
K	0.108	0.048	0.159	13.413	13.140	13.804	14.074	13.975
Ca	l.d.	l.d.	l.d.	l.d.	l.d.	l.d.	l.d.	l.d.
Ti	l.d.	l.d.	l.d.	l.d.	l.d.	l.d.	l.d.	l.d.
Fe	l.d.	l.d.	l.d.	l.d.	l.d.	l.d.	l.d.	l.d.
O	48.318	48.375	48.872	44.789	45.354	45.169	45.205	45.279
Total	99.087	99.412	100.195	97.653	98.494	98.513	98.742	98.752

Analysis	6	7	8	9	10	11	12	13
Sample	HLRL	RNMP4	ROM 1	RNMP4	ROM 1	ROM 1	RNMP4	ROM 1
Mineral	Microcline	Microcline	Microcline	Microcline	Microcline	Microcline	Microcline	Microcline
Na	0.165	0.182	0.155	0.156	0.181	0.184	1.077	0.243
Mg	l.d.	l.d.	l.d.	l.d.	l.d.	l.d.	l.d.	l.d.
Al	9.483	9.450	9.466	9.474	9.420	9.379	9.539	9.396
Si	29.748	29.844	29.701	29.837	29.970	29.900	30.164	30.017
Cl	0.040	l.d.	l.d.	l.d.	0.066	l.d.	l.d.	l.d.
K	14.023	13.987	14.257	14.124	13.892	14.215	12.600	13.982
Ca	l.d.	0.043	l.d.	0.028	l.d.	l.d.	l.d.	0.059
Ti	l.d.	l.d.	l.d.	l.d.	l.d.	l.d.	l.d.	l.d.
Fe	l.d.	l.d.	l.d.	l.d.	l.d.	l.d.	l.d.	l.d.
O	45.268	45.346	45.244	45.377	45.452	45.380	45.810	45.546
Total	98.776	98.874	98.886	99.022	99.057	99.104	99.237	99.307

Continued on next page

Analysis	14	15	16	17	18	19	20	21
Sample	ROM 1	HLRL	ROM 1	HLRL	HLRL	RNMP4	HLRL	HLRL
Mineral	Microcline	Microcline	Microcline	Microcline	Microcline	Microcline	Microcline	Microcline
Na	0.194	0.180	0.203	0.182	0.134	0.133	0.162	0.164
Mg	l.d.	l.d.	l.d.	l.d.	l.d.	l.d.	l.d.	l.d.
Al	9.531	9.540	9.477	9.394	9.580	9.502	9.499	9.535
Si	29.783	29.888	30.032	30.002	29.890	29.932	30.116	30.039
Cl	l.d.	l.d.	l.d.	0.040	0.064	l.d.	0.035	l.d.
K	14.301	14.290	14.098	14.364	14.305	14.087	14.232	14.242
Ca	0.111	l.d.	l.d.	l.d.	l.d.	l.d.	l.d.	l.d.
Ti	l.d.	l.d.	l.d.	l.d.	l.d.	l.d.	l.d.	l.d.
Fe	l.d.	l.d.	l.d.	l.d.	l.d.	l.d.	l.d.	l.d.
O	45.441	45.530	45.631	45.540	45.556	45.601	45.735	45.696
Total	99.387	99.490	99.532	99.545	99.560	99.564	99.810	99.813

Analysis	22	23	24	25	26	27	28	29
Sample	HLRL	ROM 1	RNMP4	HLRL	HLRL	RNMP4	HLRL	HLRL
Mineral	Microcline	Microcline	Microcline	Microcline	Microcline	Microcline	Microcline	Microcline
Na	0.277	0.162	0.195	0.170	0.976	0.149	0.247	0.123
Mg	l.d.	l.d.	l.d.	l.d.	l.d.	l.d.	l.d.	l.d.
Al	9.529	9.511	9.601	9.577	9.572	9.547	9.555	9.612
Si	30.098	30.077	30.129	30.176	30.371	30.212	30.101	30.160
Cl	l.d.	l.d.	l.d.	0.076	0.051	l.d.	0.079	l.d.
K	14.070	14.332	14.167	14.188	12.905	14.258	14.298	14.307
Ca	l.d.	l.d.	l.d.	l.d.	l.d.	l.d.	l.d.	l.d.
Ti	l.d.	l.d.	l.d.	l.d.	l.d.	l.d.	l.d.	l.d.
Fe	l.d.	l.d.	l.d.	l.d.	l.d.	l.d.	l.d.	l.d.
O	45.770	45.728	45.841	45.872	46.135	45.894	45.818	45.896
Total	99.852	99.870	99.990	100.106	100.123	100.130	100.148	100.164

Analysis	30	31	32	33	34	35	36	37
Sample	HLRL	ROM 1	ROM 1	RNMP4	ROM 1	RNMP4	RNMP4	RNMP4
Mineral	Microcline	Microcline	Microcline	Microcline	Microcline	Microcline	Microcline	Microcline
Na	0.115	0.201	0.150	0.116	0.218	0.185	0.153	0.177
Mg	l.d.	l.d.	l.d.	l.d.	l.d.	l.d.	l.d.	l.d.
Al	9.622	9.586	9.623	9.677	9.533	9.653	9.604	9.680
Si	30.168	30.228	30.178	30.346	30.062	30.229	30.294	30.196
Cl	l.d.	l.d.	0.042	l.d.	l.d.	0.037	l.d.	l.d.
K	14.339	14.153	14.223	13.952	14.354	14.180	14.255	14.159
Ca	l.d.	l.d.	l.d.	l.d.	l.d.	l.d.	l.d.	0.028
Ti	l.d.	l.d.	l.d.	l.d.	l.d.	l.d.	l.d.	l.d.
Fe	l.d.	l.d.	l.d.	l.d.	l.d.	l.d.	l.d.	l.d.
O	45.896	45.944	45.920	46.073	45.855	45.996	46.022	46.013
Total	100.174	100.189	100.198	100.202	100.300	100.310	100.358	100.361

Continued on next page

Analysis	38	39	40	41	42	43	44	45
Sample	HLRL	RNMP4	RNMP4	RNMP4	HLRL	RNMP4	HLRL	HLRL
Mineral	Microcline	Microcline	Microcline	Microcline	Microcline	Microcline	Microcline	Microcline
Na	0.217	0.273	0.108	0.149	0.132	0.181	0.162	0.164
Mg	l.d.	l.d.	l.d.	l.d.	l.d.	l.d.	l.d.	l.d.
Al	9.638	9.615	9.565	9.622	9.592	9.623	9.722	9.620
Si	30.260	30.318	30.329	30.302	30.289	30.377	30.146	30.255
Cl	l.d.	0.040	l.d.	0.055	l.d.	l.d.	l.d.	0.034
K	14.209	14.015	14.324	14.190	14.444	14.234	14.528	14.522
Ca	l.d.	l.d.	l.d.	0.027	l.d.	l.d.	l.d.	l.d.
Ti	l.d.	l.d.	l.d.	l.d.	l.d.	l.d.	l.d.	l.d.
Fe	l.d.	l.d.	l.d.	l.d.	l.d.	l.d.	l.d.	l.d.
O	46.026	46.066	46.032	46.046	46.053	46.148	46.023	46.048
Total	100.364	100.369	100.394	100.408	100.570	100.616	100.626	100.649

Analysis	46	47	48	49	50	51	52	53
Sample	HLRL	RNMP4	RNMP4	RNMP4	HLRL	ROMMNP	HLRL	RNMP4
Mineral	Microcline	Microcline	Microcline	Microcline	Microcline	Microcline	Microcline	Microcline
Na	0.162	0.207	0.186	0.147	0.172	0.199	0.179	0.207
Mg	l.d.	l.d.	l.d.	l.d.	l.d.	l.d.	l.d.	l.d.
Al	9.595	9.701	9.689	9.747	9.688	9.690	9.706	9.782
Si	30.366	30.422	30.442	30.452	30.383	30.439	30.373	30.401
Cl	l.d.	l.d.	0.046	l.d.	l.d.	l.d.	l.d.	l.d.
K	14.410	14.065	14.169	14.130	14.360	14.177	14.404	14.235
Ca	l.d.	0.029	l.d.	0.024	l.d.	0.029	l.d.	l.d.
Ti	l.d.	l.d.	l.d.	l.d.	l.d.	l.d.	l.d.	l.d.
Fe	l.d.	l.d.	l.d.	l.d.	l.d.	l.d.	l.d.	l.d.
O	46.138	46.256	46.266	46.320	46.228	46.291	46.250	46.337
Total	100.710	100.713	100.820	100.864	100.868	100.877	100.965	101.029

Analysis	54	55	56	57	58	59	60	61
Sample	RNMP4	RNMP4	RNMP4	RNMP4	RNMP4	HLRL	HLRL	HLRL
Mineral	Microcline	Microcline	Microcline	Microcline	Microcline	Microcline	Microcline	Microcline
Na	0.162	0.133	0.673	0.162	0.138	0.166	0.248	0.177
Mg	l.d.	l.d.	l.d.	l.d.	l.d.	l.d.	l.d.	l.d.
Al	9.805	9.761	10.126	9.747	9.751	9.728	9.758	9.784
Si	30.476	30.642	30.221	30.779	30.699	30.617	30.685	30.689
Cl	l.d.	l.d.	0.197	l.d.	l.d.	l.d.	0.057	l.d.
K	14.137	14.138	13.769	14.137	14.345	14.528	14.499	14.485
Ca	l.d.	l.d.	l.d.	l.d.	l.d.	l.d.	l.d.	l.d.
Ti	l.d.	l.d.	l.d.	l.d.	l.d.	l.d.	l.d.	l.d.
Fe	l.d.	l.d.	l.d.	l.d.	l.d.	l.d.	l.d.	l.d.
O	46.400	46.542	46.502	46.700	46.630	46.575	46.691	46.749
Total	101.031	101.289	101.540	101.586	101.600	101.681	101.959	102.063

Continued on next page

Analysis	1	2	3	4	5	6	7	8
Sample	ROM 1	ROM 1	ROM 1	RNMP4	HLRL	ROM 1	ROM 1	HLRL
Mineral	Nepheline	Nepheline	Nepheline	Nepheline	Nepheline	Nepheline	Nepheline	Nepheline
Na	11.989	11.634	12.177	11.580	11.949	11.801	11.934	11.371
Mg	l.d.	l.d.	l.d.	l.d.	l.d.	l.d.	l.d.	l.d.
Al	17.446	17.698	17.917	17.892	17.885	18.288	17.888	17.868
Si	19.984	20.404	19.378	19.981	19.600	19.363	19.918	20.236
Cl	l.d.	l.d.	l.d.	l.d.	l.d.	l.d.	l.d.	l.d.
K	4.594	4.049	5.032	4.595	4.998	5.347	4.632	4.648
Ca	l.d.	l.d.	l.d.	l.d.	l.d.	l.d.	l.d.	l.d.
Ti	l.d.	l.d.	l.d.	l.d.	l.d.	l.d.	l.d.	l.d.
Fe	0.577	0.434	0.491	0.623	0.589	0.302	0.489	0.585
O	43.646	44.048	43.490	43.923	43.667	43.660	43.915	44.101
Total	98.255	98.283	98.498	98.627	98.717	98.794	98.800	98.824

Analysis	9	10	11	12	13	14	15	16
Sample	RNMP4	ROM 1	HLRL	RNMP4	HLRL	HLRL	RNMP4	RNMP4
Mineral	Nepheline	Nepheline	Nepheline	Nepheline	Nepheline	Nepheline	Nepheline	Nepheline
Na	11.418	12.163	11.914	11.828	11.733	12.050	11.747	11.873
Mg	l.d.	l.d.	l.d.	l.d.	l.d.	l.d.	l.d.	l.d.
Al	18.191	17.834	18.320	18.293	18.306	18.093	18.138	18.420
Si	19.872	19.816	19.461	19.566	19.633	19.724	20.235	19.736
Cl	l.d.	l.d.	l.d.	l.d.	l.d.	l.d.	l.d.	l.d.
K	4.784	4.728	5.235	5.150	5.257	4.789	4.465	4.896
Ca	l.d.	l.d.	l.d.	l.d.	l.d.	l.d.	l.d.	l.d.
Ti	l.d.	l.d.	l.d.	l.d.	l.d.	l.d.	l.d.	l.d.
Fe	0.586	0.553	0.328	0.383	0.278	0.659	0.466	0.386
O	44.022	43.876	43.816	43.891	43.922	44.018	44.392	44.167
Total	98.890	98.992	99.091	99.120	99.136	99.344	99.473	99.506

Analysis	17	18	19	20	21	22	23	24
Sample	ROM 1	ROM 1	HLRL	HLRL	RNMP4	HLRL	HLRL	FROM
Mineral	Nepheline	Nepheline	Nepheline	Nepheline	Nepheline	Nepheline	Nepheline	Nepheline
Na	12.134	12.066	11.701	11.770	11.823	11.396	12.086	12.395
Mg	l.d.	l.d.	l.d.	l.d.	l.d.	l.d.	l.d.	l.d.
Al	18.068	18.171	18.398	18.268	18.446	18.461	18.331	18.086
Si	19.903	19.686	19.807	19.946	19.794	20.029	20.011	20.005
Cl	l.d.	l.d.	l.d.	l.d.	l.d.	l.d.	l.d.	l.d.
K	4.849	4.962	5.176	4.930	5.290	5.055	5.196	5.097
Ca	l.d.	l.d.	l.d.	l.d.	l.d.	l.d.	l.d.	l.d.
Ti	l.d.	l.d.	l.d.	l.d.	l.d.	l.d.	l.d.	l.d.
Fe	0.395	0.594	0.341	0.479	0.279	0.667	0.494	0.638
O	44.134	44.056	44.209	44.274	44.269	44.526	44.585	44.505
Total	99.513	99.549	99.647	99.669	99.912	100.148	100.724	100.742

Continued on next page

Analysis	25	1	2	3	4	5	6	7
Sample	FROM	HLRL	ROM 1	ROM 1	RNMP4	RNMP4	HLRL	HLRL
Mineral	Nepheline	Sodalite	Sodalite	Sodalite	Sodalite	Sodalite	Sodalite	Sodalite
Na	12.249	17.253	17.467	17.333	17.376	17.500	17.745	18.480
Mg	l.d.	l.d.	l.d.	l.d.	l.d.	l.d.	l.d.	l.d.
Al	18.165	17.186	16.486	16.215	17.085	17.220	16.934	16.424
Si	19.899	16.755	17.231	17.452	16.967	16.940	17.234	17.035
Cl	l.d.	7.272	7.258	7.489	7.338	7.447	7.130	7.326
K	5.185	l.d.	0.058	0.030	l.d.	0.027	0.036	l.d.
Ca	l.d.	l.d.	l.d.	l.d.	l.d.	l.d.	l.d.	l.d.
Ti	l.d.	l.d.	l.d.	l.d.	l.d.	l.d.	l.d.	l.d.
Fe	0.943	0.045	0.238	0.277	l.d.	l.d.	l.d.	0.284
O	44.555	40.393	40.484	40.455	40.572	40.738	40.882	40.570
Total	101.009	98.920	99.238	99.254	99.368	99.952	99.987	100.142

Analysis	8	9	10	11	12	13	14	15
Sample	RNMP4	ROM 1	ROM 1	HLRL	ROM 1	RNMP4	RNMP4	HLRL
Mineral	Sodalite	Sodalite	Sodalite	Sodalite	Sodalite	Sodalite	Sodalite	Sodalite
Na	17.288	18.649	16.946	18.398	17.543	18.212	17.431	17.589
Mg	l.d.	l.d.	l.d.	l.d.	l.d.	l.d.	l.d.	l.d.
Al	16.803	16.826	17.071	16.404	16.958	16.490	17.236	16.823
Si	17.373	16.592	17.464	17.211	17.201	17.563	17.040	17.559
Cl	7.402	7.281	7.324	7.469	7.545	7.325	7.359	7.267
K	l.d.	0.028	0.029	l.d.	0.038	l.d.	l.d.	l.d.
Ca	l.d.	l.d.	l.d.	l.d.	l.d.	l.d.	l.d.	l.d.
Ti	l.d.	l.d.	l.d.	l.d.	l.d.	l.d.	l.d.	l.d.
Fe	0.384	0.367	0.340	0.250	0.348	0.084	0.632	0.380
O	40.928	40.515	41.125	40.719	40.946	41.047	41.086	41.253
Total	100.240	100.261	100.309	100.499	100.604	100.742	100.826	100.895

Analysis	16	17	18	19	20	21	22	23
Sample	HLRL	ROM 1	RNMP4	HLRL	HLRL	RNMP4	ROM 1	HLRL
Mineral	Sodalite	Sodalite	Sodalite	Sodalite	Sodalite	Sodalite	Sodalite	Sodalite
Na	18.648	18.397	18.698	18.622	18.981	18.508	18.186	19.017
Mg	l.d.	l.d.	l.d.	l.d.	l.d.	l.d.	l.d.	l.d.
Al	16.965	16.868	16.624	16.986	16.504	16.942	16.757	17.011
Si	17.015	17.138	17.246	17.190	17.389	17.231	17.833	17.027
Cl	7.177	7.634	7.228	7.239	7.161	7.462	7.012	7.126
K	l.d.	0.034	l.d.	l.d.	0.034	l.d.	0.029	0.029
Ca	l.d.	l.d.	l.d.	l.d.	l.d.	l.d.	l.d.	l.d.
Ti	l.d.	l.d.	l.d.	l.d.	l.d.	l.d.	l.d.	l.d.
Fe	l.d.	l.d.	0.309	l.d.	l.d.	l.d.	l.d.	l.d.
O	41.000	40.945	41.071	41.183	41.150	41.159	41.579	41.183
Total	100.913	101.055	101.196	101.274	101.344	101.373	101.471	101.482

Continued on next page

Analysis	24	25	26	27	28
Sample	HLRL	RNMP4	ROM 1	ROM 1	RNMP4
Mineral	Sodalite	Sodalite	Sodalite	Sodalite	Sodalite
Na	18.234	18.478	18.767	18.606	18.452
Mg	l.d.	l.d.	l.d.	l.d.	l.d.
Al	16.722	16.569	16.793	16.927	16.703
Si	17.611	17.329	17.173	17.369	17.824
Cl	7.536	7.140	7.440	7.427	7.293
K	l.d.	0.046	0.029	0.029	l.d.
Ca	l.d.	0.060	l.d.	l.d.	0.026
Ti	l.d.	l.d.	l.d.	l.d.	l.d.
Fe	0.057	0.714	0.295	0.037	0.147
O	41.304	41.247	41.159	41.343	41.653
Total	101.483	101.591	101.660	101.762	102.118

Appendix 4. Geochemical interpretation: Spearman correlation matrix for X-Ray Fluorescence data

Correlations Spearman's rho							
		SiO_2	TiO_2	Al_2O_3	Fe_2O_3	MnO	MgO
SiO_2	Correlation Coefficient	1.000					
	Significance (α) (2-tailed)	0.000					
	N	37					
TiO_2	Correlation Coefficient	-.848(**)	1.000				
	Significance (α) (2-tailed)	0.000	0.000				
	N	37	37				
Al_2O_3	Correlation Coefficient	.719(**)	-.954(**)	1.000			
	Significance (α) (2-tailed)	0.000	0.000	0.000			
	N	37	37	37			
Fe_2O_3	Correlation Coefficient	-.860(**)	.992(**)	-.931(**)	1.000		
	Significance (α) (2-tailed)	0.000	0.000	0.000	0.000		
	N	37	37	37	37		
MnO	Correlation Coefficient	-.854(**)	.994(**)	-.945(**)	.987(**)	1.000	
	Significance (α) (2-tailed)	0.000	0.000	0.000	0.000	0.000	
	N	37	37	37	37	37	
MgO	Correlation Coefficient	-.740(**)	.893(**)	-.909(**)	.884(**)	.888(**)	1.000
	Significance (α) (2-tailed)	0.000	0.000	0.000	0.000	0.000	0.000
	N	37	37	37	37	37	37
CaO	Correlation Coefficient	-.853(**)	.980(**)	-.955(**)	.964(**)	.972(**)	.879(**)
	Significance (α) (2-tailed)	0.000	0.000	0.000	0.000	0.000	0.000
	N	37	37	37	37	37	37
Na_2O	Correlation Coefficient	-0.023	-0.322	.499(**)	-0.289	-0.299	-.408(*)
	Significance (α) (2-tailed)	0.893	0.052	0.002	0.082	0.072	0.012
	N	37	37	37	37	37	37
K_2O	Correlation Coefficient	.873(**)	-.807(**)	.666(**)	-.843(**)	-.806(**)	-.720(**)
	Significance (α) (2-tailed)	0.000	0.000	0.000	0.000	0.000	0.000
	N	37	37	37	37	37	37
Nb	Correlation Coefficient	-.706(**)	.854(**)	-.834(**)	.851(**)	.850(**)	.690(**)
	Significance (α) (2-tailed)	0.000	0.000	0.000	0.000	0.000	0.000
	N	37	37	37	37	37	37
Rb	Correlation Coefficient	-0.290	.427(**)	-.444(**)	.403(*)	.426(**)	0.283
	Significance (α) (2-tailed)	0.081	0.008	0.006	0.013	0.009	0.089
	N	37	37	37	37	37	37
Sr	Correlation Coefficient	-.558(**)	.393(*)	-0.242	.445(**)	.403(*)	0.320
	Significance (α) (2-tailed)	0.000	0.016	0.149	0.006	0.013	0.053
	N	37	37	37	37	37	37
Th	Correlation Coefficient	-.596(**)	.813(**)	-.828(**)	.805(**)	.806(**)	.647(**)
	Significance (α) (2-tailed)	0.000	0.000	0.000	0.000	0.000	0.000
	N	37	37	37	37	37	37
U	Correlation Coefficient	-.631(**)	.830(**)	-.833(**)	.823(**)	.823(**)	.666(**)
	Significance (α) (2-tailed)	0.000	0.000	0.000	0.000	0.000	0.000
	N	37	37	37	37	37	37
Y	Correlation Coefficient	-.714(**)	.766(**)	-.688(**)	.785(**)	.765(**)	.613(**)
	Significance (α) (2-tailed)	0.000	0.000	0.000	0.000	0.000	0.000
	N	37	37	37	37	37	37

**Correlation is significant at the 0.01 level (2-tailed), *Correlation is significant at the 0.05 level (2-tailed)

Continued on next page

		SiO_2	TiO_2	Al_2O_3	Fe_2O_3	MnO	MgO
Zr	Correlation Coefficient	-.695(**)	.861(**)	-.854(**)	.858(**)	.852(**)	.699(**)
	Significance (α) (2-tailed)	0.000	0.000	0.000	0.000	0.000	0.000
	N	37	37	37	37	37	37
Cl	Correlation Coefficient	0.313	-.372(*)	.381(*)	-.341(*)	-.364(*)	-0.265
	Significance (α) (2-tailed)	0.059	0.023	0.020	0.039	0.027	0.113
	N	37	37	37	37	37	37
F	Correlation Coefficient	-.656(**)	.816(**)	-.830(**)	.806(**)	.803(**)	.704(**)
	Significance (α) (2-tailed)	0.000	0.000	0.000	0.000	0.000	0.000
	N	37	37	37	37	37	37
Ba	Correlation Coefficient	0.087	-.367(*)	.497(**)	-0.309	-.352(*)	-.359(*)
	Significance (α) (2-tailed)	0.610	0.025	0.002	0.063	0.033	0.029
	N	37	37	37	37	37	37
Ce	Correlation Coefficient	-.627(**)	.570(**)	-.433(**)	.605(**)	.577(**)	.402(*)
	Significance (α) (2-tailed)	0.000	0.000	0.007	0.000	0.000	0.014
	N	37	37	37	37	37	37
La	Correlation Coefficient	-.535(**)	.768(**)	-.782(**)	.765(**)	.762(**)	.610(**)
	Significance (α) (2-tailed)	0.001	0.000	0.000	0.000	0.000	0.000
	N	37	37	37	37	37	37

		CaO	Na_2O	K_2O	Nb	Rb	Sr
CaO	Correlation Coefficient	1.000					
	Significance (α) (2-tailed)	0.000					
	N	37					
Na_2O	Correlation Coefficient	-.342(*)	1.000				
	Significance (α) (2-tailed)	0.038	0.000				
	N	37	37				
K_2O	Correlation Coefficient	-.763(**)	0.044	1.000			
	Significance (α) (2-tailed)	0.000	0.796	0.000			
	N	37	37	37			
Nb	Correlation Coefficient	.841(**)	-0.284	-.630(**)	1.000		
	Significance (α) (2-tailed)	0.000	0.088	0.000	0.000		
	N	37	37	37	37		
Rb	Correlation Coefficient	.444(**)	-0.206	-0.108	.343(*)	1.000	
	Significance (α) (2-tailed)	0.006	0.220	0.526	0.038	0.000	
	N	37	37	37	37	37	
Sr	Correlation Coefficient	.342(*)	0.216	-.623(**)	.558(**)	-0.320	1.000
	Significance (α) (2-tailed)	0.038	0.199	0.000	0.000	0.053	0.000
	N	37	37	37	37	37	37

**Correlation is significant at the 0.01 level (2-tailed), *Correlation is significant at the 0.05 level (2-tailed)

Continued on next page

		CaO	Na_2O	K_2O	Nb	Rb	Sr
Th	Correlation Coefficient	.806(**)	-0.302	-.495(**)	.944(**)	.457(**)	.342(*)
	Significance (α) (2-tailed)	0.000	0.069	0.002	0.000	0.004	0.038
	N	37	37	37	37	37	37
U	Correlation Coefficient	.815(**)	-.332(*)	-.540(**)	.977(**)	.379(*)	.446(**)
	Significance (α) (2-tailed)	0.000	0.045	0.001	0.000	0.021	0.006
	N	37	37	37	37	37	37
Y	Correlation Coefficient	.737(**)	-0.104	-.727(**)	.915(**)	0.074	.777(**)
	Significance (α) (2-tailed)	0.000	0.540	0.000	0.000	0.662	0.000
	N	37	37	37	37	37	37
Zr	Correlation Coefficient	.851(**)	-0.322	-.621(**)	.990(**)	.366(*)	.499(**)
	Significance (α) (2-tailed)	0.000	0.052	0.000	0.000	0.026	0.002
	N	37	37	37	37	37	37
Cl	Correlation Coefficient	-.388(*)	.337(*)	0.291	-.489(**)	0.205	-0.289
	Significance (α) (2-tailed)	0.018	0.041	0.081	0.002	0.225	0.083
	N	37	37	37	37	37	37
F	Correlation Coefficient	.830(**)	-.325(*)	-.592(**)	.847(**)	.535(**)	0.247
	Significance (α) (2-tailed)	0.000	0.050	0.000	0.000	0.001	0.140
	N	37	37	37	37	37	37
Ba	Correlation Coefficient	-.404(*)	.480(**)	-0.019	-0.284	-0.222	.409(*)
	Significance (α) (2-tailed)	0.013	0.003	0.910	0.089	0.187	0.012
	N	37	37	37	37	37	37
Ce	Correlation Coefficient	.520(**)	0.086	-.688(**)	.730(**)	-0.031	.867(**)
	Significance (α) (2-tailed)	0.001	0.613	0.000	0.000	0.855	0.000
	N	37	37	37	37	37	37
La	Correlation Coefficient	.736(**)	-0.306	-.436(**)	.857(**)	.486(**)	0.231
	Significance (α) (2-tailed)	0.000	0.066	0.007	0.000	0.002	0.170
	N	37	37	37	37	37	37

		Th	U	Y	
Th	Correlation Coefficient	1.000			
	Significance (α) (2-tailed)	0.000			
	N	37			
U	Correlation Coefficient	.975(**)	1.000		
	Significance (α) (2-tailed)	0.000	0.000		
	N	37	37		
Y	Correlation Coefficient	.787(**)	.851(**)	1.000	
	Significance (α) (2-tailed)	0.000	0.000	0.000	
	N	37	37	37	

**Correlation is significant at the 0.01 level (2-tailed), *Correlation is significant at the 0.05 level (2-tailed)

Continued on next page

		Th	U	Y	Zr	Cl	F
Zr	Correlation Coefficient	.960(**)	.987(**)	.894(**)	1.000		
	Significance (α) (2-tailed)	0.000	0.000	0.000	0.000		
	N	37	37	37	37		
Cl	Correlation Coefficient	-.386(*)	-.471(**)	-.467(**)	-.482(**)	1.000	
	Significance (α) (2-tailed)	0.018	0.003	0.004	0.002	0.000	
	N	37	37	37	37	37	
F	Correlation Coefficient	.872(**)	.852(**)	.740(**)	.874(**)	-0.294	1.000
	Significance (α) (2-tailed)	0.000	0.000	0.000	0.000	0.077	0.000
	N	37	37	37	37	37	37
Ba	Correlation Coefficient	-.464(**)	-.393(*)	-0.062	-.347(*)	.430(**)	-.453(**)
	Significance (α) (2-tailed)	0.004	0.016	0.715	0.035	0.008	0.005
	N	37	37	37	37	37	37
Ce	Correlation Coefficient	.518(**)	.617(**)	.895(**)	.678(**)	-.396(*)	.466(**)
	Significance (α) (2-tailed)	0.001	0.000	0.000	0.000	0.015	0.004
	N	37	37	37	37	37	37
La	Correlation Coefficient	.951(**)	.919(**)	.654(**)	.882(**)	-.385(*)	.775(**)
	Significance (α) (2-tailed)	0.000	0.000	0.000	0.000	0.019	0.000
	N	37	37	37	37	37	37

		Ba	Ce	La	
Ba	Correlation Coefficient	1.000			
	Significance (α) (2-tailed)	0.000			
	N	37			
Ce	Correlation Coefficient	0.295	1.000		
	Significance (α) (2-tailed)	0.076	0.000		
	N	37	37		
La	Correlation Coefficient	-.518(**)	.398(*)	1.000	
	Significance (α) (2-tailed)	0.001	0.015	0.000	
	N	37	37	37	

Appendix 5. Geochemical interpretation: Spearman correlation matrix for the Uniquant® 5 data compared to with WINXRF

Correlation: Spearman's rho					
		SiO_2 WinXRF	TiO^2 WinXRF	$Al2O_3$ WinXRF	Fe_2O_3 WinXRF
SiO_2 Uniquant	Correlation Coefficient	.987(**)	-.928(**)	.820(**)	-.982(**)
	Significance (α) (2-tailed)	0.000	0.000	0.000	0.000
	N	14	14	14	14
TiO_2 Uniquant	Correlation Coefficient	-.978(**)	.920(**)	-.837(**)	.991(**)
	Significance (α) (2-tailed)	0.000	0.000	0.000	0.000
	N	14	14	14	14
Al_2O_3 Uniquant	Correlation Coefficient	.739(**)	-.678(**)	.970(**)	-.779(**)
	Significance (α) (2-tailed)	0.003	0.008	0.000	0.001
	N	14	14	14	14
Fe_2O_3 Uniquant	Correlation Coefficient	-.974(**)	.900(**)	-.842(**)	.996(**)
	Significance (α) (2-tailed)	0.000	0.000	0.000	0.000
	N	14	14	14	14
CaO Uniquant	Correlation Coefficient	-.969(**)	.909(**)	-.837(**)	1.000(**)
	Significance (α) (2-tailed)	0.000	0.000	0.000	.
	N	14	14	14	14
Na_2O Uniquant	Correlation Coefficient	0.400	-0.357	.766(**)	-0.429
	Significance (α) (2-tailed)	0.156	0.210	0.001	0.126
	N	14	14	14	14
K_2O Uniquant	Correlation Coefficient	.982(**)	-.909(**)	.824(**)	-.987(**)
	Significance (α) (2-tailed)	0.000	0.000	0.000	0.000
	N	14	14	14	14
Zr Uniquant	Correlation Coefficient	-.974(**)	.913(**)	-.833(**)	.996(**)
	Significance (α) (2-tailed)	0.000	0.000	0.000	0.000
	N	14	14	14	14
Rb Uniquant	Correlation Coefficient	0.002	-0.046	-0.293	0.026
	Significance (α) (2-tailed)	0.994	0.875	0.309	0.928
	N	14	14	14	14
Sr Uniquant	Correlation Coefficient	-0.147	0.170	0.119	0.040
	Significance (α) (2-tailed)	0.615	0.562	0.686	0.893
	N	14	14	14	14
Y Uniquant	Correlation Coefficient	-.886(**)	.851(**)	-.754(**)	.899(**)
	Significance (α) (2-tailed)	0.000	0.000	0.002	0.000
	N	14	14	14	14
Nb Uniquant	Correlation Coefficient	-.968(**)	.894(**)	-.836(**)	.990(**)
	Significance (α) (2-tailed)	0.000	0.000	0.000	0.000
	N	14	14	14	14
Ba Uniquant	Correlation Coefficient	0.405	-0.324	0.308	-0.462
	Significance (α) (2-tailed)	0.151	0.259	0.284	0.096
	N	14	14	14	14
Ce Uniquant	Correlation Coefficient	-.925(**)	.876(**)	-.912(**)	.934(**)
	Significance (α) (2-tailed)	0.000	0.000	0.000	0.000
	N	14	14	14	14
La Uniquant	Correlation Coefficient	-.969(**)	.895(**)	-.824(**)	.978(**)
	Significance (α) (2-tailed)	0.000	0.000	0.000	0.000
	N	14	14	14	14

**Correlation is significant at the 0.01 level (2-tailed), *Correlation is significant at the 0.05 level (2-tailed)

Continued on next page

		CaO WinXRF	Na_2O WinXRF	K_2O WinXRF	Zr WinXRF
SiO_2 Uniquant	Correlation Coefficient	-.978(**)	0.138	.947(**)	-.978(**)
	Significance (α) (2-tailed)	0.000	0.637	0.000	0.000
	N	14	14	14	14
TiO_2 Uniquant	Correlation Coefficient	.996(**)	-0.200	-.895(**)	.987(**)
	Significance (α) (2-tailed)	0.000	0.493	0.000	0.000
	N	14	14	14	14
Al_2O_3 Uniquant	Correlation Coefficient	-.783(**)	0.493	.627(*)	-.772(**)
	Significance (α) (2-tailed)	0.001	0.073	0.016	0.001
	N	14	14	14	14
Fe_2O_3 Uniquant	Correlation Coefficient	1.000(**)	-0.204	-.899(**)	.991(**)
	Significance (α) (2-tailed)	.	0.483	0.000	0.000
	N	14	14	14	14
CaO Uniquant	Correlation Coefficient	.996(**)	-0.200	-.903(**)	.996(**)
	Significance (α) (2-tailed)	0.000	0.493	0.000	0.000
	N	14	14	14	14
Na_2O Uniquant	Correlation Coefficient	-0.433	.836(**)	0.231	-0.433
	Significance (α) (2-tailed)	0.122	0.000	0.427	0.122
	N	14	14	14	14
K_2O Uniquant	Correlation Coefficient	-.982(**)	0.143	.952(**)	-.982(**)
	Significance (α) (2-tailed)	0.000	0.626	0.000	0.000
	N	14	14	14	14
Zr Uniquant	Correlation Coefficient	.991(**)	-0.204	-.899(**)	1.000(**)
	Significance (α) (2-tailed)	0.000	0.483	0.000	.
	N	14	14	14	14
Rb Uniquant	Correlation Coefficient	0.037	-.609(*)	0.209	0.066
	Significance (α) (2-tailed)	0.899	0.021	0.472	0.822
	N	14	14	14	14
Sr Uniquant	Correlation Coefficient	0.044	.719(**)	-0.275	0.046
	Significance (α) (2-tailed)	0.881	0.004	0.341	0.875
	N	14	14	14	14
Y Uniquant	Correlation Coefficient	.903(**)	0.029	-.824(**)	.895(**)
	Significance (α) (2-tailed)	0.000	0.923	0.000	0.000
	N	14	14	14	14
Nb Uniquant	Correlation Coefficient	.995(**)	-0.189	-.893(**)	.990(**)
	Significance (α) (2-tailed)	0.000	0.517	0.000	0.000
	N	14	14	14	14
Ba Uniquant	Correlation Coefficient	-0.438	.642(*)	0.293	-0.475
	Significance (α) (2-tailed)	0.117	0.013	0.310	0.086
	N	14	14	14	14
Ce Uniquant	Correlation Coefficient	.930(**)	-0.204	-.877(**)	.930(**)
	Significance (α) (2-tailed)	0.000	0.483	0.000	0.000
	N	14	14	14	14
La Uniquant	Correlation Coefficient	.982(**)	-0.134	-.912(**)	.974(**)
	Significance (α) (2-tailed)	0.000	0.648	0.000	0.000
	N	14	14	14	14

**Correlation is significant at the 0.01 level (2-tailed), *Correlation is significant at the 0.05 level (2-tailed)

Continued on next page

		Rb WinXRF	Sr WinXRF	Y WinXRF	Nb WinXRF
SiO2 Uniquant	Correlation Coefficient	-.903(**)	-.785(**)	-.978(**)	-.982(**)
	Significance (α) (2-tailed)	0.000	0.001	0.000	0.000
	N	14	14	14	14
TiO2 Uniquant	Correlation Coefficient	.947(**)	.692(**)	.960(**)	.991(**)
	Significance (α) (2-tailed)	0.000	0.006	0.000	0.000
	N	14	14	14	14
Al2O3 Uniquant	Correlation Coefficient	-.735(**)	-0.475	-.737(**)	-.779(**)
	Significance (α) (2-tailed)	0.003	0.086	0.003	0.001
	N	14	14	14	14
Fe2O3 Uniquant	Correlation Coefficient	.943(**)	.701(**)	.965(**)	.996(**)
	Significance (α) (2-tailed)	0.000	0.005	0.000	0.000
	N	14	14	14	14
CaO Uniquant	Correlation Coefficient	.947(**)	.705(**)	.969(**)	1.000(**)
	Significance (α) (2-tailed)	0.000	0.005	0.000	.
	N	14	14	14	14
Na2O Uniquant	Correlation Coefficient	-0.440	0.015	-0.341	-0.429
	Significance (α) (2-tailed)	0.115	0.958	0.233	0.126
	N	14	14	14	14
K2O Uniquant	Correlation Coefficient	-.899(**)	-.793(**)	-.982(**)	-.987(**)
	Significance (α) (2-tailed)	0.000	0.001	0.000	0.000
	N	14	14	14	14
Zr Uniquant	Correlation Coefficient	.943(**)	.701(**)	.974(**)	.996(**)
	Significance (α) (2-tailed)	0.000	0.005	0.000	0.000
	N	14	14	14	14
Rb Uniquant	Correlation Coefficient	0.139	-0.335	0.011	0.026
	Significance (α) (2-tailed)	0.636	0.241	0.970	0.928
	N	14	14	14	14
Sr Uniquant	Correlation Coefficient	-0.077	.640(*)	0.244	0.040
	Significance (α) (2-tailed)	0.794	0.014	0.400	0.893
	N	14	14	14	14
Y Uniquant	Correlation Coefficient	.842(**)	.789(**)	.930(**)	.899(**)
	Significance (α) (2-tailed)	0.000	0.001	0.000	0.000
	N	14	14	14	14
Nb Uniquant	Correlation Coefficient	.933(**)	.722(**)	.977(**)	.990(**)
	Significance (α) (2-tailed)	0.000	0.004	0.000	0.000
	N	14	14	14	14
Ba Uniquant	Correlation Coefficient	-0.519	0.035	-0.381	-0.462
	Significance (α) (2-tailed)	0.057	0.905	0.179	0.096
	N	14	14	14	14
Ce Uniquant	Correlation Coefficient	.842(**)	.745(**)	.934(**)	.934(**)
	Significance (α) (2-tailed)	0.000	0.002	0.000	0.000
	N	14	14	14	14
La Uniquant	Correlation Coefficient	.908(**)	.785(**)	.987(**)	.978(**)
	Significance (α) (2-tailed)	0.000	0.001	0.000	0.000
	N	14	14	14	14

**Correlation is significant at the 0.01 level (2-tailed), *Correlation is significant at the 0.05 level (2-tailed)

Continued on next page

		Ba WinXRF	Ce WinXRF	La WinXRF
SiO2 Uniquant	Correlation Coefficient	-0.130	-.969(**)	-.890(**)
	Significance (α) (2-tailed)	0.659	0.000	0.000
	N	14	14	14
TiO2 Uniquant	Correlation Coefficient	0.042	.934(**)	.934(**)
	Significance (α) (2-tailed)	0.887	0.000	0.000
	N	14	14	14
Al2O3 Uniquant	Correlation Coefficient	0.031	-.693(**)	-.735(**)
	Significance (α) (2-tailed)	0.917	0.006	0.003
	N	14	14	14
Fe2O3 Uniquant	Correlation Coefficient	0.046	.938(**)	.943(**)
	Significance (α) (2-tailed)	0.876	0.000	0.000
	N	14	14	14
CaO Uniquant	Correlation Coefficient	0.042	.943(**)	.947(**)
	Significance (α) (2-tailed)	0.887	0.000	0.000
	N	14	14	14
Na2O Uniquant	Correlation Coefficient	0.475	-0.244	-0.414
	Significance (α) (2-tailed)	0.086	0.400	0.142
	N	14	14	14
K2O Uniquant	Correlation Coefficient	-0.134	-.974(**)	-.899(**)
	Significance (α) (2-tailed)	0.648	0.000	0.000
	N	14	14	14
Zr Uniquant	Correlation Coefficient	0.037	.938(**)	.943(**)
	Significance (α) (2-tailed)	0.899	0.000	0.000
	N	14	14	14
Rb Uniquant	Correlation Coefficient	-0.395	-0.095	0.150
	Significance (α) (2-tailed)	0.163	0.747	0.609
	N	14	14	14
Sr Uniquant	Correlation Coefficient	.906(**)	0.315	-0.024
	Significance (α) (2-tailed)	0.000	0.273	0.935
	N	14	14	14
Y Uniquant	Correlation Coefficient	0.345	.903(**)	.886(**)
	Significance (α) (2-tailed)	0.227	0.000	0.000
	N	14	14	14
Nb Uniquant	Correlation Coefficient	0.092	.946(**)	.946(**)
	Significance (α) (2-tailed)	0.753	0.000	0.000
	N	14	14	14
Ba Uniquant	Correlation Coefficient	.682(**)	-0.284	-0.493
	Significance (α) (2-tailed)	0.007	0.325	0.073
	N	14	14	14
Ce Uniquant	Correlation Coefficient	0.169	.916(**)	.864(**)
	Significance (α) (2-tailed)	0.563	0.000	0.000
	N	14	14	14
La Uniquant	Correlation Coefficient	0.182	.969(**)	.921(**)
	Significance (α) (2-tailed)	0.533	0.000	0.000
	N	14	14	14

**Correlation is significant at the 0.01 level (2-tailed), *Correlation is significant at the 0.05 level (2-tailed)